EFFECTS OF HIGHLY REACTIVE GASEOUS PLASMA TREATMENT ON THE GERMINATION AND GROWTH OF GARLIC

Matej Holc

Doctoral Dissertation
Jožef Stefan International Postgraduate School
Ljubljana, Slovenia

Supervisor: Prof. Dr. Miran Mozetič, Jožef Stefan Institute, Ljubljana, Slovenia
Co-Supervisor: Asst. Prof. Dr. Ita Junkar, Jožef Stefan Institute, Ljubljana, Slovenia

Evaluation Board:
Asst. Prof. Dr. Rok Zaplotnik, Chair, Jožef Stefan Institute, Ljubljana, Slovenia
Prof. Dr. Karin Stana Kleinschek, Member, Faculty of Mechanical Engineering, University of Maribor, Maribor, Slovenia
Asst. Prof. Dr. Petr Humpolíček, Member, Tomas Bata University, Zlín, Czech Republic

MEDNARODNA PODIPLOMSKA ŠOLA JOŽEFA STEFANA
JOŽEF STEFAN INTERNATIONAL POSTGRADUATE SCHOOL

Matej Holc

EFFECTS OF HIGHLY REACTIVE GASEOUS PLASMA TREATMENT ON THE GERMINATION AND GROWTH OF GARLIC

Doctoral Dissertation

UČINKI OBDELAVE Z VISOKO REAKTIVNO PLINSKO PLAZMO NA KALJENJE IN RAST ČESNA

Doktorska disertacija

Supervisor: Prof. Dr. Miran Mozetič

Co-Supervisor: Asst. Prof. Dr. Ita Junkar

Ljubljana, Slovenia, July 2019

Acknowledgments

The knowledge and research that made this dissertation possible originate from the Jožef Stefan Institute, Department of Surface Engineering and Optoelectronics (F4). The author would like to thank his supervisor and co-supervisor, Prof. Dr. Miran Mozetič and Asst. Prof. Dr. Ita Junkar, for the guidance and support received during the conception and creation of this work. Asst. Prof. Dr. Gregor Primc and Asst. Prof. Dr. Rok Zaplotnik have provided invaluable theoretical and practical support for research activities. Prof. Dr. Janez Kovač and Prof. Dr. Alenka Vesel contributed important knowledge regarding surface analysis and processes. The author is grateful to Tatjana Filipič and Janez Trtnik for the excellent technical support, as well as to the remaining team at the department for all the ideas and encouragement.

Further thanks go to Dr. Jernej Iskra, Dr. Primož Titan, and Dr. Silva Grobelnik Mlakar, for their professional help and ideas. The team at the center for electron microscopy and microanalysis (CEMM) also offered immense help with all scanning electron microscopy analyses.

Special thanks go to Darko Vernik and the staff at Semenarna Ljubljana, Selection and Testing Center in Ptuj, for their kindness and support, as well as for providing the knowledge and facilities for garlic field growth, harvest and analysis.

Funding for the research that resulted in this dissertation was provided by the Slovenian Research Agency ARRS, Young Researcher Grant PR-06950.

Abstract

Due to increasing food demands, an improvement in the growth of food crops is desired as a mechanism of increasing yields. At the same time, agricultural sustainability should be achieved to meet these food demands without harmful environmental effect. To this end, highly reactive plasma technologies have been introduced to agricultural research as "plasma agriculture". These environmentally benign alternatives to chemical-based approaches show promise regarding germination, growth and yield stimulation of various crops.

In this dissertation, we have studied the effects of inductively coupled, low-pressure radio frequency oxygen plasma on garlic cloves. Specifically, we worked with a Slovenian autochthonous garlic cultivar (*Ptujski spomladanski*) with the aim of boosting garlic growth, strengthening the plant, and improving its yield, while maintaining an ecologically friendly approach.

To treat the cloves, we have used pilot-scale and industrial-scale plasma reactors at a variety of treatment conditions. We have characterized the employed discharges using OES and a catalytic probe, as well as evaluated the effect of plasma treatment on the clove temperature. The physico-chemical and biological responses of unpeeled and peeled cloves differed due to the shielding function of the protective leaf, as well as differences in surface chemistry and biological function.

The effect of oxygen plasma on the surface properties of cloves was substantial. We have analyzed changes in the surface chemistry using XPS and ATR-FTIR. The plasma treatment increased the surface oxygen content and the O/C ratio through progressive oxidation of cuticular waxes, brought upon by functionalization mechanisms. At the same time, minor elements appeared at the surface in low amounts, indicating their exposure from deeper layers due to chemical etching of the cuticle. Surface morphology modification was evident in SEM and AFM images. In particular, with increasing oxygen atom dose, plasma treatment progressively etched the surface of the protective leaf. Conversely, protruding waxy structures appeared at the surface of plasma-treated peeled cloves, suggesting surface restructuring. The combined effect of changes to surface chemistry and morphology was increased wettability, indicated by WCA measurements, as well as improved water uptake.

Plasma treatment also affected the biological response of the cloves. During laboratory growth, treatment at suitable conditions increased sprout length, root length, and/or root number. These improvements translated into yield increases in field growth experiments, as indicated by higher mean dried bulb mass compared to garlic grown from untreated cloves. Further, the achieved yield improvements persisted into the second and third generation of garlic without the need for additional treatment.

Our findings show that at suitable plasma treatment conditions, garlic sprout and root growth is stimulated. Using properly tuned discharge parameters, plasma treatment can be a useful agricultural tool for stimulation of garlic germination and improvement of its yields.

Povzetek

Vzpodbujanje rasti poljščin, s tem pa večanje pridelka, je zaželeno zaradi stalnega večanja povpraševanja po hrani. Kmetijstvo sočasno stremi k trajnostni pridelavi, da bi lahko izpolnilo zahteve po pridelku z manj škodljivih vplivov na okolje. S tem namenom so bile tehnologije visoko reaktivne plinske plazme uvedene v kmetijske raziskave pod imenom "plazemsko kmetijstvo", kjer kot okoljsko neškodljive alternative uporabi kemikalij izkazujejo dobre obete glede vzpodbujanja kaljenja, rasti in pridelka različnih poljščin.

V tej disertaciji smo proučevali vplive nizkotlačne induktivno sklopljene radiofrekvenčne kisikove plazme na stroke česna. Pri tem smo uporabili česen slovenske avtohtone sorte *Ptujski spomladanski* z namenom vzpodbuditi njegovo rast, okrepiti rastlino ter izboljšati njen pridelek, sočasno pa ohraniti okolju prijazen pristop.

Stroke smo obdelovali v plazemskih reaktorjih pilotne in industrijske velikosti, kjer smo uporabili raznolike parametre tvorjenja plazme. Razelektritve smo okarakterizirali z uporabo optične emisijske spektroskopije in katalitične sonde, ocenili pa smo tudi vpliv plazme na temperaturo stroka med obdelavo. Fizikalno-kemijski in biološki odzivi neolupljenih in olupljenih strokov so se pri tem razlikovali zaradi zaščitne funkcije lupine česna, kakor tudi razlik v kemiji teh dveh površin in njunih bioloških vlogah.

Učinek kisikove plazme na površinske lastnosti strokov se je izkazal za znatnega. Spremembe v kemiji površine smo proučili z uporabo rentgenske fotoelektronske spektroskopije ter Fourierove transformacijske infrardeče spektroskopije. Plazemska obdelava je preko postopne oksidacije z mehanizmi funkcionalizacije povečala delež kisika na površini ter razmerje O/C. Sočasno so se na površini v manjših količinah pojavili dodatni elementi, kar nakazuje na izpostavitev globljih plasti zaradi kemijskega jedkanja kutikule. Spremembe morfologije površine so bile opazne na slikah, dobljenih s pomočjo vrstične elektronske mikroskopije ter mikroskopije na atomsko silo. Večja doza kisikovih atomov je močneje jedkala površino lupine stroka, medtem ko so se na površini olupljenega stroka pojavile izbočene voskaste strukture, kar nakazuje na preoblikovanje vrhnjih plasti. Celokupni učinek sprememb v kemiji in morfologiji površin je bila povečana omočljivost, ki jo opisujejo meritve kontaktnega kota vode, kakor tudi povečan privzem vode v strok.

Plazemska obdelava je vplivala tudi na biološki odziv strokov. Obdelava pri ustreznih pogojih je povečala povprečno dolžino kalčkov ter dolžino in število korenin med rastjo v laboratorijskem okolju. Ta izboljšanja so se med rastjo na polju prevedla v povečan pridelek, tj. višjo povprečno maso sušenih glavic česna. Nadalje je doseženo izboljšanje pridelka vztrajalo v drugo in tretjo generacijo rastlin brez potrebe po dodatni obdelavi strokov.

Naši izsledki kažejo, da je pri ustreznih pogojih plazemske obdelave mogoče vzpodbujati rast kalčkov in korenin česna. Z uporabo ustreznih plazemskih parametrov je obdelava lahko uporabno kmetijsko orodje za vzpodbujanje kaljenja česna in izboljšanja njegovega pridelka.

Contents

List of Figures **xvii**

List of Tables **xix**

Abbreviations **xxi**

Symbols **xxiii**

1 Introduction **1**
1.1 Background ... 1
1.2 Hypotheses ... 1
1.3 Plasma ... 2
1.3.1 Thermal and non-thermal plasma ... 2
1.3.2 Plasma configurations ... 2
1.3.3 Low-pressure oxygen plasma chemistry ... 3
1.3.3.1 Reactive oxygen species (ROS) ... 3
1.3.3.2 Recombination ... 4
1.3.3.3 E-mode and H-mode ... 4
1.3.3.4 Glow and afterglow ... 4
1.3.4 Plasma effects on surfaces ... 5
1.4 Plasma Agriculture ... 5
1.4.1 Germination and growth improvement of agricultural seeds ... 6
1.4.1 Mechanisms of germination and growth improvement ... 6
1.5 Garlic ... 7
1.5.1 Anatomy ... 7
1.5.2 Clove surface chemistry ... 9
1.5.3 Dormancy and germination ... 10
1.5.4 Plasma treatment of garlic cloves ... 10

2 Materials and Methods **11**
2.1 Garlic ... 11
2.2 Plasma Reactors ... 11
2.2.1 Pilot-scale system ... 12
2.2.2 Industrial-scale system ... 13
2.3 Plasma Treatment ... 14
2.3.1 Pilot-scale plasma ... 14
2.3.2 Industrial-scale plasma ... 14
2.3.3 Control treatments ... 15
2.4 Plasma Characterization ... 15
2.4.1 Optical emission spectroscopy (OES) ... 15
2.4.2 Catalytic probe ... 16
2.5 Temperature ... 17

2.6 Water Contact Angle (WCA) 17
2.7 Water Uptake (WU) 18
2.8 Surface Chemistry 18
2.8.1 X-ray photoelectron spectroscopy (XPS) 18
2.8.2 Attenuated total reflectance Fourier-transform infrared (ATR-FTIR) spectroscopy 18
2.9 Surface Morphology 19
2.9.1 Scanning electron microscopy (SEM) 19
2.9.2 Atomic force microscopy (AFM) 19
2.10 Sprout and Root Growth 19
2.11 Plant Height and Yield 20
2.12 Statistical Analysis 20

3 Results **21**
3.1 Plasma Characterization 21
3.1.1 Optical emission spectroscopy 21
3.1.1.1 Flow configuration 21
3.1.1.1.1 E-mode plasma 21
3.1.1.1.2 Garlic clove treatment 22
3.1.1.1.3 Effect of generator power 23
3.1.1.1.4 Effect of working pressure 24
3.1.1.1.5 Time courses of OH signal intensities 25
3.1.1.2 No-flow configuration 26
3.1.1.2.1 Treatment of peeled clove 26
3.1.1.2.2 Comparison of treatment of peeled and unpeeled cloves 28
3.1.2 Catalytic probe 29
3.1.2.1 n_O in the E-mode plasma 29
3.1.2.2 Probe signal increase during clove treatment 30
3.1.2.3 n_O during treatment of peeled garlic 32
3.1.2.4 n_O during treatment of unpeeled garlic 34
3.2 Temperature 36
3.3 Surface chemistry 38
3.3.1 X-ray photoelectron spectroscopy 38
3.3.1.1 Composition of untreated clove surfaces 38
3.3.1.2 Protective leaf 39
3.3.1.2.1 Pilot-scale E-mode glow treatment 39
3.3.1.2.2 Pilot-scale H-mode afterglow treatment 42
3.3.1.2.3 Pulsed treatment 43
3.3.1.3 Clove surface 44
3.3.1.3.1 Pilot-scale plasma treatment 44
3.3.1.3.2 Industrial-scale plasma treatment 46
3.3.1.3.3 Clove surface under the treated protective leaf 47
3.3.1.4 High-resolution XPS spectra 48
3.3.1.4.1 Protective leaf 48
3.3.1.4.2 Clove surface 49
3.3.2 ATR-FTIR spectra 51
3.3.2.1 Untreated surfaces 51
3.3.2.2 Unpeeled clove surface treatment 51
3.3.2.3 Peeled clove surface treatment 53
3.4 Surface Morphology 56

3.4.1 Scanning electron microscopy 56
3.4.1.1 Protective leaf 56
3.4.1.1.1 Pilot-scale glow plasma treatment 56
3.4.1.1.2 Pilot-scale afterglow plasma treatment 59
3.4.1.2 Clove surface 60
3.4.2 Atomic force microscopy 62
3.4.2.1 Protective leaf 62
3.4.2.2 Clove surface 63
3.5 Water Contact Angle 64
3.6 Water Uptake 65
3.6.1 Untreated cloves 65
3.6.2 Industrial-scale plasma 66
3.6.3 Pilot-scale plasma 67
3.6.4 Clove mass loss 69
3.6.5 Effect of initial clove mass 70
3.7 Sprout and Root Growth 71
3.7.1 Pilot-scale plasma 71
3.7.1.1 Preliminary treatment 71
3.7.1.2 Untreated controls 71
3.7.1.3 Unpeeled cloves 73
3.7.1.3.1 E-mode glow 73
3.7.1.3.2 H-mode afterglow 77
3.7.1.4 Peeled cloves 80
3.7.2 Industrial-scale plasma 85
3.8 Field Growth and Yield 87
3.8.1 Plant height 87
3.8.2 Yield 88
3.8.2.1 Pilot-scale treatment 88
3.8.2.2 Industrial-scale treatment 89
3.8.2.3 2nd and 3rd generations 89

4 Discussion **91**
4.1 Plasma Characterization 91
4.1.1 Optical emission spectroscopy 91
4.1.1.1 Flow configuration 91
4.1.1.1.1 Plasma spectra 91
4.1.1.1.2 Spectra during clove treatment 91
4.1.1.1.3 Comparison of peeled and unpeeled cloves 92
4.1.1.1.4 Plasma treatment of cloves with increasing power 92
4.1.1.1.5 Plasma treatment of cloves with increasing working pressure 93
4.1.1.2 No-flow configuration 93
4.1.2 Catalytic probe 94
4.1.2.1 n_O in the E-mode plasma without garlic sample 94
4.1.2.2 Probe signal increase during clove treatment 94
4.1.2.3 n_O during treatment of peeled garlic 95
4.1.2.4 n_O during treatment of unpeeled garlic 95
4.2 Temperature 96
4.2.1 Heating power 96
4.2.1.1 Initial heating 96
4.2.1.2 Further heating 100

4.2.2 Heating at different discharge parameters 100
4.3 Surface Chemical Composition 101
4.3.1 Untreated clove surfaces 101
4.3.2 Carbon and oxygen content 102
4.3.2.1 Unpeeled clove surface 102
4.3.2.1.1 Pilot-scale E-mode glow treatment 102
4.3.2.1.2 Pilot-scale H-mode afterglow treatment 102
4.3.2.1.3 Pulsed treatment 103
4.3.2.2 Peeled clove surface 103
4.3.2.2.1 Pilot-scale plasma treatment 103
4.3.2.2.2 Industrial-scale plasma treatment 103
4.3.2.2.3 Peeled clove surface under the treated protective leaf 103
4.3.2.3 High-resolution XPS spectra 104
4.3.2.3.1 E-mode glow treatment 104
4.3.2.3.1.1 Protective leaf 104
4.3.2.3.1.2 Clove surface 105
4.3.2.4 Surface oxidation mechanisms 105
4.3.3 Other elements 106
4.3.3.1 Sulfur 106
4.3.3.2 Calcium 107
4.3.3.3 Silicon 107
4.3.3.4 Nitrogen 107
4.3.3.5 Magnesium and potassium 108
4.3.3.6 Sodium and chlorine 108
4.3.3.7 Fluorine 108
4.3.4 ATR-FTIR spectra 109
4.3.4.1 Untreated surfaces 109
4.3.4.2 Unpeeled clove plasma treatment 109
4.3.4.3 Peeled clove plasma treatment 110
4.4 Surface Morphology 111
4.4.1 Protective leaf surface 111
4.4.1.1 Pilot-scale glow plasma 111
4.4.1.2 Pilot-scale afterglow plasma 111
4.4.2 Peeled clove surface 112
4.4.2.1 Pilot-scale glow plasma 112
4.4.2.2 Industrial-scale plasma 113
4.4.3 Atomic force microscopy 113
4.4.4 Surface reshaping processes 114
4.4.4.1 Chemical etching 114
4.4.4.2 Etching depth 114
4.4.4.3 Wax structure formation 115
4.4.4.4 Differences between plasma effects on protective leaf and peeled clove 116
4.5 Water Contact Angle 117
4.6 Water Uptake 117
4.6.1 Untreated cloves 117
4.6.2 Industrial-scale plasma 117
4.6.3 Pilot-scale plasma 118
4.6.4 Clove mass loss 118

4.6.5 Effect of initial clove mass 119
4.7 Sprout and Root Growth 120
4.7.1 Untreated controls 120
4.7.2 Unpeeled cloves 120
4.7.2.1 E-mode glow 120
4.7.2.2 Comparison of continuous and pulsed treatment 121
4.7.2.3 H-mode afterglow 122
4.7.3 Peeled cloves 122
4.7.4 Mechanisms of sprout and root growth improvement 123
4.7.4.1 Sprout growth 123
4.7.4.2 Root growth 124
4.7.4.3 Effect of low pressure 125
4.7.4.4 Effect of EM field 125
4.7.4.5 Damage to the cloves 125
4.8 Field Growth 126
4.8.1 Plant height 126
4.8.2 Yield 126
4.8.2.1 First generation 126
4.8.2.2 2nd and 3rd generation 127

5 Conclusions **129**

Appendix A Additional Results **131**
A.1 Optical emission spectroscopy 131
A.2 Scanning electron microscopy 132
A.3 Sprout and root growth 135

References **139**

Bibliography **151**

Biography **153**

List of Figures

Figure 1.1: Garlic clove anatomy. 8
Figure 1.2: Schematic cross section of the protective leaf. 8
Figure 1.3: Anatomy of the outermost layers of plant epidermis. 9
Figure 2.1: Garlic cloves. 11
Figure 2.2: The pilot-scale plasma system. 12
Figure 2.3: Photograph of the pilot-scale plasma system. 12
Figure 2.4: The industrial-scale plasma system. 13
Figure 2.5: Photograph of the industrial-scale plasma system. 13
Figure 2.6: EM control treatment in the industrial-scale plasma. 15
Figure 2.7: Catalytic probe. 16
Figure 2.8: Thermocouple measurements. 17
Figure 3.1: OES spectra comparison, pilot-scale E-mode oxygen plasma. 21
Figure 3.2: OES spectra comparison, pilot-scale E-mode clove treatment. 22
Figure 3.3: OES spectra comparison, pilot-scale E-mode, increasing power. 23
Figure 3.4: OES spectra comparison, pilot-scale E-mode, increasing working pressure. 24
Figure 3.5: Time course of OH radical spectral line (~ 309 nm) signal intensity 25
Figure 3.6: Time course of signal intensity, no-flow configuration. 26
Figure 3.7: Time course of signal intensity, no-flow configuration, increasing P_N 27
Figure 3.8: Time course of signal intensity, no-flow conf., peeled and unpeeled cloves. 28
Figure 3.9: n_O in pilot-scale E-mode plasma without a garlic sample. 29
Figure 3.10: n_O in the pilot-scale E-mode, plasma or peeled clove. 30
Figure 3.11: n_O in the pilot-scale E-mode, plasma or peeled or unpeeled clove. 31
Figure 3.12: n_O during treatment of peeled garlic, E-mode glow. 32
Figure 3.13: n_O during treatment of peeled garlic, H-mode afterglow. 33
Figure 3.14: n_O during treatment of unpeeled garlic, E-mode glow. 34
Figure 3.15: n_O during treatment of unpeeled garlic, H-mode afterglow. 35
Figure 3.16: Temperature measured by a TC in the pilot-scale plasma 36
Figure 3.17: Temperature time course, peeled and unpeeled cloves, pilot-scale plasma. 37
Figure 3.18: C and O concentration at the unpeeled garlic surface (protective leaf) 39
Figure 3.19: O/C ratio of unpeeled garlic (protective leaf) 40
Figure 3.20: Minor elements concentration at the protective leaf surface 41
Figure 3.21: O/C ratio of unpeeled garlic, pilot-scale plasma AG 42
Figure 3.22: O/C ratio of unpeeled garlic, pilot-scale plasma, pulsed treatment. 43
Figure 3.23: C and O concentration of peeled garlic (clove surface) 44
Figure 3.24: O/C ratio of peeled garlic (clove surface) 45
Figure 3.25: Minor elements concentration at the peeled clove surface. 45
Figure 3.26: O/C ratio of peeled garlic, industrial-scale plasma 46
Figure 3.27: High-resolution C 1s spectra of unpeeled garlic 48
Figure 3.28: C 1s sub-peak area of unpeeled garlic 49
Figure 3.29: High-resolution C 1s spectra of peeled garlic 50
Figure 3.30: C 1s sub-peak area of peeled garlic 50

Figure 3.31: ATR-FTIR spectra of untreated surfaces, peeled and unpeeled clove..... 51
Figure 3.32: ATR-FTIR spectra, unpeeled clove..... 52
Figure 3.33: ATR-FTIR spectra, unpeeled clove, direct comparison. 53
Figure 3.34: ATR-FTIR spectra, peeled clove..... 54
Figure 3.35: ATR-FTIR spectra, peeled clove, direct comparison. 55
Figure 3.36: SEM images, unpeeled garlic, pilot-scale E-mode glow. 57
Figure 3.37: SEM images, unpeeled garlic, pilot-scale E-mode glow, pulsed treatment. .. 58
Figure 3.38: SEM images, unpeeled garlic, pilot-scale H-mode afterglow..... 59
Figure 3.39: SEM images, peeled garlic, pilot-scale E-mode glow. 61
Figure 3.40: AFM images, unpeeled garlic, pilot-scale E-mode glow, pulsed treatment... 62
Figure 3.41: AFM images, peeled garlic, industrial-scale treatment..... 63
Figure 3.42: WCA on the surface of (A) unpeeled and (B) peeled garlic..... 64
Figure 3.43: WU of untreated cloves, peeled and unpeeled..... 65
Figure 3.44: WU of unpeeled garlic cloves treated in the industrial-scale plasma..... 66
Figure 3.45: WU of peeled garlic cloves treated in the industrial-scale plasma..... 67
Figure 3.46: WU of garlic cloves treated in the pilot-scale plasma. 68
Figure 3.47: Clove mass loss for peeled and unpeeled cloves..... 69
Figure 3.48: Clove mass loss for peeled cloves: plasma treatment and vacuum. 69
Figure 3.49: WU of peeled garlic cloves treated in the industrial-scale plasma, calculated using the initial clove mass. 70
Figure 3.50: Effect of initial clove mass on WU. 70
Figure 3.51: Peeled clove sprout growth, pulsed treatment. 71
Figure 3.52: Growth of peeled and unpeeled untreated garlic clove sprouts and roots. ... 72
Figure 3.53: Growth of unpeeled garlic clove sprouts, pilot-scale E-mode glow. 74
Figure 3.54: Growth of unpeeled garlic clove roots, pilot-scale E-mode glow..... 75
Figure 3.55: Unpeeled garlic clove root number, pilot-scale E-mode glow. 76
Figure 3.56: Growth of unpeeled garlic clove sprouts, pilot-scale H-mode afterglow. 77
Figure 3.57: Growth of unpeeled garlic clove roots, pilot-scale H-mode afterglow. 78
Figure 3.58: Unpeeled garlic clove root number, pilot-scale H-mode afterglow. 79
Figure 3.59: Unpeeled clove sprout growth, pilot-scale H-mode AG, 2nd experiment. 80
Figure 3.60: Growth of peeled garlic clove sprouts, pilot-scale E-mode glow. 81
Figure 3.61: Growth of peeled garlic clove roots, pilot-scale E-mode glow..... 82
Figure 3.62: Peeled garlic clove root number, pilot-scale E-mode glow..... 83
Figure 3.63: Peeled garlic clove control treatments..... 84
Figure 3.64: Sprout and root growth of peeled garlic cloves, industrial-scale plasma. 85
Figure 3.65: Sprout and root growth, peeled clove controls, industrial-scale plasma. 86
Figure 3.66: Plant height at harvest, pilot-scale plasma. 87
Figure 3.67: Plant height at harvest, industrial-scale plasma. 87
Figure 3.68: Average mass of dried bulb, pilot-scale plasma..... 88
Figure 3.69: Average mass of dried bulb, industrial-scale plasma system. 89
Figure 3.70: Average mass of dried bulb for 2nd and 3rd generation of garlic..... 90
Figure 3.71: Average mass of dried bulb for 2nd generation of garlic..... 90
Figure 5.1: SEM images, unpeeled garlic, pilot-scale H-mode afterglow. 133
Figure 5.2: SEM images, peeled garlic, industrial-scale E-mode glow. 134
Figure 5.3: Unpeeled clove growth after continuous and pulsed treatment..... 135
Figure 5.4: Unpeeled clove sprout and root growth after pulsed treatment. 136
Figure 5.5: Peeled cloves sprout and root growth at 70 Pa..... 137

List of Tables

Table 2.1: Treatment conditions and sample positions during garlic clove treatment in the pilot-scale plasma system.....14
Table 3.1: Surface elemental composition [at.%] and O/C ratios of untreated clove surfaces from different experiments.....38
Table 3.2: Surface elemental composition [at.%] of unpeeled garlic, pilot-scale plasma....39
Table 3.3: Surface elemental composition [at.%] of unpeeled garlic, pilot-scale AG. 42
Table 3.4: Surface elemental composition [at.%] of unpeeled garlic, pulsed treatment.....43
Table 3.5: Surface elemental composition [at.%] of peeled garlic, pilot-scale plasma.....44
Table 3.6: Surface elemental composition [at.%] of peeled garlic, ind.-scale plasma.....46
Table 3.7: Surface elemental composition [at.%] and O/C ratio of the clove surface under the treated protective leaf.....47
Table 4.1: O atom dose received by a clove during treatment. 121
Table 5.1: OES signal intensity at selected wavelengths, pilot-scale E-mode plasma.....131

Abbreviations

AFM ... atomic force microscopy
AG ... afterglow
at.% ... atomic percent
ATR ... attenuated total reflectance
DBD ... dielectric barrier discharge
DC ... direct current
DI ... deionized
EM ... electromagnetic
FTIR ... Fourier-transform infrared
G ... glow
IR ... infrared
MW ... microwave
N ... untreated control
NMR ... nuclear magnetic resonance
OES ... optical emission spectroscopy
RF ... radio frequency
ROS ... reactive oxygen species
SEM ... scanning electron microscopy
TC ... thermocouple
V ... vacuum control
WCA ... water contact angle
WU ... water uptake
XPS ... X-ray photoelectron spectroscopy

Symbols

A	... surface area
C 1s	... carbon 1s electron
c_{p}	... specific thermal capacity
γ	... recombination probability
D	... oxygen atom dose
e	... electron
E_{A}	... activation energy
H_{α}	... H-alpha hydrogen spectral line
j_{ion}	... ion flux to the surface
j_{O}	... atom flux to the surface
k	... Boltzmann constant
m	... mass
M	... ion mass
m_0	... initial clove mass
m_{t}	... clove mass after time t
n_{i}	... ion density
n_{O}	... oxygen atom density
O	... oxygen atom
O^+	... oxygen atomic ion
O_2	... oxygen molecule
O_2^+	... oxygen molecular ion
p	... working pressure
P_{EFF}	... effective power
P_{FW}	... forward power
P_{N}	... nominal power
P_{RF}	... reflected power
ρ	... density
T_{e}	... electron temperature
v_{Bohm}	... Bohm velocity
$< v_{\mathrm{O}} >$	... average velocity of O-atom thermal motion
W_{d}	... dissociation energy
W_{ion}	... ion energy

Chapter 1

Introduction

1.1 Background

The idea for plasma treatment of garlic cloves stems from the concept of "plasma agriculture", which has been a part of agricultural research trends for the last decade. The physical phenomenon of non-thermal, highly reactive gaseous plasma was found to have a variety of beneficial effects on living beings, including agriculturally important plants. At the same time, the technology is ecologically more acceptable than traditional, chemical-based approaches, as it uses abundant materials and does not introduce toxic compounds into the environment.

Non-thermal plasmas with conditions suitable for biological material treatment are commonly formed in laboratory environments, as well as scaled up to industrial-size reactors. We wanted to show that by selecting suitable discharge parameters, as well as studying the physico-chemical effects of plasma on the treated material, it is possible to achieve the desired biological responses of the treated garlic samples.

Here, we have worked with a Slovenian autochthonous garlic cultivar, *Ptujski spomladanski*. The aim was to achieve improvements in growth and yield that could strengthen its presence and availability, which are threatened by imported varieties. Thereby, local and sustainable agricultural practices could be supported by innovative technology practices.

1.2 Hypotheses

The hypotheses set for our work are the following:

- plasma treatment increases wettability of the surface exposed to the plasma (protective leaf or clove surface). Due to increased hydrophilicity, water uptake of cloves increases as well;
- increased wettability is a result of functionalization, as oxygen plasma oxidizes the cuticle surface. Oxygen-containing functional groups are introduced to the waxy cuticular compounds, initially composed primarily of carbon and hydrogen;
- etching, and the resulting nanostructuring of the surface, additionally contributes to increased wettability;
- plasma treatment of garlic cloves accelerates clove germination and early growth of sprouts and roots;

- due to the effects on germination and growth, the garlic plants grown from optimally plasma-treated cloves also exhibit a higher yield than plants grown from untreated cloves.

1.3 Plasma

Plasma is one of the four fundamental states of matter, following the solid, liquid, and gaseous states. Adding sufficient additional energy to a gas results in a plasma – a state in which a substantial amount of molecules is dissociated and ionized, while the gas remains macroscopically neutral. The plasma state is abundant in nature. It is found on Earth in the form of lightning and aurora borealis, and comprises the majority of the remaining universe, such as the interior and corona of stars, or the solar wind [1]. On the other hand, plasma is commonly formed in laboratory settings in various ways, typically by applying heat or a strong electromagnetic field to a gas. The purpose of such man-made plasmas is often tailoring of surface properties, and they are applied in material, medical, electronic, and other sciences.

1.3.1 Thermal and non-thermal plasma

A plasma state achieved by heating is a thermal plasma. If a material is in a gaseous state, and the temperature of a gas is further increased, the molecules of the gas will dissociate into atoms, which at even higher temperatures will further dissociate into charged particles: electrons and ions. Very high temperatures, in the range of several thousand Kelvin, are required for this to occur [2]. As such, thermal plasmas are unsuitable for treatment of biological materials or polymers, as at the required temperatures, thermal degradation of the treated material would take place.

Conversely, non-thermal plasmas are formed at temperatures near room temperature. They can be initiated by several types of discharges, and at a wide range of pressures. The most common distinction is between low-pressure and atmospheric pressure discharges. The discharges are electrically driven, and the primary recipients of the energy transfer are electrons, which are mobile and charged [2]. This results in a pronounced inequality between the kinetic temperatures of electrons and the heavy particles (ions, neutral particles) in the plasma. Therefore, the plasma is not in thermodynamic equilibrium, and cannot be described by the basic laws of equilibrium thermodynamics [3]. In this environment, numerous reactions occur between the plasma particles. Electron collisions with atoms and molecules bring on processes such as dissociation, excitation and ionization, which results in the occurrence of heavier particles with relatively high energy [2].

1.3.2 Plasma configurations

Plasmas created in the laboratory setting are most commonly formed by application of an electric field to a neutral gas. Such plasma systems vary widely in the possible selection of power sources, electrode configurations, reactor size, process gas, working pressure, etc. [4].

Direct current (DC) glow discharges are ignited at low pressures in closed vessels with interior electrodes. A glow discharge is then achieved when a suitable voltage and discharge current are applied [4].

Discharges formed in high-frequency electromagnetic (EM) fields at radio or microwave (MW) frequencies are also common. High frequency power generators are used as power sources. Radio frequency (RF) discharges can have different ways of power coupling to the reaction chamber [4]. Capacitively coupled RF discharges consist of two electrodes, one driven by the RF power source and one grounded, in plane parallel geometry inside a

vacuum chamber [2], between which, an electric field is generated. The electrodes may be in direct contact with the discharge, or separated from it by a dielectric. Conversely, an inductively coupled RF plasma accelerates charged particles in an induced electric field inside an electromagnetic coil [5]. The electric field is induced by a time-varying magnetic field formed by a RF current passing through a conductor, typically an electrode in the form of a coil, wrapped around the outside of a cylindrical dielectric reaction chamber. RF discharges are typically operated at low pressures. Compared to RFs, MWs have a higher frequency and a smaller wavelength, which is in the order of magnitude of many plasma reactors. MW discharges are suitable for operation at higher pressures, up to atmospheric pressure. Various configurations exist depending on the reactor structure (open or closed) and ways of coupling the electric energy to the plasma [4].

Dielectric barrier discharge (DBD) plasma systems are set up as two electrodes with a dielectric barrier and a thin gap, such as a few millimeters, in between. A large number of plasma filaments is formed in the discharge [4]. DBDs are generally operated at atmospheric pressure. Surface configurations of DBD, where the discharge is generated on a dielectric surface, also exist [6, 7].

1.3.3 Low-pressure oxygen plasma chemistry

1.3.3.1 Reactive oxygen species (ROS)

Plasma discharges in different gaseous media produce reactive species based on the chemistry of the gas. Low-pressure oxygen plasma is commonly used in experimental practice, and has been well characterized regarding the reactive species densities and behavior [5]. A wide assortment of reactive oxygen species (ROS), deriving from the ground-state oxygen molecule O_2, is found in low-pressure oxygen plasma. These include:

- O_2, the oxygen molecule in the ground state, also denoted $O_2(X^3\Sigma_g^-)$;
- O_2^+ and O_2^-, its molecular ions;
- $O_2(a^1\Delta_g)$ and $O_2(b^1\Sigma_g^+)$, the metastable, excited singlet states of O_2;
- O, the biradical neutral oxygen atom in the ground state, also denoted $O(^3P)$;
- $O(^1D)$ and $O(^1S)$, the metastable singlet states of the oxygen atom;
- O^+ and O^-, ions of the oxygen atom;
- O_3, ozone;
- O_3^+ and O_3^-, its ions [8].

In a plasma, the electrons, gas molecules, and the various reactive species interact with one another, resulting in a complex chemistry. Several types of reactions occur [5], and some of the most important are listed below. In a dissociation reaction, a molecule dissociates upon impact with an electron (e). This is an important process in low-pressure discharges, as it produces energetic neutral particles which then react with the sample surface. In case of molecular oxygen [2], the reaction proceeds as

$$e + O_2 \rightarrow 2O + e. \tag{1.1}$$

On the other hand, ionization results in the formation of an ion, either molecular (electron–molecule ionization) or atomic (electron–atom ionization), via interaction of an incident electron with a valence electron of a neutral atom or molecule [1]:

$$e + O_2 \rightarrow O_2^+ + 2e, \tag{1.2}$$

$$e + O \rightarrow O^+ + 2e. \tag{1.3}$$

At lower electron energy, ionization is less likely to occur than dissociation. However, ionization probability increases with increased electron energy, and eventually predominates [5].

1.3.3.2 Recombination

The processes of reactive species formation and loss run in parallel. The process by which reactive species combine to form parent molecules is called recombination. The most important molecular ion dissociative recombination reaction in the oxygen plasma gas phase is

$$e + O_2^+ \rightarrow 2O. \tag{1.4}$$

The loss of neutral atoms in the gas phase is predominantly in three-body collisions, so its probability at low pressures is rather low. Nonetheless, surface recombination also occurs at the surfaces of either the reaction chamber or any materials exposed to the plasma, and can be an important reactive species loss mechanism for ions as well as neutral oxygen atoms in low-pressure systems [5, 9]. However, the probability for the surface reaction

$$O + O \rightarrow O_2 \tag{1.5}$$

depends on the recombination coefficient of the material, which is rather low for borosilicate glass, so neutral atom losses are not substantial on the walls of glass reactors [10].

1.3.3.3 E-mode and H-mode

Inductively coupled RF plasma exists in two modes: a so-called E-mode, characterized by lower electron densities and lower luminosity, and an H-mode, characterized by higher electron densities and higher luminosity [11]. Density of reactive species, in particular neutral oxygen atoms and ions, increases substantially in the H-mode. Transition between the modes occurs at a specific discharge power, which depends on the gas pressure [10]. In the inductively coupled RF system, an electrostatic field is present due to potential differences between the induction coil and the ground surfaces of the system [12]. At lower input powers, in E-mode, this electrostatic field is larger than the induced field, and thus, discharges primarily form as a consequence of capacitive coupling. In H-mode, the induced electric field is larger, and is the primary factor sustaining the discharge. At the same time, the electrostatic field, and thereby some capacitive coupling, remains present as an additional aspect of plasma, known as stray capacitance [11].

1.3.3.4 Glow and afterglow

A spatial evolution of the reactive species density exists along the plasma reactor, namely between the plasma discharge (“glow”) and the post-discharge (“afterglow”) [3, 13]. Ions and excited metastable atoms will typically undergo recombination outside of the immediate discharge area, but neutral atoms and molecules will be present in the afterglow as well [14].

1.3.4 Plasma effects on surfaces

Non-thermal plasma is well known for its use in surface modification, including tuning the properties of organic materials such as polymers [3]. It is a very surface-specific technique; depending on treatment parameters and duration, it typically affects a smooth surface up to some tens of nm in depth [15]. The result is modification of physico-chemical properties of the treated surface.

One important aspect is functionalization – the introduction of new functional groups onto the surface. It is established that treatment with oxygen-containing plasma will initiate oxidation processes on the treated material [3, 16], introducing new polar functional groups and oxidizing existing ones [3, 17, 18] through grafting of oxygen atoms onto the surface of the material [19]. These oxygen-containing functional groups can include hydroxyl, ether, carbonyl, ester, and carboxyl groups, as well as unstable groups oversaturated with oxygen [3].

Additionally, morphology of the treated surfaces is affected by plasma etching, which occurs by two major mechanisms: physical sputtering and chemical etching [1]. Energetic, positively charged ions are responsible for physical sputtering of the surface [20], as they impinge on the polymeric surface with high kinetic energy, removing atoms by bond breakage in the process [1]. On the other hand, the same oxidation mechanisms responsible for functionalization result in chemical etching with prolonged exposure. Namely, oxidative degradation of organic materials occurs when oxygen-containing functional groups are further oxidized and decompose to form volatile compounds such as CO_2 and H_2O, which then enter the gaseous phase and are removed from the surface [21]. Plasma etching increases the surface roughness, resulting in an increased surface to volume ratio [22]. A combined effect of both functionalization and etching is an increase in the surface energy of the treated material, which renders the surface more hydrophilic [1]. The ratio of functionalization and etching depends on the reactive species present in the discharge, and therefore on the selected plasma parameters as well as sample position relative to the discharge.

1.4 Plasma Agriculture

Due to increasing demands, and various factors affecting production, an improvement in the germination and growth of food crops is desired as a mechanism of increasing yields. Agricultural sustainability is desired to meet increasing food demands without harmful environmental effect [23]. For example, wheat (*Triticum aestivum* L.) is one of the key cereal crops worldwide, and a major source of food. In 2015, an estimated 733 million tons of wheat were produced. Its required productivity growth was recently estimated at 1.1 % to meet consumption demands until 2020, while factors such as climate change, unpredictable environmental events, and various diseases or pests reduce yields and thereby further increase the need for production growth [24].

In agricultural research trends of the last decade, the discipline named plasma agriculture is a rapidly expanding field. It utilizes the processing capabilities of plasma treatment to improve properties of biological and food materials throughout the entire agricultural process, from seed to table. The aim of this research is to achieve optimal yields, increase food production, while simultaneously providing a high-quality, safe, environmentally friendly and affordable final product [25]. The most important applications of plasma agriculture include disinfection of biological materials and food packaging materials, enhancement of seed or plant properties [26], production and use of plasma-activated media [27], as well as plasma treatment of food [28].

1.4.1 Germination and growth improvement of agricultural seeds

In an attempt to avoid the excess use of fertilizers or chemical growth stimulants to improve plant performance in the field, plasma agriculture has delivered an environmentally acceptable alternative. The use of non-thermal plasma in agriculture is ecologically benign, does not introduce toxic compounds into the environment, and does not damage the sensitive planting material.

So far, gas plasma treatment of various agricultural seeds has been shown to affect many stages of plant germination and growth [26]. Germination rate, which is the percentage of germinated seeds at a given time point, has been improved for a variety of species, including seeds of quinoa [29], rapeseed [30], and peanut [31], using RF plasmas. After germination, various parameters of seedling growth were also improved, including sprout length, root length [6, 32, 33], seedling dry weight [32, 34], root fresh and dry weight [7], as well as other parameters. The selection of species included wheat, pea, maize, soybean, tomato, and other crops. A wide variety of plasma configurations has been used to achieve these effects, ranging from DBD plasmas in atmospheric air to low pressure RF discharges using a variety of process gases.

Further, planting of plasma-treated seeds can result in improved yield of agriculturally important crops. Increase in wheat yield was achieved by use of low-pressure helium plasma [35], low pressure air or air/He plasma [36, 37], medium pressure air and air/oxygen plasma [38], and an atmospheric pressure gliding arc discharge [39]. Tomato yield was improved by treating seeds in an atmospheric pressure air plasma, either an arc discharge [40] or a DBD [41]. A low pressure helium plasma improved peanut [31] as well as rapeseed yield [30], while the seed yield of *Arabidopsis thailana* was improved by an atmospheric pressure air DBD [42].

1.4.1 Mechanisms of germination and growth improvement

Published research on plasma-induced seed germination and growth improvement currently focuses on the elucidation of physico-chemical and biochemical mechanisms by which plasma exerts its influence on the seeds. Plasma is uniquely suitable for modifying the outer layer of the seed surface, influencing its physico-chemical properties, without disrupting the bulk of the seed. As with polymer materials, the organic materials of the seed surface are targets for functionalization and etching by the reactive plasma species. In particular, treatment with a plasma that uses an O- or N-containing working gas increases the density of polar groups on the seed surface [29, 43]. At the same time, plasma etching affects seed surface morphology by increasing its roughness [44, 45]. Both increase the seed surface energy, causing hydrophilization [46]. There appears to be a direct correlation between seed wettability and water uptake (WU) [47, 48], which is the necessary first step in the seed germination process [49]. Increased hydrophilicity of the surface is therefore desired to enhance or accelerate seed hydration. Additionally, effects of etching may further facilitate seed coat permeability by the formation of cracks and pores on the seed surface [32, 50].

In addition to these physico-chemical surface effects, the exposure of the seed to the plasma environment appears to activate certain biochemical pathways, thereby triggering a biological response. While the molecular mechanism of seed dormancy and germination are reasonably well known [51], research in the field of plasma agriculture has only recently begun to investigate the effects of plasma on the seed biochemistry. These effects may be either specific, affecting certain signaling pathways, or part of a non-specific stress response of the seed to plasma treatment [52]. The accelerated WU is a biological factor in itself, as it enables cell component mobility, restarting the seed metabolism after a period of quiescence or dormancy [49]. Further, concentrations of plant hormones involved in

germination and dormancy are affected by plasma treatment [32, 53, 54], an effect which may be related to the redox status and ROS signaling pathways of the seed. ROS are proposed to act as transmitters of environmental cues during germination, and the concept of an "oxidative window for germination" has been proposed to describe a critical range of ROS content in seeds that allows for dormancy release and germination [55]. Exposure to the reactive plasma species could thus affect these mechanisms, and thereby, germination and growth.

By all of the above, plasma treatment of seeds can be considered a physical seed priming approach. Effect of plasma on both germination and yield varies with the selected plasma parameters, as well as plant species, and should be optimized for each specific treatment case.

1.5 Garlic

Garlic (*Allium sativum* L.) is an important agricultural crop, with world production totaling over 24 million tons in 2013 [56]. Target of garlic production is a high yield of a high-quality crop [57], but production is limited by the region and climate [58].

Cereals and other agriculturally important plants are propagated sexually, through seeds. In contrast, while fertile clones of garlic were indeed discovered in central Asia some three decades ago [59], the commercially cultivated varieties of garlic are sterile. They do not produce seeds, and must thus be propagated vegetatively [60], i.e., individual cloves are planted in soil, where they germinate and produce new plants [57]. So, while improvement of crops such as cereal, and even other alliums, is possible by conventional or innovative breeding techniques [24], these are not applicable to agriculturally produced garlic, and alternative methods of crop improvement must be considered. In this way, germination and growth can be improved without the need for genetic engineering, and established or autochthonous cultivars can be propagated instead.

Depending on climate and cultivar, garlic is typically planted either in the fall (September to November) or in the spring (January to March), both for a harvest in the summer. Ideally, the timing should be such that development begins after planting, but the plant does not emerge from the soil before the first frost [61].

An autochthonous Slovenian variety of garlic, the cultivar *Ptujski spomladanski*, was used in this work with the aim of strengthening its presence and availability, which is threatened by imported varieties. The local Slovenian garlic cultivars are either fall- or spring-planted, and this cultivar is adapted for long bulb storage to enable spring planting. Any garlic planted in the spring lacks the advantage of starting its development in the fall, and thus requires early planting to properly develop its root system in time. Further, it may lack the low temperature exposure required to break dormancy and initiate clove formation and bulbing [61]. Planting at the optimal time is often hindered by external conditions such as wet soil, or freezing of the soil due to low temperatures. It is therefore desired to strengthen the garlic plant and improve its germination so that bulbs may grow efficiently, leading to high yields.

1.5.1 Anatomy

The underground part of a garlic plant is commonly called a bulb. Each bulb consists of several cloves. A clove is a storage bud consisting of a sprout leaf, found within a storage leaf, which is further covered by a protective leaf. The clove anatomy is schematically shown in Figure 1.1. The sprout leaf is the first leaf to emerge when active growth begins, followed by foliage leaves. The storage leaf provides the food reserve, and the protective

leaf envelops the storage leaf of each clove, protecting it with its tough surface. It remains tightly wrapped around the clove when the bulb is broken apart. The cloves are further enveloped by layers of dry, white sheaths, which are the bases of the foliage leaves growing over ground. The anatomy of the protective leaf is very similar to that of the foliage leaf sheath [62]. Leaves comprise of an upper and lower epidermis, and the mesophyll in between, with vascular bundles distributed throughout it [63]. In garlic, the epidermal cells are arranged in one row; a cross section of the top layers of the protective leaf is shown in Figure 1.2. The storage leaf surface, which is the surface of the peeled clove, appears similar. However, its epidermis is comparably thin and delicate [62].

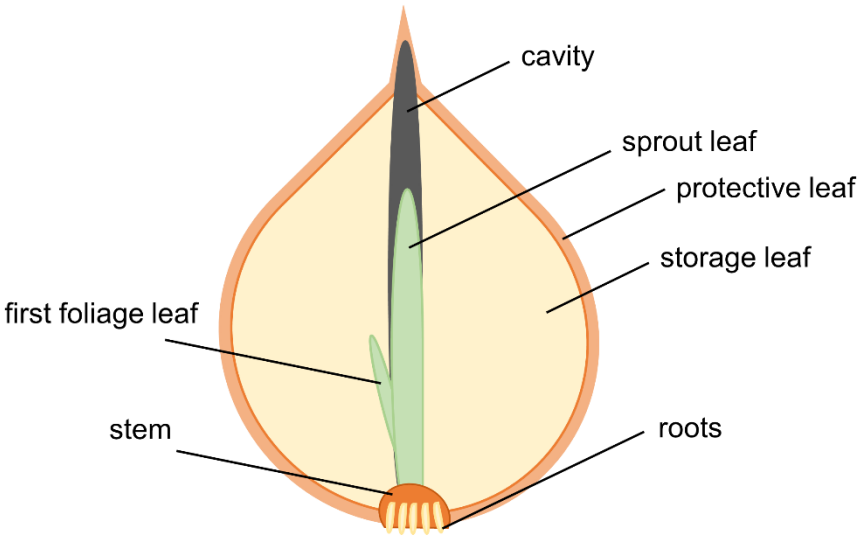

Figure 1.1: Garlic clove anatomy. Schematic representation. Adapted from [62].

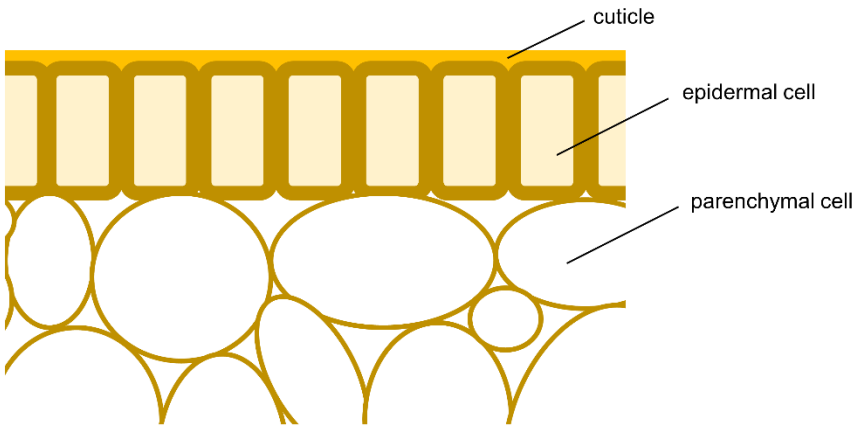

Figure 1.2: Schematic cross section of the protective leaf. Top layers are shown; the uppermost layer presents the sclerified epidermis, which is then further covered by a cuticle. Adapted from [62].

1.5.2 Clove surface chemistry

As plasma treatment primarily affects the very surface of the treated material, it is of interest to know which clove surfaces will be exposed to the plasma. The outer cellular layer of plant surfaces is the epidermis. As shown in Figure 1.3, the epidermis is covered on the outer side by a cuticle [62], which is a layered, continuous non-cellular membrane composed of a polymeric lipid matrix embedded and covered with wax.

Cuticular waxes are complex mixtures of compounds. As the name "wax" suggests, they consist of hydrophobic organic compounds. Chemically, the term wax usually refers to long-chain alkyl esters. However, in the cuticular context, it is used to also encompass compounds with different or additional functional groups, as well as other potential compounds present in this layer [64]. Two layers of cuticular wax are discussed separately: epicuticular waxes, coating the outer surface of the cuticle, and intracuticular waxes, embedded in the cuticle matrix below. In a plant species, chemical composition differs between the two [65], but mainly in the relative amounts of the particular compounds [64]. A standard array of cuticular wax compounds, found in virtually all plants studied to date, comprises fully saturated, unbranched hydrocarbon chains, from 20 to almost 40 C atoms in length, either as *n*-alkanes or containing a single terminal oxygen functional group: a hydroxyl, carbonyl, or carboxyl group, which gives a *n*-alcohol, *n*-aldehyde, or a fatty acid, respectively. In addition, the fatty acids and primary alcohols form an array of homologous esters, dimers of the aforementioned monomer compounds. The polymeric matrix of the cuticle is the biopolyester cutin, a primarily aliphatic polymer with long chains of methylene units linked by primary and secondary ester bonds [64]. Glycerol is another monomeric component of cutin, and represents between 1 and 14 % of the total polymer composition [66].

While plant cuticles have been extensively studied, there is currently no specific information regarding garlic cuticle composition. In general, plant cuticle thickness is 0.1 – 10 µm [64], however in garlic, this layer is relatively thin [62]. To the best of our knowledge, the exact thickness of the garlic cuticle is currently not known.

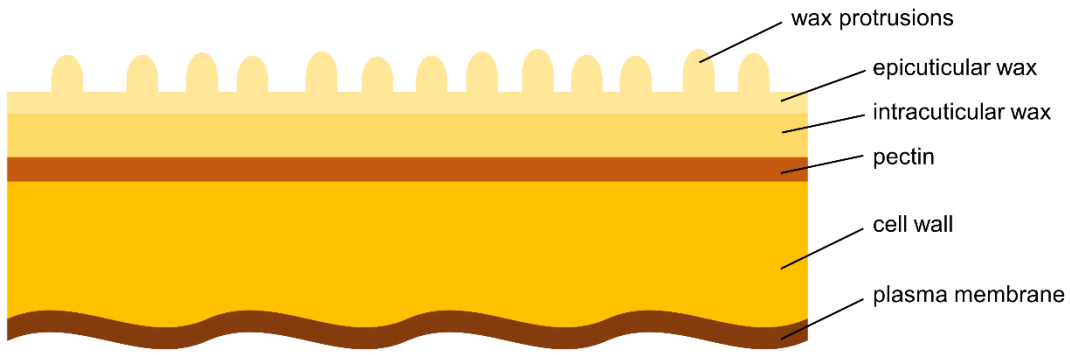

Figure 1.3: Anatomy of the outermost layers of plant epidermis. A pectin layer links the cuticle with the underlying cellulose cell wall of epidermis cells. Adapted from [67].

1.5.3 Dormancy and germination

Germination is formally defined as the process from the first water uptake by the dry seed to the emergence of the radicle, which is the embryonic root of the plant. Seedling growth after radicle emergence is referred to as seedling establishment. However, before germination and growth may begin, plant propagation material of many species is in a resting state. Indeed, in a variety of plant seeds, as well as in garlic cloves, a phenomenon known as dormancy exists to prevent germination in unfavorable seasons even if conditions are temporarily favorable. Dormancy needs to be released by additional environmental signals, such as light and temperature, before germination may begin. Release of dormancy allows for germination, which is the resumption of plant embryo growth after imbibition [49, 51].

Garlic cloves are dormant when freshly harvested, and will not readily germinate [62]. This period lasts for about 50 to 70 days, after which, growth of the sprout leaf begins within the clove. As with seeds, dormancy is controlled by the balance of plant hormones [68], and their external application accelerates germination [69]. Roots emerge more rapidly than sprouts, even with dormancy breaking pre-treatment [70]. One important factor affecting garlic dormancy is temperature, as seed cloves need to be exposed to low temperatures for an optimal amount of time to achieve proper sprouting and bulbing. Normally this occurs after planting in the field, as garlic is planted in the autumn and harvested in the spring. Instead, cloves can also be exposed to low temperatures during storage, which affects both dormancy and bulbing [57].

1.5.4 Plasma treatment of garlic cloves

To the best of our knowledge, this is the first work concerning the effect of plasma treatment on the germination, growth and yield of garlic. In parallel with methods employed for plasma treatment of seeds, we have treated garlic cloves with weakly ionized low-pressure oxygen plasma. The aim of this work was to record improvements to garlic sprout and root growth, and ultimately the yield, after exposure of cloves to plasma treatment. It was of particular interest to link any improvements in root growth to eventual yield improvement, as well as to correlate the growth of garlic to plasma-induced changes in morphology and physico-chemical properties of the garlic clove surface.

Chapter 2

Materials and Methods

2.1 Garlic

Garlic seed bulbs of a Slovenian autochthonous cultivar, *Ptujski spomladanski*, were received or purchased from Semenarna Ljubljana, d.o.o. (Ljubljana, Slovenia), and stored at suitable conditions (dry, dark, at a temperature of 4 – 10 °C). Immediately before plasma treatment, the bulbs were separated into cloves, which were either left unpeeled (with the protective leaf intact) or were peeled completely. Only undamaged and non-germinating cloves were selected for use in the experiments. Cloves are seen in Figure 2.1.

Figure 2.1: Garlic cloves. Unpeeled (left) and peeled (right) cloves of the garlic cultivar *Ptujski spomladanski*.

2.2 Plasma Reactors

Two in-house designed plasma systems were selected for the plasma treatment of cloves: a pilot-scale system and an industrial-scale system. Both used a low pressure, inductively coupled, RF oxygen plasma to treat the garlic cloves. The main difference between the systems is the size of the reactor, which in both cases is a borosilicate discharge tube.

2.2.1 Pilot-scale system

The reactor of the pilot-scale system is 800 mm in length and 36 mm inner diameter. To sustain the desired low pressure, the reactor is continuously pumped using a two-stage oil rotary vacuum pump of the nominal pumping speed of 80 m^3/h. The pump is connected to the reactor on one end through a series of stainless steel tees, onto which a simple air inlet valve is mounted for venting the whole vacuum system. Commercially available oxygen of 99.99 % purity is introduced at the opposite end of the tube by a flow controller AERA FC7700 (Advanced Energy, Fort Collins, CO, USA) calibrated for argon at 20 °C. The gas inlet is also connected to the reactor through a series of stainless steel tees, onto which a Baratron absolute pressure gauge (MKS Instruments, Andover, MA, USA) is mounted to monitor the pressure inside the reactor. A six-turn water-cooled copper coil with the length of ~ 70 mm is wrapped around the tube, and a Cesar 1310 RF power generator (Advanced Energy, Fort Collins, CO, USA) operating at 13.56 MHz is coupled to the coil via a matching network. A schematic representation of the system is seen in Figure 2.2, and a photograph is seen in Figure 2.3.

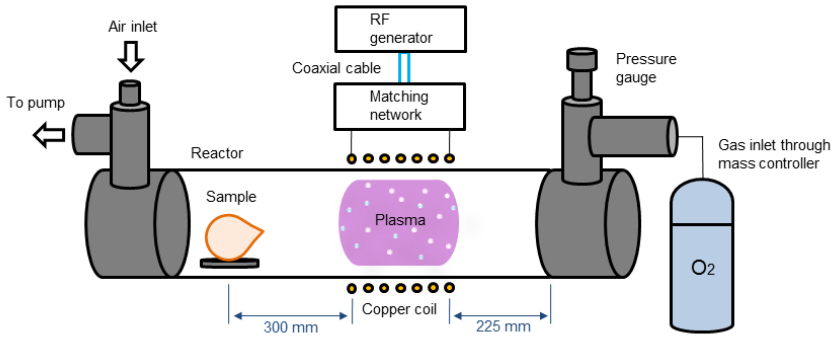

Figure 2.2: The pilot-scale plasma system. A schematic representation, showing an H-mode plasma and a sample in the afterglow treatment position.

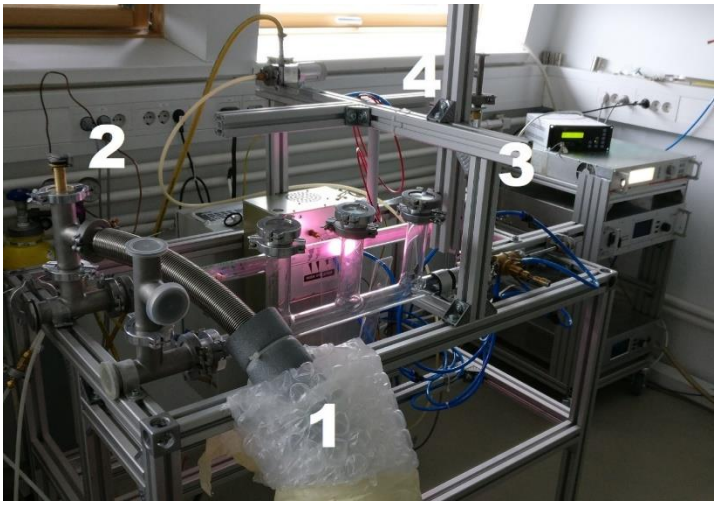

Figure 2.3: Photograph of the pilot-scale plasma system. Side view during H-mode afterglow treatment of a garlic clove, with indicated locations of the pump (1), air inlet valve (2), pressure gauge (3), and gas inlet (4).

2.2.2 Industrial-scale system

The reactor of the industrial-scale system is approximately 2000 mm in length and 200 mm in diameter. To sustain the desired low pressure, the reactor is continuously pumped using a two-stage oil rotary vacuum pump of the nominal pumping speed of 80 m^3/h connected to one end of the reactor. A simple air inlet valve for venting the whole vacuum system is mounted on the same side. Commercially available oxygen of 99.99 % purity is introduced at the opposite end of the tube by a flow controller AERA FC7700 (Advanced Energy, Fort Collins, CO, USA) calibrated for argon at 20 °C. On the same side, a Baratron absolute pressure gauge (MKS Instruments, Andover, MA, USA) is mounted to monitor the pressure inside the reactor. A double copper coil, one four- and one five-turn, is wrapped around the tube, and an RF power generator (Induktio d.o.o., Litostrojska 44d, Ljubljana, Slovenia) operating at 27.12 MHz is coupled to the coil via a matching network. A schematic representation of the system is seen in Figure 2.4, and a photograph is seen in Figure 2.5.

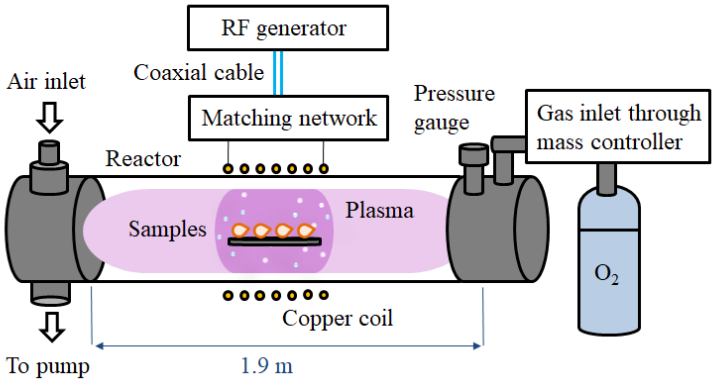

Figure 2.4: The industrial-scale plasma system. A schematic representation.

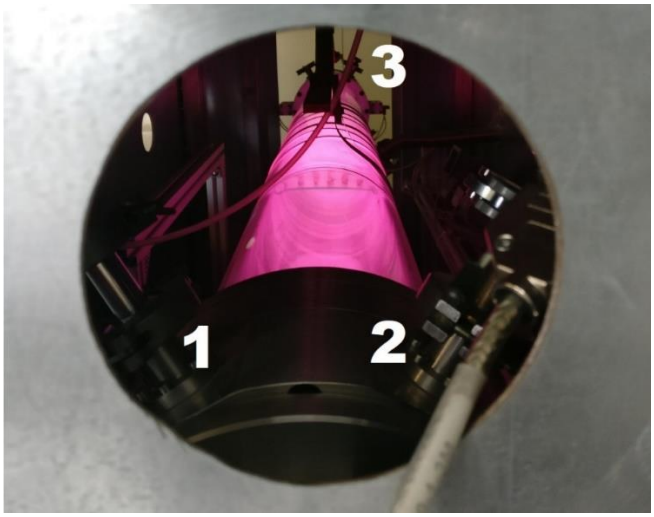

Figure 2.5: Photograph of the industrial-scale plasma system. Frontal view during the treatment of garlic cloves, with indicated locations of the gas inlet (1), pressure gauge (2), and air inlet valve (3).

2.3 Plasma Treatment

2.3.1 Pilot-scale plasma

During plasma treatment, the coil was set at a distance of 225 mm from the joint of the tube and the steel T-piece. The sample clove was placed onto a microscope slide and positioned inside the tube, with the bottom of the clove oriented toward the gas source. Each clove was treated individually unless noted otherwise. For treatment in E-mode glow plasma, cloves were placed in the center of the coil. For treatment in H-mode afterglow plasma, the cloves were positioned at a distance of 300 mm from the side of the coil, closer to the pumped end of the discharge tube, as illustrated in Figure 2.2. E-mode plasma was fairly uniformly distributed along the discharge tube. While H-mode plasma was mostly spatially enclosed within the coil, stray capacitive coupling remained present along the discharge tube. Therefore, such a treatment is clearly not a "true" afterglow. Nonetheless, for the sake of simplicity, it will be addressed simply as "afterglow" throughout this document.

The discharge was ignited at pressures ranging from 30 to 70 Pa. The nominal power (P_N) at the generator ranged from 100 to 300 W. An overview of treatment conditions and sample positions is found in Table 2.1. Treatment time varied according to the particular experiment, and in addition to continuous treatment, a pulsed treatment regimen was employed in some experiments. Treatment times and regimens are specified in the Results section. To remove any organic material or water adsorbed to the reactor walls during clove treatment, the reactor was periodically cleaned by igniting an H-mode discharge and moving the coil along the length of the tube slowly.

Table 2.1: Treatment conditions and sample positions during garlic clove treatment in the pilot-scale plasma system. Sample position: glow (G) or afterglow (AG). p is the pressure inside the tube during plasma treatment. P_N, P_{FW}, P_{RF}, and P_{EFF} are the nominal, forward, reflected and effective powers of the particular treatment, respectively.

p [Pa]	P_N [W]	P_{FW} [W]	P_{RF} [W]	P_{EFF} [W]	mode	position
30 / 50 / 70	100	100	75	25	E-mode	G
30 / 50 / 70	200	200	150	50	E-mode	G
30 / 50 / 70	300	275	200	75	E-mode	G
30	300	300	30	170	H-mode	AG
50	200	200	15	185	H-mode	AG
50	300	300	15	285	H-mode	AG

2.3.2 Industrial-scale plasma

During plasma treatment, the coil was positioned at the center of the tube. The plasma luminosity and reactive species density is highest inside the coil, but capacitive coupling is present throughout the tube. The cloves were placed on a glass plate and positioned inside the tube, with the bottoms of the cloves oriented toward the gas source. For treatment in glow plasma, the plate was placed in the center of the coil. One to five cloves were treated simultaneously. The plasma was ignited at pressures ranging from 15 to 60 Pa, at forward powers of approximately 600 – 1000 W. Treatment time varied according to the particular experiment. Particular treatment conditions and times are specified in Chapter 3.

2.3.3 Control treatments

Depending on the experiment, up to three control treatments were prepared: (1) untreated control; (2) vacuum control, which exposed cloves to low pressure and oxygen gas flow, without turning on the plasma; and (3) EM field control, which exposed cloves to the EM field of the plasma on the outside of the discharge tube. The controls are designated N, V, and EM, respectively. Duration of treatment for the vacuum and EM field controls is specified in the Results section of the particular experiment. Figure 2.6 shows the EM control treatment in the industrial-scale plasma.

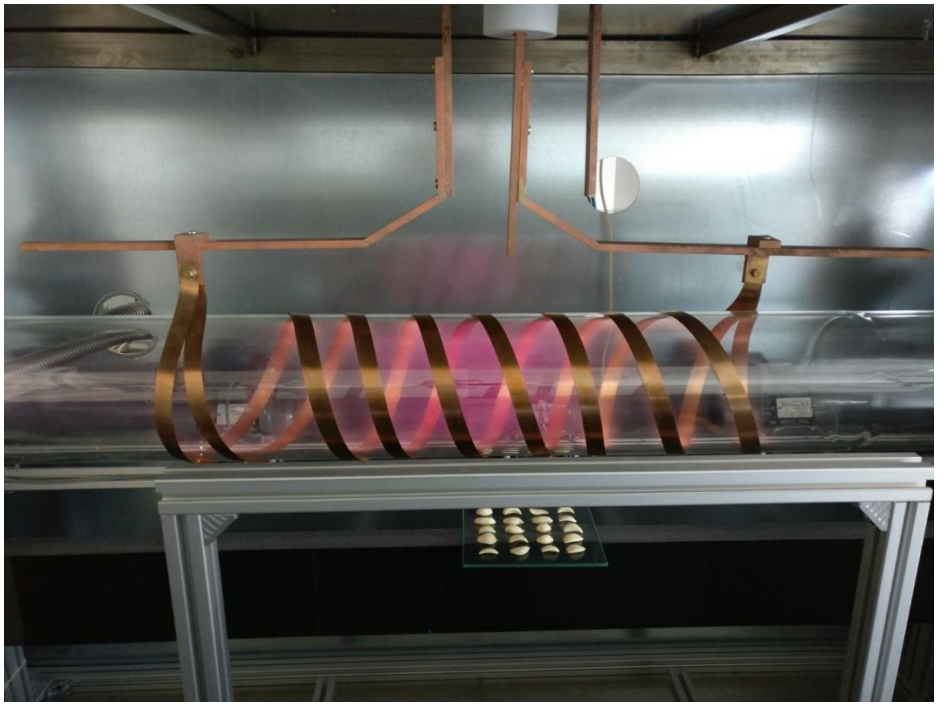

Figure 2.6: EM control treatment in the industrial-scale plasma.

2.4 Plasma Characterization

To understand and compare the properties of the used discharges, plasma with or without garlic clove samples was characterized using optical emission spectroscopy (OES) as well as a catalytic probe. For comparability of results, any plasma without a garlic sample was always ignited with a microscope slide placed in the sample position, as the presence of the microscope slide influences the plasma characteristics by blocking the path of the plasma species compared to the completely empty tube.

2.4.1 Optical emission spectroscopy (OES)

OES spectra record light intensity across a range of wavelengths. Reactive particles in the plasma emit EM radiation at wavelengths characteristic of a particular element or particle. Intensity of the signal at a specific wavelength, measured in arbitrary units, provides some information about the relative quantity of that particle, although values cannot be directly compared.

OES spectra were recorded using a 16-bit Avantes AvaSpec 3648 fiber optic spectrometer (Avantes Inc., Louisville, CO, USA). Nominal spectral resolution was 0.5 nm, and spectra were recorded in the range from 200 to 1100 nm. Integration time was 1000 ms.

Unless stated otherwise, OES spectra were recorded for discharges in the typical "flow" plasma configuration, featuring continuous pumping and gas flow. In addition, OES was measured for plasma turned on in a "no-flow" configuration, wherein the reactor was first evacuated, then the pump was turned off, and oxygen was carefully released into the reactor up to the desired working pressure. Turning on the discharge in this configuration allowed for the accumulation of plasma species appearing in very limited amounts during the course of the experiment, in particular during clove treatment, and thus facilitated the detection of these species by OES.

2.4.2 Catalytic probe

Oxygen atom density (n_O) was determined using a catalytic probe, mounted into the reactor tube opposite to the gas inlet using a flange to render it movable, as seen in Figure 2.7. We used a professional laser-heated fiber-optics catalytic probe (Plasmadis Ltd., Ljubljana, Slovenia) which employed a small catalytic tip made from pure cobalt with a surface oxide layer. The tip is mounted onto an optical fiber which connects to an electronic unit consisting of an infrared (IR) radiation detector (for measuring tip temperature) and a laser (for heating the tip to elevated temperature). Exothermic reactions – recombinations of reactive plasma species to parent molecules – occur at the probe tip when the discharge is turned on. However, the tip temperature is held constant by controlling the laser power. From the difference in the laser power between the plasma on and off conditions, the flux of reactive plasma species onto the probe tip is calculated. The probe was placed far enough (~ 15 mm) from the end of the coil to minimize the effect of ions which could additionally heat the tip surface when impinging on it.

Figure 2.7: Catalytic probe. Shown mounted onto the pilot-scale plasma system for measurements during treatment of cloves in the H-mode afterglow.

2.5 Temperature

The temperature of the garlic cloves during treatment with oxygen plasma was followed by mounting a simple thermocouple inside cloves as shown schematically in Figure 2.8. A couple of thermocouple wires of diameter 0.125 mm made from chromel and alumel alloys was spot welded on one side so that any electrical contact between the wires was only at the welded spot. Cloves were cut at the bottom and partly hollowed out to allow access, and the welded spot was inserted into the storage leaf a few mm under the surface of a clove, assuring no electrical connection between the wires except at the welded spot. The wires stretching from the clove were insulated with narrow glass tubes in order to prevent any interaction of gaseous plasma with the wires. An additional glass tube was covering the bottom part of the clove for the same purpose. On the other side, the wires were sealed hermetically onto a standard Klein flange and connected to a standard voltage meter to measure the thermocouple voltage, which is sampled automatically in 0.1 s intervals and the voltmeter is connected to a computer for data acquisition and processing. Schematic of the experimental setup is shown in Figure 2.8.

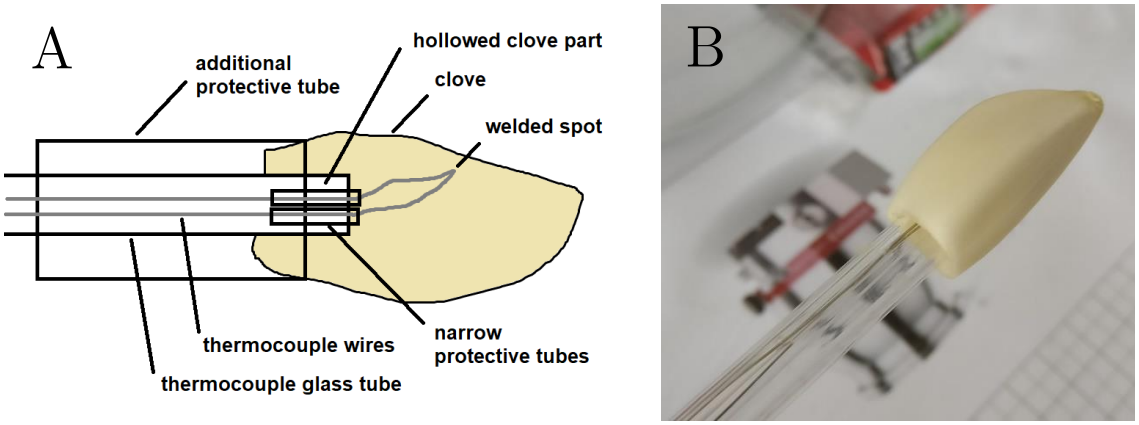

Figure 2.8: Thermocouple measurements. (A) Schematic representation of mounting a thermocouple inside a garlic clove for temperature measurement; (B) a clove with the inserted thermocouple before treatment.

2.6 Water Contact Angle (WCA)

We used water contact angle (WCA) measurements to assess surface hydrophilicity. Static WCA by the sessile drop method was evaluated via Surface Energy Evaluation System (Advex Instruments, Brno, Czech Republic) equipped with a CCD camera. A droplet ($V = 1$ µL) of deionized (DI) water was placed onto a part of the surface that was reasonably flat and not shielded from the plasma during treatment. The measurements were done at room temperature, 22 °C, and at constant relative humidity (60 %). For each treatment condition, three separately treated cloves were analyzed, and the WCA for three droplets on the surface of each was measured. A mean WCA was calculated.

2.7 Water Uptake (WU)

To determine WU by the cloves, each clove was submerged into a beaker containing 100 mL deionized (DI) water immediately after treatment. After a set soaking time, cloves were removed from the beakers, excess water was wiped off, and the cloves were weighed. WU was calculated according to the equation

$$\Delta m = \frac{(m_t - m_0)}{m_0} \times 100\%, \tag{2.1}$$

where Δm is the increase in mass, expressed as a percentage of m_0, while m_0 and m_t represent the clove mass immediately before and after t minutes of soaking, respectively. For each treatment condition, depending on the experiment, three to five separately treated cloves were used, and a mean WU was calculated. As initial clove mass affects the water uptake, only cloves within a predefined mass range (1.4 – 2.1 g) were selected for these experiments.

2.8 Surface Chemistry

2.8.1 X-ray photoelectron spectroscopy (XPS)

We used an X-ray photoelectron spectroscopy (XPS) instrument (Physical Electronics, Ismaning, Germany) to obtain elemental composition of the outermost clove surface layer (~ 5 nm), expressed in atomic percent (at.%). To analyze unpeeled cloves, the protective leaf was removed after treatment, and pieces approximately 4 mm × 4 mm in size were cut from it. To analyze peeled cloves, pieces approximately 4 mm × 4 mm in size and 1 mm in thickness were excised from the clove surface using a scalpel, then frozen in liquid nitrogen and dried inside a vacuum reactor. The samples were mounted onto an XPS sample holder, and their surfaces were excited by X-ray radiation from a monochromatic Al source at photon energy of 1486.6 eV.

The high-energy resolution spectra were acquired with an energy analyzer operating at a resolution of about 0.5 eV, and a pass energy of 29 eV. Spectra were analyzed using the MultiPak V8.0 software (Ulvac-phi, Inc., Chigasaki, Japan). They were calibrated using a C 1s peak at 284.8 eV. Sub-peaks were fitted to the high-resolution C 1s spectra to explain the chemical bond composition of the sample surface.

2.8.2 Attenuated total reflectance Fourier-transform infrared (ATR-FTIR) spectroscopy

An attenuated total reflectance Fourier-transform infrared (ATR-FTIR) spectrometer, model L1280018 (PerkinElmer, Waltham, MA, USA), was used to obtain additional information about surface chemistry, in particular, the chemical bonds present at the surface. The technique uses an IR beam that passes through the sample and becomes attenuated in regions of the IR spectrum where the sample absorbs energy. The result is an IR absorption spectrum that plots transmittance (%) against wavenumber (cm^{-1}). The spectra are roughly divided in two regions: the functional group region (4000 – 1500 cm^{-1}), where peaks correspond to specific chemical bonds, and the fingerprint region (1500 – 380 cm^{-1}), where peaks correspond to complex molecular deformations.

Spectra were recorded at the garlic surface most directly exposed to the plasma. Each spectrum comprised 10 individual acquisitions averaged. The spectra were normalized using the Origin 8.5 software (OriginLab, Northampton, MA, USA) and presented as stacked lines offset by the Y axis.

2.9 Surface Morphology

2.9.1 Scanning electron microscopy (SEM)

To obtain images of the clove surface at high magnification (up to ~ 30,000 ×), we used scanning electron microscopy (SEM). To analyze unpeeled cloves, the protective leaf was removed after treatment, and pieces approximately 4 mm × 4 mm in size were cut from it. To analyze peeled cloves, pieces approximately 4 mm × 4 mm in size and 1 mm in thickness were excised from the clove surface using a scalpel, then frozen in liquid nitrogen and dried inside a vacuum reactor. The samples were attached onto aluminum stubs using conductive carbon tape and coated with a thin layer of platinum using a Gatan 682 Precision Etching and Coating System (Gatan Inc., Pleasanton, California). The SEM images were obtained using a JSM-7600F Schottky Field Emission SEM (Jeol Ltd., Tokyo, Japan).

2.9.2 Atomic force microscopy (AFM)

We used an atomic force microscope (AFM) (Solver PRO, NT-MDT, Moscow, Russia) to characterize the topology of the samples. Pieces approximately 4 mm × 4 mm in size were cut from the protective leaf or excised from the clove surface and mounted onto aluminum holders using carbon tape. All measurements were performed in tapping mode using ATEC-NC-20 tips (Nano and More GmbH, Wetzlar, Germany) with a resonance frequency of 210–490 kHz and the force constant of 12–110 Nm^{-1}.

2.10 Sprout and Root Growth

To record sprout length, root length, and root number, we have grown garlic cloves in a laboratory setting. To begin germination and growth, each clove was placed on a layer of filter paper inside a petri dish (inner diameter 45 mm) immediately after plasma treatment and moistened with 1 mL of DI water. Cloves were incubated at room temperature in the dark; DI water was added as needed during sampling.

Depending on the experiment, sprout length was recorded up to 30 days after incubation; sprouts were measured from their lowest point of emergence from the garlic storage leaf up to the tip. Length of the longest root and total number of roots were recorded up to 15 days after incubation, after which the roots began to decay in the laboratory setting. In case of decayed sprouts or roots, the last recorded observation was used in place of missing data for the calculation of means.

2.11 Plant Height and Yield

To grow garlic plants from treated and untreated cloves, the cloves were planted in a field close to Ptuj, Slovenia, by the staff of Semenarna Ljubljana, Selekcijsko-poskusni center Ptuj. Depending on the experiment, the cloves were planted one to two days after plasma treatment. They were planted either in the fall (October) or in the spring (March) and harvested in July, after approximately nine or four months for fall- or spring-planted cloves, respectively. At harvest, plant height was recorded from the bottom of the bulb to the top of the longest leaf. The garlic was dried for a month, after which, it was cleaned, leaves and roots were removed, and the mass of each bulb was recorded. Mean height and mass were calculated.

Additionally, some of the garlic grown in the field was stored at suitable conditions until the next planting, and grown as the second or third generation of garlic without any additional plasma treatment. It was harvested, and plant height as well as bulb mass was recorded as above.

2.12 Statistical Analysis

Data from the WCA, WU, sprout and root growth, plant height and yield measurements was statistically analyzed using the JASP 0.9.2. open-source software (University of Amsterdam, Amsterdam, The Netherlands). Group means were calculated and compared using ANOVA followed by the post hoc Tukey's range test. Differences in the means were considered statistically significant at ($p < 0.05$).

Where error bars are presented in charts, they represent standard error, unless stated otherwise. In some charts, error bars are omitted for the purpose of clarity.

Chapter 3

Results

3.1 Plasma Characterization

3.1.1 Optical emission spectroscopy

3.1.1.1 Flow configuration

As specified in section 2.4.1, flow configuration is the typical configuration of the plasma system, featuring continuous pumping and gas flow.

3.1.1.1.1 E-mode plasma OES spectra of the pilot-scale E-mode plasma in the flow configuration are presented in Figure 3.1. Signal intensities at selected wavelengths are collected in Table 5.1 in Appendix A.

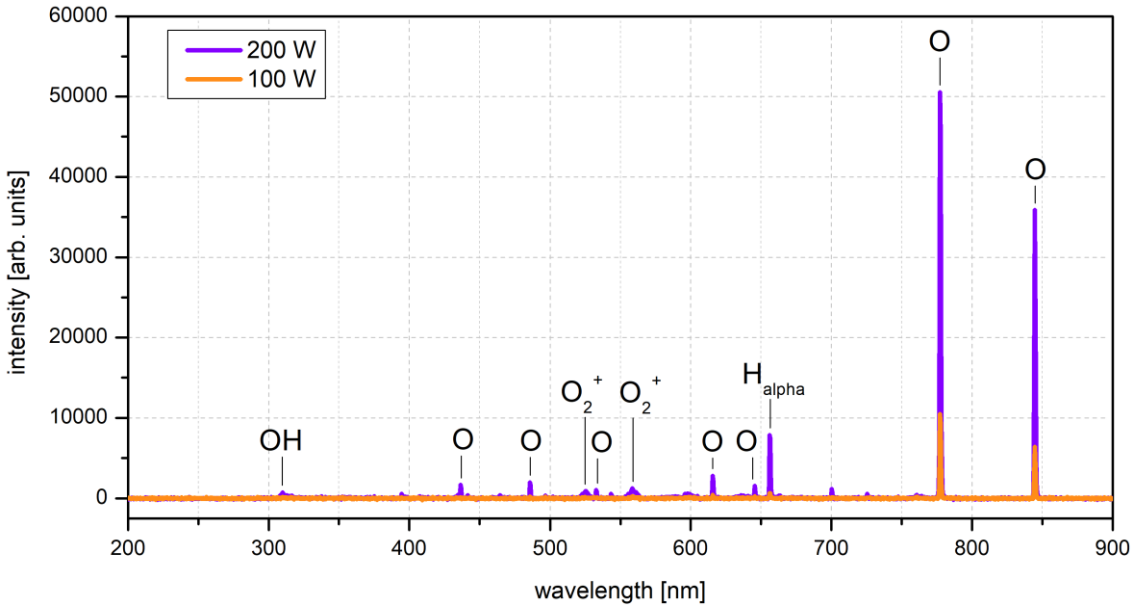

Figure 3.1: OES spectra comparison, pilot-scale E-mode oxygen plasma. $P_N = 100 - 200$ W, $p = 50$ Pa, flow configuration. Spectra were recorded approximately 60 s after turning on the discharge.

As seen in Figure 3.1, only oxygen atomic emission lines at around 777.4 and 844.6 nm are prominent at $P_N = 100$ W and $p = 50$ Pa [17]. In addition, the hydrogen Balmer line H_α is detectable at around 656 nm [71], along with additional weak lines of O (616 nm) and the oxygen molecular ion, O_2^+ (558.7 nm). After increasing P_N to 200 W, the O lines at 616,

777.4, and 844.6 nm are about 5 – 7 times more intense than at P_N = 100 W. Several additional weak O lines appear at 437, 486, 533, 544, 645 and 926 nm [72, 73]. The O_2^+ lines, e.g. at 525.5 and 558.7 nm, are also present, but still very weak. Even weaker are the O^+ lines seen at 441.5 and 464.9 nm. The H_α line is about 12 times more intense, while the OH band appears weakly at around 309 nm [17]. The spectrum of a plasma at P_N = 300 W is not included due to transitions into H-mode at both 30 and 50 Pa whenever a discharge without a garlic sample was turned on.

3.1.1.1.2 Garlic clove treatment OES spectra of the pilot-scale E-mode plasma treatment of peeled and unpeeled garlic samples are presented in Figure 3.2 – Figure 3.4. Signal intensities at selected wavelengths are collected in Table 5.1.

During treatment of peeled or unpeeled cloves in the E-mode glow plasma (Figure 3.2), the signal pattern is generally the same as without a sample. The main difference is in the intensity of the individual lines. Most prominently, as seen in Table 5.1, the oxygen atomic lines are decreased to about 50 % intensity if a garlic clove is present in the plasma. Simultaneously, the H_α and OH lines increase by a factor of about 2 and 4 for unpeeled and peeled cloves, respectively.

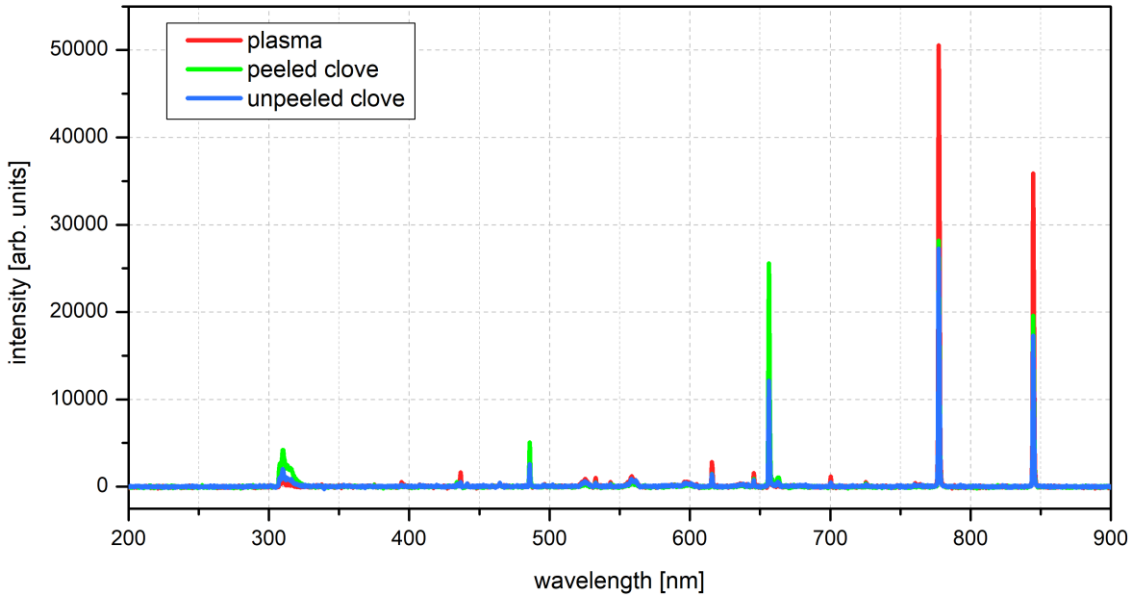

Figure 3.2: OES spectra comparison, pilot-scale E-mode clove treatment. P_N = 200 W, p = 50 Pa, plasma alone, as well as treatment of a peeled or unpeeled garlic clove in the flow configuration. Spectra were recorded approximately 60 s after turning on the discharge.

3.1.1.1.3 Effect of generator power When the P_N at which a garlic clove is treated is increased (Figure 3.3), the signal of all important emission lines increases. This includes the oxygen atom and molecular ion as well as the H and OH lines. In addition, noticeable emission lines appear at about 589, 766, and 770 nm. These lines correspond to sodium (589 nm) and chlorine (766 and 770 nm).

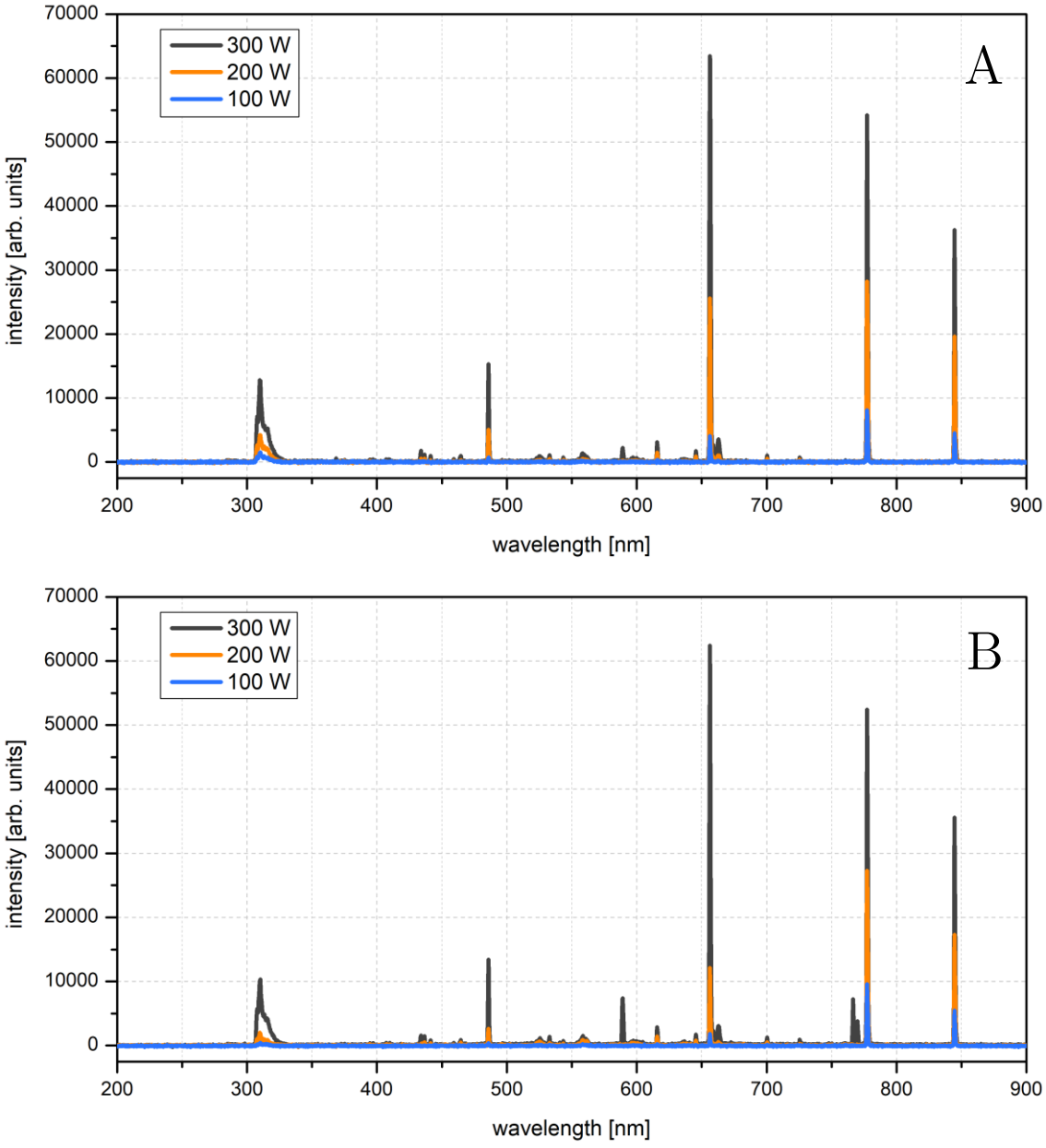

Figure 3.3: OES spectra comparison, pilot-scale E-mode, increasing power. $P_N = 100 - 300$ W, $p = 50$ Pa, flow configuration. Treatment of (A) peeled garlic cloves, (B) unpeeled garlic cloves. Spectra were recorded approximately 60 s after turning on the discharge.

3.1.1.1.4 Effect of working pressure The signal of prominent emission lines also increases when the working pressure is decreased at P_N = 200 W (Figure 3.4). However, the difference in O atom line intensities (777.4 and 844.6 nm) at the pressures of 30 and 50 Pa is barely detectable in the case of unpeeled cloves.

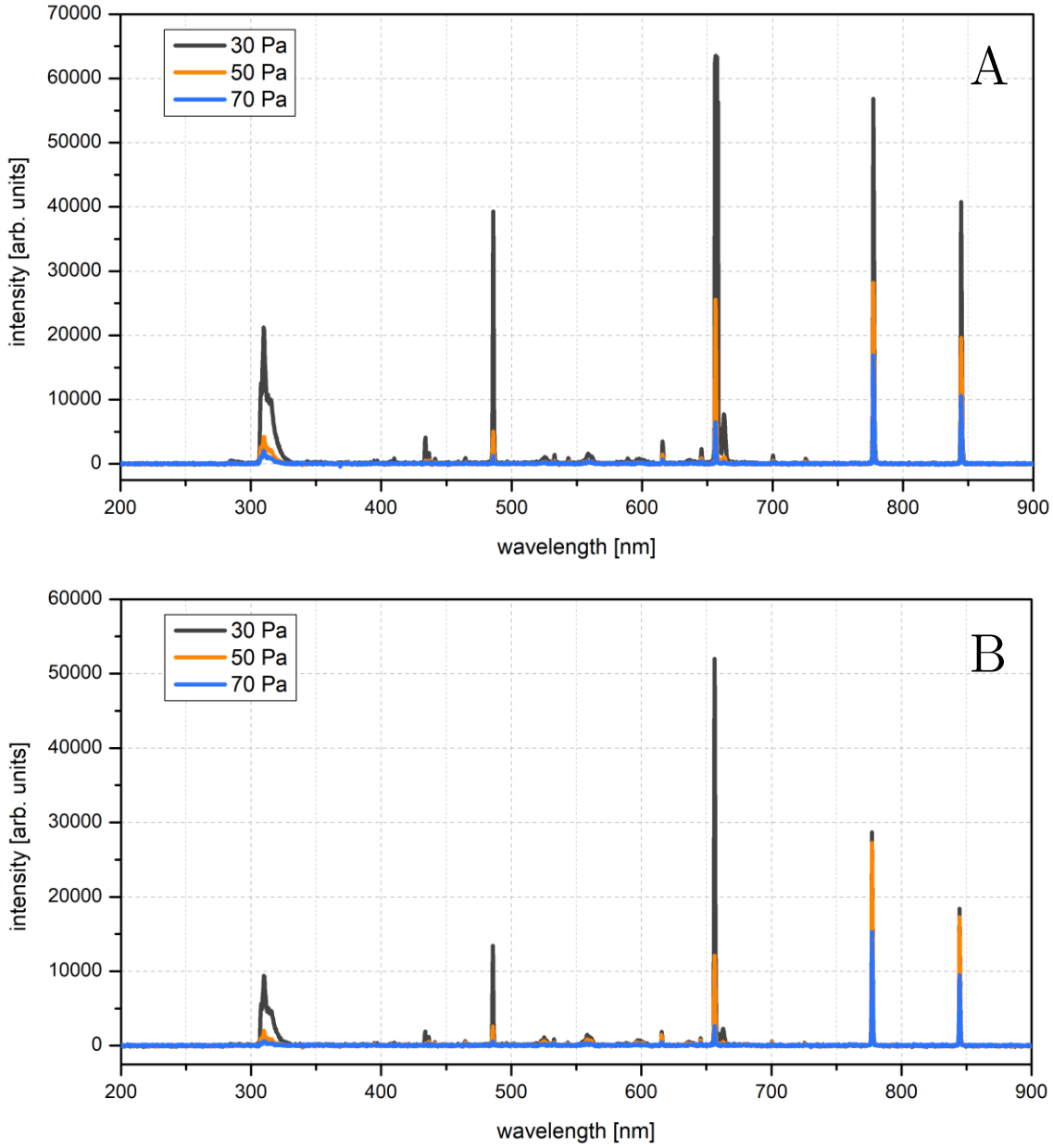

Figure 3.4: OES spectra comparison, pilot-scale E-mode, increasing working pressure. P_N = 200 W, p = 30 – 70 Pa, flow configuration. Treatment of (A) peeled garlic cloves, (B) unpeeled garlic cloves. Spectra were recorded approximately 60 s after turning on the discharge.

3.1.1.1.5 Time courses of OH signal intensities Figure 3.5 presents the time courses of the OH radical spectral line (~ 309 nm) signal intensity during plasma treatment of peeled cloves at different P_N and at different working pressure, respectively. Figure 3.5 (A) shows that, at each P_N (100 – 300 W), the signal gradually increases with time, and then reaches a plateau. However, as may be expected, the signal rise is steeper, and the plateau intensity higher, with increased treatment power. The plateau is reached in < 30 s at 300 W, in about 50 s at 200 W, and in about 90 s at 100 W. A similar development is seen for decreasing working pressure, as shown in Figure 3.5 (B).

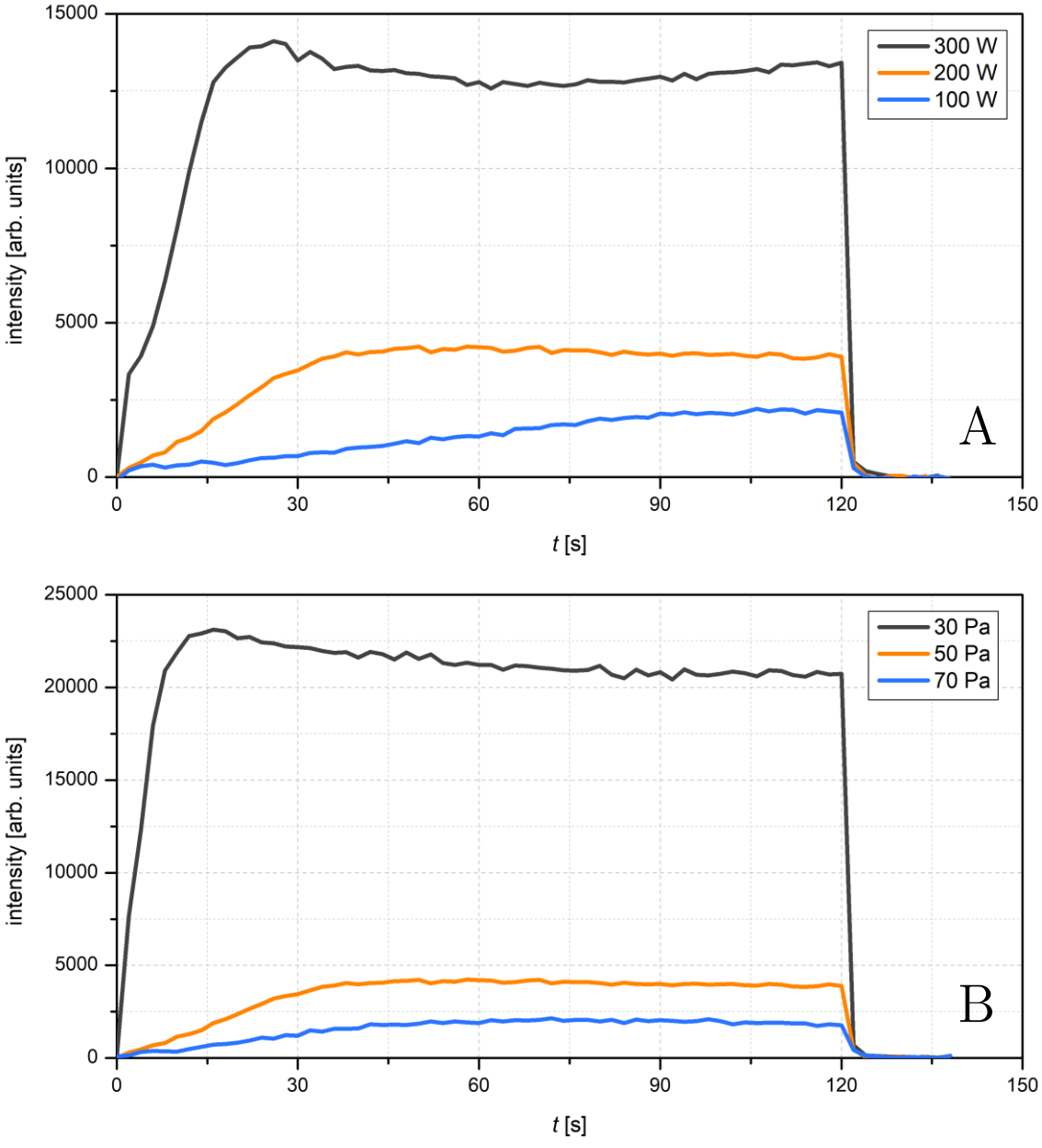

Figure 3.5: Time course of OH radical spectral line (~ 309 nm) signal intensity. Pilot-scale E-mode oxygen plasma treatment of a peeled garlic clove in the flow configuration. (A) $P_N = 100 - 300$ W, $p = 50$ Pa; (B) $P_N = 200$ W, $p = 30 - 70$ Pa. The discharge was turned on at $t = 0$ s and turned off at $t = 120$ s.

3.1.1.2 No-flow configuration

As specified in section 2.4.1, in the no-flow configuration, the reactor was first evacuated, the pump was turned off, and oxygen was carefully released into the reactor only up to the desired working pressure, after which, the gas flow was closed.

3.1.1.2.1 Treatment of peeled clove Time courses of selected signal intensities during plasma treatment of peeled cloves in the no-flow configuration are presented in Figure 3.6 and Figure 3.7. In Figure 3.6, it is apparent that H_α and OH dominate the spectrum. The remaining signals, including the O lines, rise briefly after turning on the discharge, but subside within about 20 s, when the pressure rises to about 75 – 100 Pa. The H_α and OH lines then steadily decrease while pressure increases and plasma luminosity falls. At about 200 s, the discharge extinguishes by itself due to the pressure rise.

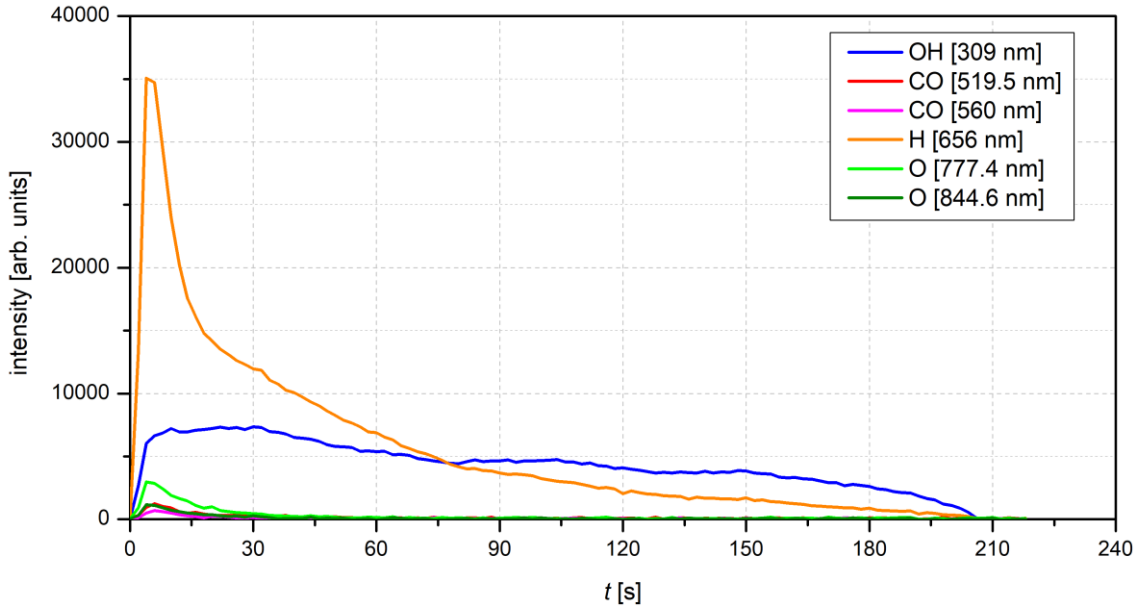

Figure 3.6: Time course of signal intensity, no-flow configuration. Pilot-scale E-mode plasma, peeled clove, $P_N = 200$ W, $p = 50$ Pa.

Figure 3.7 compares the temporal behavior of selected spectral lines between treatments with $P_N = 200$ W and $P_N = 300$ W. Interestingly, while the behavior and intensity of the OH signal is nearly identical, the remaining signals (H_α, O, and CO) are all notably more intense in the $P_N = 300$ W treatment. In particular, the initial H_α peak is nearly twice as intense (about 63000 as opposed to about 35000). However, the time course of the H_α line intensity from 20 s onward is also comparable between the $P_N = 200$ and $P_N = 300$ W treatments.

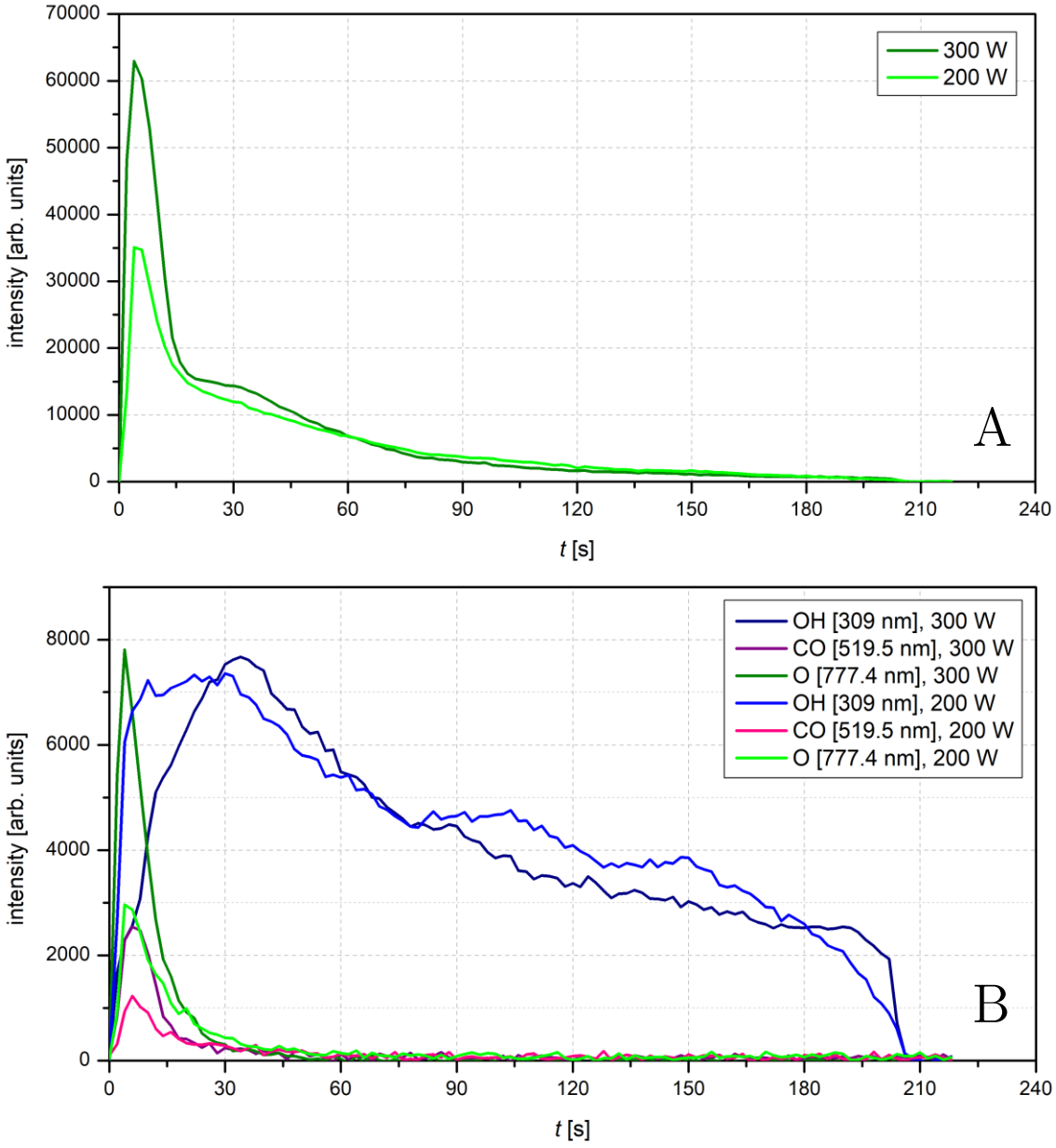

Figure 3.7: Time course of signal intensity, no-flow configuration, increasing P_N. Pilot-scale E-mode plasma, peeled clove, $P_N = 200 - 300$ W, $p = 50$ Pa. (A) H_α; (B) other signals.

3.1.1.2.2 Comparison of treatment of peeled and unpeeled cloves Comparisons of time courses of selected signal intensities during plasma treatment of peeled and unpeeled cloves in the no-flow configuration are presented in Figure 3.8. During the treatment of unpeeled cloves, the plasma lasts longer than for peeled cloves (around 330 s, compared to around 200 s). Further, signal intensities are higher during the treatment of unpeeled cloves, particularly the O and CO signals, which are twice as intense as during the treatment of a peeled clove. A notable exception is the OH band, which is more intense during the treatment of the peeled clove.

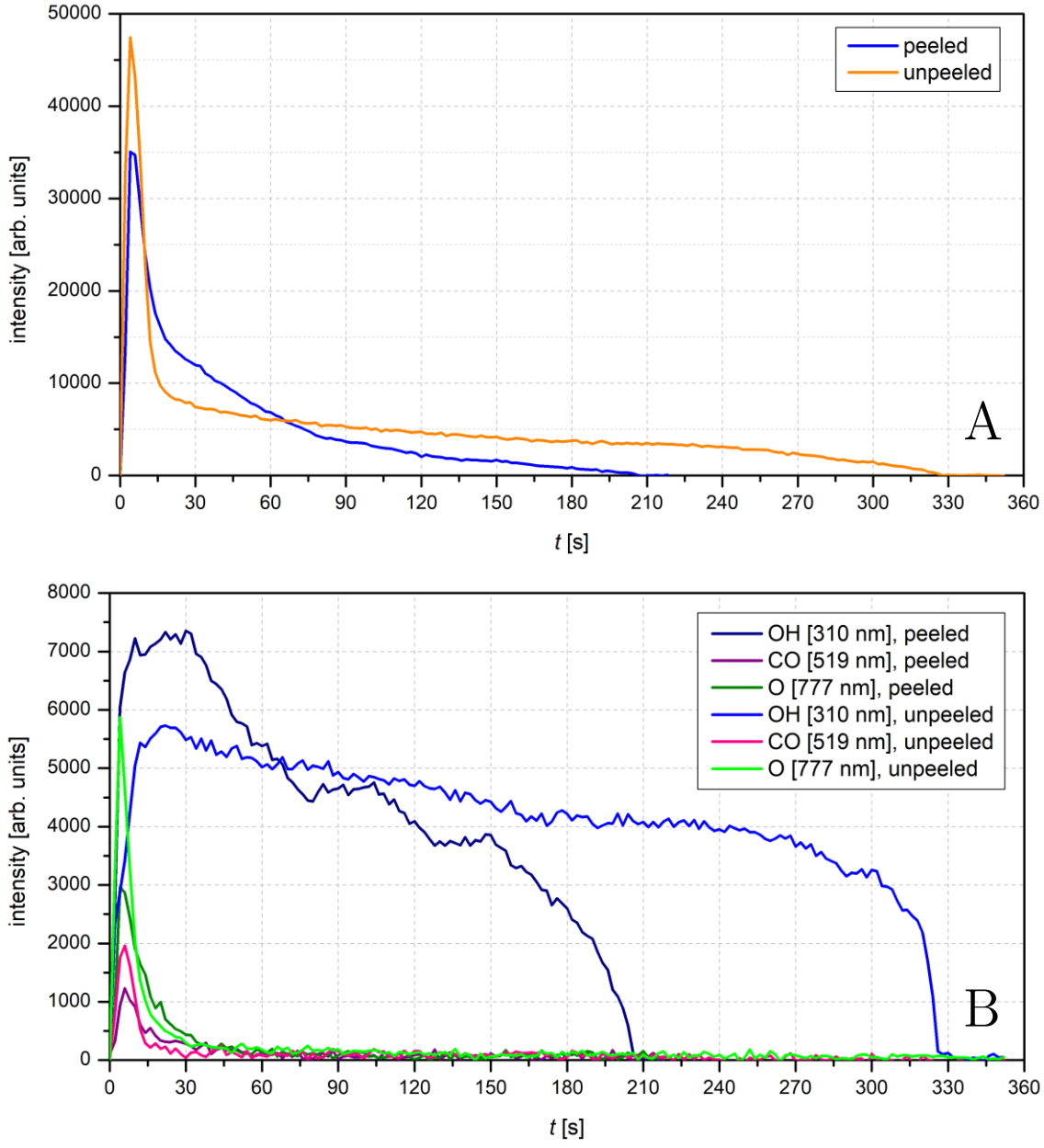

Figure 3.8: Time course of signal intensity, no-flow conf., peeled and unpeeled cloves. Pilot-scale E-mode plasma, $P_N = 200$ W, $p = 50$ Pa. (A) H_α; (B) other signals.

3.1.2 Catalytic probe

3.1.2.1 n_O in the E-mode plasma

Oxygen atom densities (n_O) recorded for the pilot-scale E-mode plasma at different plasma conditions are presented in Figure 3.9. At P_N = 100 W, the n_O was recorded at a pressure of 30, 50, and 70 Pa. At P_N = 200 W, it was only recorded at 50 and 70 Pa, and at P_N = 300 W, only at 70 Pa. This is due to the plasma assuming the H-mode at the remaining conditions in the absence of a garlic sample.

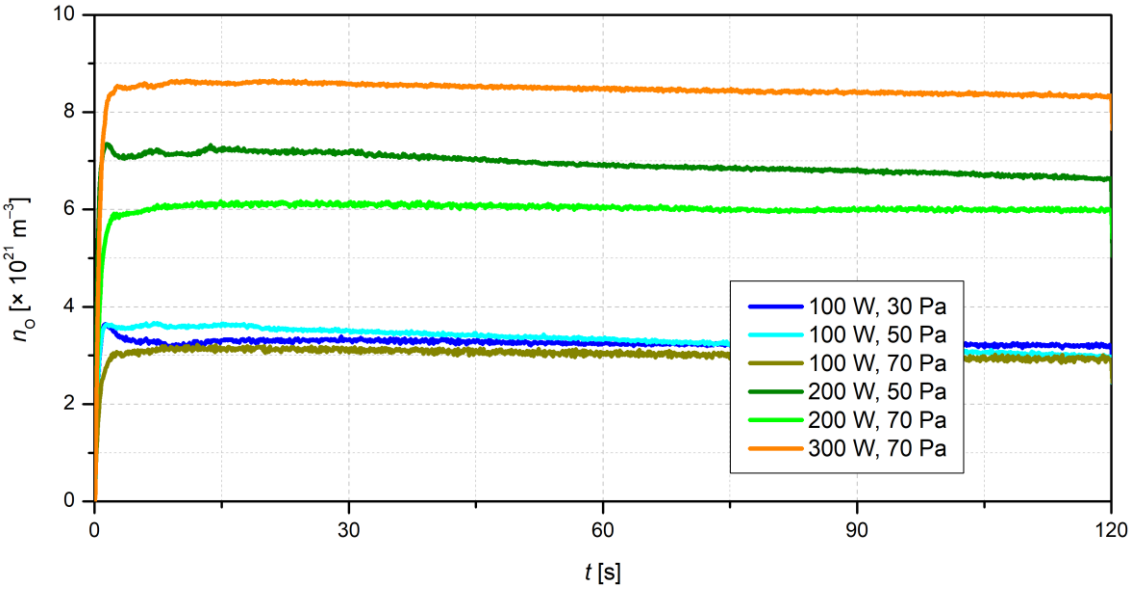

Figure 3.9: n_O in pilot-scale E-mode plasma without a garlic sample. P_N = 100 – 300 W, p = 30 – 70 Pa, t = 120 s. The discharge was turned on at t = 0 s and turned off at t = 120 s.

We know from Table 2.1 that within the selected range of plasma conditions, the P_{EFF} at a constant P_N is also constant, regardless of the working pressure. As we see in Figure 3.9, this is reflected in the n_O at P_N = 100 W, which is approximately equal (~ 3 × 10^{21} m^{-3}) at all three working pressures. At P_N = 200 W, the n_O at 50 Pa is slightly higher than at 70 Pa, about 7 × 10^{21} and 6 × 10^{21} m^{-3}, respectively. At double the P_{EFF}, these n_O values are approximately double compared to the n_O values at P_N = 100 W. The n_O at P_N = 300 W is slightly less than thrice the n_O at P_N = 100 W.

3.1.2.2 Probe signal increase during clove treatment

Figure 3.10 shows a comparison of n_O recorded during E-mode plasma alone and during treatment of a peeled clove. We see that when a garlic sample is introduced into the plasma, the recorded n_O values increase compared to plasma in an empty reactor. The initial n_O value during sample treatment is equal or larger than for plasma alone, followed by a gradual increase until a plateau is reached, whereas the n_O for plasma alone remains relatively constant throughout the experiment.

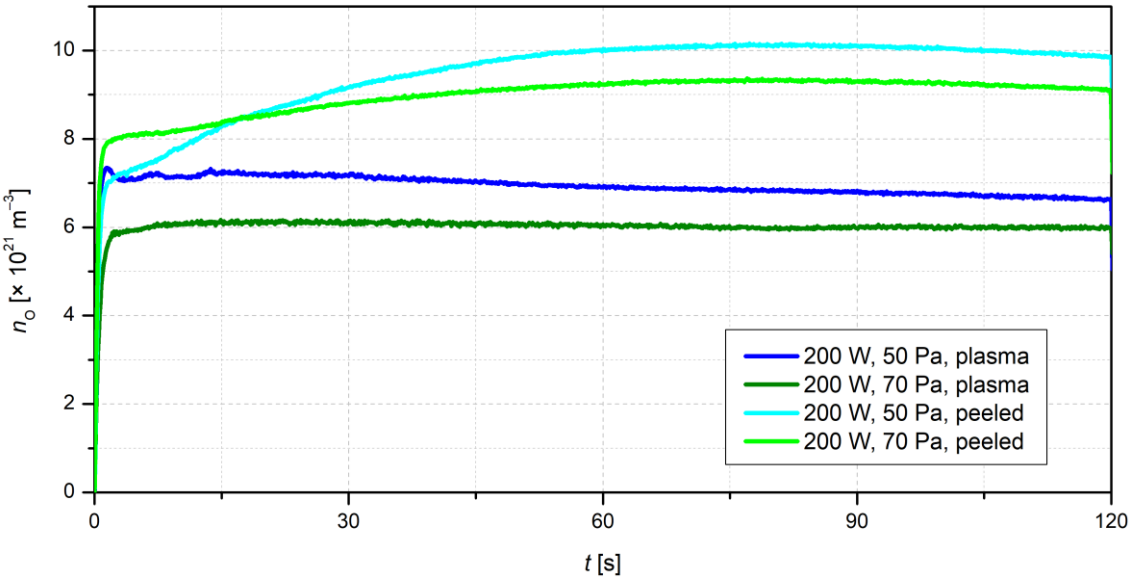

Figure 3.10: n_O in the pilot-scale E-mode, plasma or peeled clove. P_N = 200 W, p = 50 – 70 Pa, t = 120 s. The discharge was turned on at t = 0 s and turned off at t = 120 s.

Figure 3.11 shows a comparison of n_O recorded during E-mode plasma alone and during the treatment of either one or three peeled or unpeeled cloves. In all cases, the initial recorded signal is larger than the signal from the plasma alone. As in Figure 3.10, the signal during the peeled clove treatment reaches a plateau, and its value is nearly comparable between the treatment of one and three cloves. Conversely, during unpeeled clove treatment, the signal rises for about 15 – 20 s, then drops and approaches the value for plasma alone within the 60 s of treatment. The value for three cloves is higher than the value for a single clove.

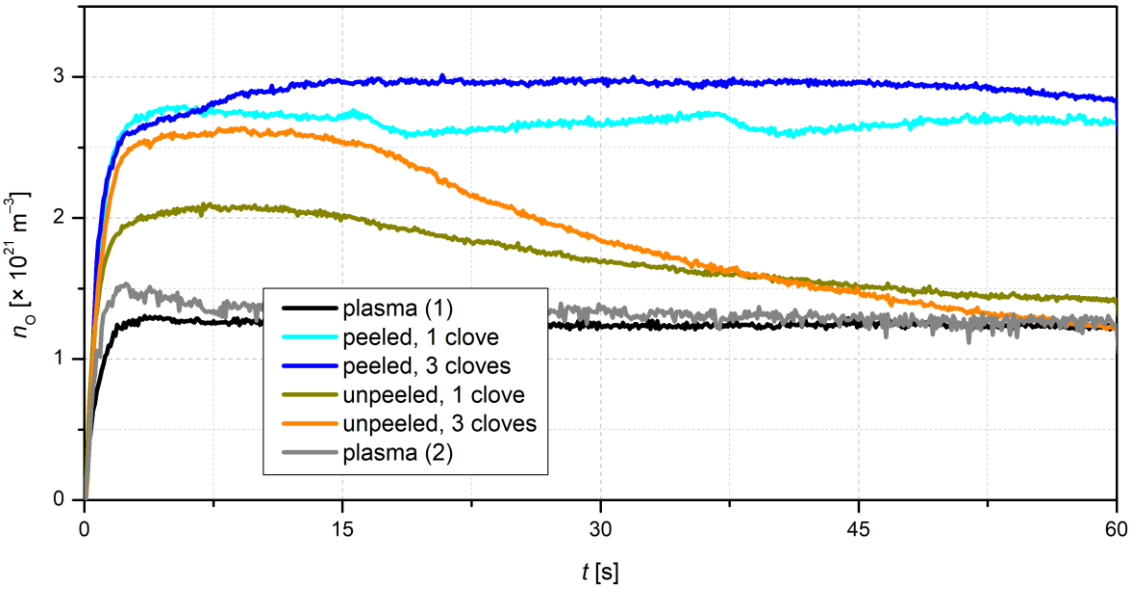

Figure 3.11: n_O in the pilot-scale E-mode, plasma or peeled or unpeeled clove. $P_N = 100$ W, $p = 30$ Pa, $t = 60$ s. Cloves were treated either individually or as three cloves simultaneously. The discharge was turned on at $t = 0$ s and turned off at $t = 60$ s.

3.1.2.3 n_O during treatment of peeled garlic

Oxygen atom densities recorded during the pilot-scale plasma treatment of peeled garlic cloves are presented in Figure 3.12 (E-mode glow) and Figure 3.13 (H-mode afterglow). We see in Figure 3.12 (A) that as above, the recorded n_O increases with increasing P_N, as well as with decreasing pressure. From Figure 3.12 (B), we see that during prolonged treatment of peeled cloves, the initial plateau value gradually begins to drop after about 100 s, and continues to do so during the 300 s of treatment.

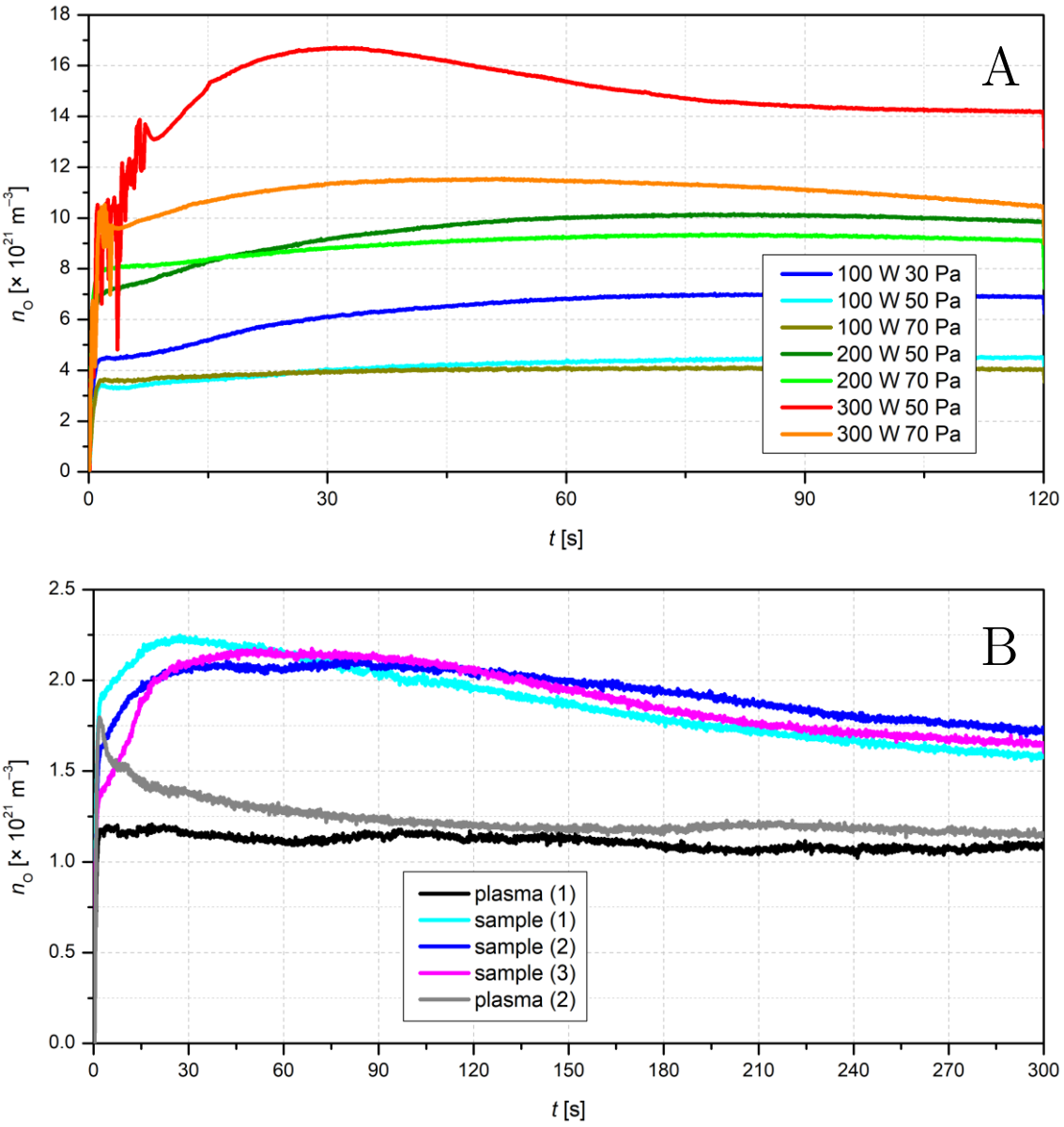

Figure 3.12: n_O during treatment of peeled garlic, E-mode glow. (A) P_N = 100 – 300 W, p = 30 – 70 Pa, t = 120 s. (B) P_N = 100 W, p = 30 Pa, t = 300 s.

In Figure 3.13, we see that the n_O during H-mode afterglow treatment of a single peeled clove at the given conditions is about $2.5 - 3 \times 10^{21}$ m^{-3}.

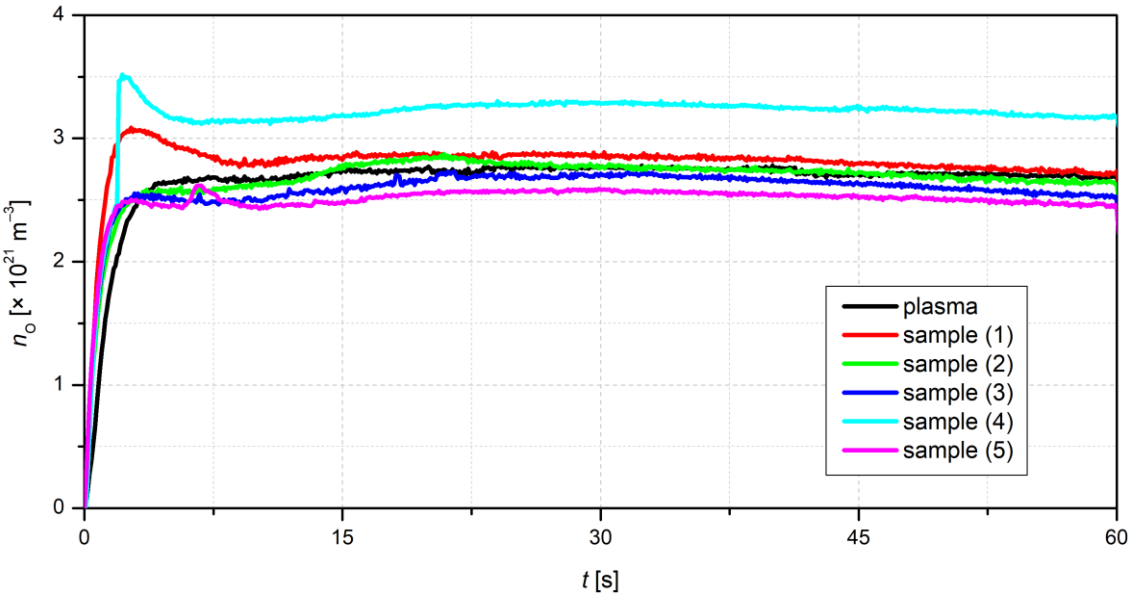

Figure 3.13: n_O during treatment of peeled garlic, H-mode afterglow. $P_N = 300$ W, $p = 30$ Pa, $t = 60$ s. The discharge was turned on at $t = 0$ s and turned off at $t = 60$ s.

3.1.2.4 n_O during treatment of unpeeled garlic

Oxygen atom densities recorded during the pilot-scale plasma treatment of peeled garlic cloves are presented in Figure 3.14 (E-mode glow) and Figure 3.15 (H-mode afterglow). We see in Figure 3.14 (A) that as above, the recorded n_O increases with increasing P_N, as well as with decreasing pressure. For the treatment at $P_N = 300$ W and $p = 50$ Pa, the recorded signal is irregular due to burning of the exposed edges of the protective leaf. For the remaining two treatments, the n_O begins to decrease slowly after approximately 20 s of treatment, and then gradually increases again with further treatment time. From Figure 3.14 (B), we see that during prolonged treatment of unpeeled cloves, the initial peak subsides within a minute and reaches a low plateau value that lasts up to about 200 s, after which the signal begins to rise once again.

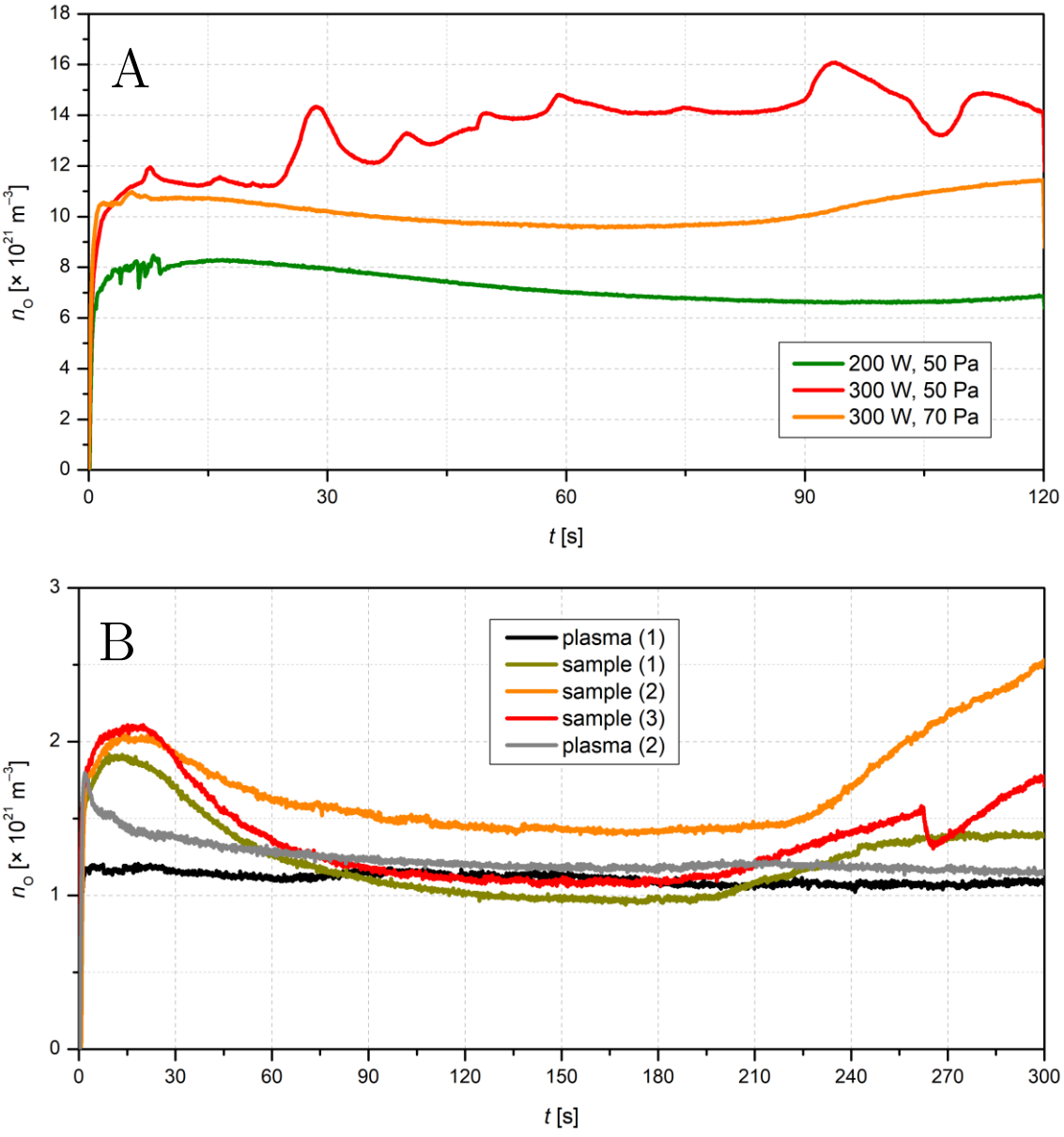

Figure 3.14: n_O during treatment of unpeeled garlic, E-mode glow. (A) $P_N = 200 - 300$ W, $p = 50 - 70$ Pa, $t = 120$ s. (B) $P_N = 100$ W, $p = 30$ Pa, $t = 300$ s.

Similar to Figure 3.13, we see in Figure 3.15 that the n_O during H-mode afterglow treatment of a single unpeeled clove at the given conditions is about 2.5 – 3 × 10^{21} m^{-3}.

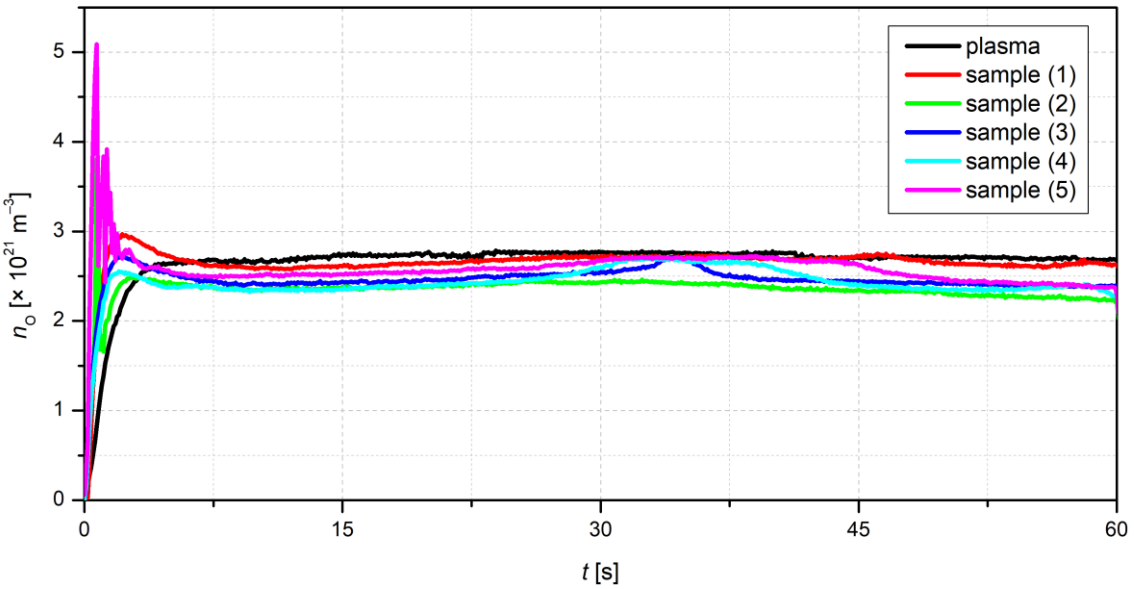

Figure 3.15: n_O during treatment of unpeeled garlic, H-mode afterglow. P_N = 300 W, p = 30 Pa, t = 60 s. The discharge was turned on at t = 0 s and turned off at t = 60 s.

3.2 Temperature

Figure 3.16 and Figure 3.17 show the time course of temperature measured by the thermocouple (TC) in selected experiments. In Figure 3.16, we have followed exposure of a peeled clove with an inserted TC, or a TC alone, to pilot-scale E-mode glow plasma with $P_N = 200$ W. The temperature progression at a working pressure of 50 Pa, when the discharge is ignited, and at atmospheric pressure, where there is no discharge, is nearly identical. A TC without a garlic sample reaches twice the temperature of the garlic measurement within the first minute, but settles at a plateau thereafter.

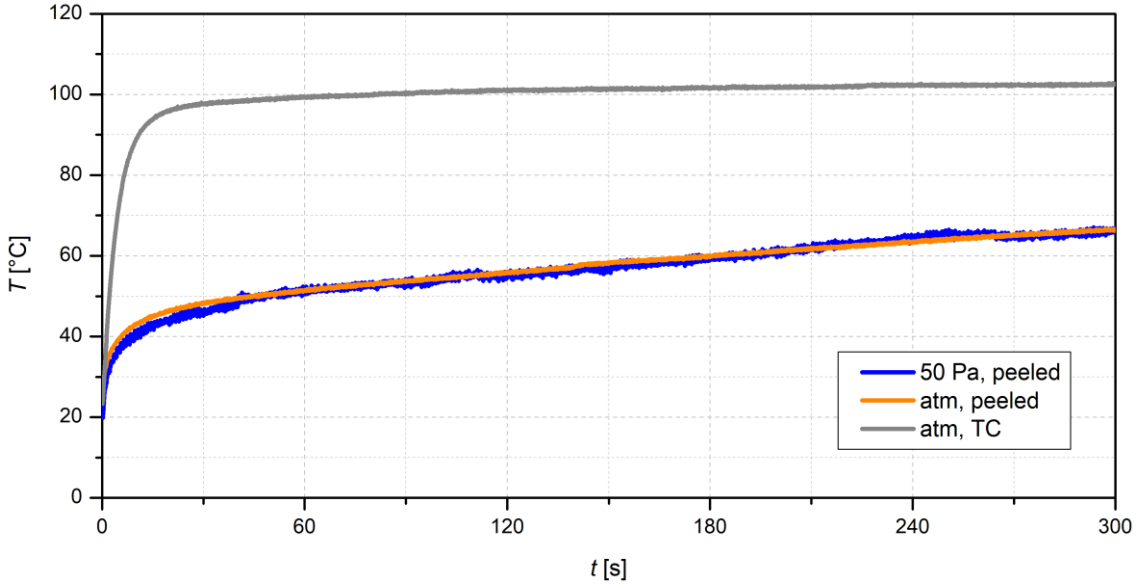

Figure 3.16: Temperature measured by a TC in the pilot-scale plasma. $P_N = 200$ W, $p = 50$ Pa or atm, $t = 300$ s, sample = peeled garlic or TC alone.

In Figure 3.17, we see a comparison of temperature time courses following exposure of a peeled or unpeeled clove with an inserted TC to one of two discharge conditions: 200 W, 50 Pa or 300 W, 70 Pa.

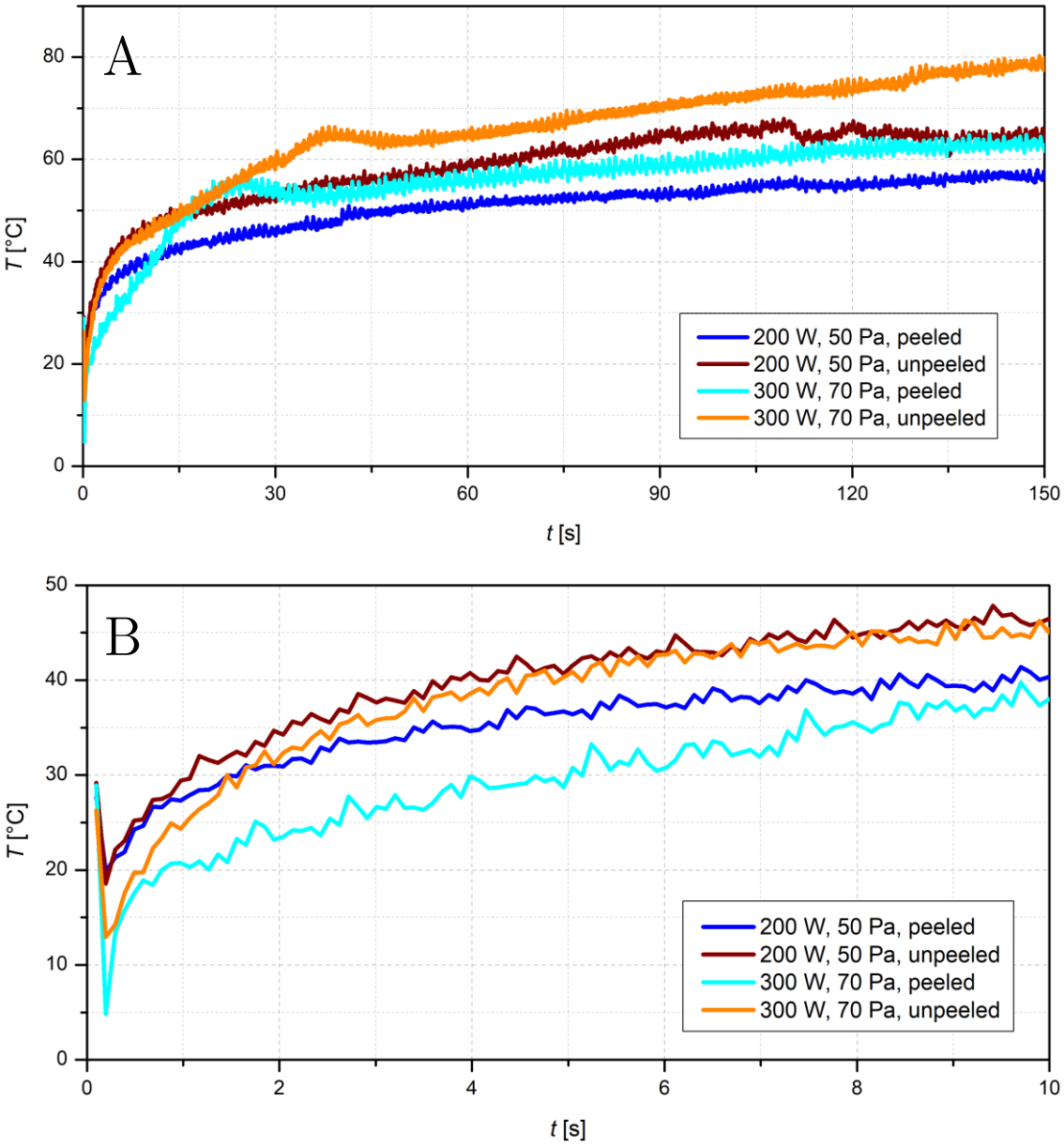

Figure 3.17: Temperature time course, peeled and unpeeled cloves, pilot-scale plasma. $P_N = 200 - 300$ W, $p = 50 - 70$ Pa, sample = peeled or unpeeled clove. (A) treatment up to $t = 150$ s; (B) the first 10 s of treatment.

3.3 Surface chemistry

3.3.1 X-ray photoelectron spectroscopy

3.3.1.1 Composition of untreated clove surfaces

Table 3.1 summarizes the surface elemental compositions of the untreated garlic clove surfaces from the various experiments, both for the protective leaf and the clove surface. The results show that these surfaces consist mainly of C and O, with minor amounts of other elements that differ depending on the particular experiment. The oxygen concentration is higher at the protective leaf surface than at the peeled clove surface. However, the protective leaf surface composition and O/C ratio also appear to vary in a wider range than those of the peeled clove surface. The mean O/C ratio is lower on the clove surface compared to the protective leaf surface.

Table 3.1: Surface elemental composition [at.%] and O/C ratios of untreated clove surfaces from different experiments. (PL) protective leaf, (C) clove. (PS) pilot-scale, (IS) industrial-scale. (G) glow, (AG) afterglow.

experiment	C	O	Ca	Si	N	Cl	Na	O/C ratio
PL, PS, G	90.2	8.2	0.1	/	1.4	0.1	/	**0.091**
PL, PS, AG	96.6	3.1	/	/	/	/	/	**0.032**
PL, PS pulsed	93.9	4.7	/	0.8	0.6	/	/	**0.050**
C, PS G	97.5	2.5	/	/	/	/	/	**0.026**
C, IS G	97.8	2.2	/	/	1.3	0.1	0.6	**0.022**

3.3.1.2 Protective leaf

3.3.1.2.1 Pilot-scale E-mode glow treatment Unpeeled cloves were treated in the pilot-scale plasma at $P_N = 200$ W, $p = 50$ Pa, $t = 0 - 120$ s. E-mode glow and H-mode afterglow sample positions were used. Surface elemental composition of the protective leaf is summarized in Table 3.2, the C and O concentrations are presented in Figure 3.18, and the O/C ratio is presented in Figure 3.19. Carbon content at the surface decreases, and oxygen content increases, with increased treatment time. The O/C ratio increases nearly linearly with glow plasma treatment time. Compared to glow treatment, the increase with the afterglow treatment is less steep.

Table 3.2: Surface elemental composition [at.%] of unpeeled garlic, pilot-scale plasma. $P_N = 200$ W, $p = 50$ Pa, $t = 0 - 120$ s, glow and afterglow (AG) treatments.

t [s]	C	O	Ca	S	Si	Mg	N	Cl	K	Na
0	90.2	8.2	0.1	/	/	/	1.4	0.1	/	/
5	77.5	20.0	0.2	0.2	/	/	1.7	/	/	0.4
15	65.3	30.1	1.6	0.5	0.4	/	1.1	0.2	/	0.9
30	44.2	46.0	6.8	1.5	0.7	0.4	0.3	/	/	/
60	38.0	48.6	9.0	2.2	0.6	0.8	0.3	/	0.4	/
120	27.6	57.2	8.6	4.4	1.0	0.6	/	/	0.7	/
AG 30	79.1	18.9	/	/	/	/	1.3	0.1	/	0.6
AG 120	46.9	43.6	4.3	1.6	0.3	0.5	0.8	0.2	0.8	1.1

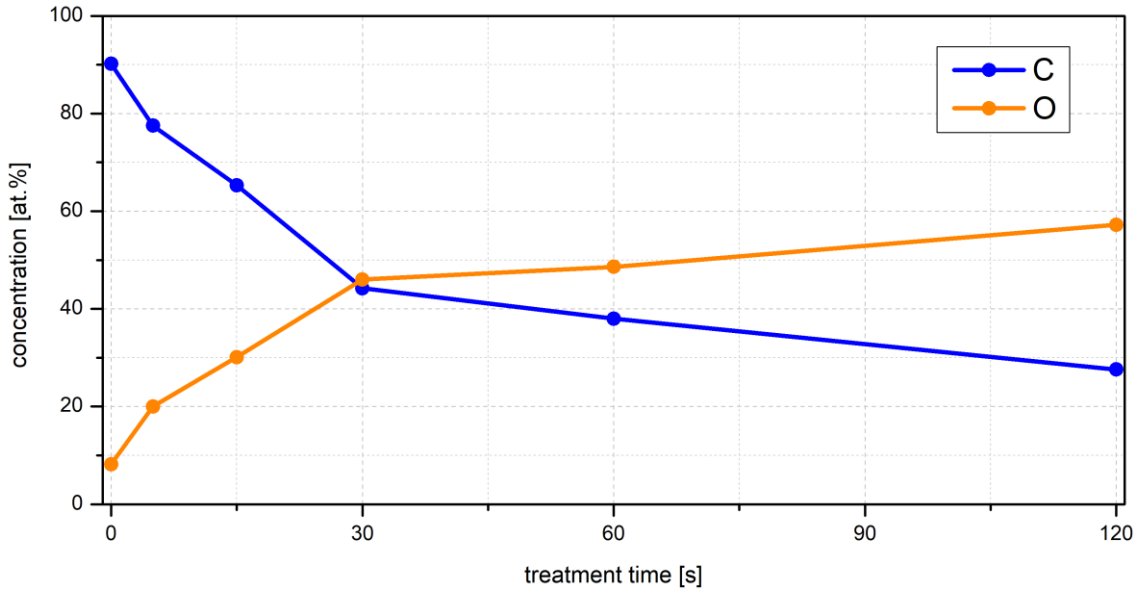

Figure 3.18: C and O concentration at the unpeeled garlic surface (protective leaf). Pilot-scale E-mode glow, $P_N = 200$ W, $p = 50$ Pa, $t = 0 - 120$ s.

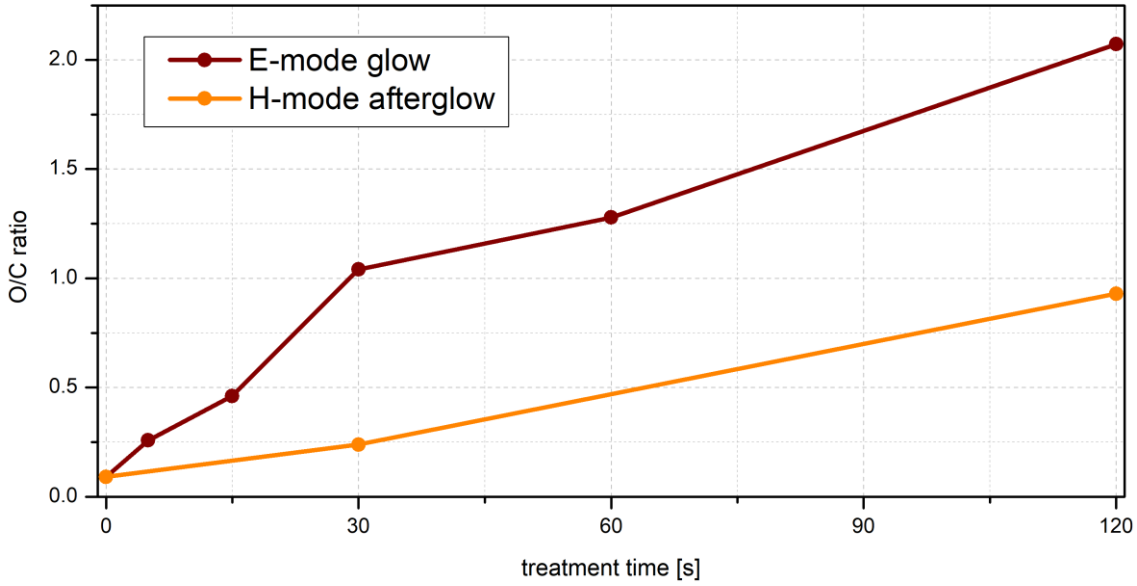

Figure 3.19: O/C ratio of unpeeled garlic (protective leaf). Pilot-scale plasma, $P_N = 200$ W, $p = 50$ Pa, $t = 0$ – 120 s, E-mode glow and H-mode afterglow treatments.

Surface concentrations of elements other than C and O are presented in Figure 3.20. These additional elements either appear at the surface with plasma treatment, or their content is increased, with the exception of nitrogen, which decreases with increased treatment time.

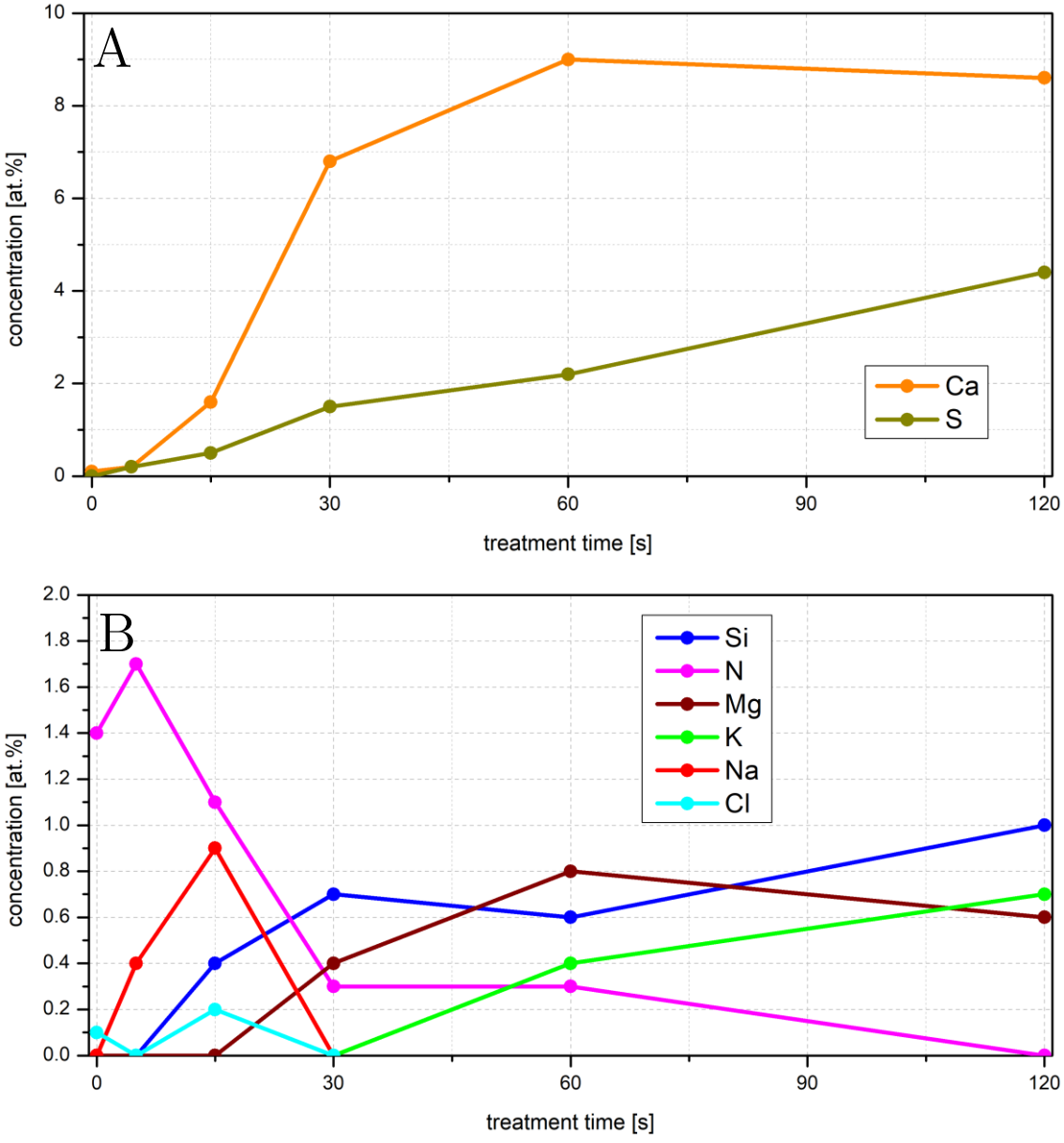

Figure 3.20: Minor elements concentration at the protective leaf surface. Pilot-scale E-mode glow, $P_N = 200$ W, $p = 50$ Pa, $t = 0 - 120$ s.

3.3.1.2.2 Pilot-scale H-mode afterglow treatment Unpeeled cloves were additionally treated in the pilot-scale plasma H-mode afterglow at different treatment conditions: $P_N = 300$ W, $p = 30$ Pa, $t = 0 – 60$ s. Surface elemental composition of the protective leaf is summarized in Table 3.3, and the O/C ratio is presented in Figure 3.21.

Table 3.3: Surface elemental composition [at.%] of unpeeled garlic, pilot-scale AG. $P_N = 300$ W, $p = 30$ Pa, $t = 0 – 60$ s.

t [s]	C	O	Ca	Si	N	K
0	96.9	3.1	/	/	/	/
15	75.8	21.4	0.6	1.5	0.7	/
30	77.4	20.4	0.5	0.9	0.8	/
45	77.9	19.4	/	0.5	2.3	/
60	56.0	39.7	1.2	0.6	1.9	0.6

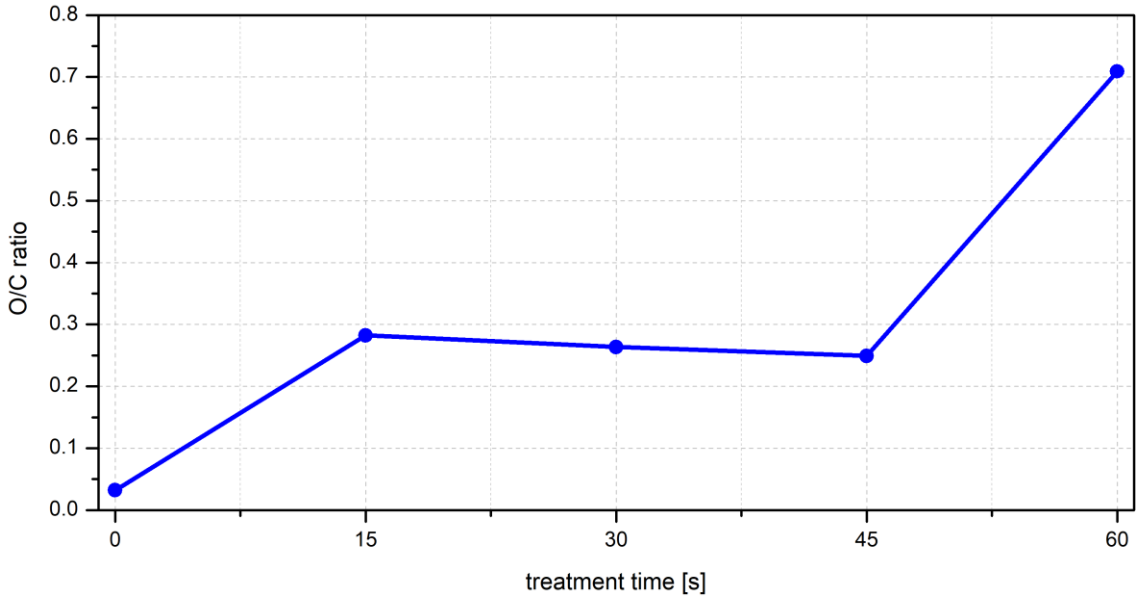

Figure 3.21: O/C ratio of unpeeled garlic, pilot-scale plasma AG. $P_N = 300$ W, $p = 30$ Pa, $t = 0 – 60$ s.

3.3.1.2.3 Pulsed treatment A pulsed treatment regimen was also applied to unpeeled cloves, with two glow treatment regimens: $P_N = 200$ W, $p = 70$ Pa, $t = 30$ s (6×5 s on, 5 s off), and $P_N = 300$ W, $p = 70$ Pa, $t = 60$ s (6×10 s on, 5 s off). Surface elemental composition of the protective leaf is summarized in Table 3.4, and the O/C ratio is presented in Figure 3.22. Not surprisingly, the O concentration and O/C ratio increases are higher in the treatment regimen with higher P_N and longer total treatment time. A variety of other elements appears prominently, in particular after the 300 W treatment regimen.

Table 3.4: Surface elemental composition [at.%] of unpeeled garlic, pulsed treatment. Pilot-scale glow plasma, pulsed treatment regimens: $P_N = 200$ W, $p = 70$ Pa, $t = 30$ s (6×5 s on, 5 s off), and $P_N = 300$ W, $p = 70$ Pa, $t = 60$ s (6×10 s on, 5 s off).

treatment	C	O	Ca	S	Si	Mg	N	K	F
untreated	93.9	4.7	/	/	0.8	/	0.6	/	/
200 W, 30 s	63.5	29.4	3.9	0.9	0.5	/	1.1	0.6	/
300 W, 60 s	44.3	43.6	4.2	2.0	1.4	1.6	0.7	1.3	1.0

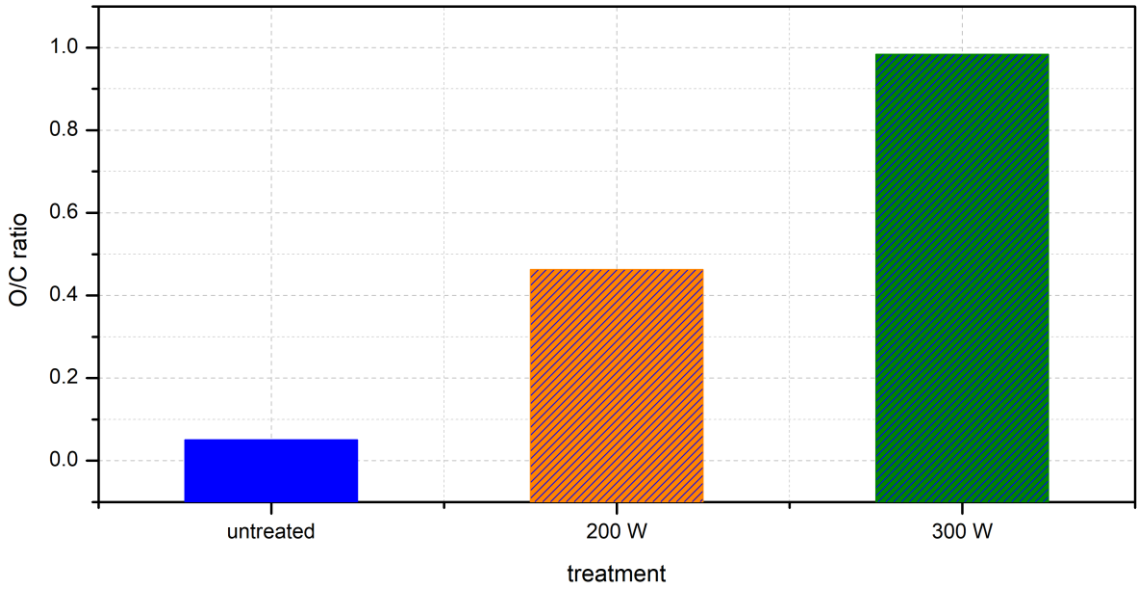

Figure 3.22: O/C ratio of unpeeled garlic, pilot-scale plasma, pulsed treatment. $P_N = 200$ W, $p = 70$ Pa, $t = 30$ s (6×5 s on, 5 s off), and $P_N = 300$ W, $p = 70$ Pa, $t = 60$ s (6×10 s on, 5 s off).

3.3.1.3 Clove surface

3.3.1.3.1 Pilot-scale plasma treatment Peeled cloves were treated in the pilot-scale E-mode glow plasma at P_N = 200 W, p = 50 Pa, t = 0 – 120 s. Surface elemental composition of the garlic clove surface is summarized in Table 3.5, the C and O concentrations are presented in Figure 3.23, and the O/C ratio is presented in Figure 3.24. Carbon content at the surface decreases, and oxygen content increases, with increased treatment time. The O/C ratio rises gradually. Further elements also appear at the surface with plasma treatment, as seen in Figure 3.25.

Table 3.5: Surface elemental composition [at.%] of peeled garlic, pilot-scale plasma. P_N = 200 W, p = 50 Pa, t = 0 – 120 s.

t [s]	C	O	Ca	S	Si	Mg	N	P	F
0	97.5	2.5	/	/	/	/	/	/	/
5	95.1	4.9	/	/	/	/	/	/	/
30	91.3	7.6	/	/	0.3	/	0.3	/	0.5
60	94.8	5.2	/	/	/	/	/	/	/
90	70.7	24.8	1.5	/	0.5	/	2	/	0.3
120	58.5	34.7	2.5	0.1	0.6	0.4	2.5	/	0.7

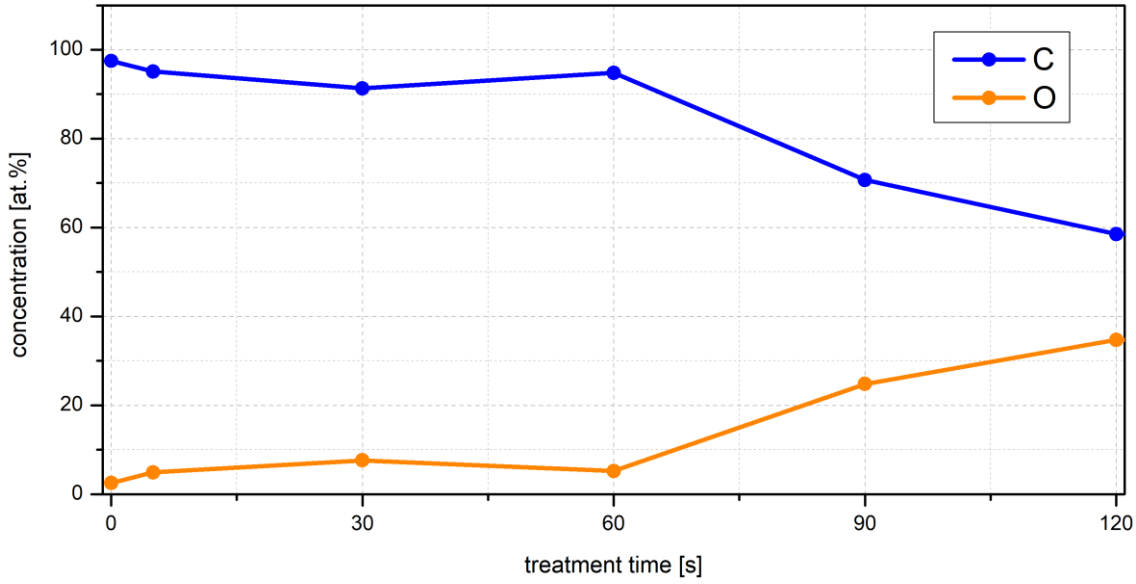

Figure 3.23: C and O concentration of peeled garlic (clove surface). Pilot-scale E-mode glow, P_N = 200 W, p = 50 Pa, t = 0 – 120 s.

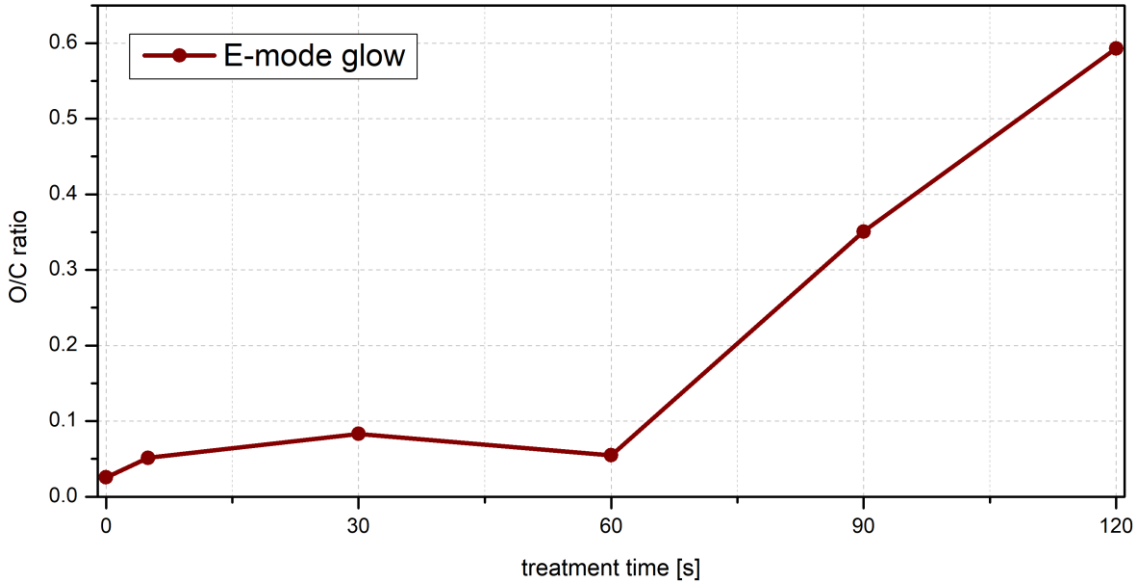

Figure 3.24: O/C ratio of peeled garlic (clove surface). Pilot-scale plasma, $P_N = 200$ W, $p = 50$ Pa, $t = 0$ – 120 s.

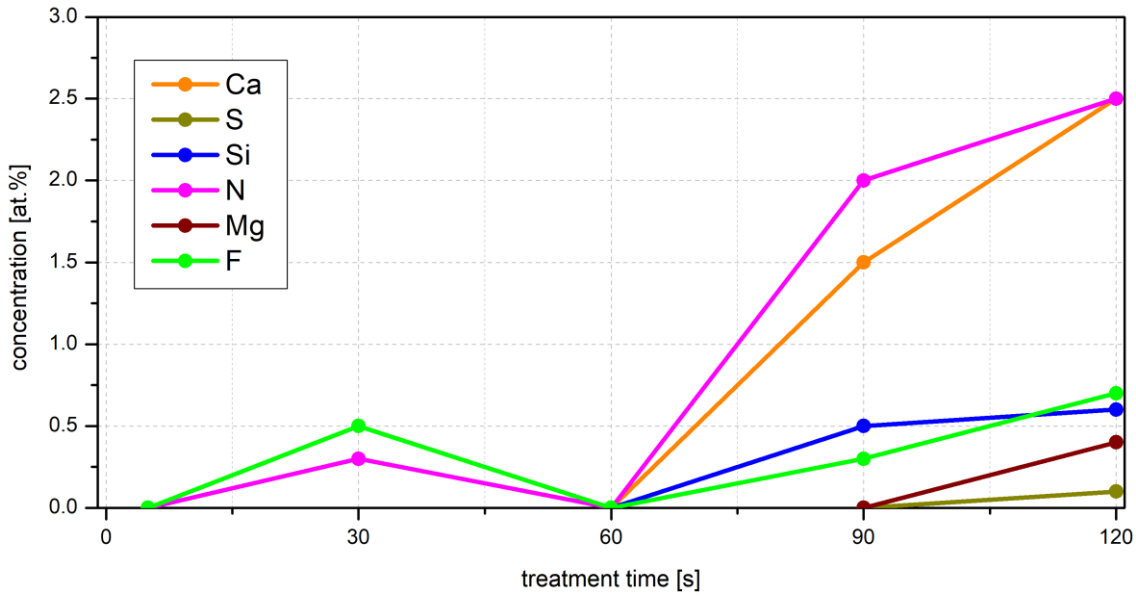

Figure 3.25: Minor elements concentration at the peeled clove surface. Pilot-scale E-mode glow, $P_N = 200$ W, $p = 50$ Pa, $t = 0$ – 120 s.

3.3.1.3.2 Industrial-scale plasma treatment Peeled cloves were additionally treated in the industrial-scale plasma at $P_N = \sim 700 - 900$ W, $p = 15 - 60$ Pa, $t = 60$ s. Surface elemental composition of the garlic clove surface is summarized in Table 3.6, and the O/C ratio is presented in Figure 3.26. The carbon and oxygen concentration changes at the surface are slight, just a few at.%, and follow no trend with treatment pressure. No elements other than C and O appear at the clove surface even after plasma treatment.

Table 3.6: Surface elemental composition [at.%] of peeled garlic, ind.-scale plasma. $P_N = \sim 700 - 900$ W, $p = 15 - 60$ Pa, $t = 60$ s.

treatment	C	O
N	97.8	2.2
60 Pa	93.8	6.2
45 Pa	94.9	5.1
30 Pa	92.2	7.8
15 Pa	94.7	5.3

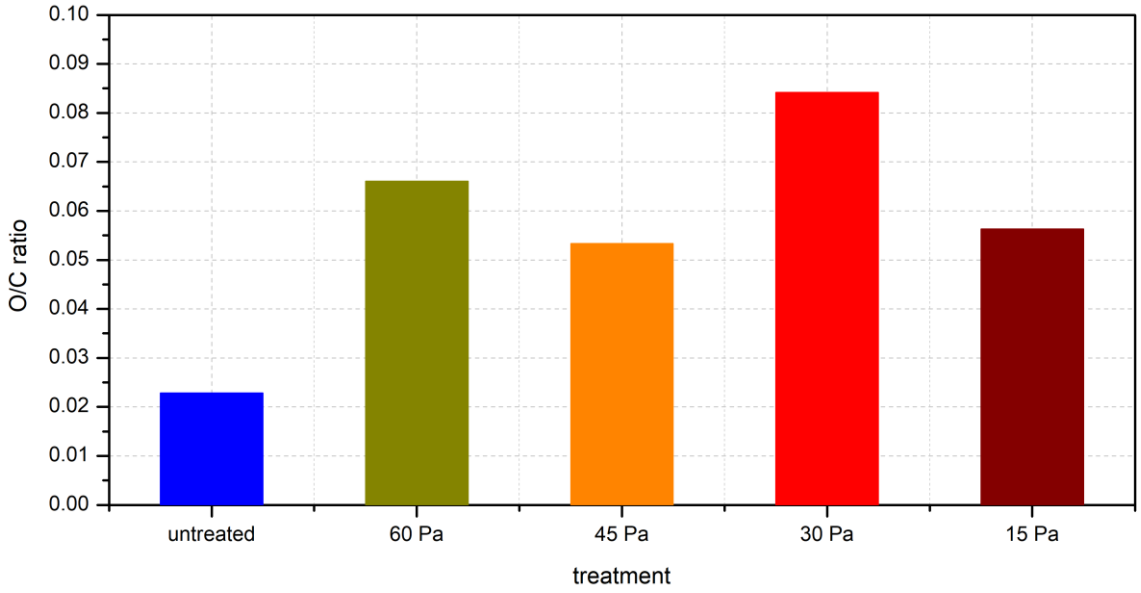

Figure 3.26: O/C ratio of peeled garlic, industrial-scale plasma. $P_N = \sim 700 - 900$ W, $p = 15 - 60$ Pa, $t = 60$ s.

3.3.1.3.3 Clove surface under the treated protective leaf In one experiment, an unpeeled clove was treated in the pilot-scale plasma. Then, its protective leaf was removed, and the clove surface under it was analyzed using XPS. The results and comparison with a peeled clove surface treated at the same conditions are presented in Table 3.7. Oxygen concentration at the surface increased only slightly, about 12 × less than when a peeled clove was treated directly.

Table 3.7: Surface elemental composition [at.%] and O/C ratio of the clove surface under the treated protective leaf. Comparison for clove surface, untreated and treated in the pilot-scale plasma system, either already peeled, or with the protective leaf removed before clove analysis. $P_N = 200$ W, $p = 50$ Pa, $t = 90$ s.

sample	C	O	Ca	Si	N	F	O/C ratio
untreated clove	97.5	2.5	/	/	/	/	**0.026**
peeled clove, 90 s	70.7	24.8	1.5	0.5	2	0.3	**0.351**
clove under treated prot. leaf, 90 s	95.1	4.3	/	0.6	/	/	**0.045**

3.3.1.4 High-resolution XPS spectra

3.3.1.4.1 Protective leaf Comparison of high-resolution C 1s spectra of the unpeeled clove (protective leaf) surface is shown in Figure 3.27. The area of sub-peaks corresponding to different chemical bonds is presented in Figure 3.28. It is seen that the area of the main sub-peak at ~ 284.8 eV, corresponding to C–C/C–H bonds, rapidly diminishes with increasing treatment time, up to including 30 s of treatment. Afterwards, the area of this peak slowly begins to increase again. Simultaneously, the area of the sub-peaks at ~ 286.1 eV for C–O bonds, ~ 287.5 eV for C=O bonds, and ~ 288.9 eV for O–C=O bonds increases within the first 15 – 60 seconds of treatment, and thereafter begins to gradually decrease again.

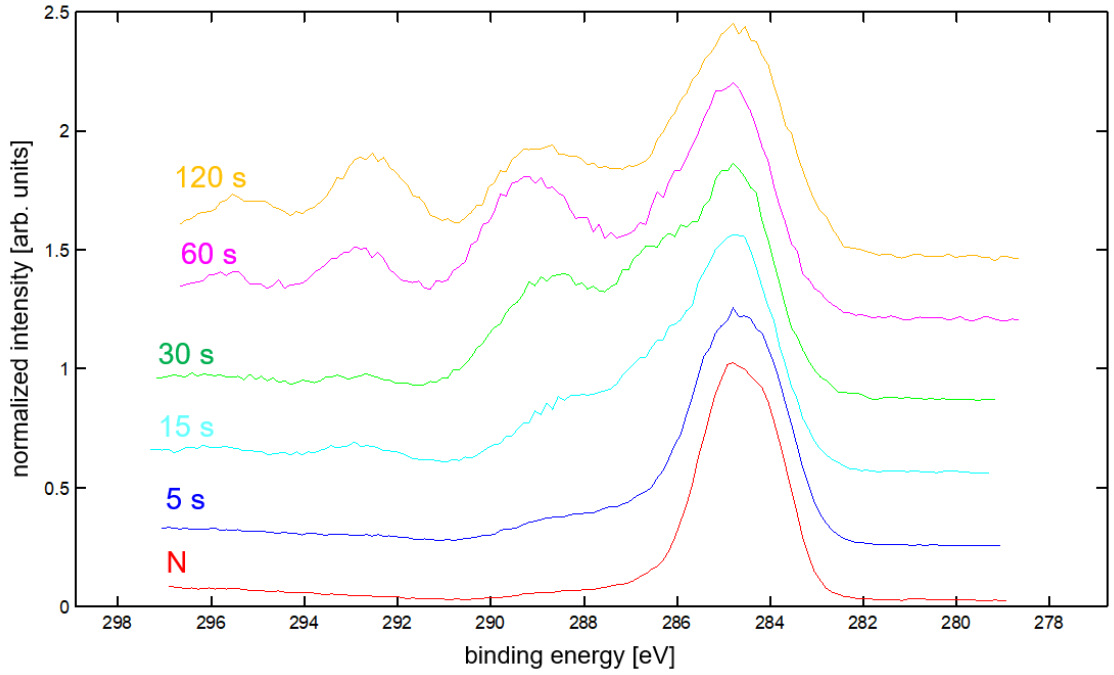

Figure 3.27: High-resolution C 1s spectra of unpeeled garlic. Pilot-scale E-mode glow, $P_N = 200$ W, $p = 50$ Pa, $t = 0$ – 120 s.

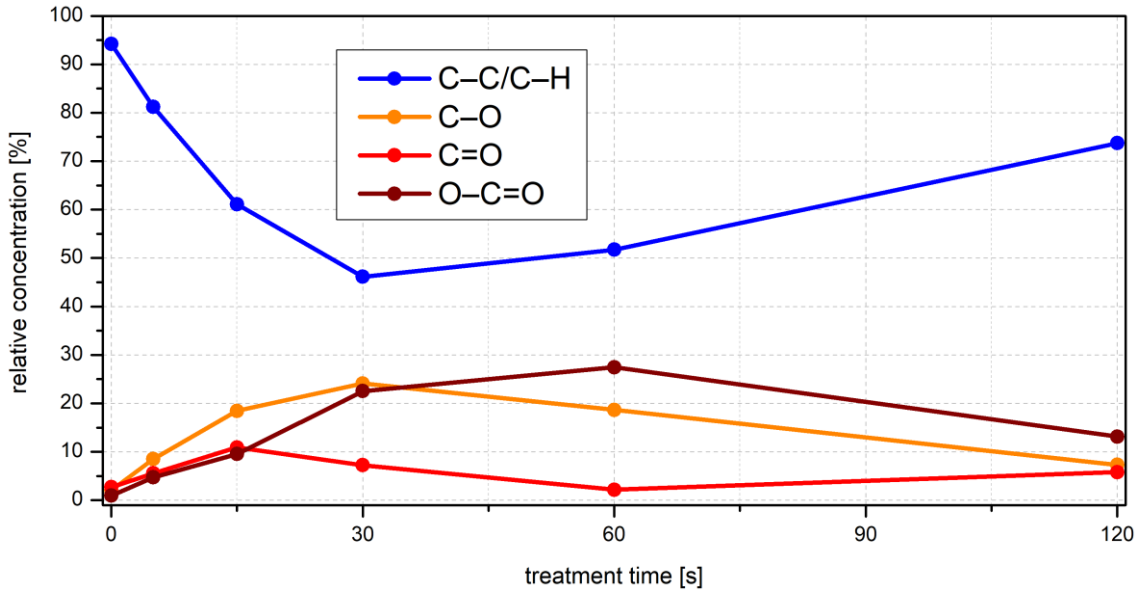

Figure 3.28: C 1s sub-peak area of unpeeled garlic. Pilot-scale E-mode glow, $P_N = 200$ W, $p = 50$ Pa, $t = 0 - 120$ s.

3.3.1.4.2 Clove surface Comparison of high-resolution C 1s spectra of the peeled clove surface is shown in Figure 3.29. The area of sub-peaks corresponding to different chemical bonds is presented in Figure 3.30. It is seen that the area of the main sub-peak at ~ 284.8 eV, corresponding to C–C/C–H bonds, diminishes with increasing treatment time, but more gradually than for unpeeled cloves. After 600 s of treatment, the area of this peak remains approximately the same. Simultaneously, the area of sub-peaks for C–O bonds very slowly decreases, while the areas of sub-peaks for C=O and O–C=O bonds increase up to 60 s. Thereafter, the presence of all listed bonds between C and O increases more rapidly up to 120 s of treatment.

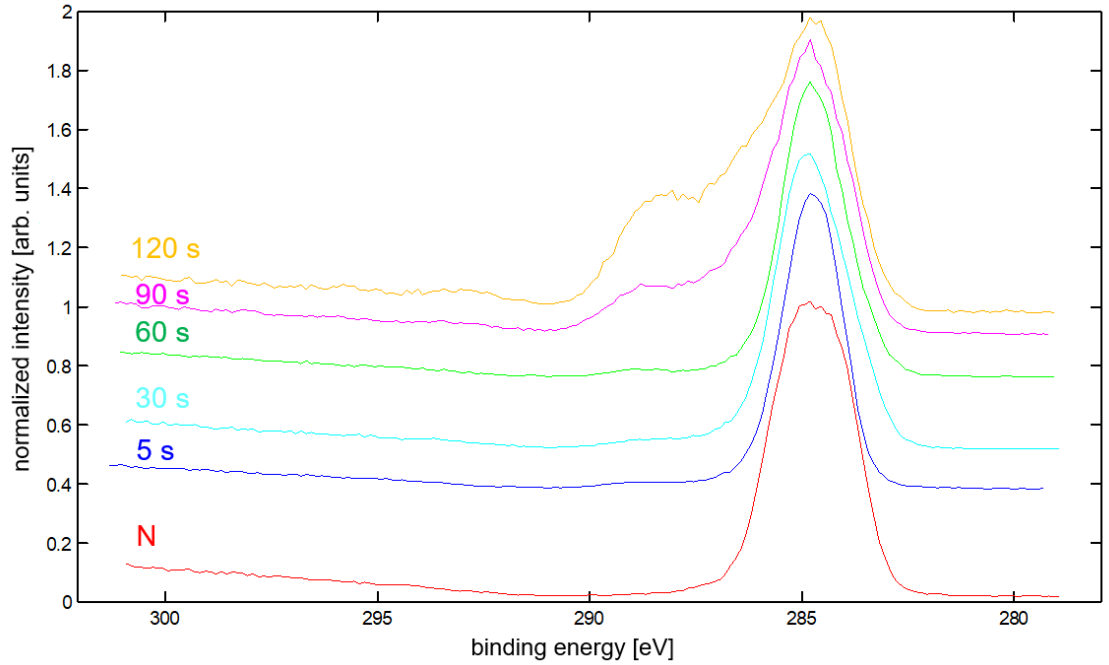

Figure 3.29: High-resolution C 1s spectra of peeled garlic. Pilot-scale E-mode glow, $P_N = 200$ W, $p = 50$ Pa, $t = 0 - 120$ s.

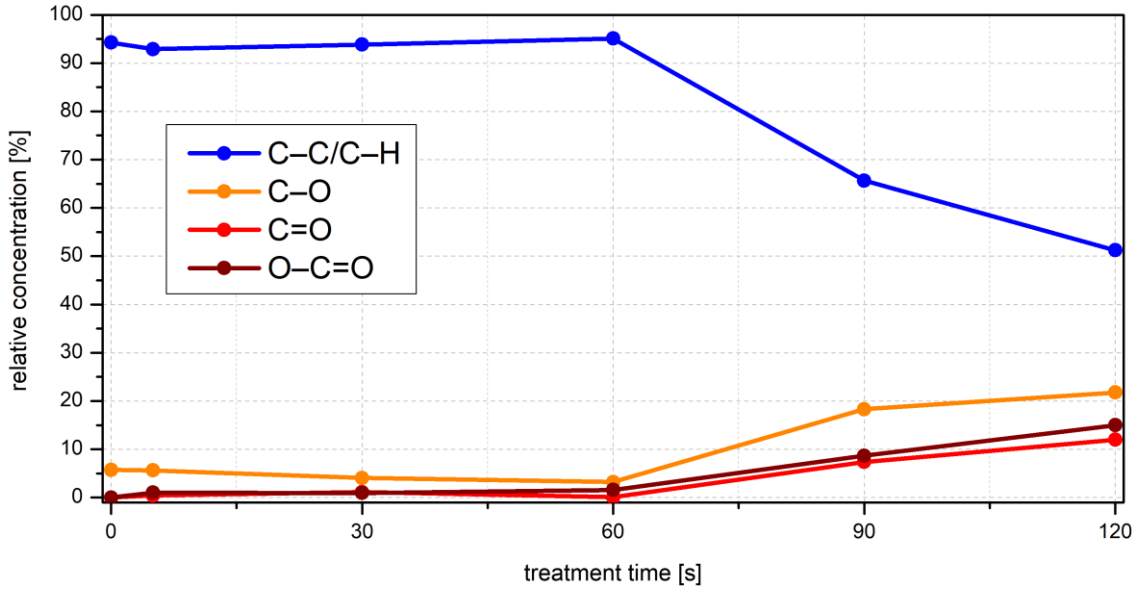

Figure 3.30: C 1s sub-peak area of peeled garlic. Pilot-scale E-mode glow, $P_N = 200$ W, $p = 50$ Pa, $t = 0 - 120$ s.

3.3.2 ATR-FTIR spectra

3.3.2.1 Untreated surfaces

Figure 3.31 shows a comparison of ATR-FTIR spectra for untreated surfaces of the protective leaf and the peeled clove. The protective leaf surface shows a much more prominent peak at ~ 3300 cm^{-1}, corresponding to the alcohol O–H stretching. On the other hand, the untreated clove surface has intense peaks at ~ 2850 and 2920 cm^{-1}, which are much less prominent on the protective leaf surface. These peaks correspond to C–H stretching in alkanes. Further differences in the spectra begin at ~ 1750 cm^{-1}, but are addressed below, or in the Discussion.

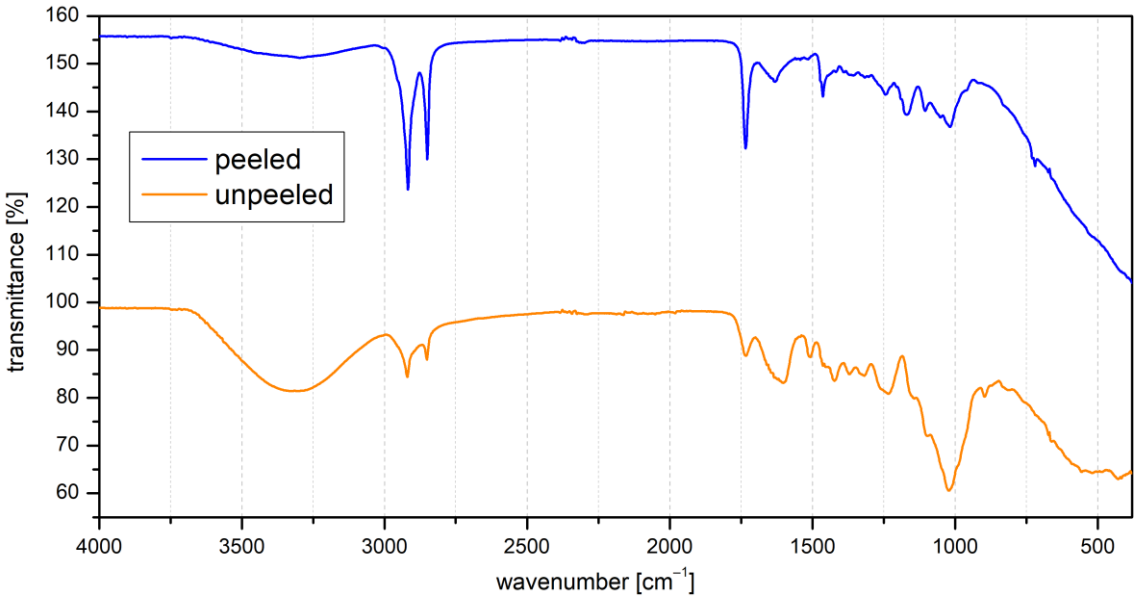

Figure 3.31: ATR-FTIR spectra of untreated surfaces, peeled and unpeeled clove.

3.3.2.2 Unpeeled clove surface treatment

Figure 3.32 shows a comparison of ATR-FTIR spectra for untreated and treated surfaces of the unpeeled clove (protective leaf). At both treatment powers, the intensity of C–H peaks at ~ 2920 and 2850 cm^{-1} diminishes with increasing treatment time. The sharp peaks become undistinguishable from the broader peak below; this happens at $t = 60$ s for $P_N = 200$ W, but already at $t = 15$ s for $P_N = 300$ W. At the same time, the O–H peak at ~ 3300 cm^{-1} remains relatively unchanged.

A peak at 1600 cm^{-1} is notably lessened at a treatment time of 120 s. It most likely represents the unsaturated C=C bonds present in the cuticular waxes, the composition of which may change with cuticle depth [64].

For all treatment times at both 200 and 300 W, the fingerprint region is completely comparable between untreated and plasma-treated protective leaf. As additionally shown in Figure 3.33, the spectra at 200 and 300 W are virtually identical at $t = 120$ s.

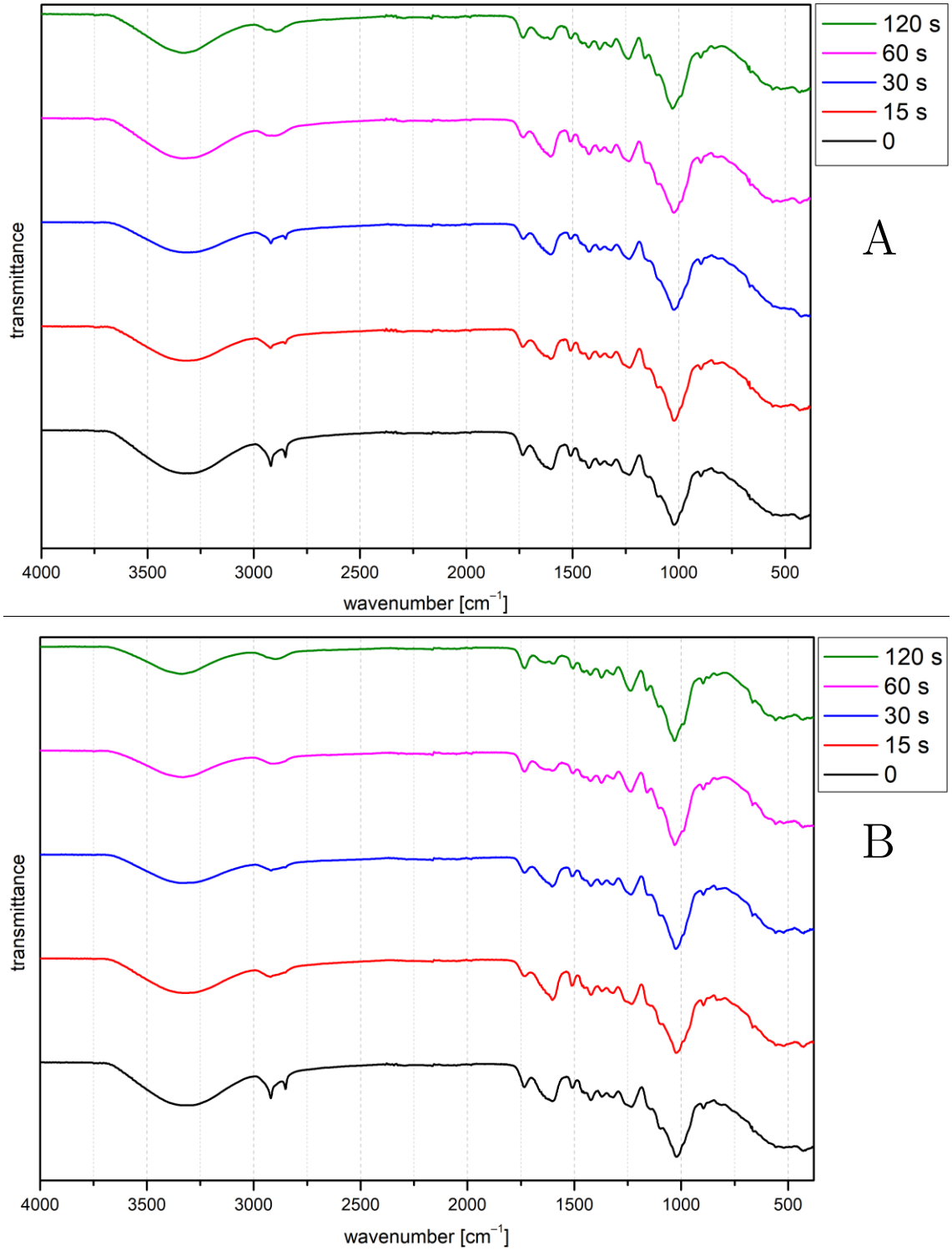

Figure 3.32: ATR-FTIR spectra, unpeeled clove. Pilot-scale E-mode glow, (A) $P_N = 200$ W, (B) $P_N = 300$ W, $p = 50$ Pa, t = 0 – 120 s.

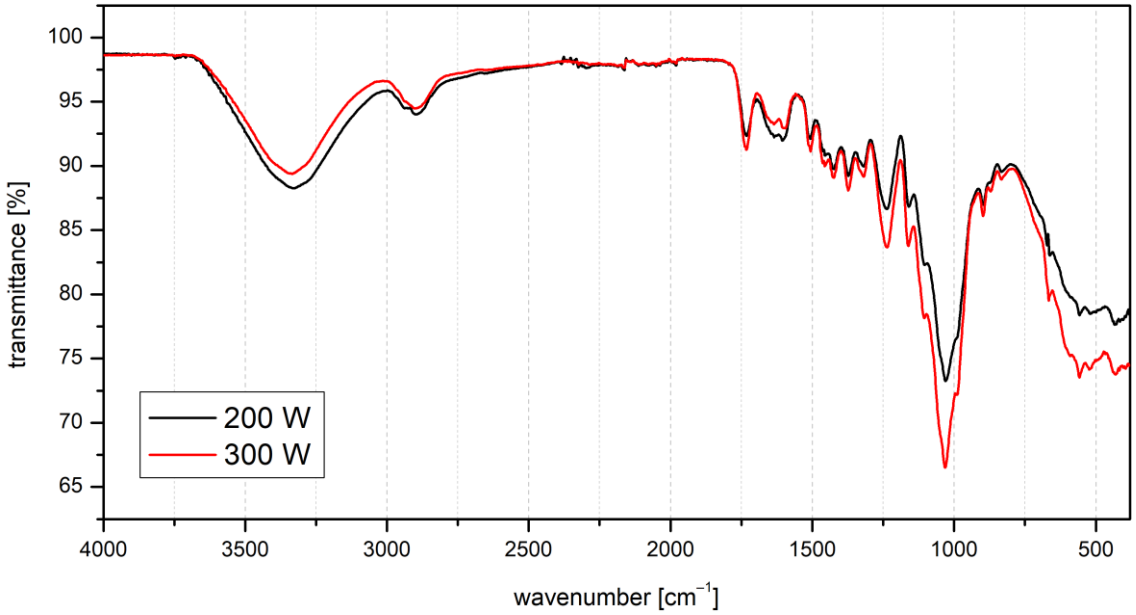

Figure 3.33: ATR-FTIR spectra, unpeeled clove, direct comparison. Pilot-scale E-mode glow, $P_N = 200 - 300$ W, $p = 50$ Pa, $t = 120$ s.

3.3.2.3 Peeled clove surface treatment

Figure 3.34 shows a comparison of ATR-FTIR spectra for untreated and treated surfaces of the peeled clove. At both treatment powers (Figure 3.34), the intensity of C–H peaks at ~ 2920 and 2850 cm^{-1} diminishes with increasing treatment time, but only after t = 60 s. After 60 s, this process appears faster for $P_N = 300$ W. The O–H peak at ~ 3300 cm^{-1} is barely noticeable on the untreated clove spectrum, but becomes more prominent with increasing treatment time.

A sharp peak at ~ 1730 cm^{-1} falls with increasing treatment time, while a slightly broader peak at ~ 1630 cm^{-1} rises. The first belongs to C=O bonds, while the second may belong to the alkene C=C bond.

The fingerprint region appears comparable between untreated and plasma-treated clove surface for short treatment times. Changes first appear at $t = 120$ s for $P_N = 200$ W, as well as at $t = 60$ s for $P_N = 300$ W. The differences in the spectra at 200 and 300 W for a treatment time of 120 s are further shown in Figure 3.35.

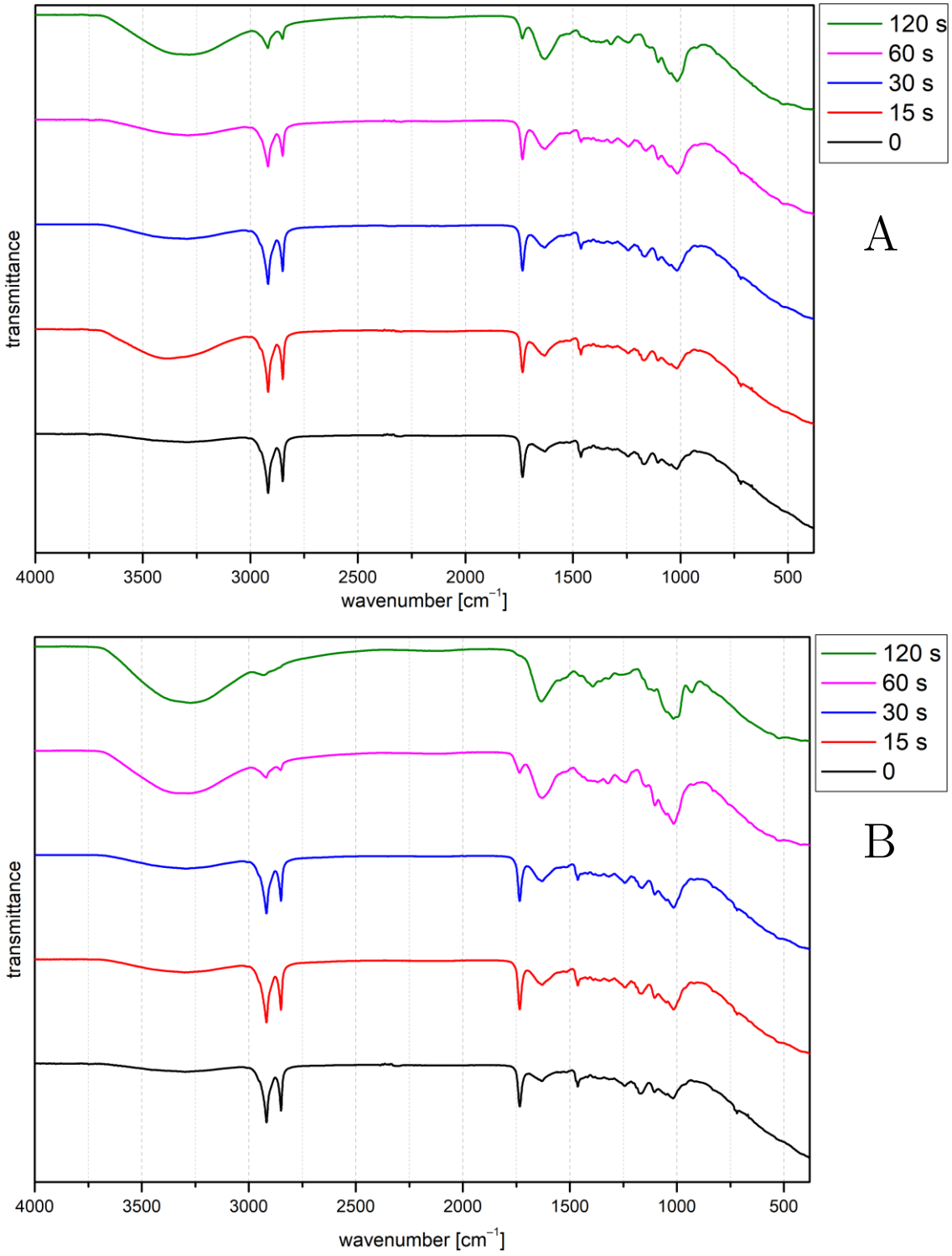

Figure 3.34: ATR-FTIR spectra, peeled clove. Pilot-scale E-mode glow, (A) $P_N = 200$ W, (B) $P_N = 300$ W, $p = 50$ Pa, $t = 0 - 120$ s.

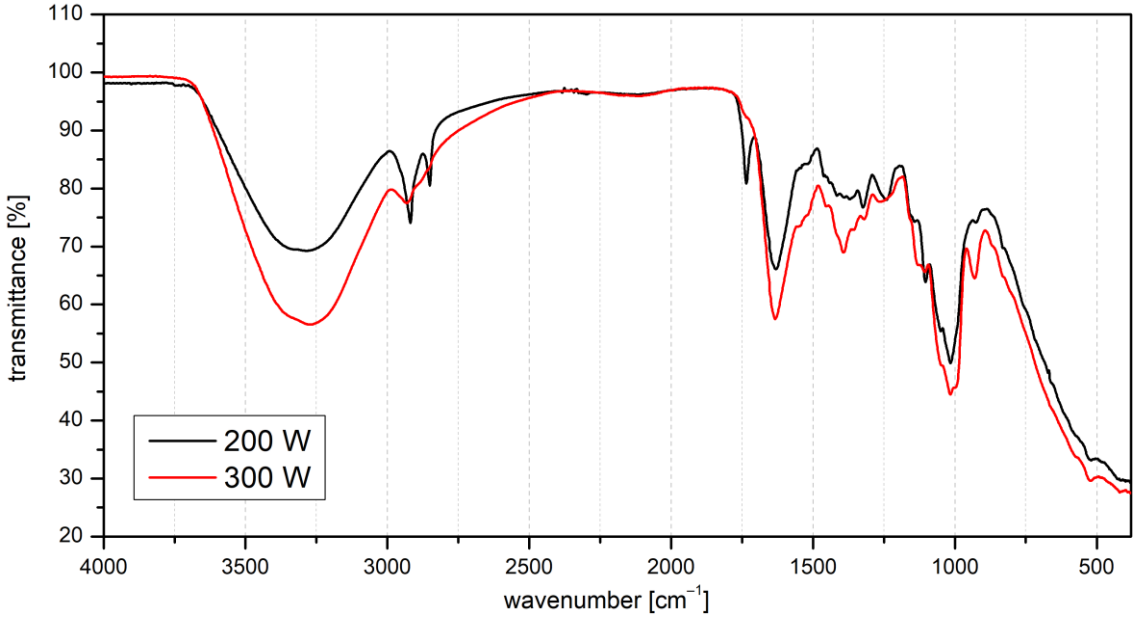

Figure 3.35: ATR-FTIR spectra, peeled clove, direct comparison. Pilot-scale E-mode glow, $P_N = 200 - 300$ W, $p = 50$ Pa, $t = 120$ s.

3.4 Surface Morphology

3.4.1 Scanning electron microscopy

3.4.1.1 Protective leaf

SEM images of untreated and plasma treated protective leaf surfaces are presented in Figure 3.36 – Figure 3.38 below. Increasing surface roughness is apparent with increasing treatment time and/or P_N.

3.4.1.1.1 Pilot-scale glow plasma treatment

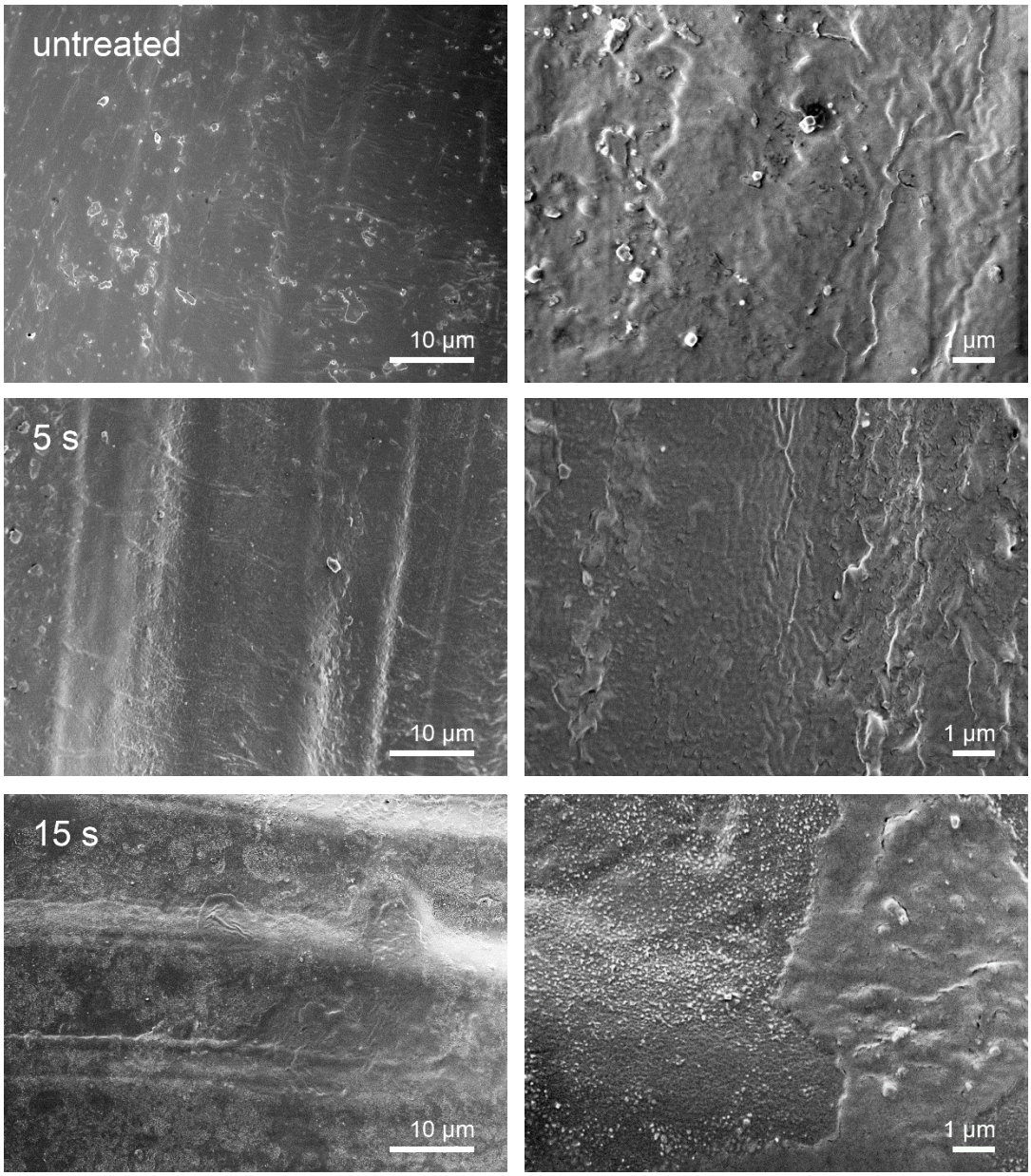

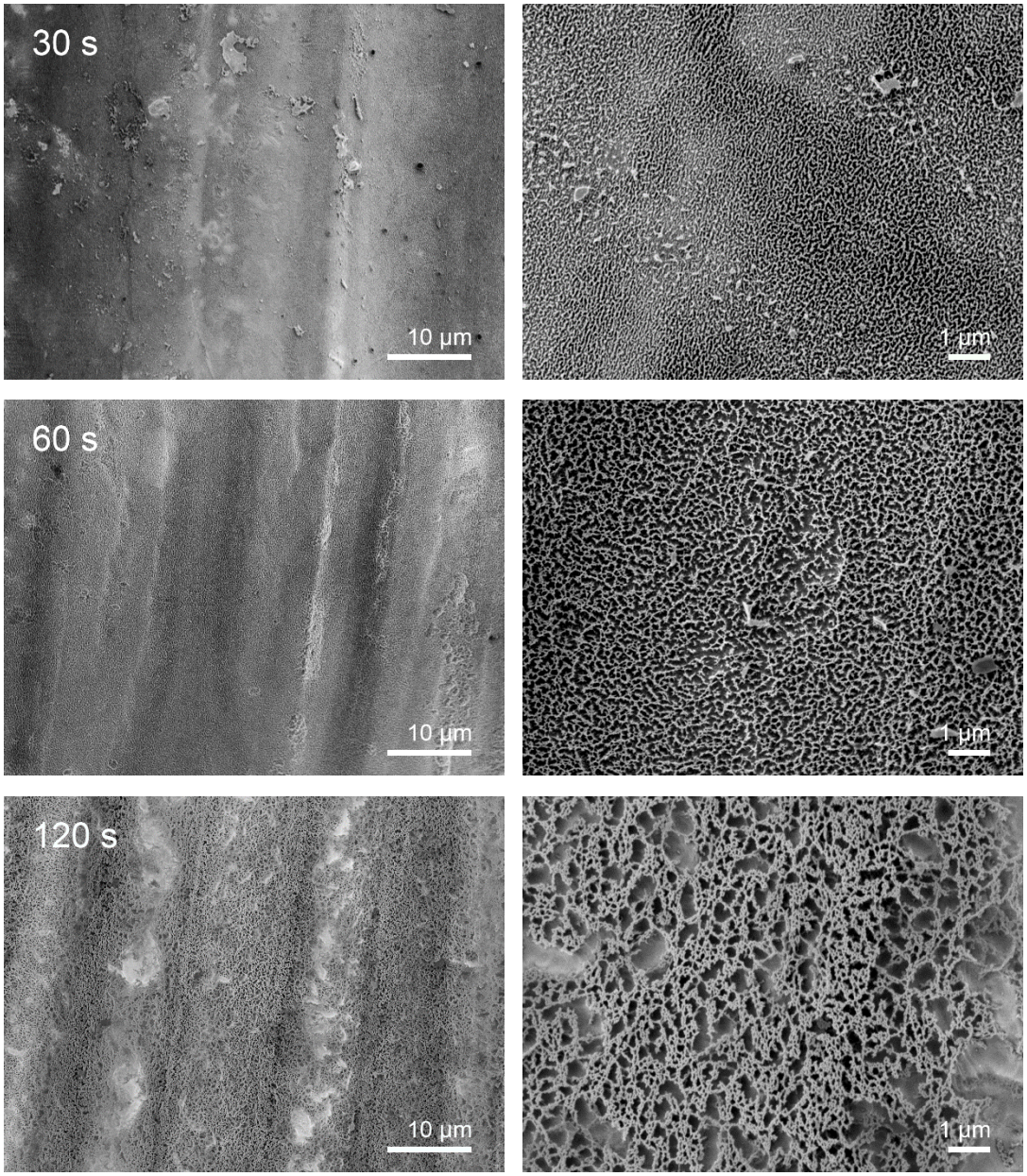

Figure 3.36: SEM images, unpeeled garlic, pilot-scale E-mode glow. P_N = 200 W, p = 50 Pa, t = 0 – 120 s. Top to bottom: untreated, 5 s, 15 s, 30 s, 60 s, 120 s. Taken at 2,000 × (left) and 10,000 × (right) magnification.

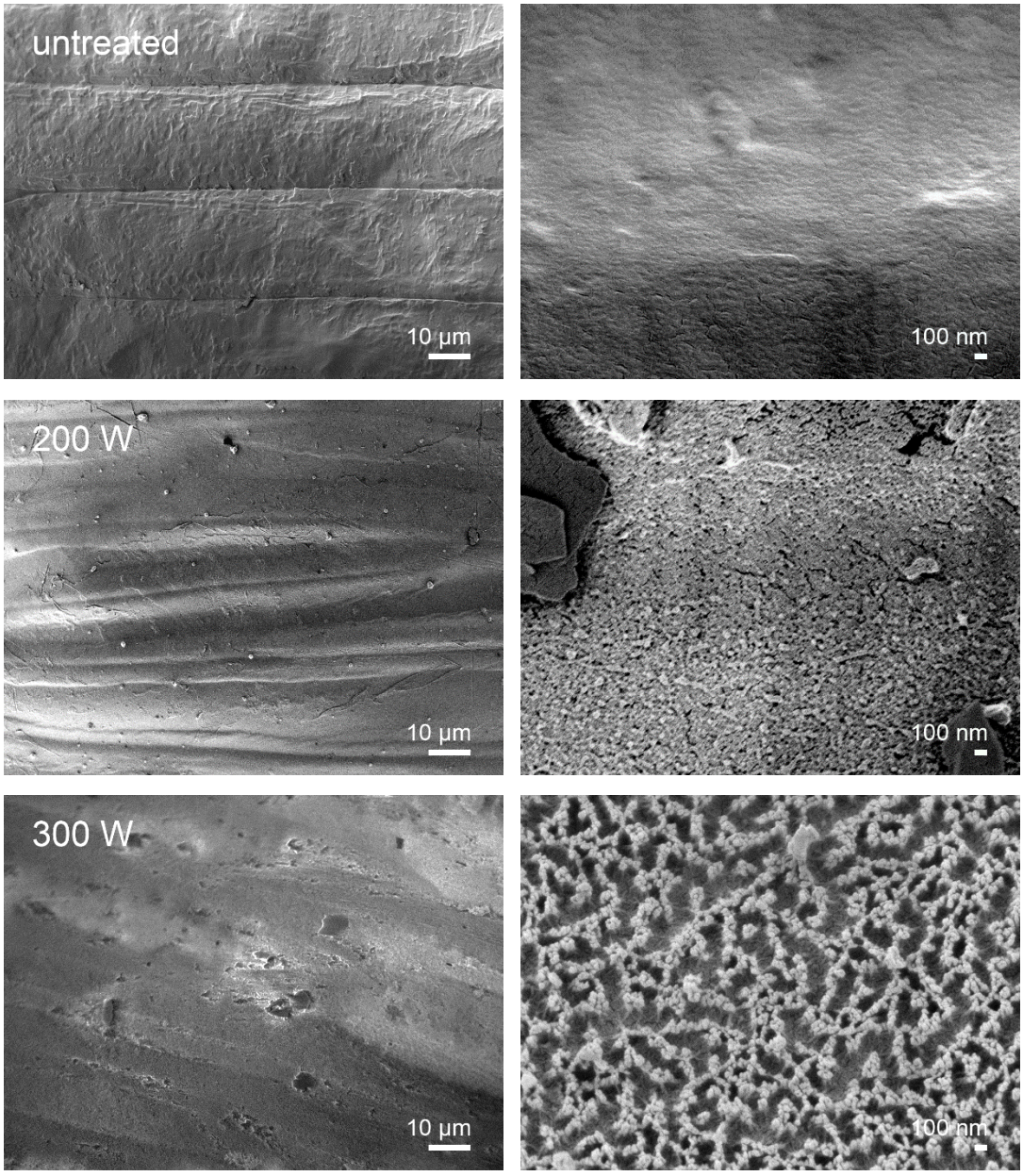

Figure 3.37: SEM images, unpeeled garlic, pilot-scale E-mode glow, pulsed treatment. Untreated; (200 W) P_N = 200 W, p = 70 Pa, t = 30 s (6 × 5 s on, 5 s off); (300 W) P_N = 300 W, p = 70 Pa, t = 60 s (6 × 10 s on, 5 s off). Taken at 1,000 × (left) and 30,000 × (right) magnification.

3.4.1.1.2 Pilot-scale afterglow plasma treatment

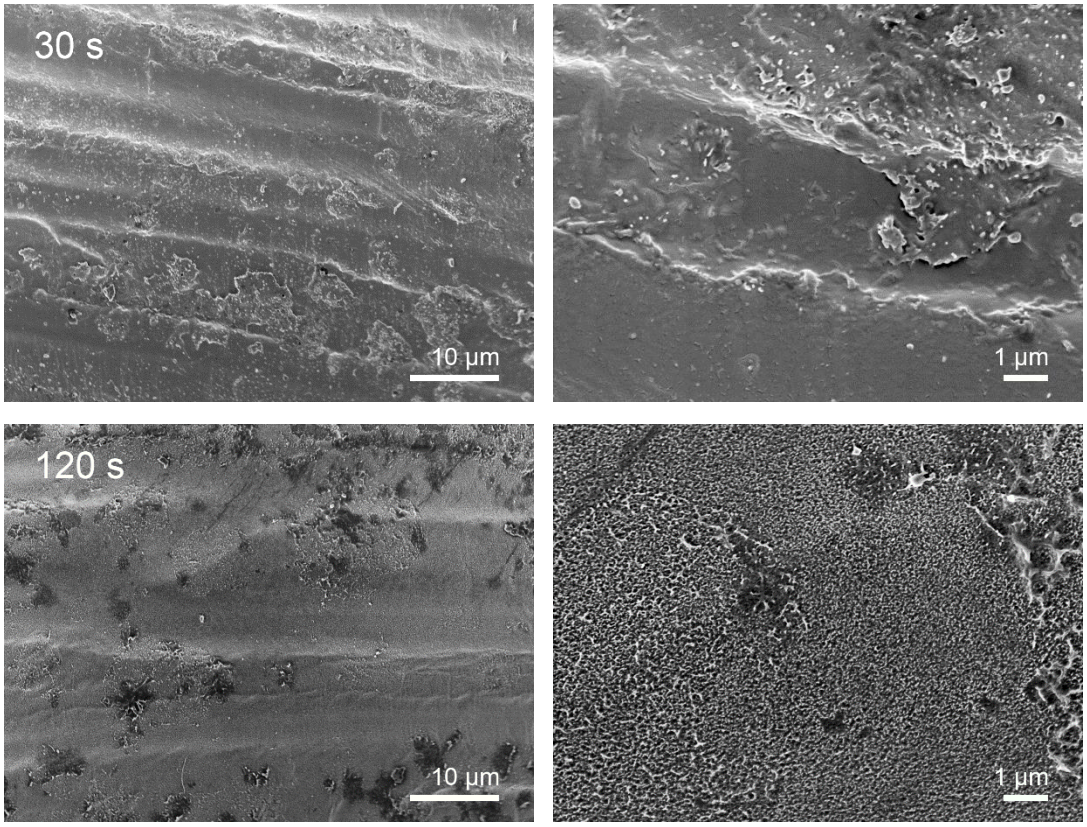

Figure 3.38: SEM images, unpeeled garlic, pilot-scale H-mode afterglow. P_N = 200 W, p = 50 Pa, t = 30 s, 120 s. Taken at 2,000 × (left) and 10,000 × (right) magnification.

Additional pilot-scale H-mode afterglow SEM images of unpeeled garlic, taken after different treatment conditions, are found in Figure 5.1 in Appendix A.

3.4.1.2 Clove surface

SEM images of untreated and plasma-treated clove surfaces are presented in Figure 3.39 below. After as little as 5 s of treatment, waxy structures appear at the clove surface. Their number and density changes with increasing plasma treatment time, followed by additional complete restructuring.

Additional SEM images of peeled garlic, taken after industrial-scale plasma treatment, are found in Figure 5.2 in Appendix A.

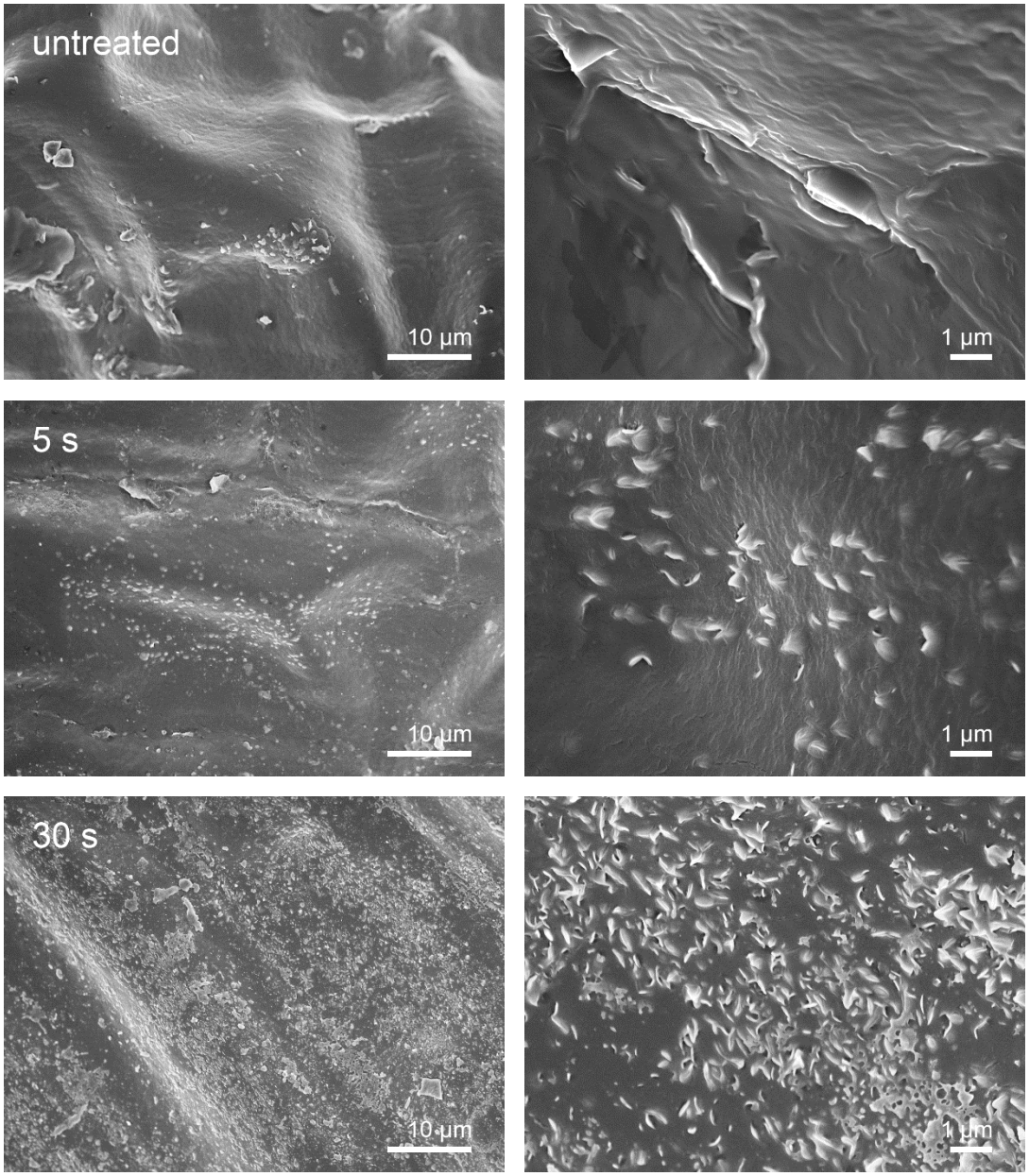

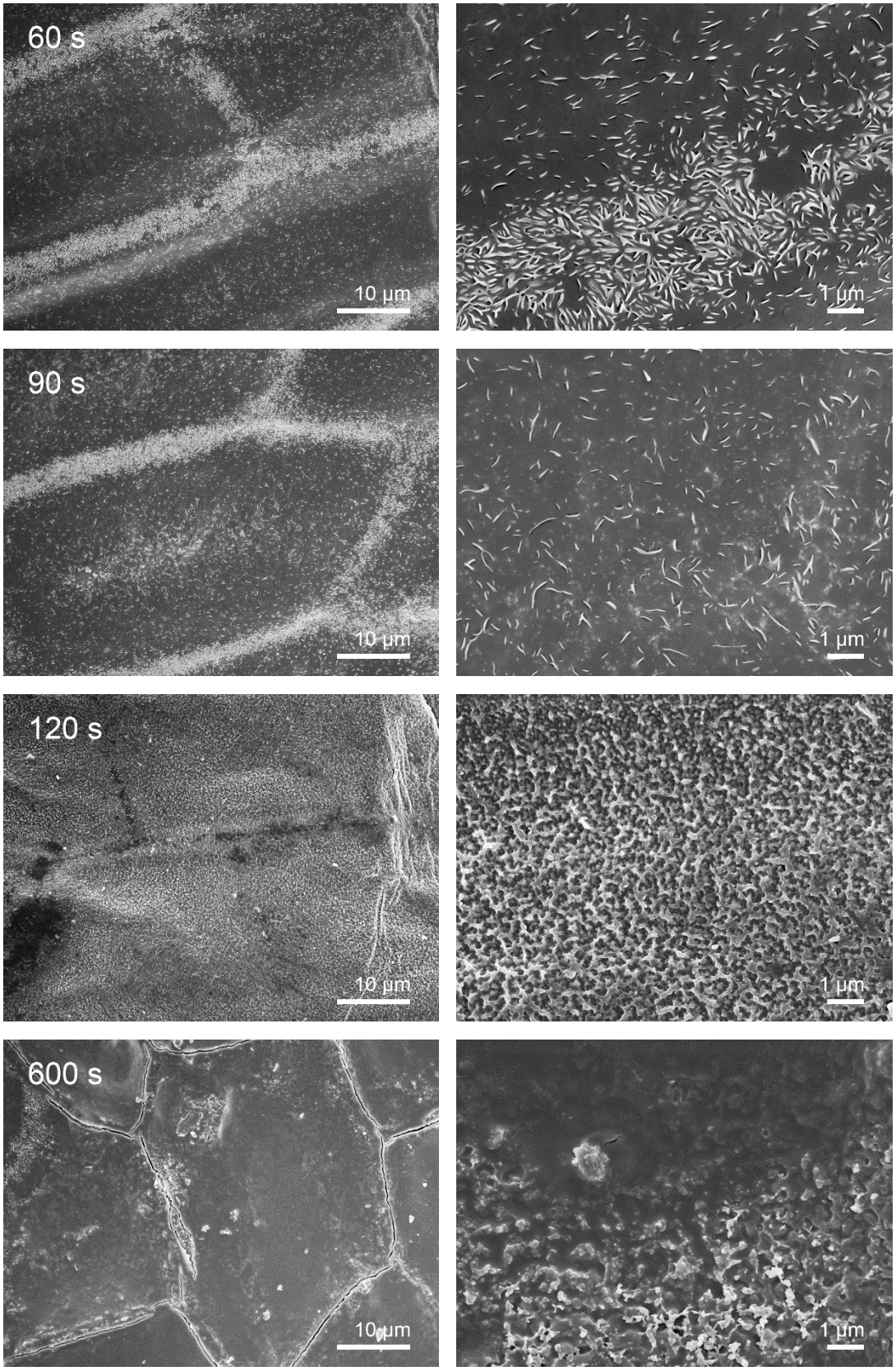

Figure 3.39: SEM images, peeled garlic, pilot-scale E-mode glow. $P_N = 200$ W, $p = 50$ Pa, $t = 0$ – 600 s. Top to bottom: untreated, 5 s, 30 s, 60 s, 90 s, 120 s, 600 s. Taken at 2,000 × (left) and 10,000 × (right) magnification.

3.4.2 Atomic force microscopy

3.4.2.1 Protective leaf

AFM images of untreated and plasma-treated protective leaf surfaces are presented in Figure 3.40 below. Increasing surface roughness is apparent with increasing treatment time and/or P_N.

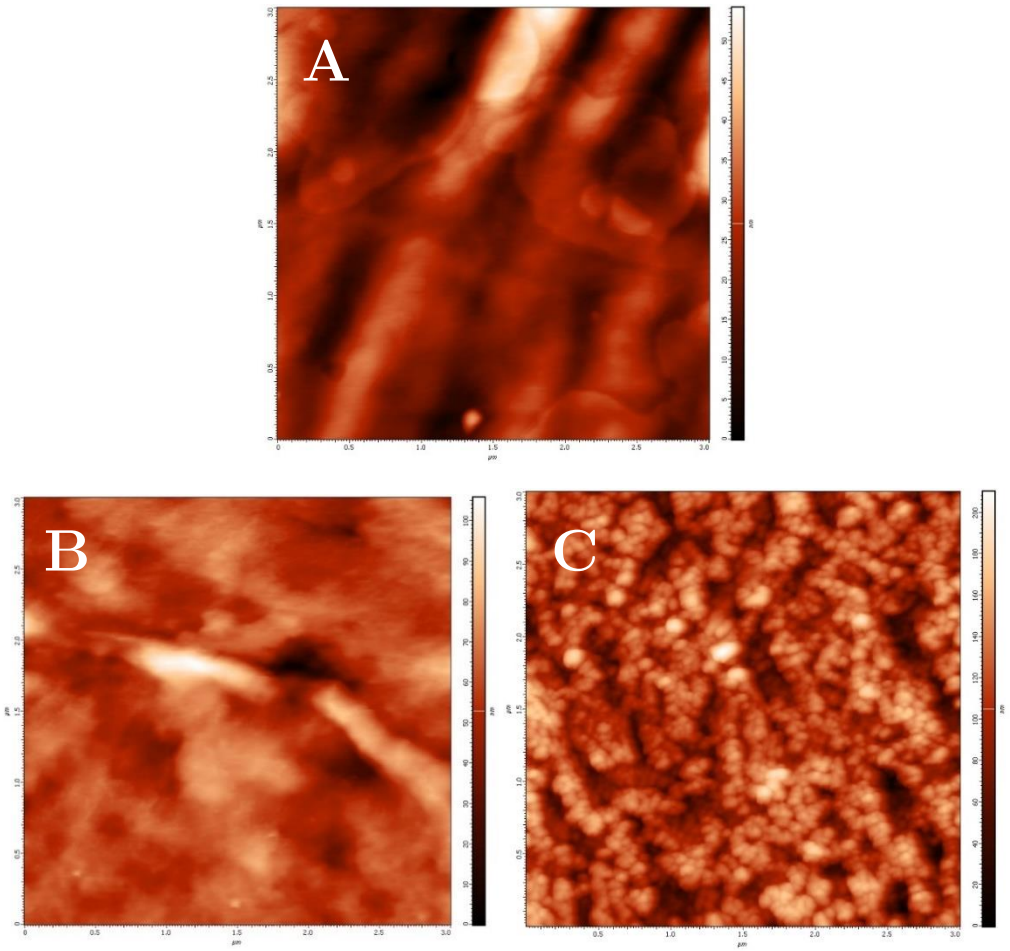

Figure 3.40: AFM images, unpeeled garlic, pilot-scale E-mode glow, pulsed treatment. (A) untreated; (B) $P_N = 200$ W, $p = 70$ Pa, $t = 30$ s (6 × 5 s on, 5 s off); (C) $P_N = 300$ W, $p = 70$ Pa, $t = 60$ s (6 × 10 s on, 5 s off). Analysis area: 3 × 3 µm.

3.4.2.2 Clove surface

AFM images of untreated and plasma-treated peeled clove surfaces are presented in Figure 3.41 below. After industrial-scale plasma treatment, roughness of the surface noticeably increases. Waxy structures, as seen in SEM images (Figure 3.39, Figure 5.2) are also visible at the sample surface (Figure 3.41 (E)).

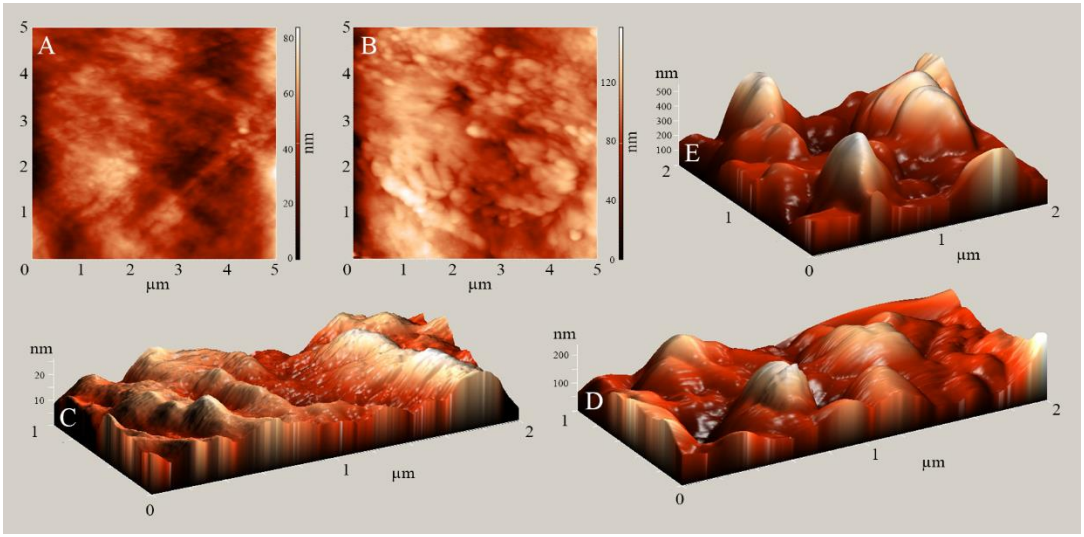

Figure 3.41: AFM images, peeled garlic, industrial-scale treatment. (A, C) untreated; (B, D, E) $P_N = \sim 800$ W, $p = 30$ Pa, $t = 60$ s. Analysis area: (A, B) 5 × 5 µm, (C, D) 2 × 1 µm, (E) 2 × 2 µm.

3.5 Water Contact Angle

WCA measurement results are presented in Figure 3.42. It is apparent that the WCA of the untreated protective leaf as well as the untreated clove surface is comparable, around 100°. With increasing plasma treatment time, the WCA decreases, as the surface gradually becomes more hydrophilic.

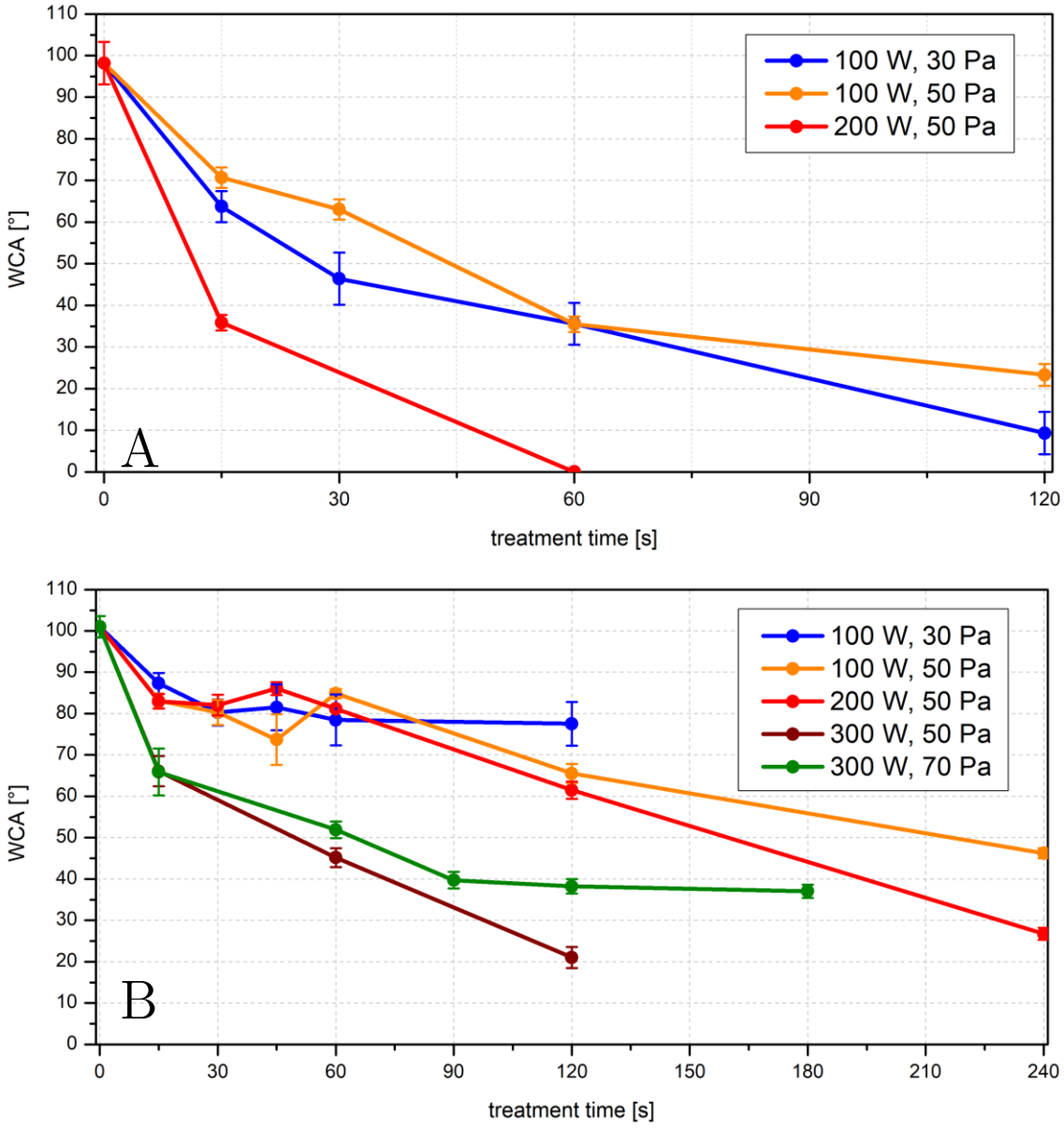

Figure 3.42: WCA on the surface of (A) unpeeled and (B) peeled garlic. Pilot-scale E-mode glow, $P_N = 100 - 300$ W, $p = 30 - 70$ Pa, $t = 0 - 240$ s. The error bars represent standard error.

3.6 Water Uptake

3.6.1 Untreated cloves

Figure 3.43 presents the WU of untreated cloves, peeled and unpeeled, when soaked in DI water.

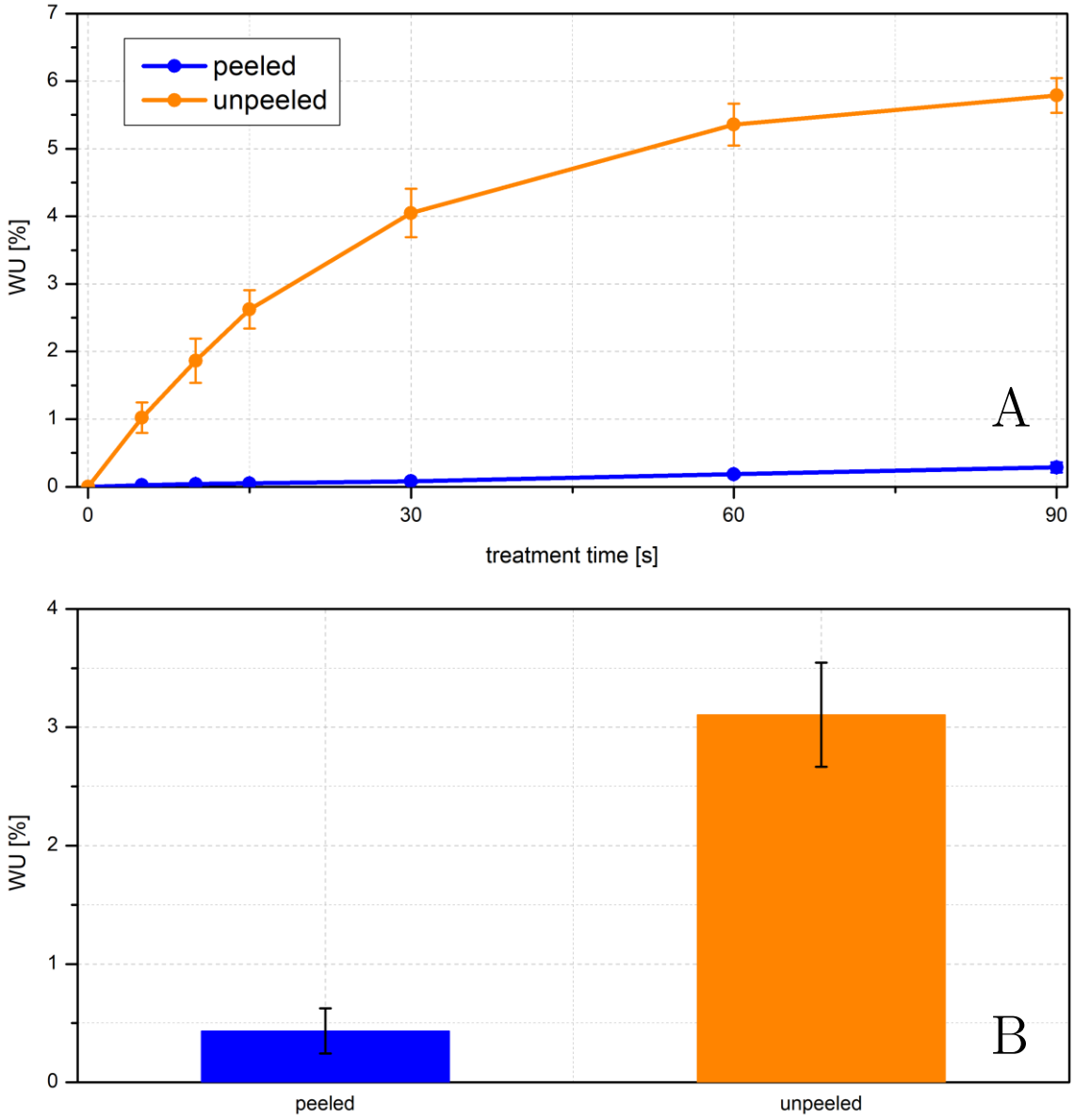

Figure 3.43: WU of untreated cloves, peeled and unpeeled. Results from two separate experiments: (A) after soaking for up to 90 minutes; (B) after soaking for 10 minutes. The error bars represent standard error.

3.6.2 Industrial-scale plasma

Preliminary tests regarding WU were carried out in the industrial-scale plasma system. Figure 3.44 and Figure 3.45 show the WU after treatment of unpeeled and peeled garlic cloves, respectively, in the industrial-scale plasma, followed by soaking in DI water for increasing amounts of time. The WU is calculated from the clove mass after plasma treatment (immediately before soaking). It is evident that the WU significantly increases after plasma treatment for both unpeeled and peeled cloves. In particular, as seen in Figure 3.45, the WU of plasma-treated peeled cloves increases much more drastically with increased soaking time compared to untreated peeled cloves. In the case of unpeeled cloves, the WU is accelerated for shorter soaking times, and then reaches a level comparable to untreated cloves after 60 minutes of soaking.

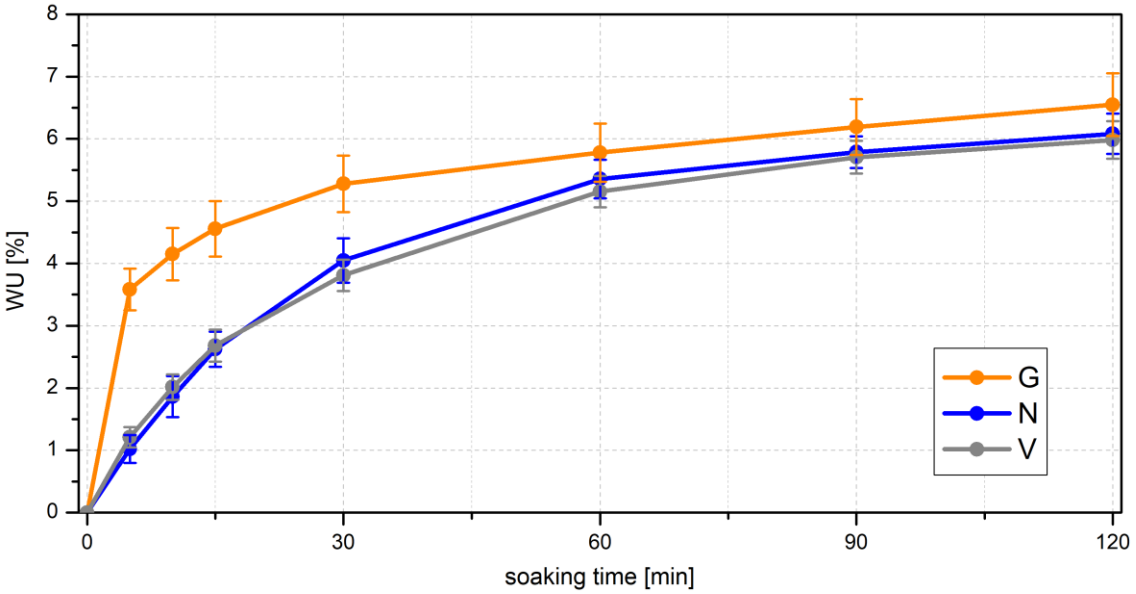

Figure 3.44: WU of unpeeled garlic cloves treated in the industrial-scale plasma. $P_N = \sim 800$ W, $p = 30$ Pa, $t = 45$ s, soaking in DI water for specified amounts of time. The same cloves were weighted each time and returned to soaking until the next measurement. G = glow plasma treatment; N = untreated control; V = vacuum control.

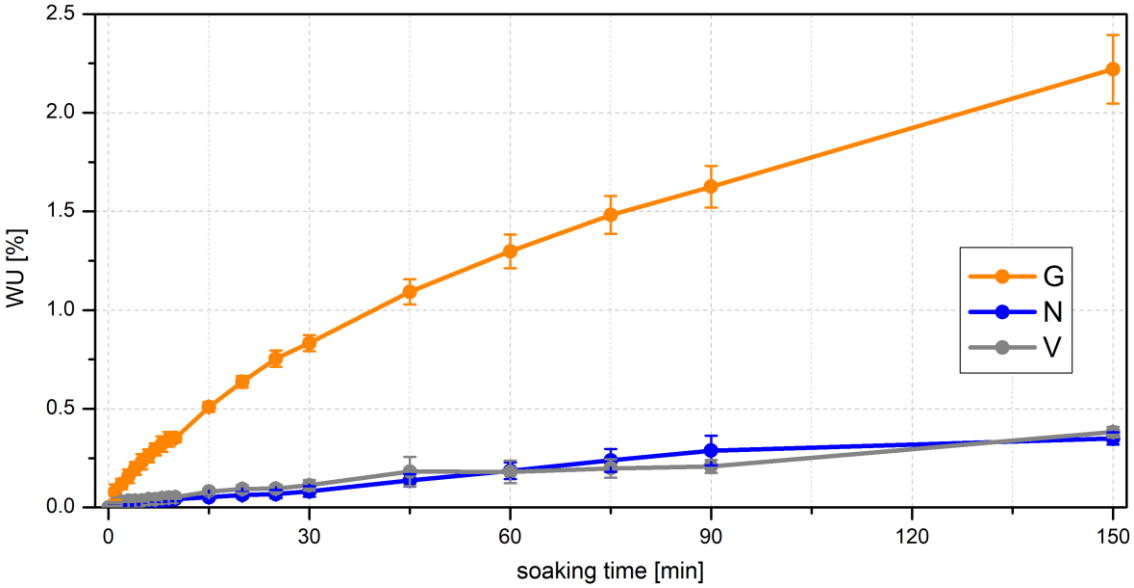

Figure 3.45: WU of peeled garlic cloves treated in the industrial-scale plasma. $P_N = \sim 900$ W, $p = 40$ Pa, $t = 60$ s, soaking in DI water for specified amounts of time. The same cloves were weighted each time and returned to soaking until the next measurement. G = glow plasma treatment; N = untreated control; V = vacuum control.

3.6.3 Pilot-scale plasma

Figure 3.46 shows the WU of garlic cloves treated in the pilot-scale plasma for different amounts of time, followed by soaking in DI water for 10 minutes. With increased treatment time, the WU increases for both peeled and unpeeled cloves linearly. The WU after exposure to vacuum alone is unchanged regardless of vacuum exposure time.

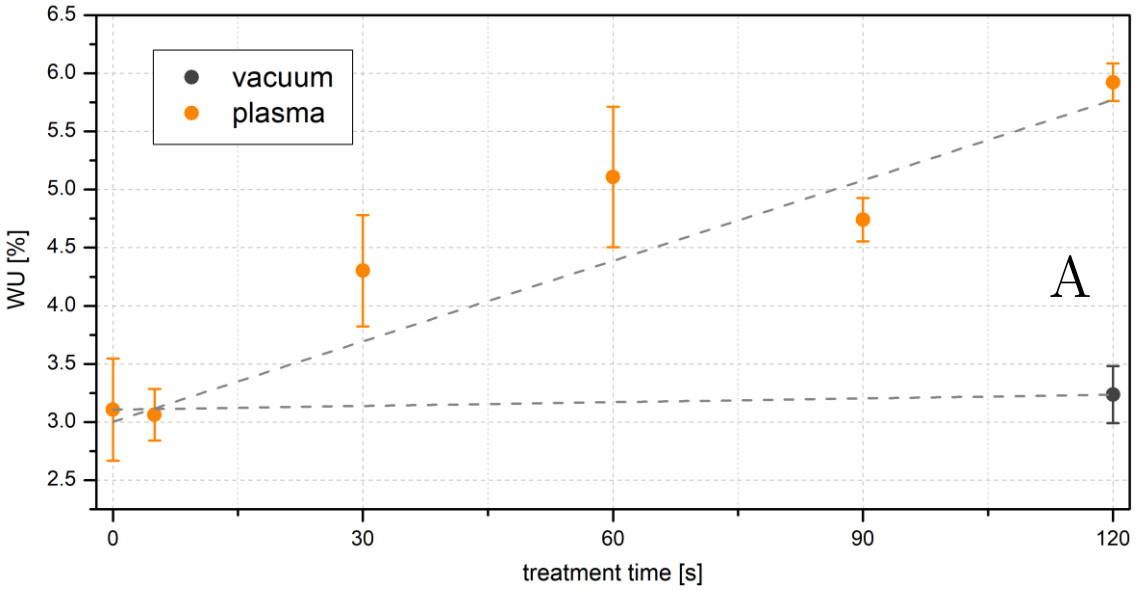

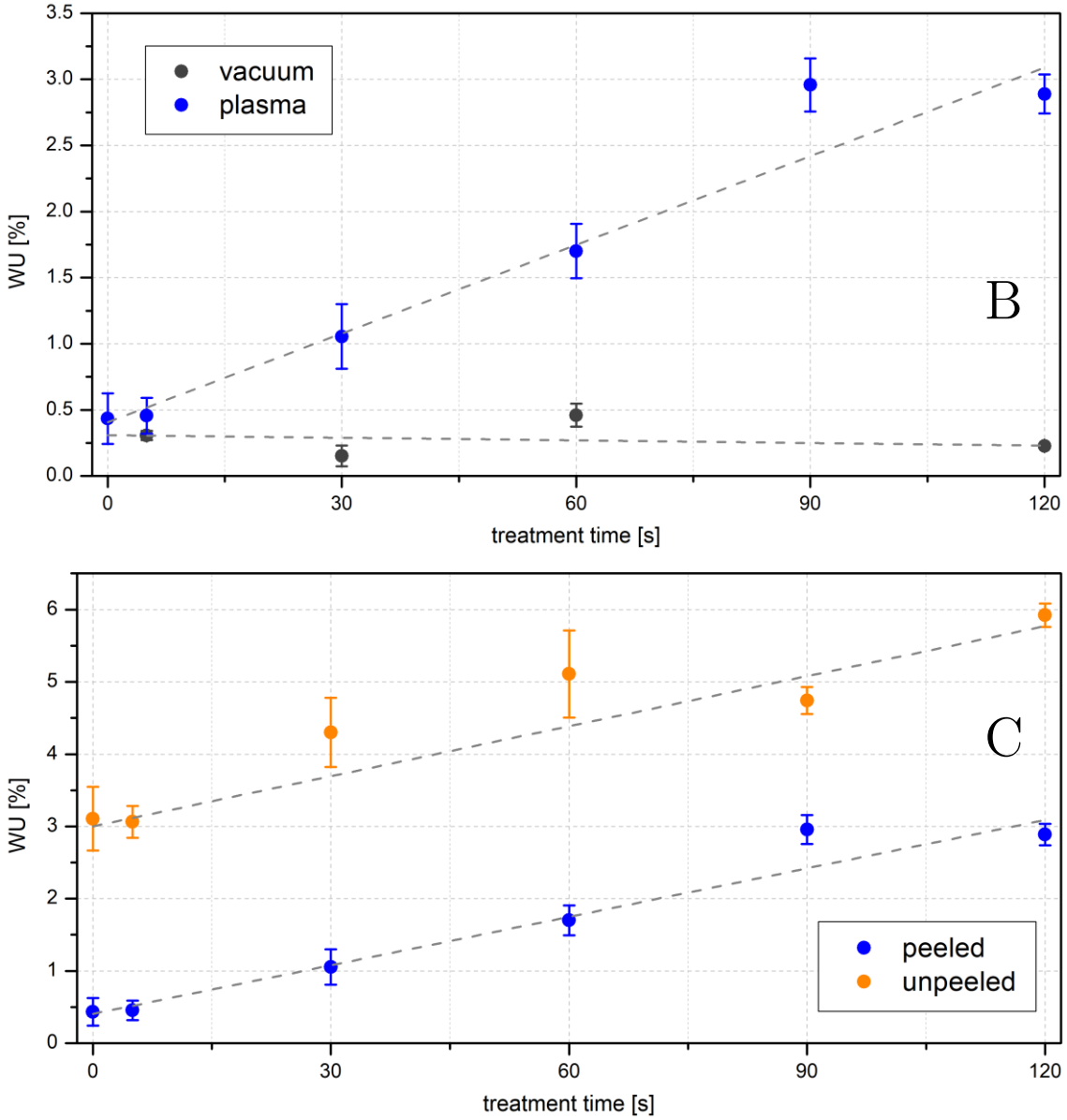

Figure 3.46: WU of garlic cloves treated in the pilot-scale plasma. (A) unpeeled cloves; (B) peeled cloves; (C) comparison. $P_N = 200$ W, $p = 50$ Pa, $t = 0 - 120$ s, or equivalent exposure to low pressure and gas flow alone, followed by soaking for 10 min. The error bars represent standard error. Linear trend lines are added.

3.6.4 Clove mass loss

Loss of clove mass during treatment in the pilot-scale plasma is presented in Figure 3.47 and Figure 3.48. The clove mass steadily decreases during plasma treatment for both peeled and unpeeled cloves, but loss of clove mass during plasma treatment is significantly larger for peeled cloves compared to unpeeled (Figure 3.47). Loss of peeled clove mass is further significantly greater for plasma-treated cloves compared to those exposed to low pressure and gas flow for the same amount of time (Figure 3.48).

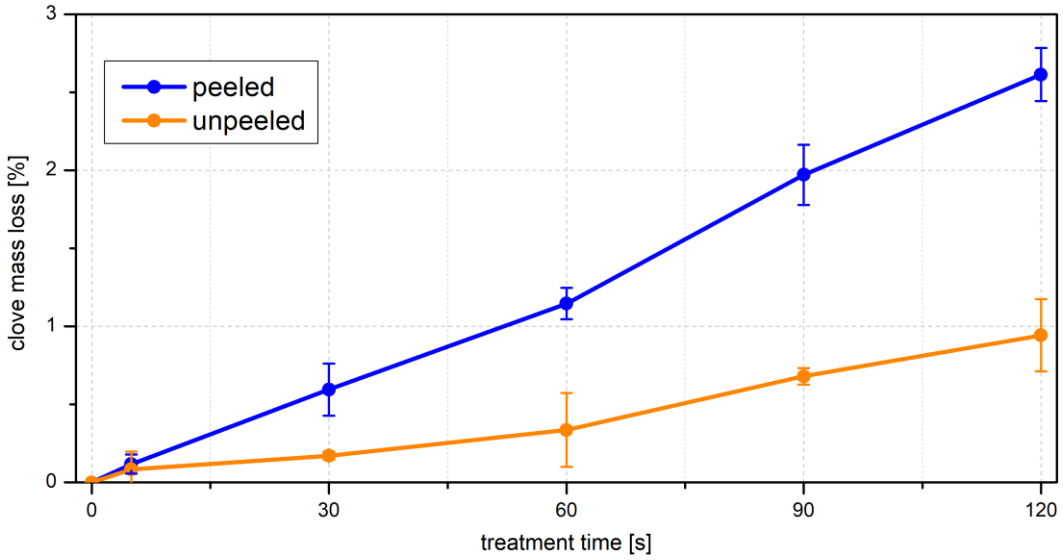

Figure 3.47: Clove mass loss for peeled and unpeeled cloves. Pilot-scale E-mode glow, $P_N = 200$ W, $p = 50$ Pa, $t = 0 - 120$ s. The error bars represent standard error.

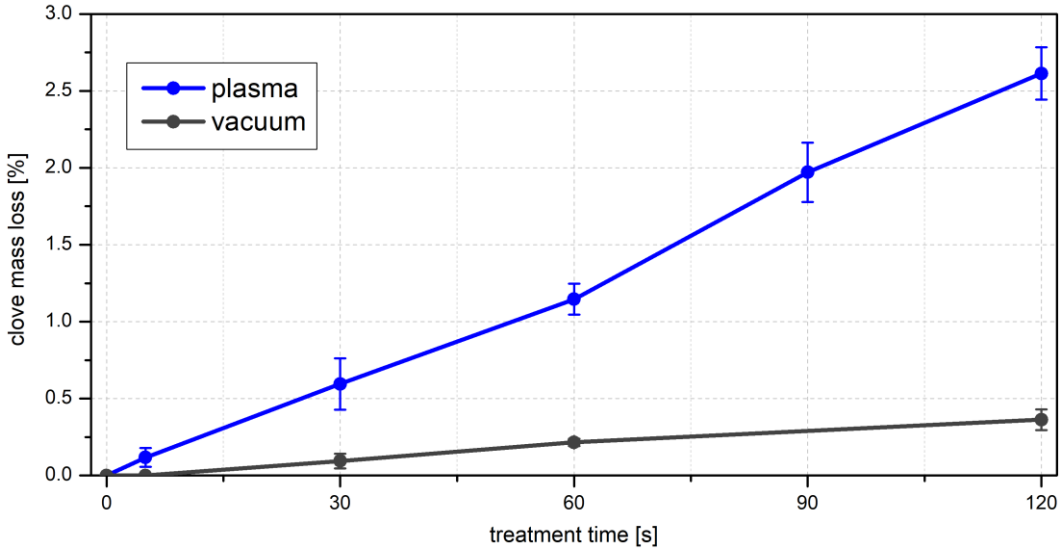

Figure 3.48: Clove mass loss for peeled cloves: plasma treatment and vacuum. Pilot-scale E-mode glow, $P_N = 200$ W, $p = 50$ Pa, $t = 0 - 120$ s, or exposure to low pressure and gas flow for the same treatment times. The error bars represent standard error.

Figure 3.49 shows the WU of peeled cloves already presented in Figure 3.45, but here, the WU is calculated using the initial clove mass, before plasma treatment, in Equation (2.1). We see that due to clove mass loss, the initial WU only covers the mass lost during treatment, and reaches the initial clove mass only after about 30 minutes of soaking. However, even after that point, WU is accelerated compared to untreated cloves.

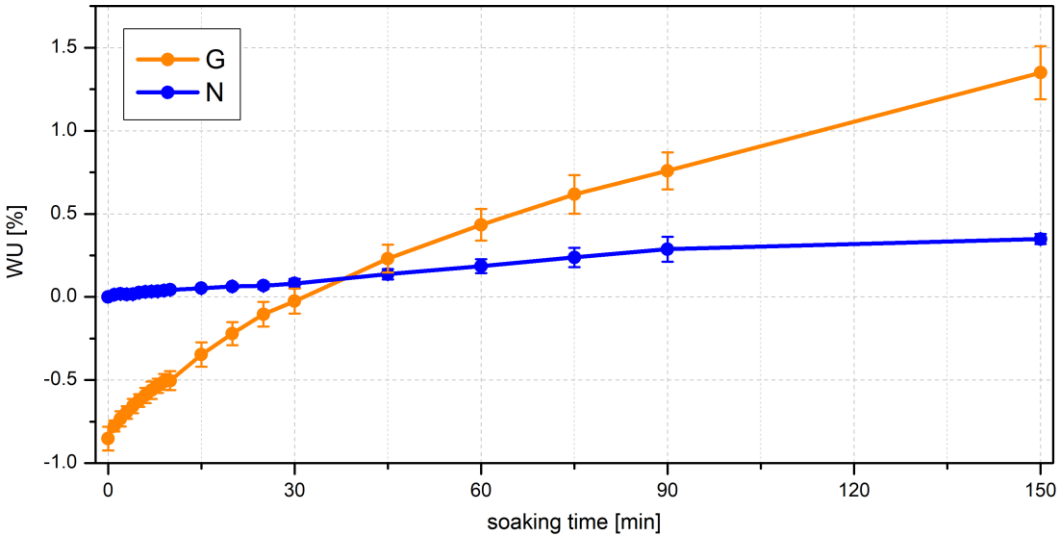

Figure 3.49: WU of peeled garlic cloves treated in the industrial-scale plasma, calculated using the initial clove mass. $P_N = \sim 900$ W, $p = 40$ Pa, $t = 60$ s, soaking in DI water for specified amounts of time. G = glow plasma treatment; N = untreated control. The error bars represent standard error.

3.6.5 Effect of initial clove mass

Figure 3.50 presents the relationship between the WU at a single plasma treatment condition and initial mass of the treated clove samples.

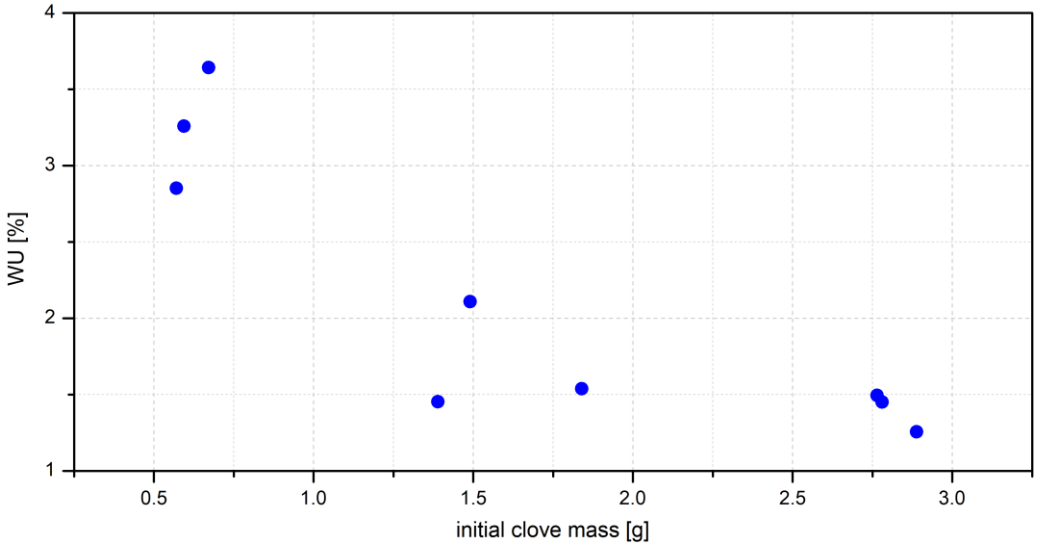

Figure 3.50: Effect of initial clove mass on WU. Pilot-scale E-mode glow, $P_N = 200$ W, $p = 50$ Pa, $t = 60$ s. The data points represent individual values.

3.7 Sprout and Root Growth

3.7.1 Pilot-scale plasma

3.7.1.1 Preliminary treatment

In a preliminary experiment, we have shown that pilot-scale plasma treatment can positively affect sprout growth of garlic cloves. The result is presented in Figure 3.51.

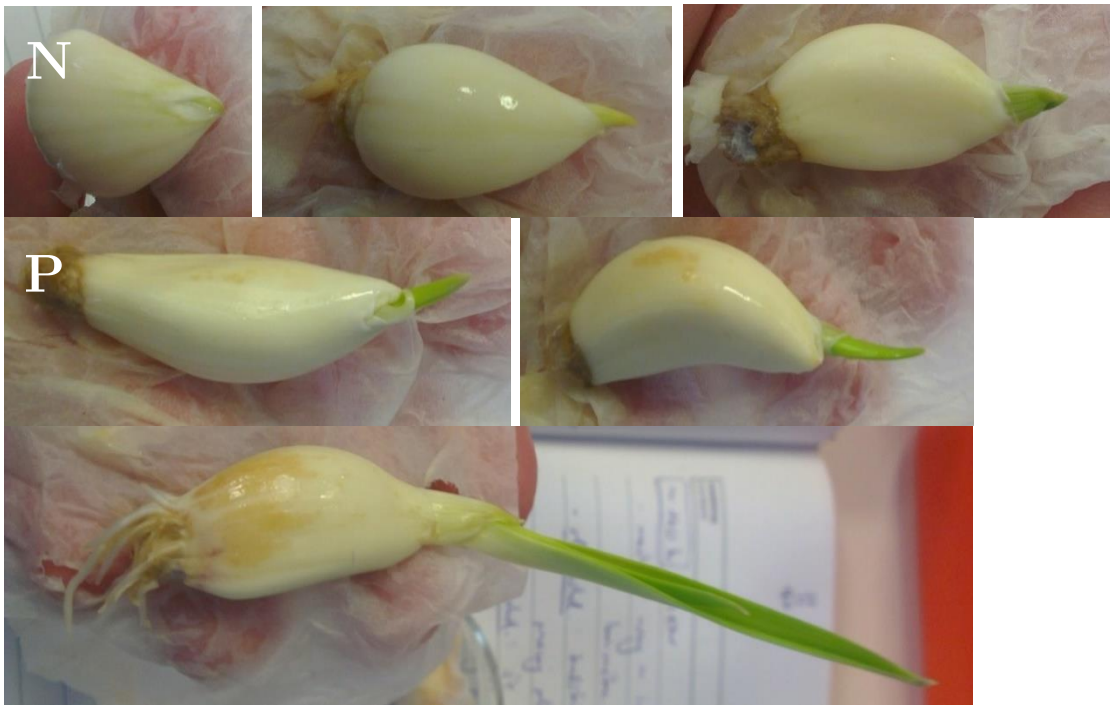

Figure 3.51: Peeled clove sprout growth, pulsed treatment. Pilot-scale E-mode glow plasma, $P_N = 200$ W, $p = 70$ Pa, $t = 30$ s (6×5 s on, 5 s off). N = untreated control; P = plasma treated. Recorded after 140 h of growth.

3.7.1.2 Untreated controls

The results of untreated control sprout and root growth are collected in Figure 3.52. We see that sprout length, root length, and root number all increase faster when the cloves are unpeeled.

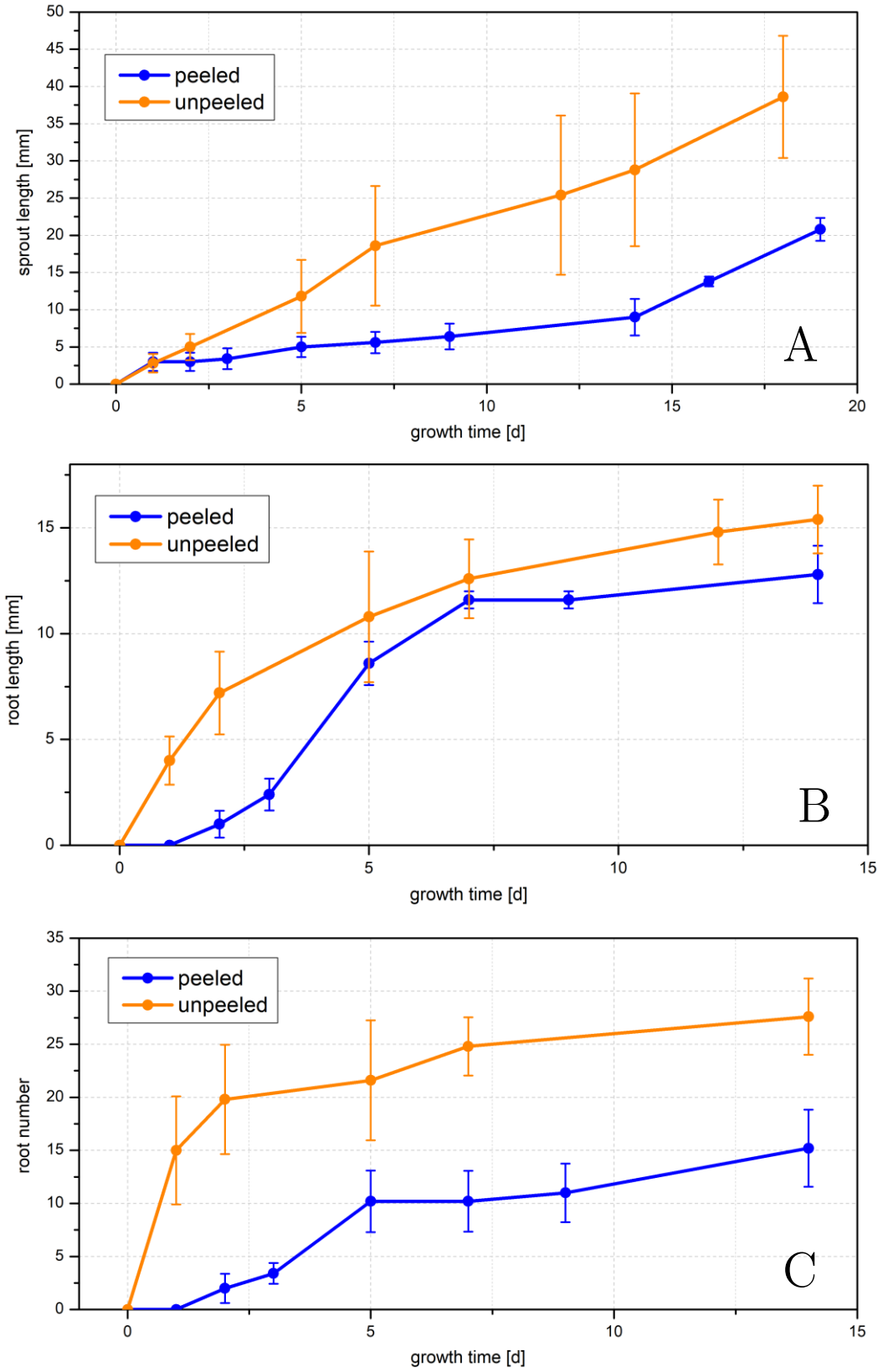

Figure 3.52: Growth of peeled and unpeeled untreated garlic clove sprouts and roots. The error bars represent standard error. (A) sprout length; (B) root length; (C) root number.

3.7.1.3 Unpeeled cloves

3.7.1.3.1 E-mode glow Figure 3.53 – Figure 3.55 present the growth of unpeeled clove sprouts and roots after treatment in the pilot-scale plasma E-mode glow at different treatment conditions.

In Figure 3.53, we see that at $p = 50$ Pa, the treatment at $P_N = 100$ W does not significantly affect sprout growth. The treatment at $P_N = 200$ W, for a treatment time of 60 s, significantly improves sprout growth from 12 days of growth onward. A non-significant improvement trend is also seen for $t = 45$ s. The treatment at $P_N = 300$ W does not significantly affect sprout growth, although a trend is apparent for the treatment times of 30, 45 and 60 s.

In Figure 3.54, we see that the treatment at $P_N = 100$ W slightly improves root length at several treatment times, but the improvement is not significant. The same is true for $P_N = 200$ W for treatment times of 15 – 60 s, as well as for $P_N = 300$ W for 15 and 30 s. In both cases, longer treatments retard root length. The negative effect is statistically significant for $t = 120$ s at both P_N.

In Figure 3.55, we see that root number is not significantly positively affected at any P_N or treatment time. Further, at $P_N = 200$ W and $t = 120$ s, as well as at $P_N = 300$ W and $t = 45$ – 120 s, the root number is significantly negatively affected at most growth times.

A comparison of sprout and root growth results between continuous and pulsed treatment is found in Figure 5.3 and Figure 5.4 in Appendix A.

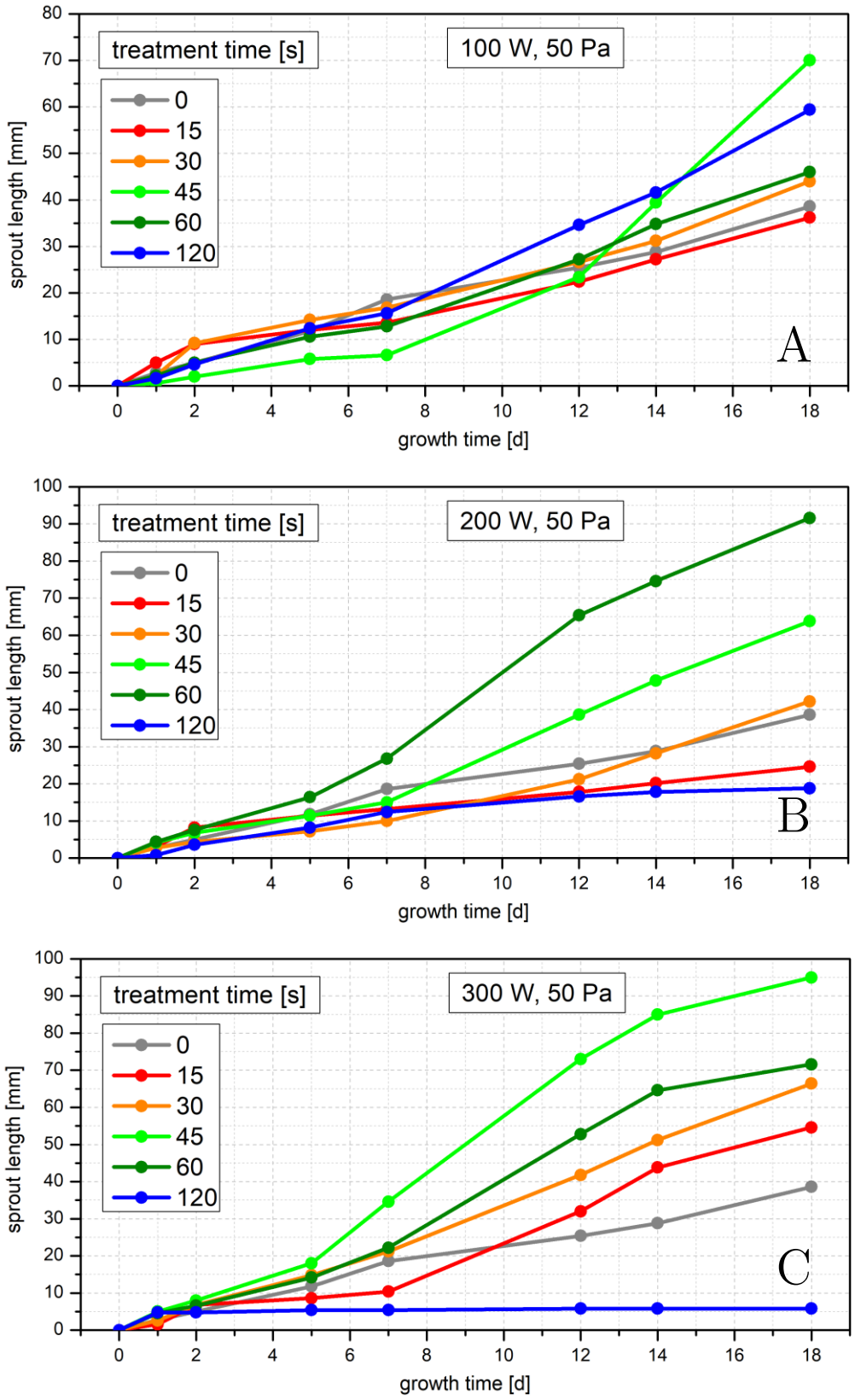

Figure 3.53: Growth of unpeeled garlic clove sprouts, pilot-scale E-mode glow. (A) $P_N = 100$ W; (B) $P_N = 200$ W; (C) $P_N = 300$ W. $p = 50$ Pa, $t = 0 - 120$ s.

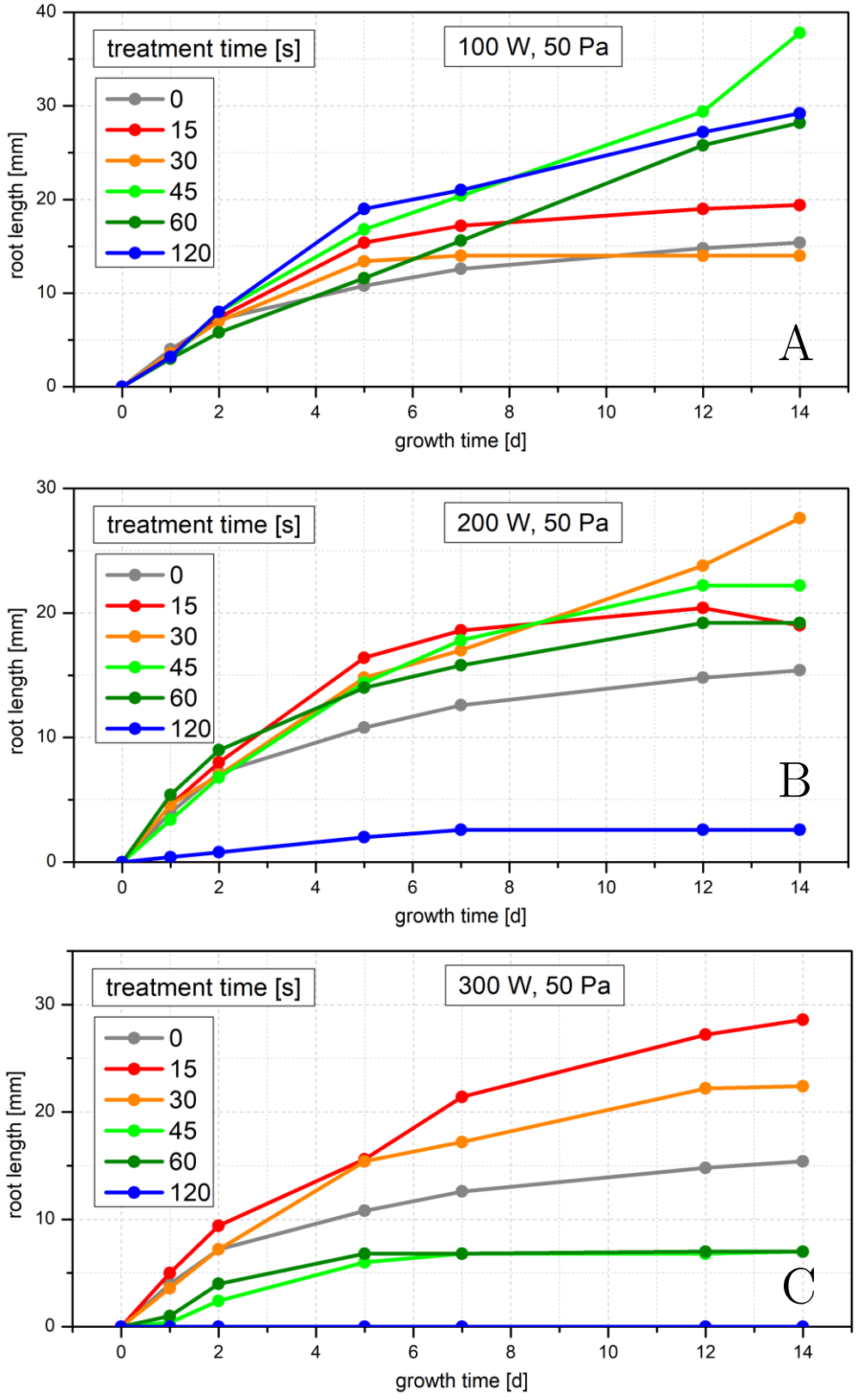

Figure 3.54: Growth of unpeeled garlic clove roots, pilot-scale E-mode glow. (A) $P_N = 100$ W; (B) $P_N = 200$ W; (C) $P_N = 300$ W. $p = 50$ Pa, $t = 0 - 120$ s.

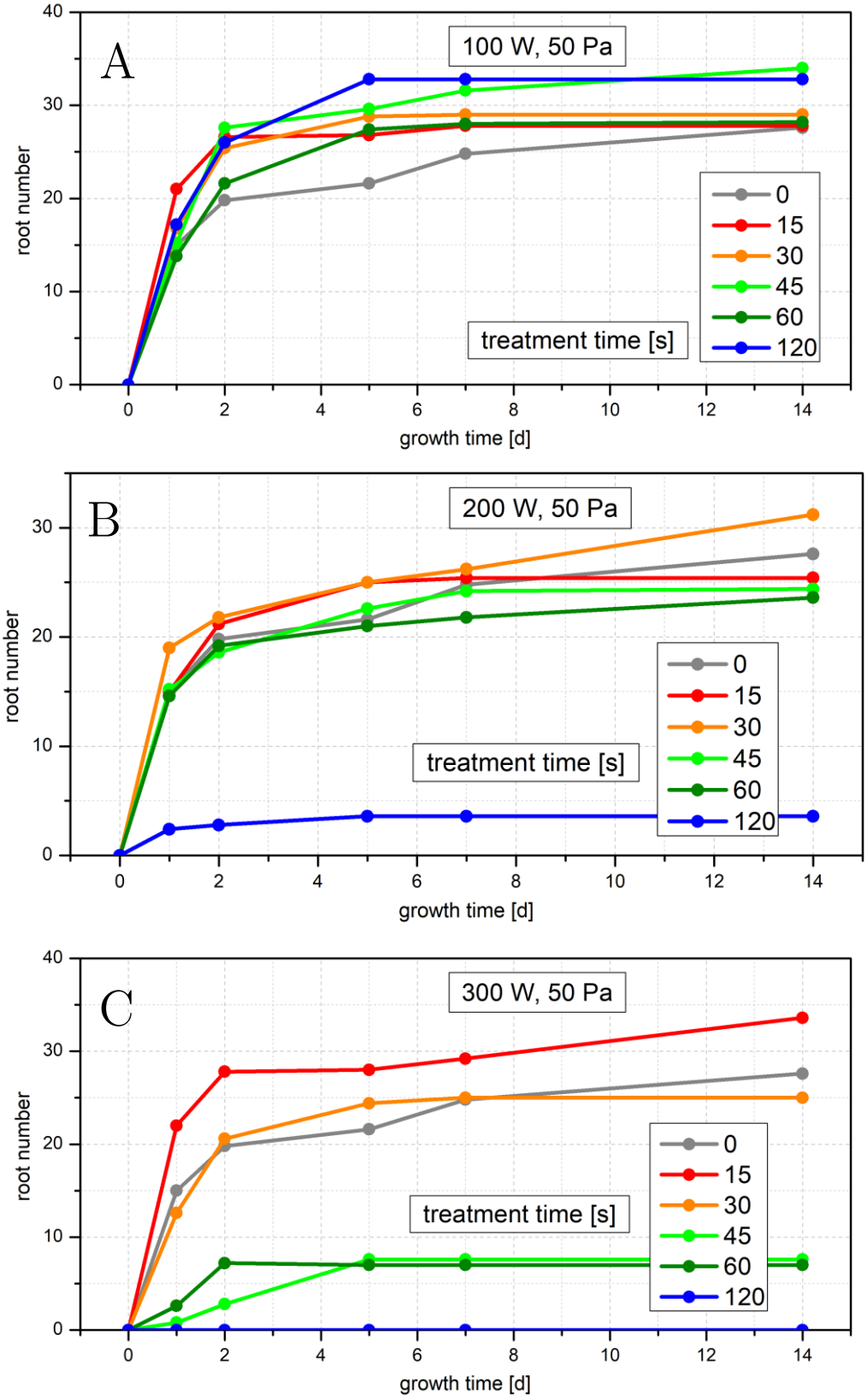

Figure 3.55: Unpeeled garlic clove root number, pilot-scale E-mode glow. (A) $P_N = 100$ W; (B) $P_N = 200$ W; (C) $P_N = 300$ W. $p = 50$ Pa, $t = 0 - 120$ s.

3.7.1.3.2 H-mode afterglow Figure 3.56 – Figure 3.59 present the growth of unpeeled clove sprouts and roots after treatment in the pilot-scale plasma H-mode afterglow at different treatment conditions.

In Figure 3.56, sprout growth after H-mode afterglow treatment at $P_N = 200$ or 300 W, $p = 50$ s, is presented. While some mean sprout length values considerably exceed those of the untreated control, no clear trend is apparent, and there are no statistically significant differences at any of the treatment times.

Root length, as shown in Figure 3.57, does not significantly deviate from the untreated control for either of the treatment conditions. The same is true for root number, seen in Figure 3.58, with the exception that the root number at $P_N = 200$ W, $t = 120$ s is significantly lower than at all of the remaining treatment times at $P_N = 200$ W.

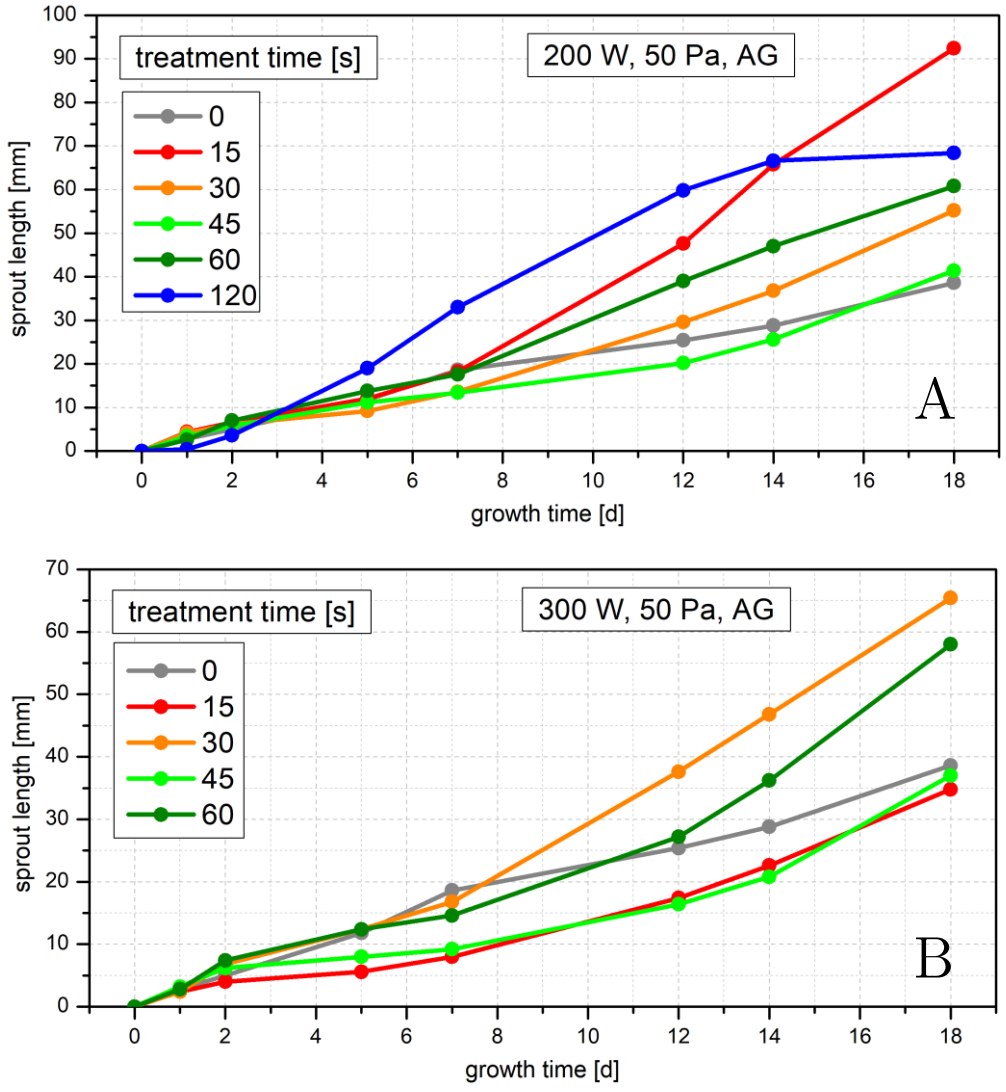

Figure 3.56: Growth of unpeeled garlic clove sprouts, pilot-scale H-mode afterglow. (A) $P_N = 200$ W; (B) $P_N = 300$ W. $p = 50$ Pa, $t = 0$ – 120 s.

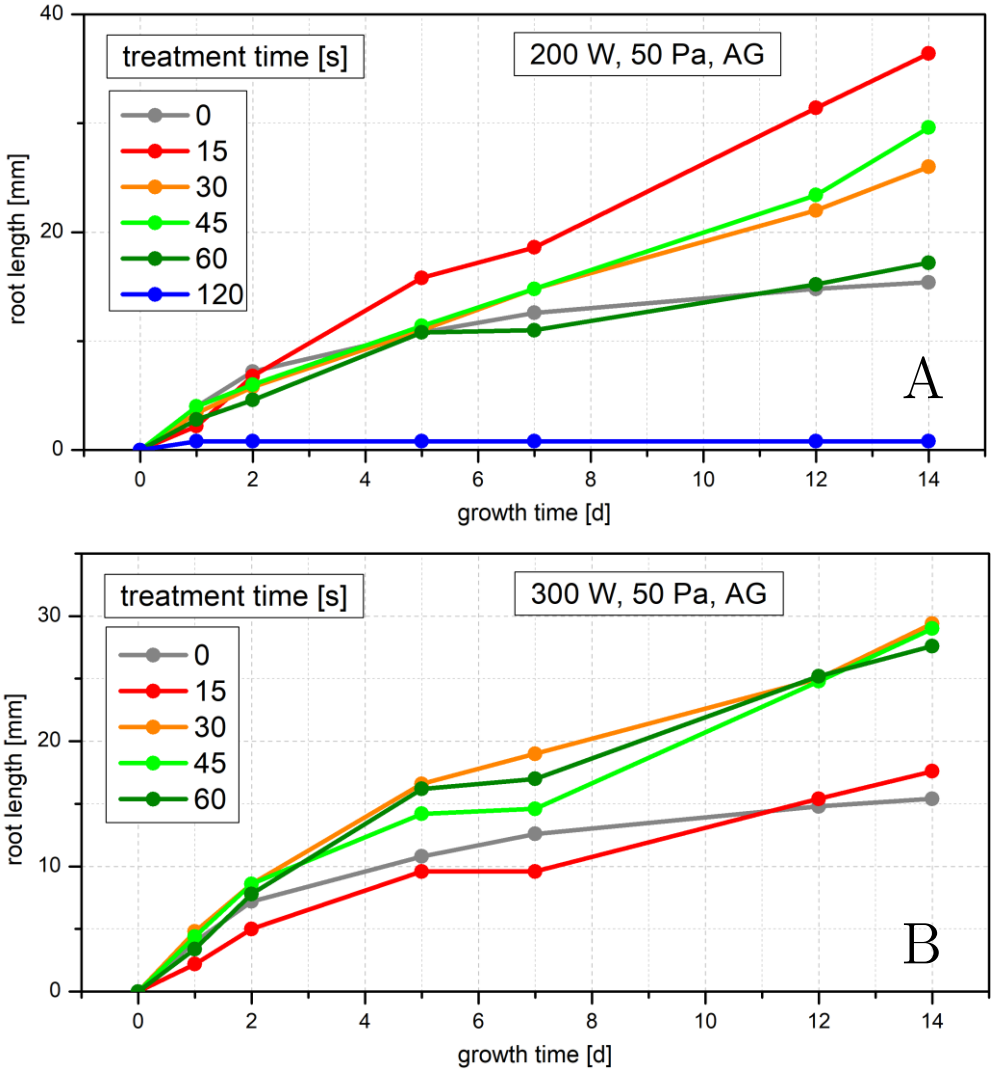

Figure 3.57: Growth of unpeeled garlic clove roots, pilot-scale H-mode afterglow. (A) $P_N = 200$ W; (B) $P_N = 300$ W. $p = 50$ Pa, $t = 0 - 120$ s.

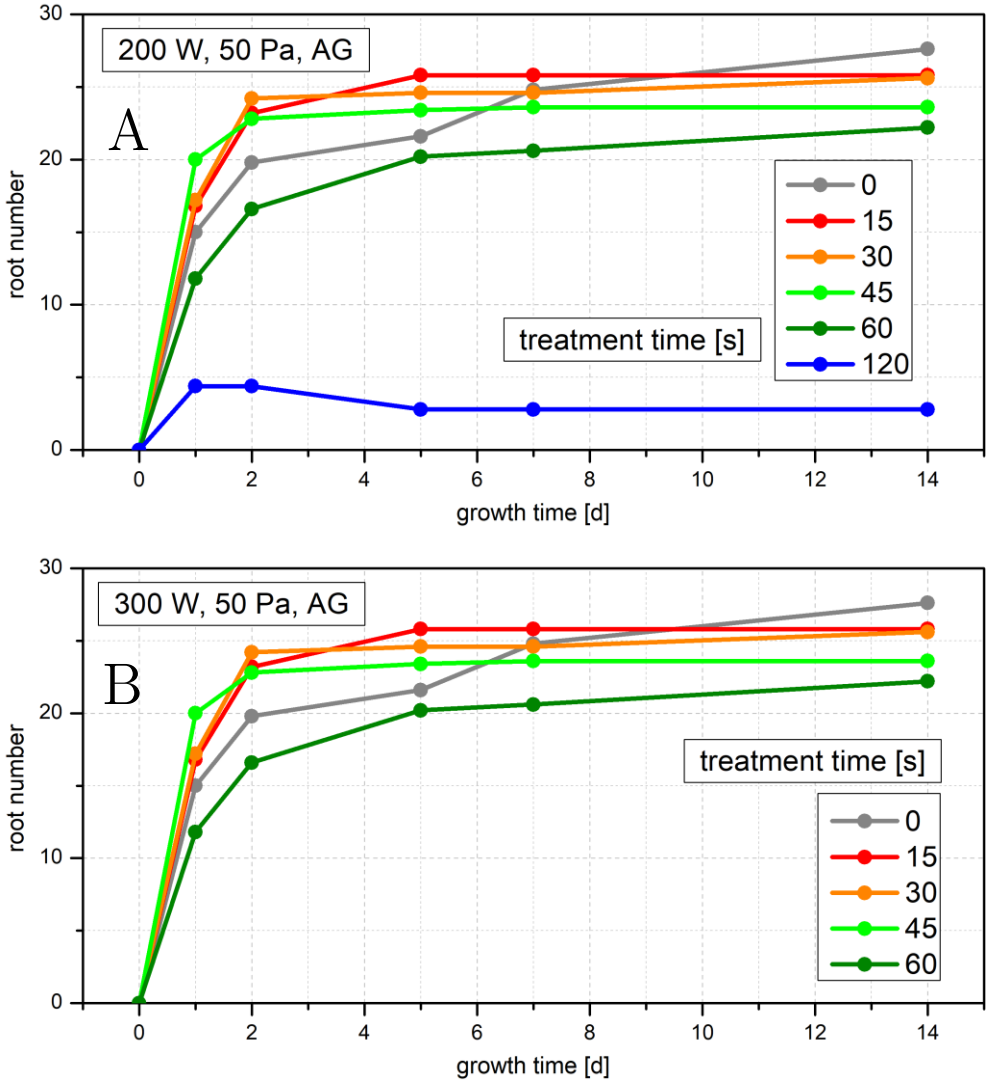

Figure 3.58: Unpeeled garlic clove root number, pilot-scale H-mode afterglow. (A) $P_N = 200$ W; (B) $P_N = 300$ W. $p = 50$ Pa, $t = 0 - 120$ s.

Figure 3.59 presents the sprout growth after pilot-scale H-mode afterglow treatment in a separate experiment, with different discharge conditions. Treatments at the times of up to 45 s increase the mean sprout length and follow a clear trend. Nonetheless, due to the dispersion of the individual results, none of the improvements are statistically significant. Root growth was not followed in this experiment.

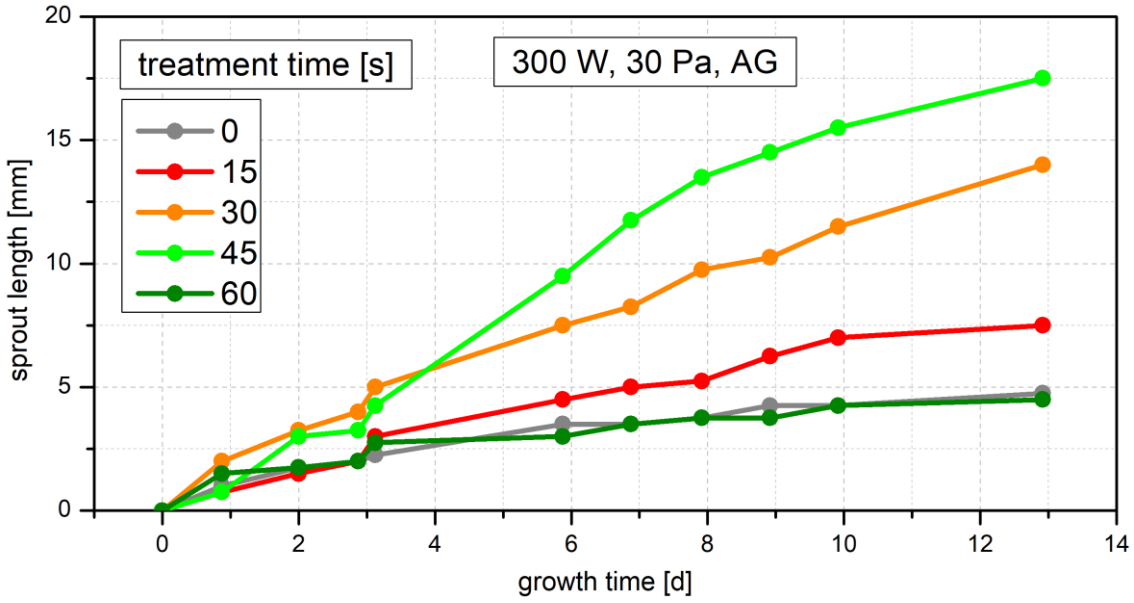

Figure 3.59: Unpeeled clove sprout growth, pilot-scale H-mode AG, 2nd experiment. $P_N = 300$ W, $p = 30$ Pa, $t = 15 - 60$ s.

3.7.1.4 Peeled cloves

Figure 3.60 presents the growth of peeled clove sprouts after treatment in the pilot-scale E-mode glow plasma at different treatment conditions. At $P_N = 100$ W, we see no improvement for shorter treatment times, but the sprout length increase is significant for the 90 s and 120 s treatment times from 9 days onward, as well as for the 60 s treatment time from 14 days onwards. Similarly, at $P_N = 200$ W, the sprout length is significantly improved for the 90 s treatment time from 7 days onward, and at $P_N = 300$ W, for the 90 s treatment time from 5 days onward. The treatment times that show no significant improvement nonetheless all exhibit a trend of mean sprout length increase up to $t = 90$ s, followed by a decrease at $t = 120$ s.

In Figure 3.61, root length improvement after plasma treatment is presented. The root length is not consistently significantly improved compared to the untreated control at any of the treatment conditions. Nonetheless, the mean root length is affected by treatment time. At each discharge condition, there is a treatment time that affects mean root length the most, which at a working pressure of 50 Pa decreases with increasing P_N (and thus increasing n_O). These treatment times are 60 s, 30 s, and 15 s, for $P_N = 100$ W, 200 W, and 300 W, respectively. The remaining treatment times either do not improve the mean root length to that degree, or in the case of $P_N = 300$ W, even decrease it.

Root number, presented in Figure 3.62, is also not consistently significantly improved compared to the untreated control. Nonetheless, the mean root number is affected by treatment time, but there is lack of a clear trend. At $P_N = 100$ W and 200 W, 60 s seems to be the optimal treatment time, and longer treatment times also positively affect the mean root number. In the case of $P_N = 300$ W, the effect of the treatment times appears to be comparable, with the exception of 120 s, which decreases the root number.

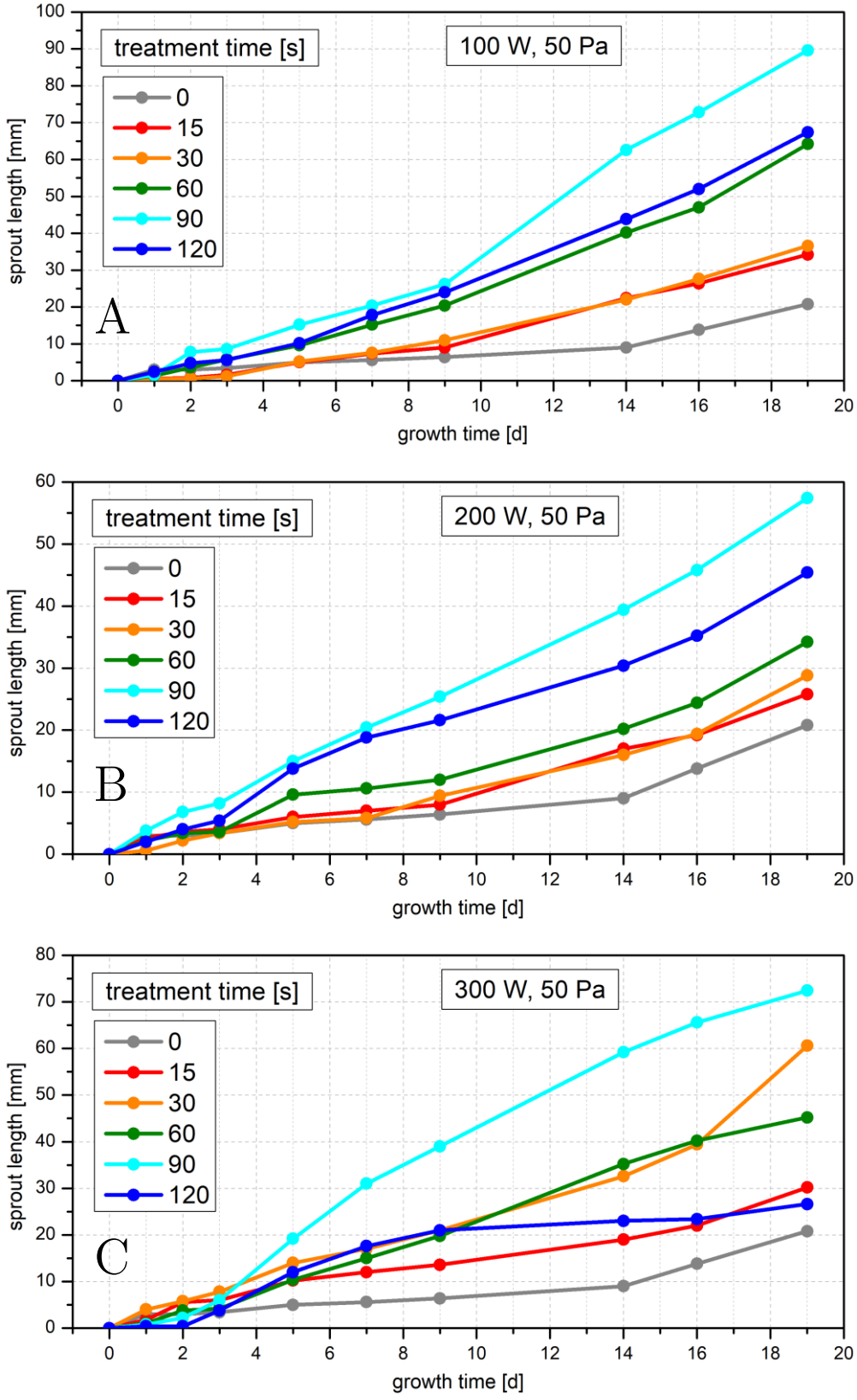

Figure 3.60: Growth of peeled garlic clove sprouts, pilot-scale E-mode glow. (A) $P_N = 100$ W; (B) $P_N = 200$ W; (C) $P_N = 300$ W. $p = 50$ Pa, $t = 0$ – 120 s.

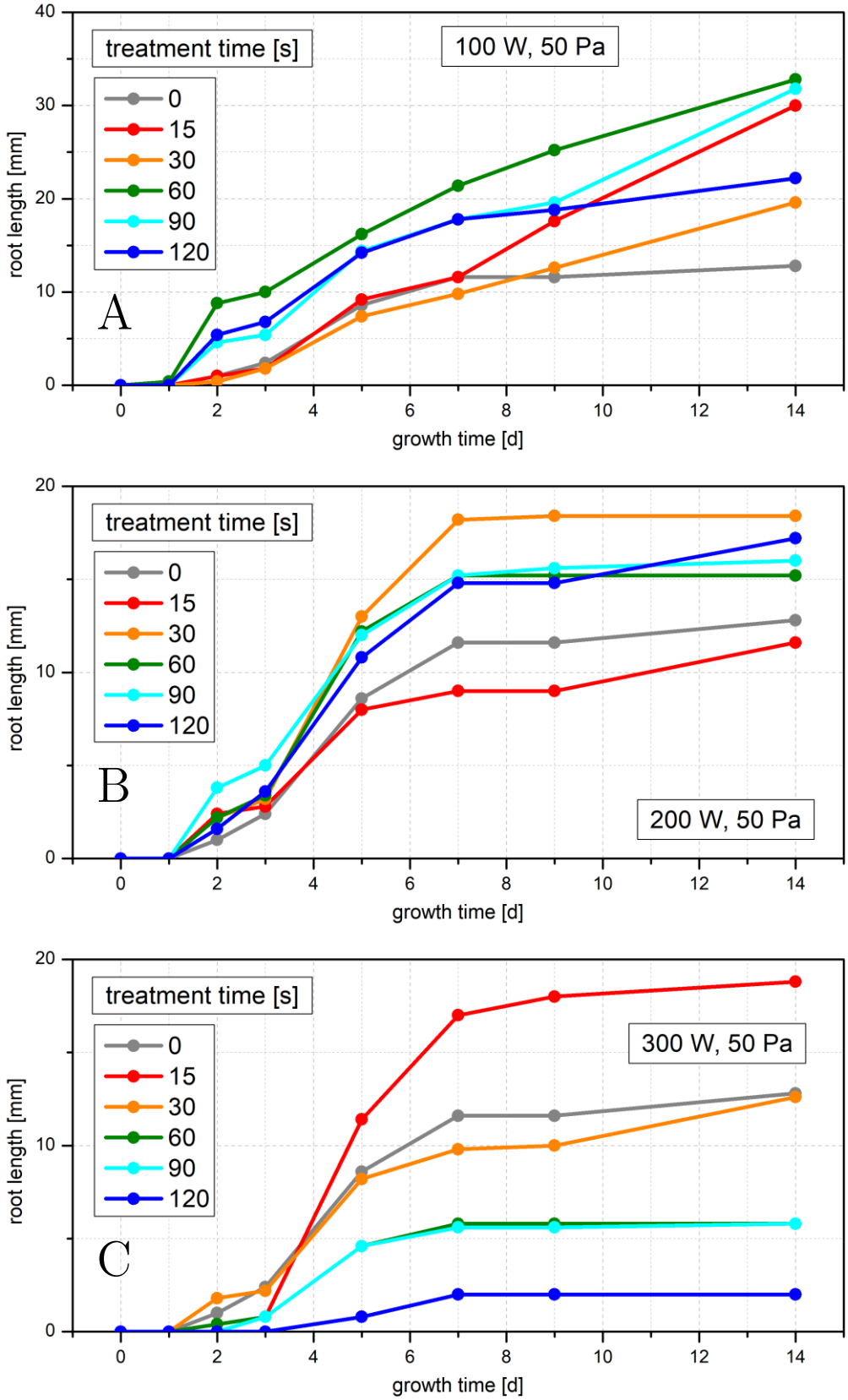

Figure 3.61: Growth of peeled garlic clove roots, pilot-scale E-mode glow. (A) $P_N = 100$ W; (B) $P_N = 200$ W; (C) $P_N = 300$ W. $p = 50$ Pa, $t = 0$ – 120 s.

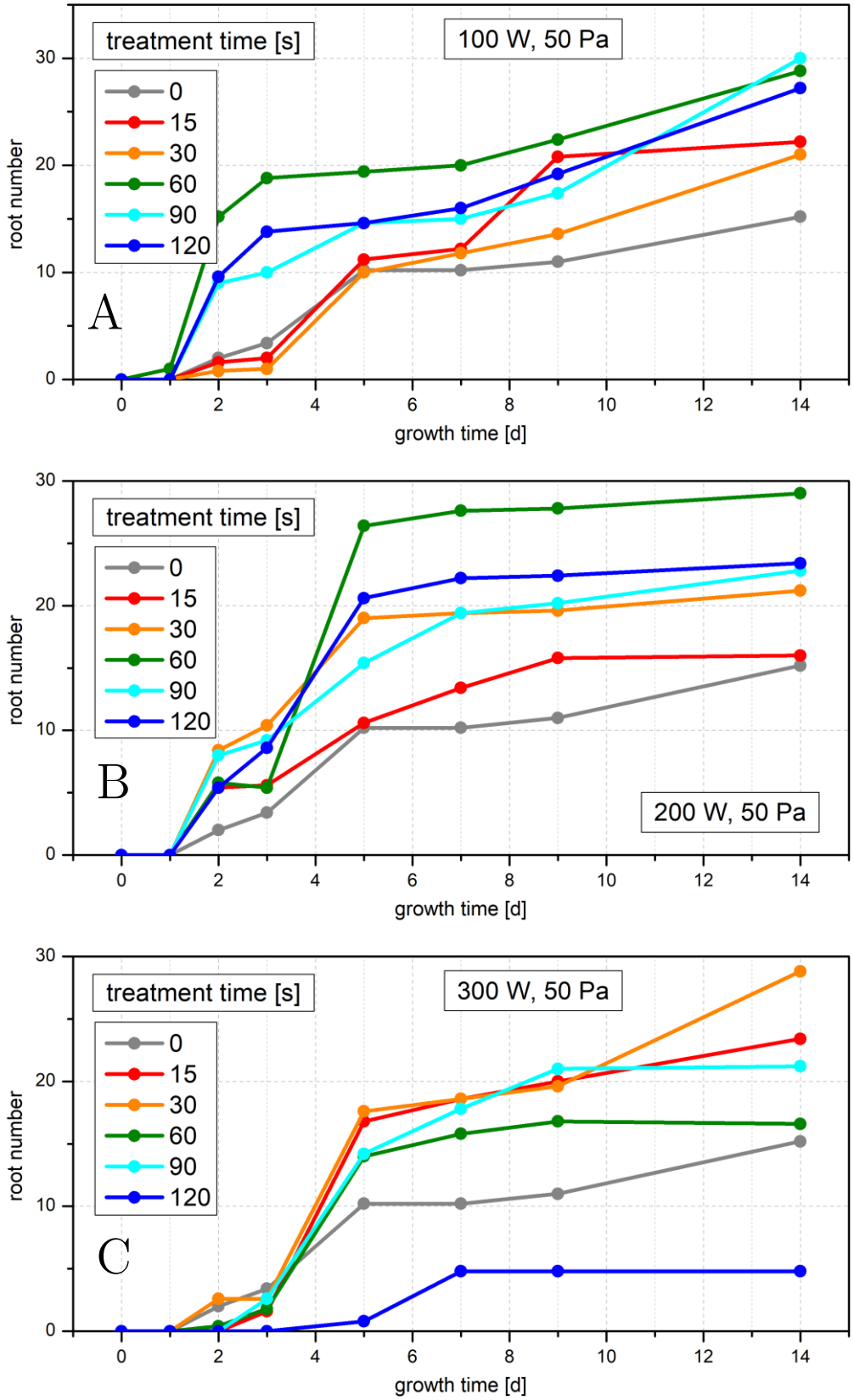

Figure 3.62: Peeled garlic clove root number, pilot-scale E-mode glow. (A) $P_N = 100$ W; (B) $P_N = 200$ W; (C) $P_N = 300$ W. $p = 50$ Pa, $t = 0 - 120$ s.

Figure 3.63 shows the sprout and root growth of peeled cloves exposed to control treatments. There are no statistically significant differences between the control treatments at any treatment condition, treatment time, or time since germination.

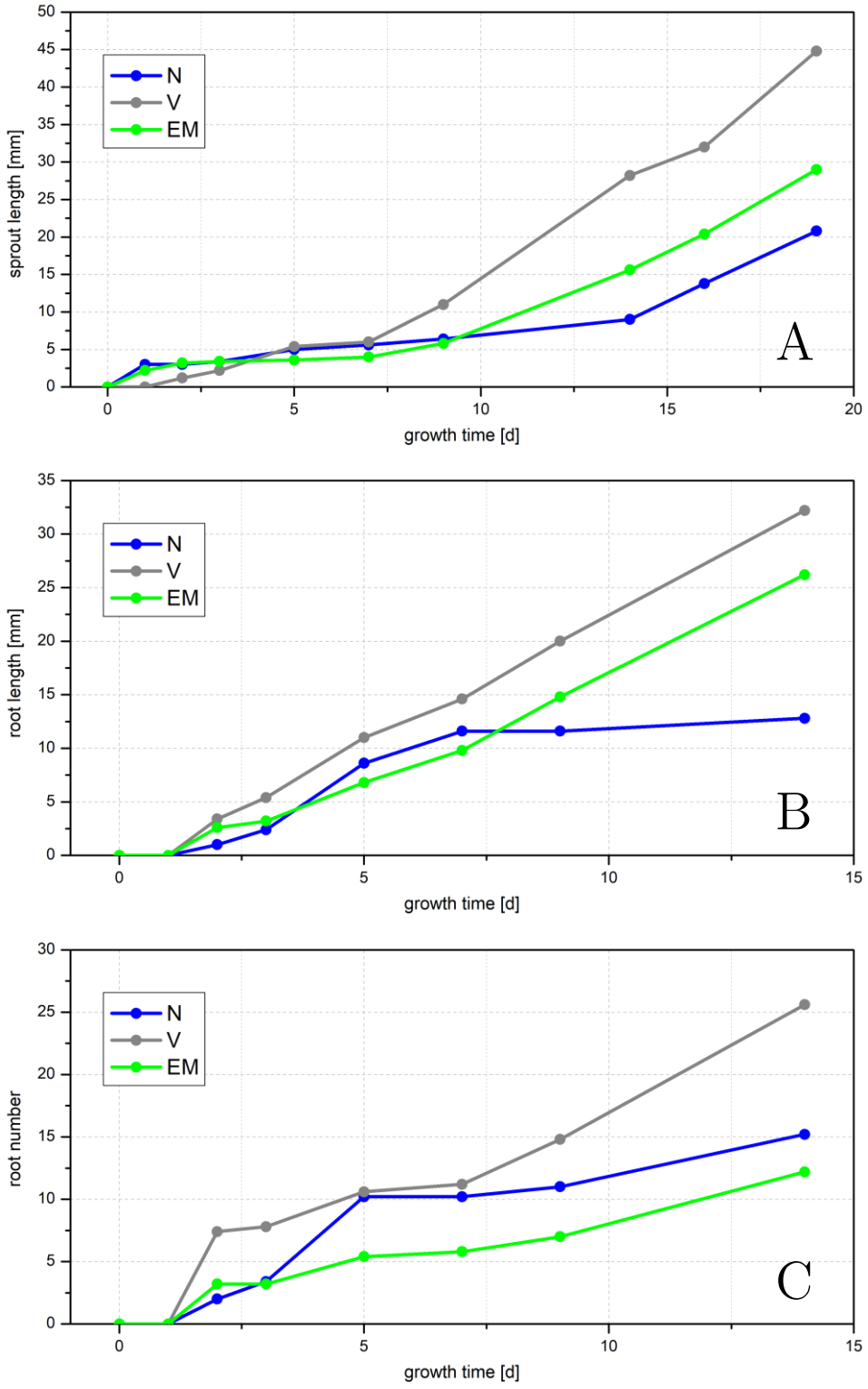

Figure 3.63: Peeled garlic clove control treatments. Sprout length (A), root length (B), and root number (C). Pilot-scale plasma. N = untreated control; V = vacuum control; EM = EM field control. V and EM control: $t = 60$ s.

3.7.2 Industrial-scale plasma

Figure 3.64 shows the growth of peeled clove sprouts and roots after treatment in the industrial-scale plasma at increasing pressure, while Figure 3.65 shows the comparison of control treatments in the same configuration.

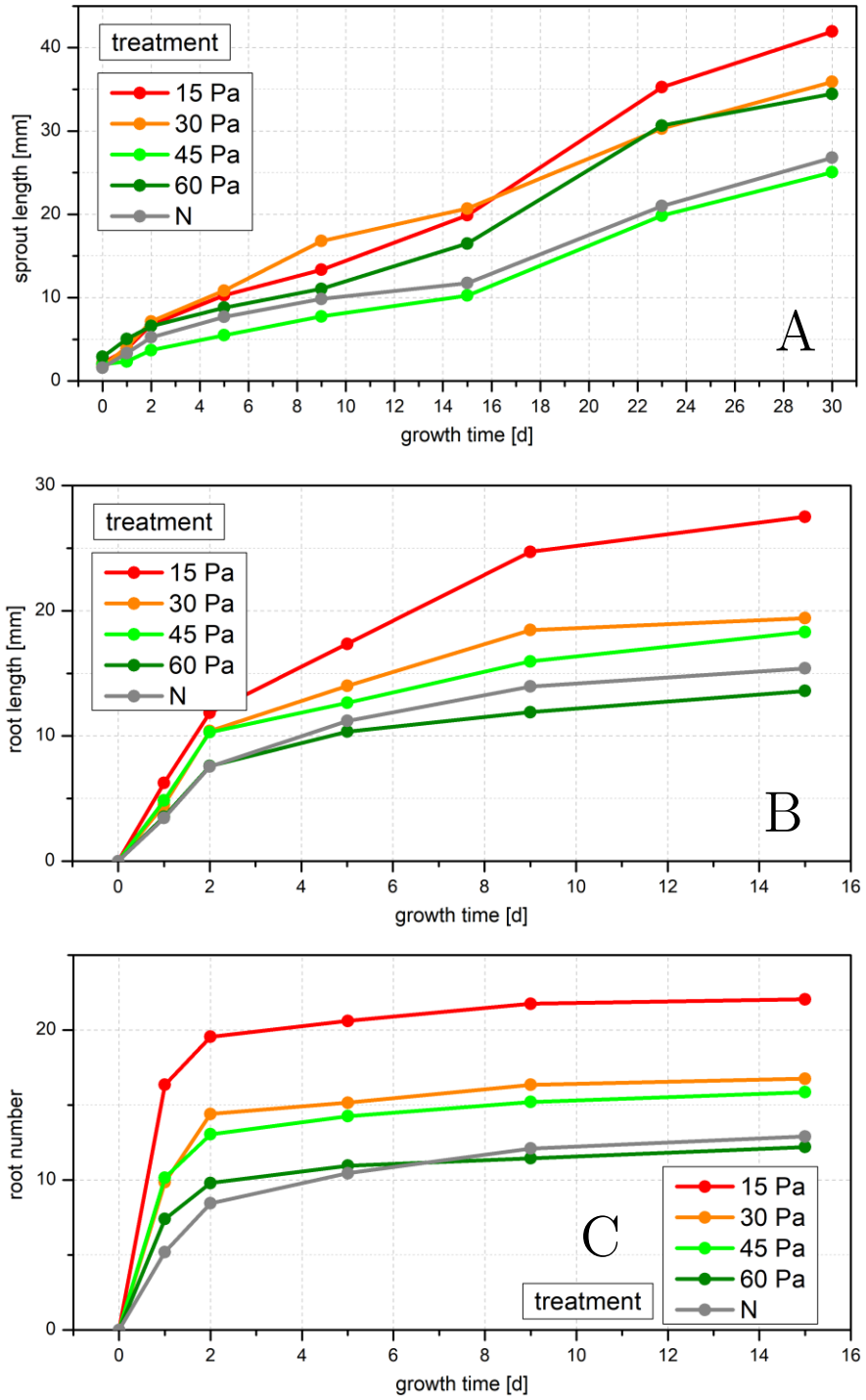

Figure 3.64: Sprout and root growth of peeled garlic cloves, industrial-scale plasma. (A) sprout length; (B) root length; (C) root number. $P_N = \sim 700 - 900$ W, $p = 15 - 60$ Pa, $t = 60$ s. N = untreated control.

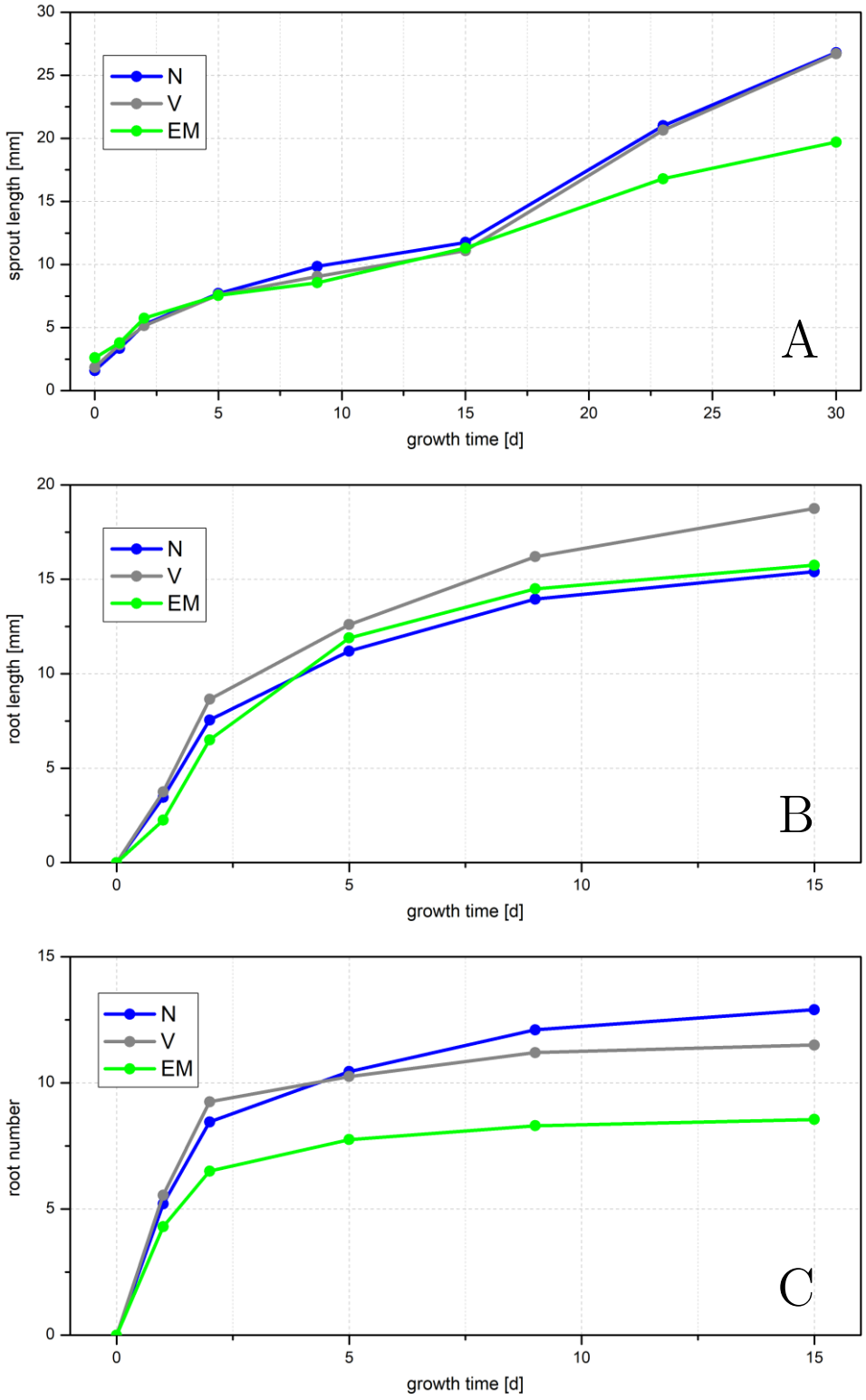

Figure 3.65: Sprout and root growth, peeled clove controls, industrial-scale plasma. (A) sprout length; (B) root length; (C) root number. N = untreated control; V = vacuum control; EM = EM field control. V and EM control: $t = 60$ s.

3.8 Field Growth and Yield

3.8.1 Plant height

Plant height of garlic plants at harvest is presented in Figure 3.66 and Figure 3.67. The differences between the mean plant height are not statistically significant in either of the presented cases.

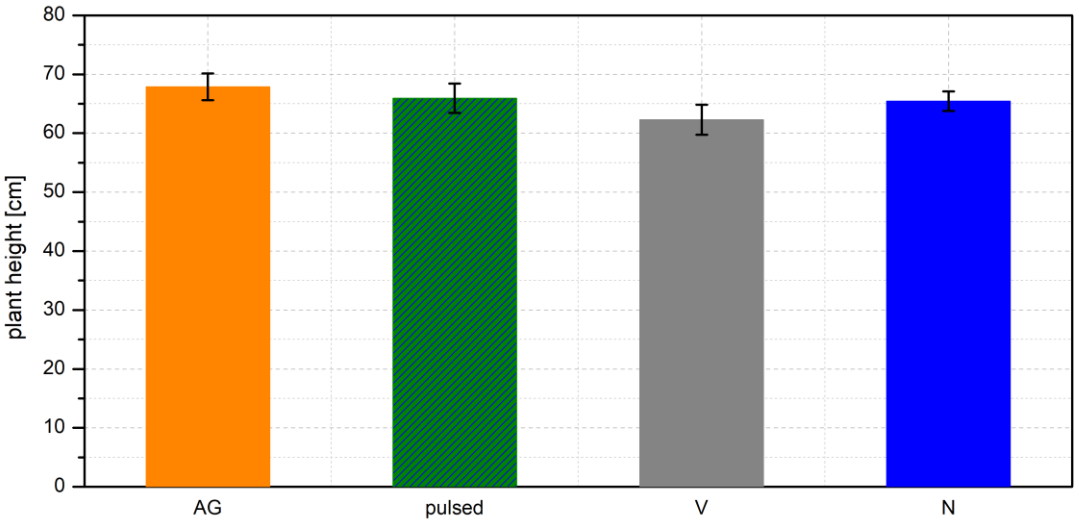

Figure 3.66: Plant height at harvest, pilot-scale plasma. Grown from unpeeled cloves. Planted in October 2017, harvested in July 2018. AG = H-mode afterglow, $P_N = 300$ W, $p = 30$ Pa, $t = 45$ s. Pulsed = E-mode glow, $P_N = 200$ W, $p = 70$ Pa, $t = 30$ s (6×5 s on, 5 s off). N = untreated control; V = vacuum control. Error bars represent standard error.

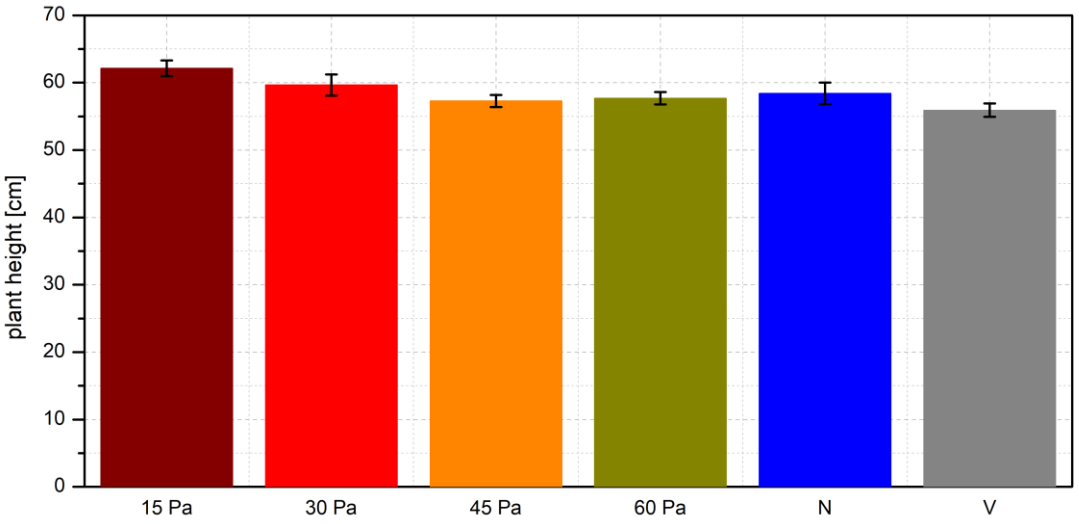

Figure 3.67: Plant height at harvest, industrial-scale plasma. Grown from peeled cloves. Planted in March 2018, harvested in July 2018. $P_N = \sim 700 - 900$ W, $p = 15 - 60$ Pa, $t = 60$ s. N = untreated control; V = vacuum control. Error bars represent standard error.

3.8.2 Yield

3.8.2.1 Pilot-scale treatment

Figure 3.68 shows the yield of garlic grown from plasma-treated and untreated unpeeled cloves. The mean mass of bulbs grown from afterglow-plasma-treated cloves is significantly higher than that of the treated control, while the one of bulbs grown from pulsed glow plasma-treated cloves is not.

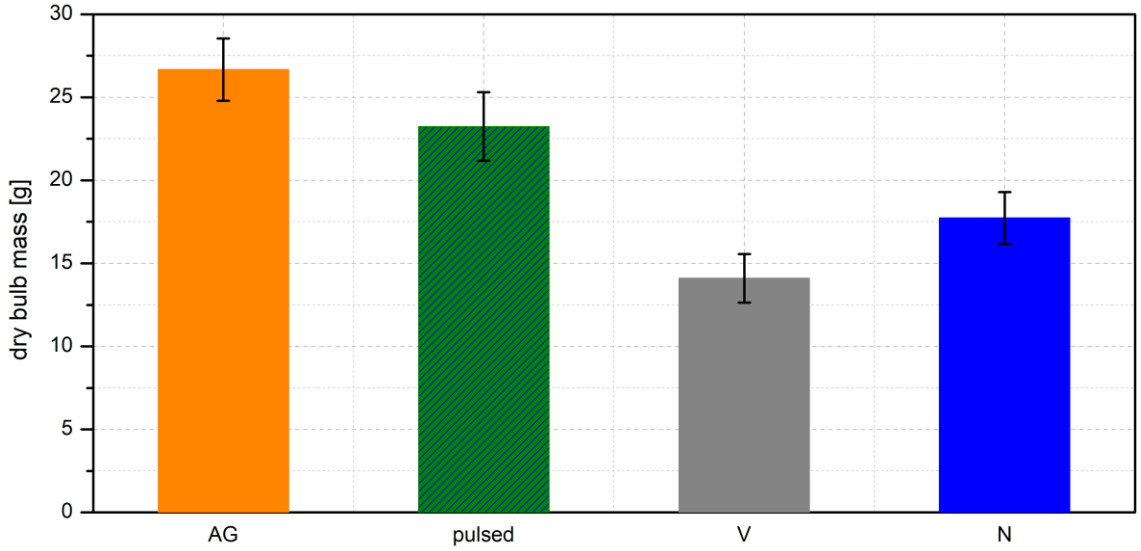

Figure 3.68: Average mass of dried bulb, pilot-scale plasma. Grown from unpeeled cloves. Planted in October 2017, harvested in July 2018. AG = H-mode afterglow, $P_N = 300$ W, $p = 30$ Pa, $t = 45$ s. Pulsed = E-mode glow, $P_N = 200$ W, $p = 70$ Pa, $t = 30$ s (6×5 s on, 5 s off). N = untreated control; V = vacuum control. Error bars represent standard error.

3.8.2.2 Industrial-scale treatment

Figure 3.69 shows the yield of garlic grown from plasma-treated and untreated peeled cloves. We see an 11 % increase of dried bulb mass for the 15 Pa treatment. Very limited increases are also seen for the 30 Pa and 45 Pa treatments, while the dried mass for the 60 Pa treatment is decreased. The differences are not statistically significant.

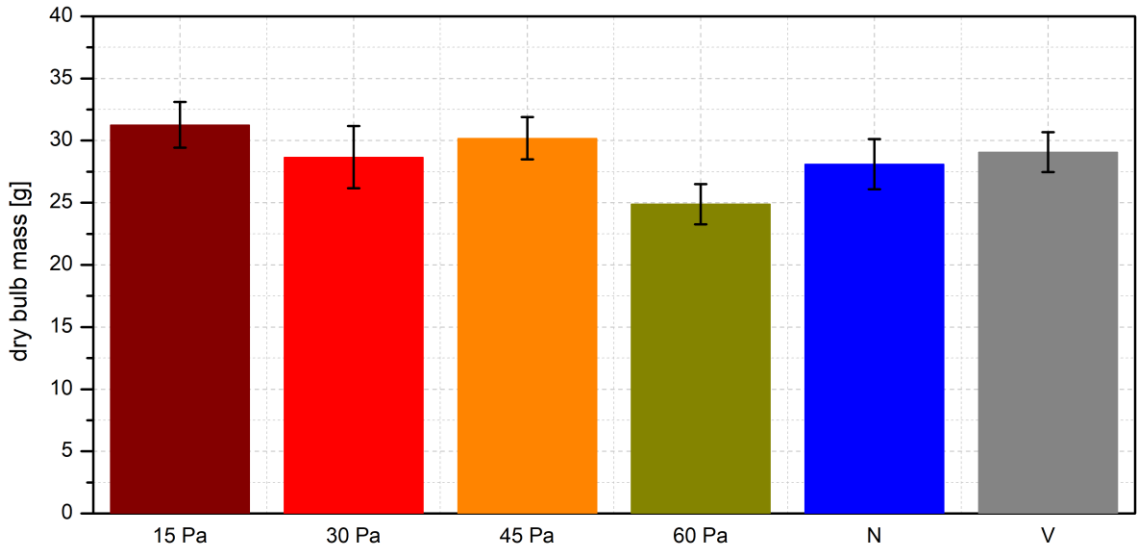

Figure 3.69: Average mass of dried bulb, industrial-scale plasma system. Grown from peeled cloves. Planted in March 2018, harvested in July 2018. $P_N = \sim 700 - 900$ W, $p = 15 - 60$ Pa, $t = 60$ s. N = untreated control; V = vacuum control. Error bars represent standard error.

3.8.2.3 2nd and 3rd generations

Figure 3.70 and Figure 3.71 show dry bulb mass of the 2nd and 3rd generation of garlic grown from cloves treated in plasma before 1st generation planting. No additional treatment took place between the 1st and 2nd generation or between the 2nd and 3rd generation. All garlic was stored, planted and maintained as per the standard procedure.

For the garlic treated with the pulsed regimen in the first generation (Figure 3.70), the mean bulb mass was increased compared to the bulb mass of untreated garlic. This trend continued throughout to the third generation. However, none of the differences between treated and untreated conditions within the same generation are statistically significant.

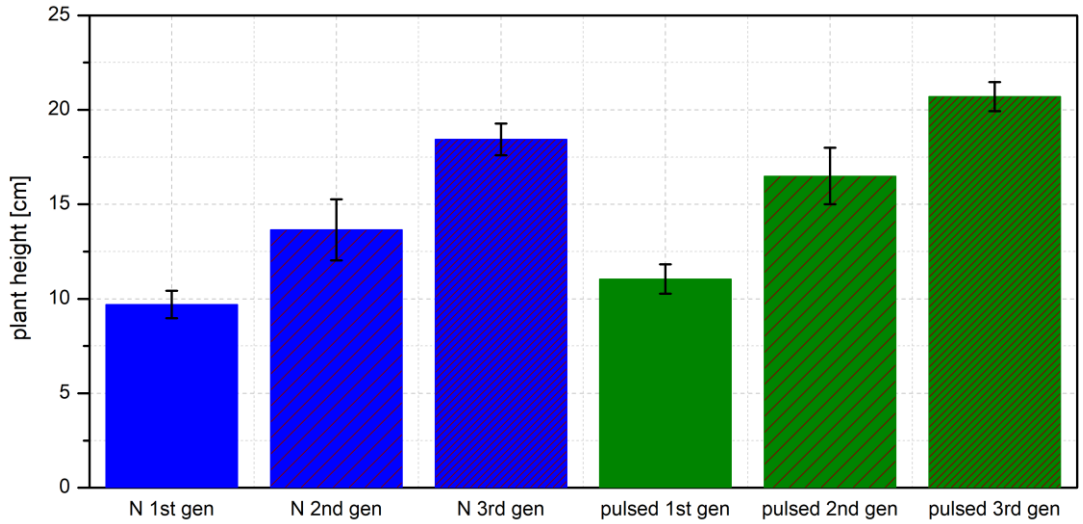

Figure 3.70: Average mass of dried bulb for 2nd and 3rd generation of garlic. Grown from unpeeled cloves, 1st generation planted in May 2016, harvested in July 2016. 2nd generation planted in October 2016, harvested in July 2017. 3rd generation planted in October 2017, harvested in July 2018. Plasma treatment of 1st generation: pilot-scale plasma pulsed E-mode glow, $P_N = 200$ W, $p = 70$ Pa, $t = 30$ s (6 × 5 s on, 5 s off). Error bars represent standard error.

For the garlic treated with the afterglow regimen in the first generation (Figure 3.71), the mean bulb mass was also increased compared to the bulb mass of untreated garlic, in both generations. The difference was not statistically significant in the first generation, but was in the second.

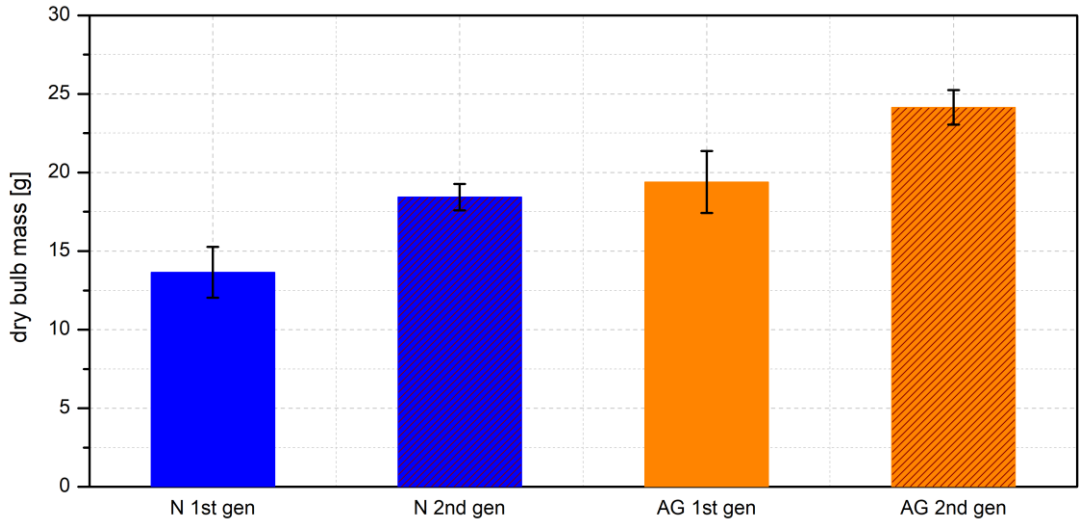

Figure 3.71: Average mass of dried bulb for 2nd generation of garlic. Grown from unpeeled cloves, 1st generation planted in October 2016, harvested in July 2017. 2nd generation planted in October 2017, harvested in July 2018. Plasma treatment of 1st generation: pilot-scale plasma H-mode afterglow, $P_N = 200$ W, $p = 70$ Pa, $t = 45$ s. Error bars represent standard error.

Chapter 4

Discussion

4.1 Plasma Characterization

4.1.1 Optical emission spectroscopy

4.1.1.1 Flow configuration

4.1.1.1.1 Plasma spectra As seen in Figure 3.1, the main species detected by OES in E-mode plasma alone is the neutral oxygen atom (O). The prevalence of oxygen atoms as the primary reactive species is typical for low-pressure RF oxygen plasma [10], and the density of positive ions in such plasma is several orders of magnitude smaller than that of neutral atoms. The reasons for this general rule have been elaborated elsewhere [74], but for the sake of completeness, let us mention the key reason relevant for plasma sustained in glass tubes by electrodeless RF discharges: while the probability for surface neutralization of positively charged ions is almost 100 % regardless of the surface properties, the probability for the surface loss of atoms depends enormously on the type of material facing plasma. For many glasses, the probability for the loss of atoms by heterogeneous surface recombination is below 10^{-3} [75]. Furthermore, the dissociation energy of oxygen molecule is about 5 eV, while the ionization energy is close to 12 eV. There are a couple of long-living metastable states of neutral oxygen molecule at potential energy of about 1 and 2 eV, so stepwise dissociation is likely to occur. For these reasons, as shown in Figure 3.9, the atom density is as large as 8.5×10^{21} m^{-3} in the pilot-scale reactor in these experiments.

As seen by the presence of O_2^+ and O^+ lines, ionization still occurs, but is not nearly as prominent [5]. It is also not expected that ions would have high kinetic energy in a RF discharge. The relevant positive ions in oxygen plasmas are O_2^+ and O^+, but dissociative ionization is energetically less favorable than ionization of molecules [18], which explains why the O_2^+ lines are relatively more intense than the O^+ lines. The presence of the OH band and hydrogen H_α line is the consequence of residual water vapor present in the vacuum system as an impurity [76].

4.1.1.1.2 Spectra during clove treatment OES spectra recorded during treatment of garlic cloves (Figure 3.2) show considerable changes in the intensity of the spectral lines. This indicates an important change in the plasma chemistry. Decreased signal intensity of oxygen atomic lines suggests a decreased production rate or an increased loss rate [76], and can be described by several contributing factors. The garlic clove, peeled or unpeeled, facilitates O atom loss due to the reactions occurring at the clove surface. In the process of functionalization, O atoms chemically incorporate into the surface structure [16]. With further oxidation, due to chemical etching, they are lost from the surface in the form of CO_2, via a mechanism which will be further addressed below. In addition, recombination

of O atoms to parent molecules may also occur. While to the best of our knowledge, no data is available regarding recombination coefficients for plant surfaces or waxes, recombination coefficients for polymers are typically on the order of 10^{-3} [9]. This value is rather low, but still 1 – 2 orders of magnitude greater than that of borosilicate glass [77], which forms the reactor walls. Even further, the chemical species released from the clove intervene with the formation of reactive species, or react with them in the plasma volume [78], thereby decreasing their density.

Simultaneously, the H_α and OH lines increase. This indicates that the water present in the system is no longer a residual impurity, but actively added into the plasma. The source of the water is the clove itself. Two mechanisms are possible. Firstly, if chemical etching occurs at the surface, OH radicals form by hydrogen abstraction by the oxygen atom, and may then abstract another hydrogen to form water [78]. Secondly, if cracks or fissions form in the cuticle [32], this may facilitate water release from the bulk of the clove in the low-pressure environment. The dissociation energy of the water molecule is rather low. Therefore, once in the gas phase, water is dissociated to OH and H radicals by the plasma electrons [79]. This is seen in the OES spectra as an increase in the intensity of the corresponding spectral lines.

4.1.1.1.3 Comparison of peeled and unpeeled cloves Figure 3.3, Figure 3.4, as well as Table 5.1, all show that the increase in H_α and OH line intensity is larger for peeled than unpeeled cloves, especially at $P_N = 100$ or 200 W. This indicates that more water is present in the system when a peeled clove as opposed to an unpeeled clove is treated. Since both the protective leaf and the peeled clove are covered with a cuticle, no considerable differences in the etching products are expected. However, compared to the clove itself, which contains about 65 % water [61], the protective leaf is relatively dry, with the cells of its parenchyma mainly collapsed [62]. Its function is protection of the clove from environmental effects, including water loss. Therefore, under the assumption that etching and cracking of the treated surface takes place, less water is present in the system during the treatment of the unpeeled clove, firstly, due to a lesser quantity of water in the treated surface, and secondly, due to protection of the water-containing clove from the plasma by the protective leaf.

4.1.1.1.4 Plasma treatment of cloves with increasing power Figure 3.3 (A) and Table 5.1 present OES spectra recorded during treatment of a peeled clove at increasing P_N, and thus at increasing P_{EFF}. Unsurprisingly, the signal of all important emission lines increases with increasing P_N. In the E-mode plasma, at fixed pressure, reactive species density will gradually increase with increased treatment power [80], explaining the O and O_2^+ signal intensity increase. This is also seen in our own catalytic probe measurements of n_O (Figure 3.9). This increase, in turn, accelerates surface modification, resulting in accelerated etching and water release from the clove, which is evident in the increased H_α and OH lines. In Figure 3.5 (A), the time course of the OH line signal intensity during the treatment of a peeled clove at increasing P_N is plotted. The steeper increase and higher plateau are also in agreement with the above explanation.

In parallel, Figure 3.3 (B) and Table 5.1 present the results of OES measurements during treatment of an unpeeled clove at increasing P_N, and thus at increasing P_E. The observed signal increases are very similar to the ones seen for peeled clove treatment. One prominent difference is the appearance of spectral lines at approximately 588, 766, and 770 nm. These lines appear due to the presence of sodium and chlorine. Out of all treatment conditions used in our experiments, the 300 W, 50 Pa condition has the highest O atom density. When treating unpeeled cloves, exposed parts of the protective leaf (the thin tip,

or any cracks that form due to the heat) may begin to sear due to intense heat generated in the reactions with the plasma species. This causes thermal degradation of the organic compounds in the protective leaf, releasing material into the gaseous phase. This may be the source of elements such as sodium and chlorine detected during this treatment.

4.1.1.1.5 Plasma treatment of cloves with increasing working pressure As seen in Figure 3.9, oxygen atom density within the selected plasma parameters range either does not change ($P_N = 100$ W) or decreases ($P_N = 200$ W) with increased working pressure. At low pressures, the mean free path that particles can travel is larger, so the electron temperature is increased. Consequently, ionization probability is also higher, and thus the electron density is increased [76]. This results in a more intense excitation of reactive plasma species, detected as an increase in the OES signal intensity.

The accelerated etching allows for more rapid water loss from the clove, resulting in an increased OH emission line signal (Figure 3.5 (B)). The plateau is reached when an equilibrium is established between the water release from the clove and the pumping speed.

4.1.1.2 No-flow configuration

Etching is definitely present during plasma treatment of cloves, as confirmed by SEM images of the surface (Figure 3.36 – Figure 5.2) and further explained below. During this process, the organic material is gradually degraded, and C is released into the system in the form of volatile compounds, in particular, CO and CO_2 [81]. When organic material is oxidized in this way, emission lines of CO are typically seen in OES spectra, commonly including CO Angstrom bands at around 519.5 and 560 nm [82].

Interestingly, in our experiments in the flow configuration, the CO emission lines are either not present, or seen very weakly. Because the system is pumped throughout, the CO is steadily removed by the pump, and may remain under the detection limit of the OES. To further confirm the presence of CO, and thereby the occurrence of etching, spectra were also recorded in the no-flow configuration. In these discharges, the signal intensity changes with time are significantly more dramatic than in the flow configuration. To better present these dynamic changes, the data is plotted in Figure 3.6 through Figure 3.8 as time courses of signal intensities at selected wavelengths, rather than "static" spectra at a specific time point.

The initial presence of the CO lines in these charts confirms the occurrence of etching, but the CO signal intensity is still rather low, and subsides rapidly. This is due to the plasma conditions in the no-flow configuration. Firstly, the reactor is not pumped, but the etching and water loss introduce new molecules into the gaseous phase, resulting in constantly rising pressure in the reactor, mainly due to water accumulation. At the same time, no additional O_2 is introduced into the system. All of the above strongly influence the plasma chemistry. As the plasma conditions and chemistry change due to the lack of pumping and oxygen supply, etching subsides, and the CO signal decreases rapidly.

When comparing the temporal behavior of the spectral lines between treatments of the peeled and unpeeled clove (Figure 3.8), most spectral lines are more intense for the unpeeled clove, with the exception of OH. This indicates more intense etching of the unpeeled clove, but more water presence for the peeled one. More water released during peeled clove treatment also contributes to faster pressure rise, and therefore a shorter-lasting plasma.

4.1.2 Catalytic probe

4.1.2.1 n_O in the E-mode plasma without garlic sample

In Figure 3.9, n_O values recorded in the pilot-scale E-mode plasma without garlic sample are seen. The n_O increases with increasing P_N. This corresponds well to the OES spectra in Figure 3.1, where the O emission lines intensity increases with increased P_N. At fixed working pressure, n_O is known to increase with increasing generator power [83], and the parameters selected here appear to be in a range of approximately linear increase.

The n_O also appears to increase with decreasing working pressure, at least at $P_N = 200$ W. As explained above, the larger mean free path at low pressures increases the electron temperature, and thereby, the electron density via higher ionization probability [76]. Via Eq. (1.1), this results in an increased n_O due to increased production of O from the parent O_2 molecules.

4.1.2.2 Probe signal increase during clove treatment

From Figure 3.10, it is evident that when a garlic sample is introduced into the plasma, the recorded catalytic probe signal increases. The observed increase is contrary to what would be expected for polymers or other materials that are functionalized by oxygen plasma. In a plasma system, the oxygen atom density will depend on the equilibrium between the production and loss of the atoms. If a material treated in a plasma is functionalized, the n_O should decrease, as the oxygen atoms are "spent" introducing new functional groups to the surface.

The signal detected by the catalytic probe depends on the amount of recombinations of reactive plasma species that occur at the probe tip surface [84]. To calculate n_O, we assume that the signal increase is due to oxygen atom recombinations ($O + O \rightarrow O_2$), which is true for plasma alone if the effect of ions is excluded. However, the probe is not specific to O recombinations, as other exothermic reactions also affect the signal. This includes recombinations of OH ($OH + H \rightarrow H_2O$) and CO ($CO + O \rightarrow CO_2$) radicals.

From this reasoning, it follows that the signal increase recorded in the presence of garlic does not represent the recombination of O atoms alone. As explained above, etching and water loss from the clove introduce new species into the gaseous phase during plasma treatment of cloves. The OH and CO radicals released in this way then recombine at the probe tip surface and increase the recorded signal. Thus, Figure 3.10 confirms the occurrence of etching and water desorption from the clove.

Further, in Figure 3.11, we compare the signal increase between plasma alone, treatment of one or three peeled cloves, and treatment of one or three unpeeled cloves. We see that the recorded signal is higher in all cases of garlic sample treatment. Further, it is higher during the treatment of three cloves compared to one clove, as well as during the treatment of peeled cloves compared to unpeeled cloves. This is explained by the amount of CO and OH radicals released from the cloves. A higher number of cloves has a larger surface exposed to the plasma than a single clove, and thus releases more CO and OH during treatment. Similarly, the peeled clove is a practically limitless supply of water to serve as a source of OH radicals, while the water content in the protective leaf is rather low, and thus likely exhausted soon after the beginning of treatment.

4.1.2.3 n_O during treatment of peeled garlic

Figure 3.12 (A) shows that the recorded probe signal during treatment of a peeled clove increases with increasing P_N and decreasing working pressure, similar to the plasma alone. However, in addition to the equilibrium of O atom formation and loss, the introduction of OH and CO into the system must be accounted for in the explanation of signal behavior. We see that the signal increases during the course of the treatment become steeper with increasing P_N. This is explained by the intensity of etching and water loss, which is higher at increased P_N. The intensity of the OH line in OES spectra indicates the importance of the OH radical in shaping the signal recorded by the catalytic probe. The OH signal in Figure 3.5 (A) is about 1.5 × higher for P_N = 300 W compared to P_N = 200 W, and so is the signal recorded at the catalytic probe (Figure 3.12 (A)).

From Figure 3.12 (B), we see that the plateau reached during short treatment (< 120 s) gradually begins to drop once the treatment time crosses ~ 100 s. This is likely due to the exhaustion of the water adsorbed on the surface and found in the upper surface layers. Water from deeper layers of the clove is more difficult to bring to the surface during treatment, and takes a longer time to do so. Thus, with the density of OH radicals slowly dropping, the signal at the catalytic probe begins to gradually decrease.

During treatment of peeled cloves in the H-mode afterglow position (Figure 3.13), we see that the recorded n_O is about 2.5 – 3 × 10^{21} m^{-3}. Compared to the measurements in Figure 3.12 (A), this value is quite modest. In addition to a smaller n_O due to the distance from the coil, this is also a consequence of less intense surface etching, and thereby less intense water loss, in the afterglow position.

4.1.2.4 n_O during treatment of unpeeled garlic

As above, Figure 3.14 (A) shows that the recorded probe signal during treatment of a peeled clove increases with increasing P_N and decreasing working pressure. The irregular signal obtained at 300 W, 50 Pa is the consequence of burning of the exposed edges of the protective leaf.

It is interesting that during prolonged treatment of unpeeled cloves in E-mode plasma (Figure 3.14 (B)), the signal on the catalytic probe rises to a peak at about 15 s, falls to a low plateau at about 100 s, and begins to rise again at about 200 s. The initial peak may present either loss of water from the protective leaf (which is more plausible), or intense initial etching (which is less likely due to the low P_{EFF} and the absence of etching products in OES spectra at these plasma parameters). As the protective leaf is dryer than the clove itself, it is possible that most of its water is lost in the first minute, after which, there is a period of functionalization, followed by etching after about 200 s.

As above, the n_O results in the H-mode afterglow position (Figure 3.15) are a result of the distance from the coil, less intense surface etching, and less intense water loss.

4.2 Temperature

4.2.1 Heating power

4.2.1.1 Initial heating

To evaluate the effect of heating during plasma treatment on garlic cloves, TC measurements during treatment were performed. In Figure 3.16, we see that as expected, the temperature starts increasing upon turning on the discharge, which is explained by exothermic surface effects rather than immediate increase of the gas temperature. Namely, the neutral gas kinetic temperature in oxygen RF plasma sustained with an electrodeless discharge created in a glass tube at low pressure and power remains practically at room temperature due to the lack of gas-phase collisions that would cause transfer of available power to the kinetic energy of gaseous molecules [85].

The initial stage of heating (for the first 10 seconds of plasma treatment) is shown in Figure 3.17 (B). The initial temperature is about 25 – 30 °C. Just after turning on the discharge, the temperature for all four cloves drops for 10 °C or more. There is no reason for immediate cooling of a clove in a fraction of a second, so this effect is explained by RF interferences. Although both the thermocouple wires and the voltage meter are kept at floating potential, there is some interference, so the sudden drop of the temperature just after turning on the discharge is an artifact. Following that, the measured temperature during plasma treatment of a peeled clove increases rather intensely for the first few s. It rises from about 20 °C to about 40 °C within the first 10 s of treatment. After this initial rise, the temperature assumes a rather slow increase.

Neglecting the interference artifact, it is possible to explain the heating of the cloves after turning on the discharge. If the heating power were constant and the thermal conductivity of the cloves infinite, the initial increase of the clove temperature would have been linear with time for the first second after turning on the discharge. Namely, after turning on the discharge, any cooling effects are easily neglected since the temperature difference between the clove and surrounding gas is marginal. The linear approximation of the temperature curves after turning on the discharge enables determination of the heating power. At the conditions presented in Figure 3.17, the time derivative of a clove is about 15 K/s. One can calculate the power taking into account a standard relation, i.e.

$$P = m\ c_{\mathrm{p}}\ \frac{\Delta T}{\Delta t}\ . \tag{4.1}$$

Here, P is the heating power, m the mass of the clove, c_{p} the specific thermal capacity of garlic at room temperature, and $\Delta T/\Delta t$ the slope of the linear approximation of the temperature curve after turning on the discharge. The specific thermal capacity of garlic is unknown, but can be replaced with a value typical for fresh fruit, i.e., 3.5×10^3 J kg^{-1} K^{-1} [86]. This assumption is reasonable since the major component (~ 65 %) of a garlic clove is water, same as for fresh fruit. The rest is biological matter (complex hydrocarbons of lower thermal capacity), so the specific heat capacity is somewhat lower than for pure water (4.2×10^3 J kg^{-1} K^{-1}). Still, one can take into account the numerical values using available data and calculate the heat dissipated on a clove surface in unit time after turning on the discharge using Eq. (4.1). The mass of a clove was about 1 g and the time derivative about 15 K/s, so the initial heating power was

$$P = 10^{-3}\ \mathrm{kg} \times 3.5 \times 10^3\ \mathrm{J\ kg^{-1}\ K^{-1}} \times 15\ \mathrm{K\ s^{-1}} = 50\ W. \tag{4.2}$$

From Table 2.1, we know that the P_{EFF} at these discharge conditions is 50 W. If the above calculation is correct, this would mean that all available discharge power is used for heating of the clove. As shown below, other processes, namely functionalization and etching, also take place, so this is obviously untrue. In Figure 3.16, we additionally see that at the same experimental conditions, but in atmospheric air instead at 50 Pa of oxygen, the temperature time course is practically identical than in the above experiment. At atmospheric pressure, no discharge appears when the generator is turned on. This means that the temperature increase in this case is due to induction heating, as the sample is exposed to the EM field formed by the coil. Therefore, we can state that the temperature increase of garlic during plasma treatment is not as high as suggested by the TC measurements.

As explained above, the power used for clove heating is dissipated on the surface of the clove, so the relevant parameter is the power per unit surface. Cloves are not geometrically simple, but a useful approximation of the surface area is to take into account spherical geometry. Such an approximation underestimates the real surface of a clove, but on the other hand, a significant part of clove surface is shaded from plasma since the clove is placed onto a microscope slide during treatment. The surface of a sphere is calculated as

$$A = 4\pi \left(\frac{3m}{4\pi\rho}\right)^{2/3}. \tag{4.3}$$

Here, ρ is the density of garlic. In a reasonable approximation, the density is close to the water density, i.e., $\rho = 10^3$ kg m^{-3}. The surface of a garlic clove with a mass of 1 g facing plasma is therefore close to

$$\begin{aligned} A = 13 \left(\frac{3 \times 10^{-3} \text{ kg}}{13 \times 10^3 \text{ kg m}^{-3}}\right)^{2/3} = 13 \left(0.23 \times 10^{-6} \text{ m}^{-3}\right)^{2/3} = 5 \times 10^{-4} \text{ m}^{-2} \\ = 5 \text{ cm}^2. \end{aligned} \tag{4.4}$$

The power density (i.e., power per unit surface area, as determined from the measured temperature from Figure 3.17) is therefore around 10^5 Wm^{-2} = 0.1 W mm^{-2}:

$$\frac{P}{A} = \frac{50 \text{ W}}{5 \times 10^{-4} \text{ m}^{-2}} = 1 \times 10^5 \text{ W m}^{-2}. \tag{4.5}$$

Gaseous plasma was characterized by electrical and catalytic probes. The density of oxygen ions at the position of the sample was previously estimated using a double electrical probe and the value was about $n_{\text{i}} = 8 \times 10^{15}$ m^{-3}. The density of neutral oxygen atoms at the same position as determined with a fiber-optics catalytic probe (Figure 3.9) was $n_{\text{O}} = 7 \times 10^{21}$ m^{-3} at these discharge conditions.

The effects of weakly ionized highly reactive oxygen plasma are highly surface specific. There are two dominant heating mechanisms of solid materials facing this kind of plasma: (1) heating by positively charged molecular ions due to both surface neutralization and bombardment, and (2) heterogeneous surface recombination of oxygen atoms to parent molecules. Other effects like absorption of light quanta, surface relaxation of metastables, accommodation of any vibrational-excited molecules, and exothermic chemical reactions (low temperature "burning") are regarded marginal for such plasma, as explained in detail elsewhere [3].

Let us first consider the heating of cloves by positively charged ions. The ions move randomly in bulk plasma and their temperature is close to the neutral gas kinetic temperature, i.e., 300 K. Once approaching a surface, they first enter the pre-sheath, where they assume directed velocity which is calculated as the "Bohm velocity", i.e.

$$v_{\mathrm{Bohm}} = \sqrt{\frac{kT_{\mathrm{e}}}{M}}. \tag{4.6}$$

Here, k is the Boltzmann constant, T_{e} the electron temperature in plasma, and M the ion mass. Taking into account the typical electron temperature in weakly ionized oxygen plasma, 5×10^4 K, and the ion mass, 32 Da, the Bohm velocity is

$$v_{\mathrm{Bohm}} = 3 \times 10^3 \text{ m s}^{-1}. \tag{4.7}$$

The positively charged ions are accelerated in the sheath next to any floating object immersed into gaseous plasma. In the collision-less approximation, which is justified for such a plasma at the pressure of 50 Pa, the power dissipated on the surface of a garlic clove per unit surface area is

$$\frac{P_{\mathrm{ion}}}{A} = j_{\mathrm{ion}} W_{\mathrm{ion}}, \tag{4.8}$$

where j_{ion} is the flux of ions towards the surface (product of ion density and Bohm velocity), and W_{ion} the available energy, i.e., the sum of potential and kinetic energies. Both energies are close to 10 eV, so one can use the value $W = 20$ eV $= 3 \times 10^{-18}$ J. Inserting numerical values, i.e. $n_{\mathrm{i}} = 8 \times 10^{15}$ m^{-3}, $j_{\mathrm{ion}} = 2.4 \times 10^{19}$ m^{-2} s^{-1} and $W_{\mathrm{ion}} = 3 \times 10^{-18}$ J, one calculates the power dissipated per unit area on the surface of a garlic clove due to interaction of positively charged molecular ions as

$$\frac{P_{\mathrm{ion}}}{A} = 2.4 \times 10^{19} \text{ m}^{-2} \text{ s}^{-1} \times 3 \times 10^{18} \text{ J} = 72 \text{ W m}^{-2}. \tag{4.9}$$

The value in Eq. (4.9) is three orders of magnitude smaller than the measured power density presented in Eq. (4.5). Although several approximations were used to estimate the heating of garlic cloves by positively charged ions, it is clear that the ions play a marginal role.

We have established that the density of neutral oxygen atoms in weakly ionized oxygen plasma is orders of magnitude larger than the ion density, around $n_{\mathrm{O}} = 7 \times 10^{21}$ m^{-3} in the pilot-scale reactor experiment at the given parameters (Figure 3.9). The atoms are neutral, so they are not accelerated in the sheath next to the sample surface, but move thermally, so the flux of atoms onto the surface of any object facing plasma is

$$j_{\mathrm{O}} = \frac{1}{4} n_{\mathrm{O}} < v_{\mathrm{a}} >. \tag{4.10}$$

Here, $<v_{\mathrm{O}}>$ is the average velocity of O-atom thermal motion, which is calculated from Boltzmann law as

$$< v_{\mathrm{O}} > = \sqrt{\frac{8kT}{\pi \frac{M}{2}}}. \tag{4.11}$$

Taking into account numerical values and assuming a room temperature of $T = 300$ K, one gets the average random velocity of O-atoms

$$< v_{\mathrm{O}} > = 630 \text{ m s}^{-1}. \tag{4.12}$$

The heating due to interaction of O-atoms with the garlic surface is calculated using Eq. (4.8), except that W from Eq. (4.8) should be replaced with "average energy an atom brings to the surface". If all atoms recombine to molecules, and the molecules leaving the surface are in thermal equilibrium with the solid material, the heating by heterogeneous surface recombination of O-atoms to parent molecules will be

$$\frac{P_{\mathrm{O}}}{A} = \frac{1}{2}\, j_{\mathrm{O}} W_{\mathrm{d}}. \tag{4.13}$$

Here, W_{d} is the dissociation energy of the oxygen molecule: $W_{\mathrm{d}} = 5.2$ eV $= 8 \times 10^{-19}$ J. The factor 1/2 comes from the fact that an oxygen molecule contains 2 atoms. The heating by atoms in the approximation of 100 % surface recombination would be

$$\frac{P_{\mathrm{O}}}{A} = \frac{1}{8}\, 7 \times 10^{21}\ \mathrm{m^{-3}} \times 6.3 \times 10^{2}\ \mathrm{m\ s^{-1}} \times 8 \times 10^{-19}\ \mathrm{J} = 4 \times 10^{5}\ \mathrm{W\ m^{-2}}. \tag{4.14}$$

The calculated value is larger than the measured heating power as shown in Eq. (4.5) by a factor of 4. The discrepancy is explained by the fact that the surface recombination probability is not 100%. As mentioned earlier, the recombination coefficient depends on the type of material and its morphology [75]. The value as deduced from Eq. (4.5) and (4.14) is surprisingly large and worth discussing. Namely, dividing the calculated value in (4.14) with the measured one in (4.5) gives a recombination probability of

$$\gamma = 0.25. \tag{4.15}$$

This value is typical for smooth catalytic materials and definitely well above the order of 10^{-3} typical for many polymers [9]. Such a large recombination coefficient could be explained by several effects, the most obvious of which are (1) surface roughness, (2) the presence of catalytic materials on the surface of an object facing plasma. The surface roughness plays an important role in surface recombination of oxygen atoms. In fact, the largest recombination coefficients exceeding the value $\gamma = 0.5$ have been measured for a rather inert material of extremely rich morphology on the sub-micron scale [87]. The effect was explained by trapping O-atoms into pores of dimension well below the mean free path of O-atoms, which is roughly 200 µm at a pressure of 50 Pa. In the SEM images of untreated peeled clove surface shown in Figure 3.39, we see that the surface is rather smooth, and despite its roughening with increased treatment time, certainly not rough enough to cause such trapping of O atoms. From this consideration, one can conclude that the surface roughness is not sufficient to explain the recombination coefficient presented in Eq. (4.15). The surface composition of an untreated peeled garlic clove as determined by XPS is shown in Table 3.1. The surface is composed predominantly of hydrocarbons with a few at.% of oxygen and a few other elements in marginal amounts. There is obviously no catalytic material on the surface of untreated garlic. This confirms our earlier conclusion that the calculated heating power is overestimated due to the effect of induction heating on the recorded temperature values. As such, the TC measurements cannot be used to determine the absolute temperature of the treated clove, but a relative comparison is still possible.

4.2.1.2 Further heating

After several seconds of plasma treatment, the increase of the garlic temperature is not as extensive as initially. Figure 3.17 (A) reveals that the temperature still increases with increasing time for the first few minutes, but the increase is slower. If the curve from about 30 to 300 s in Figure 3.17 (A) is interpolated with a line, the temperature increase in this region will be a bit below 0.1 K/s. Such a slow increase could be explained by several effects, including the slow modification of the surface morphology, weak variation of the recombination coefficient, or increased temperature of gas surrounding the clove. The latter explanation is preferred. Such a slow increase is typical for thermal effects, since the entire discharge tube slowly warms up, allowing gas molecules to accommodate on warm surfaces and thus causing an increase of the gas temperature.

4.2.2 Heating at different discharge parameters

Figure 3.17 shows the time course of temperature during peeled and unpeeled clove treatment at two different discharge conditions: 200 W at 50 Pa, as well as 300 W at 70 Pa. As mentioned earlier, these temperature values are not absolute due to induction heating effects, but can be used for relative comparison.

In Figure 3.9, we see that the oxygen atom density is around 7×10^{21} m^{-3} at 200 W and 50 Pa, while it is around 8.5×10^{21} m^{-3} at 300 W and 70 Pa. Therefore, it is unsurprising that the clove treated at the higher P_N heats slightly more rapidly than the one treated at the lower P_N.

It is further interesting to note that unpeeled cloves heat somewhat more rapidly than peeled cloves. This is due to the nature and function of the protective leaf, which prevents water and heat from leaving the clove. For this reason, heat damage affects unpeeled cloves earlier, i.e., at shorter treatment times than peeled cloves, as will be shown below in the sprout and root growth section.

4.3 Surface Chemical Composition

4.3.1 Untreated clove surfaces

XPS is a very surface-sensitive technique, analyzing the chemical composition of the surface about 5 nm in depth. Given a plant cuticle thickness of 0.1 – 10 μm [64], XPS only analyzes a thin outermost layer of the cuticle, specifically, the epicuticular waxes coating its outer surface. Our results indicate that the epicuticular wax composition of the protective leaf and the clove surface differs somewhat, which is commonly the case between different plant organs in the same species [64].

The oxygen concentration is higher at the untreated protective leaf surface compared to the untreated clove surface (Table 3.1). This indicates a higher degree of initial oxygenation of the protective leaf cuticular waxes. As will be shown in ATR-FTIR spectra (Figure 3.31), the oxygen is mainly present in the form of –OH and C=O groups, which are typically present as terminal functional groups of cuticular wax compounds [64].

While the WCA of the native protective leaf and clove surfaces is comparable, the WU of untreated unpeeled cloves is much higher than that of untreated peeled cloves (Figure 3.43). This indicates a higher hydrophobicity of the native clove surface compared to that of the native protective leaf surface, and the lower O/C ratio we recorded at the clove surface is therefore expected. This result indicates that the peeled clove cuticular waxes contain a higher fraction of non-functionalized hydrocarbons, which are more hydrophobic than their equivalents with polar, oxygen-containing functional groups.

The greater variability of C and O content in the protective leaf may be attributed to biological variability, which is presumably higher in the protective leaf than the clove itself. Often, a difference in the protective leaf of different cloves, from the same garlic batch or even the same bulb, is already easily detectable in the protective leaf color, thickness, or texture. On the other hand, all healthy peeled cloves appear uniformly white and smooth.

To the best of our knowledge, the only XPS analyses of garlic in available literature were performed on garlic peel that was processed and ground before analysis, with emphasis on the detection of externally added adsorbed materials [88, 89]. On the other hand, there are instances of XPS analyses of other native plant cuticles found in the literature. In tomato fruit cuticles, 96.4 % C and 3.6 % O were detected on the cuticle surface, corresponding to an O/C ratio of 0.037 [90]. On the adaxial leaf surfaces of two clones of willow, the concentration of C, O and N was either 86.4, 12.0 and 1.6 %, or 89.7, 8.8 and 1.5 % [91]. Cherry laurel leaf surfaces showed an average of 94.0 % C, 4.7 % O, 0.9 % N, and 0.4 % Si [92]. This confirms that plant cuticle waxes vary in their surface chemical composition, but nonetheless consist mainly of hydrocarbons with some oxygen-containing functional groups [64].

4.3.2 Carbon and oxygen content

4.3.2.1 Unpeeled clove surface

4.3.2.1.1 Pilot-scale E-mode glow treatment After oxygen plasma treatment of organic materials, in particular aliphatic hydrocarbons, O concentration at the surface typically increases with increased dose of plasma reactive species [93, 94]. This is true for all results of XPS measurements performed on the garlic protective leaf, where increased treatment time and/or generator power has resulted in an increased O concentration and an increased O/C ratio. A notable decrease in C and increase in O content was observed after as little as 5 s of treatment, particularly for the protective leaf of cloves treated in the pilot-scale plasma (Table 3.2). The fastest increase in surface O content is achieved within the first 30 s of treatment, and with increasing treatment time, the O content rise becomes more gradual. Saturation of organic material surface with oxygen-containing functional groups is typical, and is complemented by chemical etching, which is further explained below. Within the treatment times used in our experiments, saturation of the clove surface has not been completely achieved, but is gradually approached. This behavior could also be the consequence of simultaneous functionalization and etching, during which, organic material is removed from the surface, deeper layers of varying chemical composition are uncovered, and thus analyzed with XPS at the given treatment time. The unpeeled clove was not treated for longer than 120 s in the pilot-scale plasma to avoid burning of the dry protective leaf, which was almost completely burned away at the exposed side of the clove during a preliminary treatment of 600 s at the same conditions.

The seed coats of many plant species' seeds are also covered with cuticles [95], and a comparable effect of cuticular wax oxidation was found in quinoa seeds treated with air plasma, either as an atmospheric pressure surface DBD or low pressure capacitively coupled RF discharge [29]. Nasturtium seed treatment with an atmospheric pressure DBD in an air/He mixture also increased O with treatment time, rapidly reaching saturation [15].

4.3.2.1.2 Pilot-scale H-mode afterglow treatment The O/C ratio of the protective leaf surface increases more gradually during pilot-scale H-mode afterglow treatment compared to the E-mode glow treatment. When the same plasma conditions are used to produce both the E-mode glow and the H-mode afterglow plasma (Figure 3.19), the slope at which the O/C ratio increases in the afterglow treatment is approximately half the slope of the glow treatment. At a higher P_N and lower working pressure (Table 3.3), the increase is somewhat higher, and the O/C ratio reaches a value of ~ 0.7, as opposed to ~ 0.5, within 60 s of treatment (Figure 3.21).

In our plasma system, neutral oxygen atoms are reasonably long-lived species, as they do not readily recombine on the glass reactor walls due to the low recombination coefficient of glass [77]. While n_O drops with increasing distance from the immediate glow discharge, it is nevertheless maintained at a considerable level throughout the discharge tube, assisted by the gas flow downstream of the discharge [13]. In addition, for discharges like the one used in this experiment, weak capacitive coupling is present throughout the reactor. The combination of these two effects exposes the sample in the afterglow treatment position to a lower, but still considerable flux of O atoms compared to that of the E-mode glow.

In the two experiments considering treatment in the pilot-scale reactor afterglow, the XPS analysis result at the only repeated treatment time (30 s) is comparable, despite the difference in P_{EFF} and working pressure (200 W and 50 Pa as opposed to 300 W and 30 Pa). This may indicate that treatment time is the most important functionalization parameter when treating the garlic clove with H-mode afterglow. In the same plasma system, it has

previously been shown that after transition to the H-mode, increasing the generator power does not critically increase O atom density, especially at low pressures [80]. While the considerable increase in the density of charged and highly excited species in the H-mode must be considered, the effect of these species is practically negligible outside of the immediate H-mode glow discharge.

4.3.2.1.3 Pulsed treatment Two different pulsed treatment regimens were used in the pilot-scale E-mode glow plasma. The O concentration and O/C ratio increases are higher in the treatment regimen with higher P_N and longer total treatment time. Comparing the O/C ratio between the 200 W treatments, pulsed (Figure 3.22) and continuous (Figure 3.19), it is evident that at the same treatment time (30 s), the O/C ratio is higher in the continuous treatment. This is due to the lower working pressure in that experiment (50 as opposed to 70 Pa), which produces a higher n_O (Figure 3.9). As will be shown below, the effect of the continuous and pulsed treatments on the sprout and root growth does not differ significantly if the treatments are performed using the same plasma parameters.

4.3.2.2 Peeled clove surface

4.3.2.2.1 Pilot-scale plasma treatment As with the protective leaf, oxygen plasma treatment increases O concentration at the peeled clove surface (Table 3.5). Compared to the protective leaf, the O increase at the peeled clove surface is more gradual at the same treatment condition. The same is true for the O/C ratio, which within 120 s of treatment increases up to ~ 0.6 (Figure 3.24), as opposed to ~ 2.0 for the protective leaf (Figure 3.19). While in the wax oxidation process, the most important initialization reaction is abstraction of a hydrogen atom from the alkyl chain, oxidation after abstraction of H from a terminal alcohol group is the most important mechanism for further oxidation [96]. Therefore, cuticle waxes already containing terminal –OH groups may undergo more rapid further oxidation, as well as the etching that follows. This is further explained below.

4.3.2.2.2 Industrial-scale plasma treatment The oxidation seen at the peeled clove surface after industrial-scale plasma treatment is limited to a few at.% (Table 3.6, Figure 3.26), despite higher P_N at the generator. While it is difficult to directly compare the treatments in the pilot-scale and industrial-scale plasma systems, we can ascribe this difference to the experimental conditions. Although the nominal power is about 4 × larger in the industrial-scale experiment (~ 800 W, as opposed to 200 W), the volume of the industrial-scale reactor is larger than that of the pilot-scale reactor by nearly a factor of 100 (~ 63 L, as opposed to ~ 0.8 L). Even without the assumption of uniform plasma distribution throughout the discharge tube, we can see that the plasma power density will be much larger in the more compact pilot-scale reactor. Therefore, the treatment in the industrial-scale plasma in this case is gentler. Further, no presence of mineral elements (silicon, calcium, potassium) was detected, indicating that no substantial etching of the surface took place during plasma treatment.

4.3.2.2.3 Peeled clove surface under the treated protective leaf When an unpeeled clove was treated in the pilot-scale plasma, peeled, and the clove surface under the treated protective leaf was analyzed with XPS, the O concentration increased only slightly (Table 3.7). In comparison, the O concentration increase at the surface of a peeled clove treated at the same conditions for the same amount of time (90 s) increased over 12 times as much. This indicates that when still properly attached, the protective leaf presents an effective barrier against plasma reactive species penetration to the clove surface.

4.3.2.3 High-resolution XPS spectra

To obtain additional data regarding surface chemistry, high-resolution C 1s spectra were analyzed (Figure 3.27, Figure 3.29). Differences in the area of sub-peaks were detected, corresponding to the relative frequency of different chemical bonds appearing on the surface. Four sub-peaks were considered: (1) ~ 284.8 eV for C–C/C–H bonds, (2) ~ 286.1 eV for C–O bonds, (3) ~ 287.5 eV for C=O bonds, and (4) ~ 288.9 eV for O–C=O bonds [93].

4.3.2.3.1 E-mode glow treatment

4.3.2.3.1.1 Protective leaf In case of untreated protective leaf (Figure 3.27), the main peak appears at the binding energy of 284.8 eV, corresponding to C–C/C–H bonds. The main peak takes up > 90 % of the total peak area, which is expected, as the cuticular waxes are made up mostly of long hydrocarbon chains, where C–C and C–H bonds are ubiquitous. The sub-peaks of C–O, C=O and O–C=O bonds appear at the higher binding energy side of the main peak. They represent the terminal oxygen-containing functional groups of the cuticular wax compounds, as well as the ester bonds of the wax compound dimers which form from the alcohol and carboxylic acid monomers [64]. In comparison, a native, untreated cherry laurel leaf cuticle was analyzed to have relative peak areas of 87.1, 7.6, 3.4, and 1.9 %, for C–C/C–H, C–O, C=O, and O–C=O peaks, respectively [92]. The higher relative presence of all oxygen-containing functional groups compared to garlic is due to the differences in cuticular wax composition between species and plant organs.

As treatment time progresses up to 30 s, the area of the main peak (C–C/C–H at 284.8 eV) diminishes from ~ 94 % to ~ 46 % (Figure 3.28). This is in line with the rapid decrease of the surface C concentration in the same time frame (Figure 3.18). The concurrent increase in the area of the remaining sub-peaks corresponds to the O concentration increase. All of this indicates that functionalization of the protective leaf surface is taking place, as oxygen is introduced onto the surface through mechanisms further presented below. Further oxidation of already present functional groups also takes place. This evolution in the C 1s peak shape is typical for organic material exposure to oxidant plasmas [93], and was also recorded on agricultural seed surfaces. A low-pressure RF discharge and an atmospheric DBD, both in air, decreased the C–C/C–H peak and increased the presence of oxygen-containing functional groups on quinoa seeds [29]. On nasturtium seeds treated in air/He atmospheric DBD, increases in C=O and O–C=O also occurred, but the relative sub-peak areas reached saturation already after 30 s [15].

Out of the sub-peaks for carbon-oxygen bonds, the C–O peak increases the most rapidly. This represents the introduction of new –OH groups onto the alkyl chains, and is therefore consistent with the functionalization which is taking place. The C=O and O–C=O peaks increase comparably up to 15 s of treatment. Then, the C=O peak begins to decrease, and the O–C=O peak keeps increasing up to 60 s of treatment. As aldehydes are not particularly likely to form in the oxidation process, and are likely to be rapidly oxidized further to carboxylic acids [96], it makes sense that the O–C=O peak is more prominent than the C=O peak at most of the treatment times.

Looking at the surface morphology (Figure 3.36), it is clear that up to 30 s of treatment, there is no intense etching, and the surface changes appear more as reshaping of the existing morphology. However, at t = 30 s and onward, etching is clearly evident. As seen in Figure 3.28, after 30 s, the C–C/C–H peak area increases again, while the remaining sub-peaks decrease. This is due to the intense chemical etching which begins around that time and exposes deeper, not yet oxidized layers. This equilibrium between functionalization and etching is reflected in the more gradual surface C content decrease and O content increase, as well as in the increasing relative area of the C–C/C–H component of the C 1s peak.

4.3.2.3.1.2 Clove surface On the clove surface, within the first 60 s of treatment, the relative area of C 1s sub-peaks barely changes (Figure 3.30), just as the O/C ratio remains relatively unchanged within this time frame (Figure 3.24). The C–O peak decreases, and the C=O and O–C=O peaks increase slightly, likely as oxidation of existing terminal –OH groups takes place. After 60 s, with the increase of O concentration and decrease of C concentration (Figure 3.23), the C–O peak increases, along with more gradual increases of the C=O and O–C=O peaks. The behavior of curves for all sub-peaks between 60 and 120 s of treatment is very similar to what we see within the first 15 s of treatment of the unpeeled clove. This indicates that the same processes are taking place on the peeled clove surface, however, they start and progress more slowly.

Naturally, the initial chemical composition of the cuticle affects the behavior during plasma treatment. Cucumber and pepper seeds, which had a strongly oxygenated surface (18 – 21 at.% O) already when untreated, also showed relative C–O peak areas over 40 % after as little as 4 s of atmospheric air surface DBD treatment [97]. As the peeled clove surface contains less oxygen than the protective leaf, it is expected that its oxidation will proceed more slowly.

4.3.2.4 Surface oxidation mechanisms

We have shown that during exposure to oxygen plasma, oxygen concentration at the garlic clove surface increases, and that the chemical functionality also changes with plasma exposure time. As with polymer materials, the hydrocarbon chains of the cuticle compounds are targets for functionalization by the reactive plasma species, particularly ROS in oxygen-containing discharges [98]. The neutral oxygen atom, O, is the most relevant oxidizing agent in oxygen plasma. The initial oxidation steps of cuticular wax components result in the introduction of hydroxyl and carbonyl groups into the hydrocarbon chain structure. The main products will be (secondary) alcohols, as well as their corresponding ketones. The alcohols can be further oxidized to carbonyl or carboxyl groups [99, 100]. This is supported by our own results (Figure 3.28, Figure 3.30), as well as results of chemical characterization of tomato fruit cuticle by nuclear magnetic resonance (NMR) [101].

The oxidation of hydrocarbon chains is initiated by the formation of an alkyl radical, which occurs via a hydrogen abstraction by atomic oxygen:

$$\mathrm{RH} + \mathrm{O} \longrightarrow \mathrm{R}^{\bullet} + {}^{\bullet}\mathrm{OH}. \tag{4.16}$$

In linear hydrocarbon chains, such as those of cuticular waxes, this reaction would preferentially take place on secondary atoms (somewhere within the chain, as opposed to on either end) [100]. Further, a cuticular wax reaction with an oxygen atom may also split an alkyl chain directly. However, the activation energy (E_A) for this reaction is higher than the E_A for hydrogen abstraction [96].

It should be noted that while in our experiments, pure oxygen gas was introduced into the vacuum system, we have established that a significant amount of OH radicals is present in the system during plasma treatment, especially of peeled cloves (Figure 3.2). We have attributed this in part to water originating from the cloves during treatment. However, water vapor plasma is mildly oxidizing as well, and OH radicals may dissociate further to form O and H radicals [79]. Further, in addition to those formed by dissociation of the water molecule, OH radicals form in oxygen plasma anyway through hydrogen abstraction (Eq. (4.16)). Therefore, the effect of oxygen plasma containing some water vapor will likely be similar to that of pure oxygen plasma, just somewhat milder. This may also contribute to the slower oxidation process of the peeled clove surface compared to the protective leaf surface.

4.3.3 Other elements

With longer treatment of the garlic cloves, elements other than C and O began to be detected at the protective leaf and clove surfaces. In the case of the unpeeled cloves treated in the pilot-scale E-mode glow plasma (Table 3.2, Figure 3.20), we recorded increases in Ca, S and Si concentration at the treated protective leaf surface. Mg an K also appeared in concentrations under 1 at.%, Na was detectable for treatment times of 5 and 15 s, and Cl for treatment times of 0 and 15 s. Interestingly, N was present on untreated and briefly treated surfaces, but gradually disappeared with longer treatment.

At the clove surface (Table 3.5, Figure 3.25), no element other than C and O appeared earlier than after 30 s of treatment. Ca, S and Si concentration all began to increase later and reached lower values within 120 s of treatment than at the protective leaf surface. Mg only appeared after 120 s, but N began to increase after as little as 30 s. F also appeared from 30 s onward.

The etching effect, and thereby the exposure of deeper layers of the protective leaf, could be responsible for the appearance of some of the elements. It is clearly seen in SEM images (Figure 3.36) that with longer plasma exposure time, particularly over 30 s, etching gradually uncovers deeper layers of the protective leaf. Thereby, elements or compounds not found at the cuticle surface may also be uncovered. The reshaping of deeper layers of the storage leaf surface appears to begin only with longer treatment times (Figure 3.39), which is reflected in the time of appearance of additional elements. Some of the differences between the behavior of the two surfaces may also reflect differences in cuticle composition between the two organs.

4.3.3.1 Sulfur

While the main constituents of cuticular wax, as well as the cutin polymer scaffold, only consist of C, O and H, it is generally possible to find compounds such as alkaloids, which include heteroatoms in their structure, within the cuticle [64]. The majority of sulfur in garlic is found in non-protein amino acids, including volatile flavor compound precursors [61], and so, it is likely that the detected sulfur originates from allicin or other garlic thiosulfinates. The allicin precursor, alliin, is primarily produced in leaves and translocated to other parts of the plant [102], where it is typically located inside of cells. After damage to the plasma membrane, an enzymatic reaction converts alliin to allicin, which gives garlic its pungent smell and taste [103]. It was shown that allicin does not permeate cuticle waxes efficiently when sprayed onto plant surfaces [104], and its precursor compound is even more polar. However, as we will show during the discussion of ATR-FTIR results below, it appears that plasma treatment at the selected discharge parameters does not affect the garlic surfaces deeply enough to affect the epidermal cells beneath the cuticle. Further, sulfur-containing compounds are mainly found in the storage leaf, while in the protective leaf, their concentration is much lower [105]. Nonetheless, if the etching was deep enough to release any of the sulfur-containing garlic compounds to the surface, or if they are normally found in the cuticle in small amounts, this may account for S appearance in the XPS spectra. Another possible origin of S would be proteins, but in that case, we would need to also detect an increase in N. However, with increasing treatment time, N concentration at the surface clearly decreases.

Sulfur only appears in the XPS profile of peeled cloves after 90 s of treatment, and in very low amounts. This is surprising, as the concentration of thiosulfinates in the fresh storage leaf is around 700 × higher than in the fresh protective leaf [105]. While most of these compounds are found in cells in the bulk of the storage leaf, the only plausible explanation for such a late appearance of sulfur during peeled clove treatment is the milder treatment due to increased water presence, and thereby, the slower chemical etching process.

4.3.3.2 Calcium

On the unpeeled clove surface, the most prominent element concentration increase with treatment time was Ca, up to ~ 9 at.% (Figure 3.20). Ca^{2+} ions are capable of penetrating the cuticle despite their polar nature, likely at the site of stomata, or aqueous pores in the cuticle [106]. However, on the garlic protective leaf surface, stomata are practically missing [62], and it is therefore unlikely that the calcium originates from within epidermal cells. On the other hand, Ca^{2+} ions are bound by free carboxyl groups of the pectin in the layer which connects the cuticle and the plant cell wall [107]. If the pectin layer is at least partly exposed during plasma treatment, this would explain the increase in Ca concentration at the surface.

Similar as with sulfur, Ca content also begins to increase with peeled clove treatment, but is detected only after longer treatment times, and in lesser amounts (Figure 3.25).

4.3.3.3 Silicon

The origin of the detected silicon is not completely clear. In polymers, Si may be detected at the surface after plasma treatment, as it is an additive in polymer production or processing, and is then exposed during plasma etching of the polymer [108]. However, the garlic used here is unprocessed, lacking any additives. Although XPS analysis of processed garlic peel did not detect any Si [88], it is known that certain plants may accumulate Si in a layer underneath the cuticle, possibly due to its beneficial mechanical effects in protection from plant stress [109]. This accumulation, and the subsequent exposure of Si with progressing plasma treatment time, seems like the most likely origin for the Si detection.

Similar as with S and Ca, Si concentration also begins to increase with peeled clove treatment, but is detected only after longer treatment times, and in lesser amounts (Figure 3.25).

4.3.3.4 Nitrogen

Interestingly, N concentration at the protective leaf surface starts at ~ 1.5 at.% and decreases with plasma treatment time, until none is detected at 120 s of treatment (Figure 3.20). The most obvious source of N in living matter is protein. Protein content of the entire garlic protective leaf is about 8 % [110], but the protein is found as cellular components, and therefore, in deeper layers of the protective leaf than are accessed by etching. None of the cuticular waxes, polymers or other outer layer components contain any nitrogen in their structure. It is therefore reasonable to suggest that the source of nitrogen is external, for example, that N is present on the protective leaf surface due to fertilization of garlic with N-containing fertilizer.

This suggestion is supported by the fact that on the peeled clove surface, which is tightly wrapped from the outside by the protective leaf, no N is detected initially, although N appears at the surface after 90 s of treatment and onwards (Figure 3.25). This later appearance of N on the peeled clove surface may be due to the presence of enzymes in the cell wall, which in opposition to the protective leaf epidermal cell wall, is not sclerified [62].

4.3.3.5 Magnesium and potassium

Mg an K increases were also detected by XPS. As suggested for plasma-treated quinoa seeds, these elements likely diffuse toward the treated surface as a consequence of plasma etching [29]. Indeed, they only appear in XPS spectra at treatment times where etching of the protective leaf is already apparent in the morphology as observed by SEM (Figure 3.20). At the peeled clove surface (Figure 3.25), Mg only appears after 120 s of treatment, and K does not appear at all.

4.3.3.6 Sodium and chlorine

On the protective leaf surface (Figure 3.20), the random appearance of Na and Cl hints at contamination, possibly through touching the clove with an unprotected hand. Neither element appears at the peeled clove surface.

4.3.3.7 Fluorine

On the storage leaf surface, from 30 s of treatment onward, minor amounts of fluorine appear (Figure 3.25). To the best of our knowledge, fluorine has no physiological function in garlic, but may be accumulated in plants from the environment, either from pollution or compounds such as pesticides or fertilizers. It is also possible that fluorine contamination originates from the plasma system in case a fluorine-containing gas was used in the system prior to the performed experiments.

4.3.4 ATR-FTIR spectra

4.3.4.1 Untreated surfaces

The differences between the ATR-FTIR spectra of untreated protective leaf and clove surfaces (Figure 3.31) emphasize the difference in their chemical composition and correspond well to XPS results of the untreated surfaces (Table 3.2). The higher oxygen content of the protective leaf is reflected here in the prominent O–H peak at ~ 3300 cm^{-1}, which indicates the presence of more –OH functional groups in the waxy compounds of the cuticle. Conversely, the sharp, tall peaks of C–H bond stretching (~ 2850 and 2920 cm^{-1}) seen in the peeled clove spectrum correspond to the high alkane chain content of that surface, which is seen in XPS results as a high concentration of carbon. The peak at 1465 cm^{-1}, seen only in the peeled clove spectrum, further stands for C–H bending of methylene groups in alkanes [111].

The major differences between the two spectra start at ~ 1750 cm^{-1} and extend into the fingerprint region. The peak at ~ 1732 cm^{-1} represents the C=O bond [46, 111]. It is taller and thinner in the peeled clove, indicating a stronger presence of the C=O bond, either as an aldehyde/ketone, or as part of a carboxylic acid or ester. As the XPS results indicate less initial oxygen presence at the peeled clove surface (Table 3.2), it is likely that C=O bond signal derives from groups present in deeper layers of the clove surface, perhaps the ester bonds of the cutin polymer scaffold.

In addition to the O–H stretching peak at ~ 3300 cm^{-1}, both untreated spectra exhibit a peak at ~ 1632 cm^{-1}, indicating O–H absorption [112]. On the peeled clove surface, this peak is clearly distinct, but slightly smaller. On the protective leaf surface, it is taller, but hidden as a shoulder within another peak. This peak, found at ~ 1600 cm^{-1} only in the unpeeled clove spectrum, appears to represent C=C stretching. It is complemented by the peak at 897 cm^{-1} for C=C bending [111, 113]. Unsaturated analogues of the typically saturated compounds may be present in cuticular waxes [64], and are a possible source of the C=C signal.

The differences in the peak intensities for O–H, C=O and C=C groups, as well as almost fully distinct fingerprint regions, hint at differences in the chemical composition of untreated protective leaf and storage leaf surfaces analyzed by FTIR. They could either be the consequence of different cuticular wax composition, or stem from a difference in cuticular wax thickness, which influences the depth of further layers included in the FTIR analysis, and thus the obtained spectrum. As cuticular wax composition within the same plant species is somewhat consistent, the second option seems more likely. We know that, as the clove is already protected by the protective leaf, the epidermis of the storage leaf is thin and delicate [62]. It makes sense, then, that the cuticle covering it is also thinner, and that the IR beam during FTIR analysis penetrates into deeper layers, resulting in a difference in the fingerprint region of the FTIR spectrum.

4.3.4.2 Unpeeled clove plasma treatment

As seen in Figure 3.32, O–H and C–H peak intensity in FTIR spectra of the unpeeled clove changes with pilot-scale plasma treatment. With treatment at both $P_N = 200$ and 300 W within 120 s, the intensity lowers for both the O–H peak at ~ 3300 cm^{-1} and the C–H peaks at ~ 2850 and 2920 cm^{-1}. The sharp C–H peaks also turn dull and indistinguishable from one another, which happens earlier at larger P_N. From XPS results (Figure 3.18), we know that surface oxidation occurs, and O-containing groups replace hydrogen at the methylene chain surface, leading to C–H peak decrease. While new –OH groups are introduced, we also still see an O–H peak decrease, as these groups are also rapidly oxidized further.

Another feature of the spectrum that decreases in intensity is the C=C peak at ~ 1600 cm^{-1}. This is due to preferential oxidation of cuticular wax compounds at any available double bonds.

Interestingly, no changes are seen in the 1800 – 1650 cm^{-1} region, where C=O stretching peaks typically appear. The C=O peak at ~ 1732 cm^{-1} remains comparable throughout the treatment. In addition, no changes at all are seen in the fingerprint region of the spectra, between 1500 and 400 cm^{-1}. This is due to the analysis depth of the method. ATR-FTIR is a less surface-sensitive technique than XPS. Its analysis depth, which depends on the depth of IR beam penetration, is typically between 0.5 and 2 µm [114]. Thus, in addition to the cuticle with its outermost, plasma-affected layer, the analyzed volume includes deeper layers of the protective leaf or clove [49]. The plasma functionalization processes affect only one atomic layer at a time, which are then gradually removed by chemical etching. Therefore, the depth in which chemical changes occur is very thin compared to the thickness of the layer analyzed by FTIR. If the composition of the cuticular waxes is fairly uniform along the cuticle depth, then these oxidative changes at the very surface do not detectably affect the fingerprint region. In available literature, this was also suggested as the reason why for radish seeds after low pressure capacitively coupled RF oxygen plasma treatment, there were no changes in ATR-FTIR spectra [98]. Similarly, there were no changes for nasturtium seeds treated in atmospheric pressure DBD in an air/He mixture with increasing treatment times, with the exception of a decrease in the O–H peak, which could be related to loss of water [15].

In addition, this result confirms that the plasma treatment within the selected conditions does not etch the cuticle away completely, or damage the epidermal cells. If that was the case, the fingerprint region of the spectrum would noticeably change, as the IR beam would penetrate deeper through a different set of compounds contained in the cells.

4.3.4.3 Peeled clove plasma treatment

Changes due to plasma treatment are also reflected in FTIR spectra of the peeled clove surface (Figure 3.34). The initially more prominent C–H stretching peaks decrease more slowly than at the unpeeled clove surface, indicating a slower surface oxidation process. The C–H bending peak decreases as well. As the plasma introduces new –OH groups to the surface, the O–H stretching and absorption peaks gradually increase. As above, the changes are more pronounced at longer treatment times, and occur earlier during treatment with higher P_N.

The remaining changes to the spectra occur mainly at the longest treatment times (120 s at P_N = 200 W, and 90 – 120 s at P_N = 300 W). The C=O peak at ~ 1732 cm^{-1} gradually diminishes. In addition, reshaping of the fingerprint region begins. As we will show below, these are treatment times that begin to negatively affect the sprout growth (Figure 3.60). Therefore, it is plausible that these treatment times begin to affect the epidermal cells, and damage the clove, or increase its vulnerability.

4.4 Surface Morphology

4.4.1 Protective leaf surface

4.4.1.1 Pilot-scale glow plasma

As seen in Figure 3.36, the morphology of the protective leaf surface at low magnification (2,000 ×) consists of parallel grooves that run along the surface. The width of the grooves is about 15 – 20 µm, which suggests that they are the outlines of the outer epidermis cells, which are known to be about 500 µm long, and thus run over the protective leaf surface like long parallel stripes. Their cell walls are lignified, and they are covered by a thin, smooth cuticle [62]. This is seen at larger magnification (10,000 ×) of the untreated protective leaf as a wrinkled, but reasonably smooth surface.

The protective leaf surface treated in the pilot-scale E-mode glow plasma becomes increasingly rougher with increased plasma exposure time (Figure 3.36). After as little as 5 s of treatment, increased roughness is apparent in the form of surface bumps, which become more prominent after 15 s of treatment. The bumps are visually reminiscent of the roughness increase seen after oxygen plasma etching of polyethylene [115], a polymer chemically related to cuticular waxes, as it is composed of long methylene chains. From 30 s onward, extensive etching is apparent. As the wax is etched away, the surface becomes nanostructured, and an irregular, ridge- or scaffold-like structure remains at the surface. The effect is increased with increasing the treatment time, and thereby, with the plasma reactive species dose received by the clove. This is seen as further changes to the structure roughness and compactness with increased treatment time.

In the case of pulsed treatment at two different discharge conditions (Figure 3.37), as expected, the etching at the condition with higher P_N and longer treatment time (300 W, 6 × 10 s on, 5 s off) is significantly more extensive than at the less intense one (200 W, 6 × 5 s on, 5 s off). Further, in comparison with the continuous treatment (Figure 3.36), the pulsed treatment at 200 W shows slightly less intense etching at the same total treatment time (30 s). However, the pulsed treatment was performed at higher working pressure (70 as opposed to 50 Pa), where the oxygen atom density at P_N = 200 W is somewhat lower (around 6×10^{21} m^{-3} as opposed to 7×10^{21} m^{-3}). So, the observed result is expected.

It is well known that oxidative plasma etches polymer surfaces [3]. This is also true for the waxy compounds that compose plant cuticles. Low pressure RF oxygen plasma has etched cuticular waxes on lamb's lettuce leaves [116] and tomato fruits [101]. In plasma treatment of agricultural seeds, etching or erosion of the seed surface was seen after atmospheric pressure DBD treatment of wheat kernels in O_2, air, Ar, or N_2 plasma [44], or cotton seeds in air or N_2 plasma [45], as well as atmospheric pressure micro DBD treatment of coriander seeds in N_2 plasma [117], or spinach seeds in air or N_2 plasma [53]. Etching intensity often increases with treatment time [32, 44, 53, 117]. However, no authors so far have quantified the etching rate or the thickness of the cuticle layer eroded during plasma treatment.

4.4.1.2 Pilot-scale afterglow plasma

SEM images of unpeeled cloves treated in the pilot-scale H-mode plasma afterglow were prepared for samples treated at two discharge conditions: (1) P_N = 200 W, p = 50 Pa (Figure 3.38) and (2) P_N = 300 W, p = 30 Pa (Figure 5.1). As seen in Figure 3.15, the oxygen atom density at the sample position was around $2.5 – 3 \times 10^{21}$ m^{-3} for the 300 W, 30 Pa condition. While we have not directly measured the oxygen atom density for the

200 W condition, we know that due to lower P_N and higher pressure, the value is lower than at the 300 W condition. This is reflected in the morphological changes seen in the SEM images. After afterglow treatment at the 200 W condition for 30 s (Figure 3.38), the morphology is virtually unchanged from the untreated sample seen in Figure 3.36. After 120 s, etching is apparent, but still not to the degree seen in the glow plasma treated samples at much shorter treatment times. On the other hand, the afterglow treatment at the 300 W condition causes clearly visible etching already after 15 s of treatment (Figure 5.1). The etching appears to progress with treatment time, but is uneven across the clove surface area.

The etching at the afterglow position is practically exclusively chemical in nature. Even though the shift of plasma from E- to H-mode causes a dramatic increase in charged particle density [80], the ions are immediately lost on the reactor surfaces [75]. In addition to the oxygen atoms flowing downstream from the H-mode plasma to the sample position, some atoms are also formed at the sample position itself due to the stray capacitive coupling still present throughout the tube. The combined effect of these atoms is the chemical etching seen in the afterglow position.

4.4.2 Peeled clove surface

4.4.2.1 Pilot-scale glow plasma

The untreated peeled clove surface, as seen in Figure 3.39, appears wavy at low magnification. Elongated, roughly rectangular shapes with raised ridges and concave surfaces cover the area, arranged in irregular rows. Given their size (approximately 70 × 25 µm) and shape, these are the outlines of the cells of the outer epidermis of the storage leaf [62]. Similar as the protective leaf surface, the cells give shape to the cuticular layer covering them.

At higher magnification, the surface appears wrinkled, but reasonably smooth, similar to the surface of the protective leaf. After as little as 5 s of treatment in the pilot-scale E-mode glow plasma, distinct structures begin to appear at the clove surface. They are reminiscent of flat semicircular disks protruding from the cuticle surface, and fully achieve this shape during the first 60 s of plasma treatment. Approximate size of the structures is up to 500 nm in length and up to 100 nm in width. We estimate that their height is no larger than their length, up to a few hundred nm. When their density increases, most prominently at 60 s of treatment and longer, they begin to blend and create a mesh-like structure. Their density first increases at the physically exposed parts of the surface, that is, on the raised ridges dividing the individual cells. At 90 s of treatment, they more densely cover the areas between the ridges, and by 120 s, they have covered virtually the entire clove surface, creating a continuous, rough nanostructure. By 600 s, the surface appears devoid of the structures, which seem to have flattened or crumpled, blending in with the remaining area.

Considering this evolution of the wax morphology with treatment time, it appears as if the structures are not formed by etching away the material around them, but rather protrude from the existing surface. The clove surface area not covered by the wax structures does not appear to become rougher or more wrinkled with increased treatment time. This is in stark contrast with the extensive etching seen at the surface of the protective leaf (Figure 3.36). In both cases, the untreated cuticle appears as a flat film, yet the outcome of plasma treatment at the same discharge conditions is dramatically different.

After longer treatment (120 s, 600 s), it appears as if etching begins to take place in parallel to the reshaping. The morphological changes become uniform across the surface, and the typical irregular structures appear.

This delay in the etching process compared to the unpeeled clove does not explain the more intense water loss from the peeled clove. One explanation is that the water lost during peeled clove treatment is adsorbed water, normally prevented from evaporation by the protective leaf. If, however, the source of the water is the bulk of the clove, it is possible that water is lost through small cracks in the cuticle. As seen in Figure 3.39, the untreated peeled clove surface is completely smooth even at magnifications as large as 30000 ×. After as little as 5 s of plasma treatment, cracks appear at the surface. If these cracks increase the porosity of the cuticle and allow for water loss, this explains the OES and catalytic probe results that show more OH radicals during peeled clove treatment. Cracks in the cuticle surface have often been detected after plasma treatment of agricultural seeds, for example pea [32], *Andrographis paniculata* [118], cotton [45], or wheat [119], and are seen as signs of improved water permeability of the seed coat.

4.4.2.2 Industrial-scale plasma

After industrial-scale plasma treatment of peeled cloves (Figure 5.2), similar wax structures appear at the clove surface. They appear somewhat larger than the ones after treatment in the pilot-scale plasma (up to 1 µm in length). They are visually most similar to what was seen in the pilot-scale plasma (Figure 3.39) after 5 – 30 s of treatment. There are also differences in their density and distribution. They do not appear primarily on ridges, but are seemingly distributed randomly, and appear in discreet areas reminiscent of islands or stripes. In areas where they are present, their density appears uniform. While it is difficult to estimate the total covered area, it appears to increase with decreasing pressure, suggesting that the structures are more abundant after treatment with a higher reactive species dose, in parallel with increasing treatment time in the pilot-scale plasma.

As described above, the treatment in the industrial-scale plasma in this case is gentler as a consequence of lower power density in the larger reactor volume. This results in a lower density and different distribution of the observed wax structures.

4.4.3 Atomic force microscopy

The AFM images of the protective leaf surface (Figure 3.40) and clove surface (Figure 3.41) both confirm the SEM findings for the respective plasma treatment used. The unpeeled garlic surface treated in the pilot-scale E-mode glow pulsed regimen (Figure 3.40) shows subtle roughness increases after the 200 W treatment, but intense nanostructuring after the 300 W treatment, just as in the SEM images (Figure 3.40). On the other hand, along with some roughness increase, we can clearly see the protruding wax structures on the industrial-scale plasma-treated clove surface (Figure 3.41).

4.4.4 Surface reshaping processes

4.4.4.1 Chemical etching

Chemical etching is seen in particular after plasma treatment of unpeeled cloves. Pure oxygen plasmas are especially efficient in the removal of organic material from surfaces [120], since oxygen atoms are particularly useful for oxidative degradation of organic materials due to their number of valence electrons and high electronegativity [21]. As discussed earlier, oxygen atoms are the dominant reactive species in weakly ionized oxygen plasmas like the one used in these experiments. This suggests that chemical etching, and not ion bombardment, is the prevalent mechanism of material removal from the surface. In this mechanism, the wax components are oxidatively degraded by oxygen atoms, which first oxidize the structure by the functionalization mechanisms presented earlier, and then oxidize it further to form CO_2 (via formaldehyde and carbon monoxide [96]) and H_2O. These molecules are then removed from the surface due to their volatility. This was previously confirmed for low pressure oxygen plasma-treated lamb's lettuce leaves using FTIR [116] as well as for tomato fruit cuticles using NMR [101], and correlates with our surface chemistry analysis results showing gradual oxidation of the cuticle surface (Table 3.2).

4.4.4.2 Etching depth

Due to the surface-specific nature of its effects, we expect the plasma treatment to only affect outer cuticle layers, and to not have any direct physico-chemical impact on the cells of the underlying epidermis. This is also suggested by the ATR-FTIR results, as explained above. To gain insight into which layers are etched away by the plasma treatment and which are exposed, we need to consider the etching depth. Etch rate of the garlic clove surface was impossible to measure directly by clove mass measurements due to simultaneous loss of water from the clove, which greatly impacted the total loss of clove mass during plasma treatment. However, we can estimate the etching depth from available data for related compounds. Polyethylene foil etch rates in a capacitively coupled RF oxygen plasma were up to about 8 µg cm^{-2} min^{-1} [121]. If, based on the densities of polyethylene and paraffin wax, we assume a cuticular wax density of $\rho = 1$ g cm^{-3}, we can calculate an etching depth of up to 80 nm per minute:

$$h = \frac{V}{s} = \frac{m}{\rho s} = \frac{kt}{\rho} = \frac{8 \times 10^{-6}\ \text{g cm}^{-2}\ \text{min}^{-1} \times 1\ \text{min}}{1\ \text{g cm}^{-3}} = 80\ \text{nm}. \tag{4.17}$$

Here, h is the etching depth, s is the surface area, and k is the etch rate. As plant cuticles can be as thin as 100 nm [64], it is entirely plausible that any treatment longer than a minute could etch away the cuticle completely and expose the underlying layers of pectin and the epidermal cell walls. However, this scenario assumes a high etch rate as well as the thinnest possible cuticle. Linear hydrocarbon polymers are in general not as easily chemically etched due to the absence of tertiary C atoms, which are preferential targets for hydrogen removal by O atoms [100], and thereby for initiation of the etching mechanisms presented above. Considering this, along with ATR-FTIR results, it appears much more likely that the cuticle is not completely etched away by the plasma treatment, but remains at least partly intact, and that the structures observed in SEM images are either cuticular components or directly connected to the cuticle. Such a scenario was also suggested for low-pressure RF oxygen plasma treatment of tomato cuticles, where the epidermis was deemed to remain intact in the experiment, with the possibility to be damaged with prolonged exposure times [101].

Regardless of the chemical nature of the material, what we observe may be the selective plasma etching of cuticular components, which is a well-known concept for polymers [122]. In oxygen plasma, polymer etch rate depends on the energy required to break the chemical bonds of the polymer backbone. Some polar and aromatic functional groups appear to stabilize the polymer against plasma etching [123], while on the other hand, ester bonds (such as in the cutin structure) seem to increase the degradation rate of hydrocarbons in oxygen plasma, possibly due to resonance stabilization of radicals formed in this way ($RCO^{\bullet}$, $RCOO^{\bullet}$) [78]. We assume what we see in the SEM images is a distinct cuticle component found in the deeper cuticle layers which is less readily etched, or remains in place and is slowly oxidized further. This is impossible to confirm by the performed XPS analyses, since all cuticular components, as well as pectin and cell wall components, including lignin, are strictly oxygenated hydrocarbons. ATR-FTIR also does not give useful information in this regard due to its analysis depth, which extends far beyond the layers of interest in this case. However, this idea could be correlated with the rapid increase of the surface O concentration in the first 30 s of plasma treatment and the much more gradual increase thereafter. Based on the scaffold-like structure seen after etching, the less-etched component could be cutin. If the etching depth is higher, another possibility is lignin, a polyphenolic polymer which deposits in the plant cell wall, between the cellulose micro-fibrils, where as an additional protective measure, it strengthens and waterproofs the cell wall [124]. In the protective leaf outer epidermis, lignification does occur, and the cells thereby form a continuous hardened layer, which is then covered by the cuticle [62]. Due to its chemical structure, specifically its many aromatic rings, we expect lignin to be less susceptible to degradation by oxygen plasma than cuticular waxes [123].

4.4.4.3 Wax structure formation

To elaborate on the origin of the wax structures that appear on the peeled clove surface after plasma treatment, we can look into cuticular wax chemistry and morphology. On many plant cuticle surfaces, epicuticular waxes are known to readily self-assemble into crystalline structures. The morphology of these structures varies widely; it is associated with plant species and determined by chemical constituents of the wax. If such wax is deposited on an artificial surface after extraction or evaporation, it will reassemble into structures typical for its composition [64, 125]. While in our findings, the cuticle of untreated protective leaf exhibits a smooth wax film, it is possible that the appearance of wax structures is brought upon by the combined action of wax oxidation and surface heating during plasma treatment. The gradual increase in the C=O and O–C=O bonds seen in high-energy-resolution XPS spectra (Figure 3.30) indicates the appearance of aldehydes/ketones and carboxylic acids. C=O groups, along with –OH groups, typically imply the presence of platelet-like structures on epicuticular wax. In fact, the waxes on leaves of onion and leek – both, like garlic, of the genus *Allium* – were shown to form wax platelets, albeit more densely packed, and having serrated edges [64], as opposed to the smooth circular edges seen in our case. Size of the structures appears roughly comparable. In leek, the symmetric C_{31} ketone palmitone was found a major component of epicuticular wax, and may be the substance prevalent in the wax crystals on leek leaf surface [126].

In Figure 3.16, we have shown that due to processes such as surface neutralization and recombination, the temperature of the clove during plasma treatment rises with plasma treatment time. The reactive plasma species exert their exothermic effects at the surface, so the temperature increase of the treated material is the highest at its surface as well. For an array of studied plant species, it was found that the cuticular wax melting point is typically around 60 – 80 °C [127]. However, even annealing at temperatures below the wax melting point may be sufficient for wax structure formation, as long as they allow for

mobility of the wax molecules [125]. After treatment, the chemically altered waxes may recrystallize in the form of platelets like the ones seen in our SEM images. For comparison, at the surface of Thuringian mallow seeds, plasma treatment led to a restructuring, or "sharpening", of the cuticle, which also improved germination parameters. However, longer exposure times also led to surface erosion and cracking, followed by weaker germination improvement [128, 129].

Based on all of the above, we propose that the appearance of wax structures on the garlic clove cuticle, as opposed to etching, is a consequence of (1) a more delicate cuticle and epidermis anatomy, (2) altered plasma chemistry due to water loss from the clove, and (3) the resulting recrystallization of epicuticular wax. Points (1) and (2) are further elaborated below.

We should allow for the possibility that some of the distortions and cracks seen at the clove surface at high magnifications are artifacts of the sample preparation process, particularly the freeze drying step. However, we can state that the sample preparation does not result in the formation of the wax structures, as they are completely absent from the surface of the untreated control sample, which was prepared for SEM observations in parallel with the treated samples.

4.4.4.4 Differences between plasma effects on protective leaf and peeled clove

There are several potential reasons for the different behavior of the protective leaf and the storage leaf when exposed to oxygen plasma. They can roughly be explained in terms of differences between the surface anatomy and chemistry, as well as in their influence on plasma chemistry.

First, the anatomy of the epidermis and cuticle differs slightly between the two organs. In contrast to the lignification seen in the outer epidermis of the protective leaf, the outer epidermis of the storage leaf is thin and delicate [62]. Second, as seen from XPS analysis of the untreated surface (Table 3.1), the composition of the cuticle differs. The clove surface has a higher C concentration at the surface and a lower O/C ratio, indicating a more "waxy" composition – the presence of more non-functionalized hydrocarbons, or perhaps longer aliphatic chains in the functionalized compounds. This influences the functionalization process. At the protective leaf surface, where O concentration is higher, and cuticle waxes already containing terminal –OH groups, such waxes may undergo more rapid further oxidation, as there is no need to introduce the initial O-containing functional group onto the alkyl chain. Therefore, the chemical etching that follows functionalization also proceeds more rapidly.

Third, while the protective leaf appears almost completely dry, and all its cells except the outer epidermis collapse when the leaf is mature [62], there is a significant amount of water – around 65 % of the clove mass – present in the storage leaf. When the peeled clove is treated in the plasma, water is lost from the clove, as indicated by loss of clove mass during treatment (Figure 3.47) as well as the prominent presence of the OH radical band at 309 nm in the OES spectra (Figure 3.2 – Figure 3.4). In Figure 3.2, we see that the OH band is relatively more prominent during peeled clove treatment, compared to the protective leaf treatment. Naturally, the increased presence of water influences the plasma chemistry, and further, has an effect on the etching and functionalization mechanisms. As we have noted earlier, the oxidizing effect of oxygen plasma containing some water vapor should be similar to that of pure oxygen plasma, only milder. If this contributes to the slower oxidation process of the peeled clove surface, it also results in a delayed chemical etching compared to the protective leaf surface.

4.5 Water Contact Angle

WCA measurement results on the unpeeled clove are presented in Figure 3.42 (A). The WCA for cloves treated at $P_N = 100$ W gradually decreases, and the values are comparable regardless of working pressure (30 or 50 Pa). This corresponds to the catalytic probe n_O measurements (Figure 3.9), where the n_O at $P_N = 100$ W does not vary in the pressure range of 30 – 70 Pa. The WCA of the unpeeled clove treated at $P_N = 200$ W decreases more rapidly compared to $P_N = 100$ W, and is impossible to measure at a treatment time of 60 s already, due to practically complete wetting, as the droplet spreads across the surface fully.

The WCA of the peeled clove surface is seen in Figure 3.42 (B). The WCA decreases approximately equally for the treatment conditions of 100 W at 30 Pa, 100 W at 50 Pa, and 200 W at 50 Pa, up to the treatment times of 120 s, even though the n_O at 200 W at 50 Pa is twice as large as at the remaining two conditions. The WCA decreases more rapidly, but also approximately equally, for the treatment conditions of 300 W at 50 Pa and 300 W at 70 Pa. The n_O for the 300 W at 50 Pa was not measured, as the plasma without a garlic sample assumed the H-mode at these conditions. From the available results, it appears that the nominal power is a more important parameter in influencing the garlic WCA than the working pressure.

It should be considered that both the functionalization and the etching play a role in determining the wettability of a surface, and thereby, the WCA. By introducing new, oxygen-containing functional groups onto the surface, the chemistry of the seed surface changes, and surface energy as well as wettability increase. Concurrently, an increase in surface roughness also increases the surface wettability [1]. The two effects complement and affect each other, and the final WCA decrease is a product of both.

4.6 Water Uptake

4.6.1 Untreated cloves

In Figure 3.43, which compares the WU of untreated peeled and unpeeled garlic cloves, we see that the WU of unpeeled cloves is significantly greater than that of the peeled ones. WCA measurements of untreated surfaces show that the wettability of both untreated surfaces is comparable (Figure 3.42). However, we know from the results of XPS analysis (Table 3.1) that the oxygen concentration of the protective leaf surface is several at.% higher than that of the peeled clove, and as such, is more hydrophilic than the clove surface. In addition, the protective leaf of the unpeeled clove is dry, and is the component of the clove that easily soaks up large quantities of water. It follows that when soaking the peeled clove, the protective leaf acts as a water reservoir, taking up the water much more easily compared to the peeled clove, which is hydrophobic and does not readily take up water if not exposed to plasma beforehand.

4.6.2 Industrial-scale plasma

The WU increase after plasma treatment of cloves (Figure 3.44, Figure 3.45) arises from the physico-chemical surface modifications discussed above. The functionalization of the surface with O-containing functional groups, as well as increased surface roughness, increase the wettability of the cuticle. Concurrently, the etching effect facilitates water permeation through these layers. Consequently, the surface affinity for water increases, and water penetrates into the clove more easily. The combined effect is important; while

physical removal of the cuticle, such as scraping, will enhance WU by the seeds, it is not as effective as plasma treatment, which additionally functionalizes the surface [130].

The peeled clove WU increases steadily with soaking time (Figure 3.45). On the other hand, the WU of plasma-treated unpeeled cloves is accelerated in the first 60 minutes of soaking, after which, there is no significant difference between the WU by plasma treated and untreated cloves, as the WU approaches a plateau (Figure 3.44). The protective leaf mass is very low compared to the clove itself, so its capacity for WU is limited. Simultaneously, as we have seen in XPS results (Table 3.7), the clove surface under the treated protective leaf is much less affected by the plasma treatment, meaning that the water will not penetrate such a clove more readily than the untreated one. Therefore, the WU increase for plasma-treated unpeeled cloves is limited, and manifests only as a WU acceleration in the beginning of soaking. It is reasonable to expect that a similar effect would be seen after significantly prolonged soaking of peeled cloves.

For both peeled and unpeeled cloves, there is no difference in WU between the untreated control and the vacuum control. While some clove mass is lost during vacuum exposure alone, this value is insignificant compared to the mass lost during plasma treatment (Figure 3.48). Further, in the absence of plasma reactive species, no surface modification takes place which could affect the WU of the clove.

4.6.3 Pilot-scale plasma

In the pilot-scale plasma experiments, we have checked the effect of treatment time on the WU. Based on the result of the industrial-scale plasma experiments, we have selected a soaking time of 10 minutes as a time where the WU of both peeled and unpeeled cloves differs as much as possible between treated and untreated cloves.

In Figure 3.46, it is clearly seen that the WU linearly increases with treatment time for both peeled and unpeeled cloves, and that the difference is significant after 30 s of plasma treatment. Initial WU of the untreated unpeeled clove is about six times higher than that of the untreated peeled clove (~ 3 % as opposed to ~ 0.5 %). However, the slope at which the WU increases with treatment time is nearly identical for peeled and unpeeled cloves treated at the same discharge condition. Further, in both cases, the vacuum control trend line is nearly horizontal, indicating that the WU does not significantly increase with vacuum exposure within the time frame of 120 s.

As with the industrial-scale system treatment, the WU increase corresponds to the progressive changes to the clove surface seen in the XPS, SEM and WCA analysis results, which increase the clove wettability and thereby facilitate the WU.

4.6.4 Clove mass loss

It is evident from the WU results of the vacuum control (Figure 3.44, Figure 3.45) that exposure to low pressure alone is not sufficient for increased WU. Loss of clove mass during exposure to vacuum alone is also minimal, no more than 0.4 % within 120 s in the pilot-scale plasma (Figure 3.48). It is possible that only water adsorbed onto the clove is removed in this way.

The increased mass loss during plasma treatment (Figure 3.48) indicates that plasma affects the surface in a way that allows for additional loss of clove mass. The reasons for the mass loss may be either water loss from the clove bulk or surface chemical etching. During the treatment of cloves, OH radical presence in the plasma system is considerable. While OH may originate from water presence in the system as well as from chemical etching, the source of CO is chemical etching alone. The difference in the intensity of peaks representing OH and CO in the OES spectra (Table 5.1) indicates that more water than

carbon is lost from the clove. This suggests that during plasma treatment, the clove does indeed lose water due to the loss of protective function of the cuticle. Fresh garlic cloves contain about 65 % of water [61]. The plasma effects on the cuticle facilitate water penetration through this otherwise hydrophobic layer to the surface, where it gets removed from the clove due to the low pressure inside the plasma reactor. Compared to the mass of water lost in this way, material loss due to etching is likely negligible.

The loss of clove mass during plasma treatment is higher for peeled than unpeeled cloves (Figure 3.47). This is due to the function of the protective leaf, which is a barrier to the clove against water loss, and plasma treatment in the absence of any cracks or damages only affects the protective leaf surface, without affecting the surface of the clove itself. Loss of clove mass is no larger than about 2.5 % for treatment times up to 120 s in the pilot-scale plasma, which is the longest feasible treatment time for any practical application in agriculture.

In Figure 3.49, we see the same peeled clove WU results as in Figure 3.45, with the difference that here, WU is calculated using the clove mass before plasma treatment in the calculation (m_0 in Eq. (2.1)). The results in Figure 3.49 therefore take into account the loss of clove mass during plasma treatment. Mean loss of clove mass during treatment is less than 1 %. It is apparent that WU is accelerated even past the point when the initial clove mass is reestablished during soaking. This confirms that the WU increase or acceleration after plasma treatment is not just due to water loss from the clove during treatment, but due to changes to the surface chemistry and morphology discussed earlier.

In experiments performed on beans, it was found that the micropylar region is particularly important for seed imbibition, but nonetheless, plasma treatment strengthens water permeation through the entirety of the seed coat surface [131]. While no micropylar region exists in the clove, a similar cavity-like structure at the tip of the storage leaf could contribute to the steady mass loss during clove exposure to vacuum. Plasma exposure then lessens the protective function of the cuticle and allows for additional water loss through the clove surface.

4.6.5 Effect of initial clove mass

To show whether the initial clove mass before treatment affects WU, the relationship between these two variables is shown in Figure 3.50. At the same treatment conditions and treatment time, the WU of lighter cloves is proportionally larger. This is due to the surface-to-mass ratio, which decreases with increasing clove mass. A heavier clove therefore has a proportionally smaller surface area through which water can be taken up into the clove.

We have shown that material is lost from the clove surface due to etching as well. However, considering the relative intensities of the relevant reactive species in OES spectra (Table 5.1), it is safe to deduce that the mass of the etched material is negligible compared to water loss.

4.7 Sprout and Root Growth

4.7.1 Untreated controls

In the comparison of sprout and root growth of untreated controls (Figure 3.52), we see that sprouts and roots of unpeeled cloves grow significantly faster than those of peeled cloves. As we have mentioned earlier, the protective leaf is a water reservoir, and is aligned to the storage leaf tightly. Therefore, during laboratory growth of unpeeled cloves, the protective leaf takes up water, making it more directly available to the storage leaf, which then takes it up slowly over a large area. Even if this is not reflected in the WCA measurements (Figure 3.42), the untreated storage leaf itself is noticeably more water-repellent, and therefore the contact area between the storage leaf and water is smaller in the case of untreated peeled cloves, resulting in less water availability and slower sprout and root growth.

4.7.2 Unpeeled cloves

4.7.2.1 E-mode glow

Sprout and root growth was also systematically followed for unpeeled cloves treated in the pilot-scale E-mode glow plasma. From the results (Figure 3.53 – Figure 3.55), we see that the treatment at $P_N = 100$ W is too weak to significantly affect either sprout length, root length or root number. Root growth is somewhat affected, and shows a slight trend of improvement with increasing treatment time. For treatments at $P_N = 200$ W and 300 W, sprout length improvements are seen for specific treatment times. This indicates that a particular dose of oxygen atoms which the clove receives positively affects its sprout growth. We can calculate the O atom dose a clove receives at the given discharge conditions from the oxygen atom flux, clove surface area, and treatment time:

$$D = j_O \, A \, t. \tag{4.18}$$

From Eq. (4.10), it follows that

$$D = \frac{1}{4} n_O < v_O > A \, t. \tag{4.19}$$

We have established in Eq. (4.4) that the surface of a clove with a mass of 1 g is ~ 5 cm^2, and in Eq. (4.12) that the $<v_O>$ at the given conditions is 630 m s^{-1}. The n_O at the particular discharge condition is taken from Figure 3.9, and t is the treatment time. Considering this, one gets

$$D = \frac{1}{4} n_O \times 630 \frac{\text{m}}{\text{s}} \times 5 \text{ cm}^2 \times \ t = 787.5 \, n_O t. \tag{4.20}$$

For the treatment conditions used in the present experiments, we can calculate the O atom dose received by a clove as presented in Table 4.1.

Table 4.1: O atom dose received by a clove during treatment. Pilot-scale E-mode glow plasma, $p = 50$ Pa.

t [s]	100 W	200 W	300 W
0	0	0	0
15	3.5×10^{25}	8.3×10^{25}	1.1×10^{26}
30	7.1×10^{25}	1.7×10^{26}	2.2×10^{26}
45	1.1×10^{26}	2.5×10^{26}	3.4×10^{26}
60	1.4×10^{26}	3.3×10^{26}	4.5×10^{26}
90	2.1×10^{26}	5.0×10^{26}	6.7×10^{26}
120	2.8×10^{26}	6.6×10^{26}	9.0×10^{26}

Considering the sprout growth results from Figure 3.53, we can estimate the required O atom dose for sprout growth improvement of unpeeled cloves. The only significantly improved treatment condition is $P_N = 200$ W, $t = 60$ s, which equals an O atom dose of approximately 3.3×10^{26}. If we include treatment conditions that non-significantly improve sprout growth, ($P_N = 200$ W, $t = 45 - 60$ s, as well as $P_N = 300$ W, $t = 30 - 60$ s), then the required O atom dose bracket for sprout growth improvement is around $2 - 4.5 \times 10^{26}$.

Following the same reasoning, we can calculate the required O atom dose for root length improvement. While none of the improvements in Figure 3.54 are significant, some of the treatments non-significantly improve root length, in particular: $P_N = 100$ W, $t = 45$ s; $P_N = 200$ W, $t = 15 - 45$ s; and $P_N = 300$ W, $t = 15 - 30$ s. This suggests that a degree of root length improvement may be achieved with an O atom dose of about $1 - 2.5 \times 10^{26}$. Conversely, from the negative effects seen at longer treatment times for $P_N = 200$ and 300 W, we can state that an O atom dose over $\sim 3.5 \times 10^{26}$ will negatively affect root length.

The required O atom dose for root number improvement is estimated less easily due to the lack of clear trends in the non-significant improvements (Figure 3.55). A rough estimate is about $1 - 2 \times 10^{26}$. As with root length, any O atom dose over $\sim 3.5 \times 10^{26}$ will negatively affect root number.

Based on all of the above, a pilot-scale plasma treatment that positively affects both sprout and root growth of unpeeled cloves in the laboratory conditions would require an O atom dose of about $2 - 2.5 \times 10^{26}$. Out of the selected treatments, this is true for $P_N = 200$ W, $t = 45$ s, as well as $P_N = 300$ W, $t = 30$ s. Of course, many other P_N/working pressure/treatment time combinations can be used to achieve this range, and are, disregarding other factors, potentially effective.

4.7.2.2 Comparison of continuous and pulsed treatment

We have compared the sprout and root growth of unpeeled cloves treated in either continuous or pulsed pilot-scale E-mode glow plasma, and the results are presented in Figure 5.3. While in this experiment, there was no positive effect on any of the measured parameters at the given discharge condition and treatment times, there was also no significant difference between the results of the continuous and pulsed treatments.

Pulsed treatment was initially used to reduce any potential negative effects of clove heating during treatment. From Figure 5.3, it is clear that the continuous and pulsed treatments have an entirely comparable effect on sprout and root growth of unpeeled cloves. This confirms the suggestion that it is the O atom dose received by the clove that

ultimately determines the biological effect. Further, it suggests that at least at the selected treatment conditions (P_N = 200 W, p = 50 Pa, t = 15 – 120 s, pulsed: 5 s on, 5 s off), the temperature increase of the clove during plasma treatment does not impact sprout and root growth to a degree where pulsed treatment would be of particular benefit.

A pulsed treatment was also selected for an additional experiment at a higher pressure (p = 70 Pa) due to promising sprout growth results from the preliminary treatment (Figure 3.51). The results are presented in Figure 5.4. The treatment significantly negatively affected the sprout growth, which barely occurred for treated cloves, as well as root growth, which was also severely retarded. The reason for this result is that the experiment was performed in October, using garlic harvested in July of the same year. The cloves were therefore still in a state of dormancy, which is reflected in the very late start of sprout growth (~ 20 days post-treatment). Due to the long time between treatment and start of sprout growth, the cloves may become negatively affected, either by loss of water or other environmental factors, such as fungal attack.

4.7.2.3 H-mode afterglow

The H-mode afterglow did not significantly affect sprout growth in our experiments. Nonetheless, non-significant improvements are seen in Figure 3.56, and a trend is even present in Figure 3.59. We see a similar effect on root length (Figure 3.57) and number (Figure 3.58), although the non-significant positive effect is primarily an acceleration of root growth, as a comparable plateau is gradually approached by untreated and treated cloves.

Although exact numbers are not available for all treatment conditions, the O atom dose received by samples in the H-mode afterglow is generally lower than during exposure to the E-mode glow at the same discharge parameters. For example, as seen in Figure 3.13, the n_O in the afterglow position at P_N = 300 W, p = 30 Pa, is about 2.5 – 3 × 10^{21} m^{-3}. This is comparable to the n_O at P_N = 100 W in the E-mode glow position. It is clear that for the same O atom dose to be received, treatment times in the H-mode afterglow must be longer. As we have shown that if suitable treatment times are used, there are no drastically negative effects on the clove with E-mode glow treatment, there is no reason to not prefer its use over that of the H-mode afterglow.

4.7.3 Peeled cloves

Sprout and root growth was also followed for peeled cloves treated in the pilot-scale plasma with a P_N of 100 to 300 W, at p = 50 Pa, for times of 15 – 120 s. The results are collected in Figure 3.60 – Figure 3.62.

It is particularly interesting to note that at all treatment conditions at p = 50 Pa, the treatment time to induct significant sprout length improvement was the same: 90 s. In addition, treatment times of 15 – 60 s had a positive effect on sprout growth regardless of P_N, while the longer treatment time of 120 s again diminished the positive effect, especially at P_N = 300 W. This observation is in contrast with the results of unpeeled cloves treatment, where the optimal treatment time varied with P_N, suggesting the importance of the received O atom dose over treatment time.

Here, considering these results and referring back to Table 4.1, we can attempt to again calculate the optimal O atom dose for peeled clove treatment. The results are not as uniform as for unpeeled cloves, as the approximate O atom dose ranges for sprout improvement are 1.4 – 2.8 × 10^{26} (P_N = 100 W), 5 – 6.6 × 10^{26} (P_N = 200 W), and 2.2 – 6.7 × 10^{26} (P_N = 300 W). The overlap of these ranges is only partial, suggesting that for sprout growth of peeled cloves, treatment time is a more important parameter than P_N.

Root growth was affected in a different pattern than sprout growth. The most pronounced positive effect on longest root length at the P_N of 100, 200, or 300 W was seen at the treatment time of 60, 30, and 15 s, respectively. Below these treatment times, root length was typically comparable to the untreated control, while above, it was increased, but not as much as in the optimal case. The exception is treatment at $P_N = 300$ W, where all treatments longer than 15 s have decreased root length. Despite this, the number of roots was at least somewhat increased for all P_N and treatment times, with the exception of 300 W at 120 s. Here, the O atom dose range for optimal root length improvement, as discerned from Table 4.1, is more uniform across P_N, about $1 - 2 \times 10^{26}$.

A treatment condition of $P_N = 300$ W, $p = 70$ Pa was also added for comparison, and the results are found in Figure 5.5, Appendix A. When the pressure is increased to 70 Pa, there is no significant benefit to sprout growth, except for the improvement at the 60 and 120 s treatment time from 14 days onward. Further, there is no obvious improvement of root length, while some improvement to root number is seen. This is due to the lower dose of oxygen atoms received by the cloves at these treatment conditions.

4.7.4 Mechanisms of sprout and root growth improvement

4.7.4.1 Sprout growth

If we compare responses of unpeeled (Figure 3.53) and peeled cloves (Figure 3.60) sprout growth to plasma using the same discharge parameters, we see that their behavior differs. The effect on peeled cloves is more immediate, as we already see a sprout length response at $P_N = 100$ W, which leaves unpeeled cloves unaffected. On the other hand, at higher P_N (200 and 300 W), the optimal response of unpeeled cloves appears at a shorter treatment time, but the improvement is less drastic than for peeled cloves.

Considering all of the above, we suggest that with treated unpeeled cloves, the protective leaf acts as a sort of "buffer". On the one hand, it prevents the immediate contact of plasma species with the storage leaf surface, leaving it essentially unaffected (Table 3.7). On the other hand, as shown by XPS surface analysis (Table 3.2), WCA measurements (Figure 3.42), and WU results (Figure 3.46), the treatment causes hydrophilization of the protective leaf surface and accelerates its WU. Therefore, it allows for increased, uniform exposure of the clove surface to water taken up by the protective leaf, ensuring a steady moisture supply. We know that WU is the first and essential step required for the start of germination in seeds [49], and if exposure of cloves to plasma facilitates this process, then germination and early growth can be improved by these primarily physico-chemical mechanisms.

Conversely, with treated peeled cloves, the reactive plasma species directly affect the clove surface. This also causes increased water uptake into the clove, but without the "buffer" function of the protective leaf like with unpeeled cloves.

In addition, peeled clove treatment results in potentially direct biological effects: an influence of reactive plasma species on the biochemical pathways of the clove. We know that during plasma treatment, the clove is exposed to a steady flux of ROS. In living beings, ROS are traditionally considered damaging due to their oxidative nature and subsequent damage to the molecular components of the cell. However, it is now widely established that ROS in plants play a dual role, as they are also involved in cellular signaling pathways. Indeed, the concept of an "oxidative window for germination" has been proposed to describe a critical range of ROS concentration in seeds that allows for dormancy release and germination [55]. During seed storage, ROS levels gradually increase, reducing dormancy [51] by affecting the ratio of plant hormones, particularly abscisic acid and gibberellins, through an influence on the expression of relevant genes [49]. Using

electron paramagnet resonance, one study suggested a higher radical level in plasma-treated seeds; they noted improved germination, and related this to an acceleration of seed metabolism and stimulation of biochemical and physiological processes [132]. Another group concluded that redox reactions in plasma irradiated radish sprout seeds are influenced by the plasma treatment [133]. We suggest that parallel mechanisms positively influence the germination and early growth of plasma-treated garlic cloves.

It is at present unclear how the plasma ROS influence the plant signaling pathways. In seeds, it is suggested that to some degree, plasma species do not only affect the very surface, but can also penetrate the partially permeable seed coat, influencing the seed cells directly [134]. In parallel, we have seen in SEM images that small cracks appear in the cuticle of the treated peeled clove (Figure 3.39), which could allow for ROS to access deeper layers, including epidermal cells, and act as signal transmitters. Indeed, ROS are proposed to act as transmitters of environmental cues during germination. Therefore, it is possible to imagine that ROS produced in oxygen plasma would act on the clove as an environmental signal or stressor, activating its biochemical pathways [55].

Viscosity of the cytoplasm, influenced by seed hydration, also plays a role in ROS signaling, enabling mobility of the ROS, allowing them to act as messenger molecules [55]. In this way, the previously described WU improvement also contributes to the activation of biochemical processes in the clove.

It should be noted that even though in our results, we see mean sprout length improvements at many of the discharge conditions and treatment times, only few of those improvements are statistically significant. The lack of statistical significance is a consequence of a small sample size, typically $n = 5$, in the laboratory germination and growth experiments. This is complemented by biological variability of the cloves, which adds considerable variation to the results.

4.7.4.2 Root growth

In a mature garlic clove, 20 – 40 unelongated roots develop in the base of the storage leaf, some of which penetrate through the base even before germination begins [62]. It appears that plasma treatment stimulates, or at least accelerates, the growth of these roots. We suggest that this effect, as with sprout growth above, is due to biochemical activation as a result of plasma treatment, as well as the increased water availability thereafter. The required O atom dose for root growth improvement, as calculated above, is comparable for the treatment of peeled and unpeeled cloves.

As seen from Figure 3.54 and Figure 3.55, root growth is positively affected by plasma earlier than sprout growth, but also the first to be negatively affected if the received O atom dose is too large. From comparing Figure 3.54 and Figure 3.55 with Figure 3.61 and Figure 3.62, we notice that just as the positive effect, the negative effect on the roots of treated unpeeled and peeled cloves is also approximately equal at the same discharge conditions and treatment times. As roots are delicate structures, which may already be partially exposed to the environment in a treated clove, an O atom dose that is too large may damage the root tips, including the apical meristem required for root elongation.

In addition, we have seen during laboratory growth of cloves that the roots are preferential targets for fungal attack. Due to their function of water and nutrient absorption, roots generally lack a cuticle [49], and as such, are more vulnerable to pathogen attack. Any damage to the outer epidermis by the reactive plasma species further increases this susceptibility. As root growth is perhaps the most important factor of plant establishment in the early phases of growth, such damage should necessarily be avoided if improved field growth should be achieved. Discharge parameters should be adjusted accordingly.

4.7.4.3 Effect of low pressure

We have shown in several experiments that exposure of cloves to low pressure and oxygen flow alone does not affect their laboratory germination and growth (e.g., Figure 3.63, Figure 3.65). This was previously shown for agricultural seeds as well, where exposure to vacuum alone was also found insufficient for germination improvement [135].

4.7.4.4 Effect of EM field

In the case of agricultural seeds, exposure to EM field alone can also stimulate germination [135, 136], and germination, growth and yield of onion has previously been improved by exposure to magnetic fields [137]. Contrary to these findings, we have shown in Figure 3.63 that a control exposure to EM field alone does not significantly affect sprout or root growth of garlic cloves. The EM field may be one of several important components that affect the cloves during plasma treatment, and the results may depend on the characteristics of the applied EM field.

4.7.4.5 Damage to the cloves

At prolonged treatment times, in particular at the highest discharge power (300 W), the cloves have sustained significant damage. This was already evident from the sensory properties of cloves, particularly a glassy appearance and an odor of cooked garlic, both indicating excessive temperature increase. It is further reflected in the sprout and root growth response. With longer treatment times, the sprout length, but especially the root length and number, is considerably decreased.

This is especially evident when comparing sprout growth of unpeeled and peeled cloves (Figure 3.53 and Figure 3.60). Prolonged treatment at the same discharge conditions affects unpeeled cloves much more severely than peeled cloves; sprout growth is negatively affected at shorter treatment times. This is due to the function of the protective leaf, which confines heat and water to the clove, causing the negative effects of increased temperature to appear earlier due to faster heating (Figure 3.17).

4.8 Field Growth

4.8.1 Plant height

In the results presented in Figure 3.66 and Figure 3.67, we see that there are no statistically significant differences between height of garlic plants grown in the field. In several cases, plant height increase after plasma treatment of agricultural seeds has translated to an improvement of yield [30, 31, 35]. However, in our experiments, the plant height was recorded at harvest, a time when the foliage leaves are already somewhat dry, and often damaged by the heat and dryness of the summer months. Therefore, plant height results are not expected to be very informative. In addition, a garlic clove planted in the field may develop along several paths in response to environmental stimuli [57], and an unchanged or even decreased plant height may in fact be desired, as it could indicate that the plant devotes more energy and resources to bulbing than growth of the parts above ground.

4.8.2 Yield

4.8.2.1 First generation

We see from Figure 3.68 that both used plasma treatment regimens increased the mean bulb mass compared to the control treatments, although only the increase caused by the afterglow treatment was significant. The plants grown from the industrial-scale treated cloves (Figure 3.69) also show a hint of mean bulb mass improvement, but the increase is minimal, and not significant. As described above, this is due to the gentler treatment conditions as a consequence of lower power density. A further factor affecting these results is the time of planting. The pilot-scale treated cloves from Figure 3.68 were planted in the fall, while the industrial-scale planted cloves from Figure 3.69 were planted in the spring. The overwintering of the clove in the soil is important for the garlic plant development, and yields are higher if garlic is planted in the fall [138]. The spring-planted garlic has less time for bulb development, and therefore, the differences between the yield of differently treated groups will be less pronounced.

The mechanism of yield improvement stems from the biological effects of plasma treatment on the clove, as outlined earlier. For the afterglow treatment, the improvements in bulb mass (Figure 3.68) correlate with the improvement in sprout growth (Figure 3.59). For the pulsed treatment, there is no directly correlated result, but improved sprout growth was recorded in a preliminary experiment (Figure 3.51). For the industrial-scale treatment, we also see a correlation, as the treatment at 15 Pa caused the highest mean sprout length increase (Figure 3.64) as well as mean bulb mass increase (Figure 3.69), although none are statistically significant. Parallel findings from plasma treatment of seeds confirm the correlation. Rapeseed seedling height increased after seed plasma treatment, and was accompanied by an increase in yield [30]. In plasma treatment of wheat, medium pressure air/oxygen plasma treatment similarly induced seedling length increase, which translated to a subsequent yield increase [38]. Further, after low-pressure He plasma treatment, wheat yield increase in the field was preceded by increases in plant height and root length at both seedling and booting stage [35].

This effect could relate to a general stimulation of plant vigor. One factor is the increased imbibition due to increased hydrophilicity, which, on the one hand, signifies enhanced transmission of water and oxygen [6] as well as nutrients [139] into the clove. On the other hand, in seeds, imbibition is also essential for the start of physiological activities associated with germination. Germination is related to the activation of many biochemical pathways within the cells [53]; for example, an increase in chlorophyll content in plants

from plasma-treated seeds was recorded [35]. All these factors can strengthen the plant and improve its growth. Further, root growth improvement is particularly important. As root is the plant organ responsible for nutrient absorption, increased root growth and activity after plasma treatment is linked to increased nutrient uptake [34], which again improves plant growth. In particular, when garlic is planted in the spring, it is important that the root system is established quickly and efficiently in order for the plant to grow properly.

It should also be noted that any plasma-treated garlic cloves should be planted as soon as possible after treatment. Firstly, the functionalization effect is at least partly reversible due to a process known as aging, wherein the surface oxygen content decreases after treatment [140], as oxygen is lost from the surface, the newly introduced functional groups re-orientate, and impurities are adsorbed [141]. This effect increases with time after treatment. And secondly, due to the plasma effects on the cuticle surface, the clove is more vulnerable to dehydration, attack by pathogens, and general decay. If the cuticle is partly or fully removed from the surface, the storage and shelf life of the cloves will be reduced [101].

4.8.2.2 2nd and 3rd generation

In the field growth experiments where 2nd and 3rd generation of plants was grown from initially plasma-treated cloves (Figure 3.70, Figure 3.71), we have shown that the stimulating effect of plasma treatment on yield is preserved throughout the generations, without additional treatment.

To the best of our knowledge, no studies so far have considered potential effects of plasma treatment on the yield of the next generation. One study has used plasma on seeds of perennial woody plants to find long-term positive effects on plant morphometric traits, such as stem and root branching or leaf number and surface [136]. This shows that the effects of plasma treatments on plants can be long-lasting. However, our yield results are the first instance indicating that the effects can be carried over into the next generation through non-sexual propagation.

We see in Figure 3.70 and Figure 3.71 that the mean mass of bulbs from treated and untreated cloves also increases from generation to generation. Potential reasons for this are mainly agricultural and include longer development time (fall planting as opposed to spring planting) and better conditions for garlic growth in that particular year.

Chapter 5

Conclusions

From our results, it is clear that using suitably selected parameters, low pressure, inductively coupled RF oxygen plasma can stimulate the growth of garlic clove sprouts and roots, as well as have a positive effect on the yield of garlic grown from such cloves. Further, this yield improvement can persist throughout generations of the garlic plant without the need for additional plasma treatment. This improvement is most likely a consequence of combined physico-chemical and biological action of the reactive plasma species. In cases where the results are not statistically significant, clear trends of improvement are nonetheless often present. The non-significant results are often due to biological variability, which is considerable in garlic cloves, as they may vary in size, shape, water content, or other parameters, even within a single bulb.

There are differences between the physico-chemical and biological responses of peeled and unpeeled cloves to plasma treatment. This is due to a variety of differences between the two. The initial chemical composition of the peeled and unpeeled surface differs, and the peeled clove is more hydrophobic than the unpeeled clove. Further, the protective leaf offers a shielding function to the clove within, and retains at least some of this function during plasma treatment. A larger amount of water is released from the peeled clove during exposure to plasma, which affects the plasma chemistry, making it less oxidizing, and the functionalization and etching processes slower. As a result, the time course of changes to the surface chemistry is different. The surface morphological changes are considerably different as well; whereas the protective leaf is quite easily etched, the reshaping of the peeled clove surface is a more complex process at the same discharge conditions.

All of this also affects sprout and root growth. Sprouts of untreated unpeeled cloves grow more readily due to uniform water exposure. However, the relative stimulating effect on the peeled cloves is larger due to the comparably more direct exposure to reactive plasma species. In addition, during plasma exposure, the temperature of unpeeled cloves increases faster than for peeled cloves, resulting in earlier clove damage. On the other hand, with peeling, the clove loses its protective barrier, making it more vulnerable to negative environmental effects. This includes plasma, which may negatively affect cloves with prolonged exposure. Roots are particularly vulnerable, and the required O atom dose for root growth improvement is lower than for sprout growth improvement. The decision to use peeled or unpeeled cloves should be taken based on processing capabilities, time from treatment to planting, and preliminary tests in the particular plasma system used for treatment.

We suggest that the plasma treatment conditions used in our experiment only manipulate the garlic clove cuticle, and do not negatively affect the epidermal cells, with the exception of the longest treatment times in plasma with high n_O. This is supported by

the lack of difference in the fingerprint region of the ATR-FTIR spectra, as well as the lack of nitrogen detection in XPS spectra of etched cloves, which would indicate the presence of proteins from the cells. If etching is extensive enough to damage the cells, the negative effects become apparent due to the clove vulnerability to drying out as well as pathogen attack.

All of the above indicates the presence of an optimal dose of plasma reactive species that a clove should receive to improve sprout growth, root growth and/or yield, as well as avoid damage. This dose can be adjusted by tuning the discharge power, pressure, or treatment time. The selected parameters, in the presence of a sample clove, should also result in an E-mode plasma, where the reactive species density is low enough to not damage the clove.

Many of the findings run in parallel with available literature on plasma treatment of agricultural seeds, and can also be applied to that related field of research. Despite biological differences between garlic cloves and other plant seeds, several parallels exist regarding the biological processes of dormancy, germination, and growth.

Given our understanding of plant biochemical processes, it is reasonable to propose that the suitable dose of O atoms not only physico-chemically modifies the garlic clove surface, but also affects signaling pathways in a way that stimulates germination and growth, possibly by breaking clove dormancy or affecting its hormonal balance.

Appendix A

Additional Results

A.1 Optical emission spectroscopy

Table 5.1: OES signal intensity at selected wavelengths, pilot-scale E-mode plasma. Flow configuration, recorded approximately 60 s after turning on the discharge. Recorded with or without peeled or unpeeled garlic samples. $P_N = 100 - 300$ W, $p = 50$ Pa. Any signal not distinguishable from noise (up to an intensity of ~ 100) is not included.

		no sample		peel	unp	peeled			unpeeled		
peak	wl	100	200	200	200	100	200	300	100	200	300
OH	309	133	731	4186	2016	1417	4186	12792	332	2016	10032
O	437	/	1643	541	516	140	541	1176	/	516	1483
O^+	441.5	/	371	149	167	/	149	723	/	167	596
O^+	464.9	/	363	233	454	/	233	953	/	454	873
O	485.7	190	1977	5053	2589	678	5053	15295	386	2589	13412
C_2	516	/	/	/	108	/	/	111	/	108	263
CO	519.5	/	/	/	109	/	/	247	/	109	444
O_2	525.5	/	882	331	602	/	331	918	/	602	1143
O	533	/	1002	492	432	/	492	1072	129	432	1347
O	544	/	522	240	304	/	240	704	/	304	736
O_2	558.7	255	1214	480	806	155	480	1264	137	806	1524
CO	560	/	/	401	639	/	401	1037	141	639	1060
O	616	392	2793	1452	1438	180	1452	3125	216	1438	2847
O	645	238	1538	884	755	/	884	1702	/	755	1708
H_α	656	641	7859	25562	12105	4049	25562	63429	1832	12105	62396
O	700	128	1136	501	501	/	501	1033	142	501	1244
O	777.4	10447	50506	28187	27273	8061	28187	54194	9582	27273	52391
O	844.6	6400	35866	19581	17283	4476	19581	36224	5446	17283	35569
O	926	/	838	452	389	/	452	1109	/	389	1111

A.2 Scanning electron microscopy

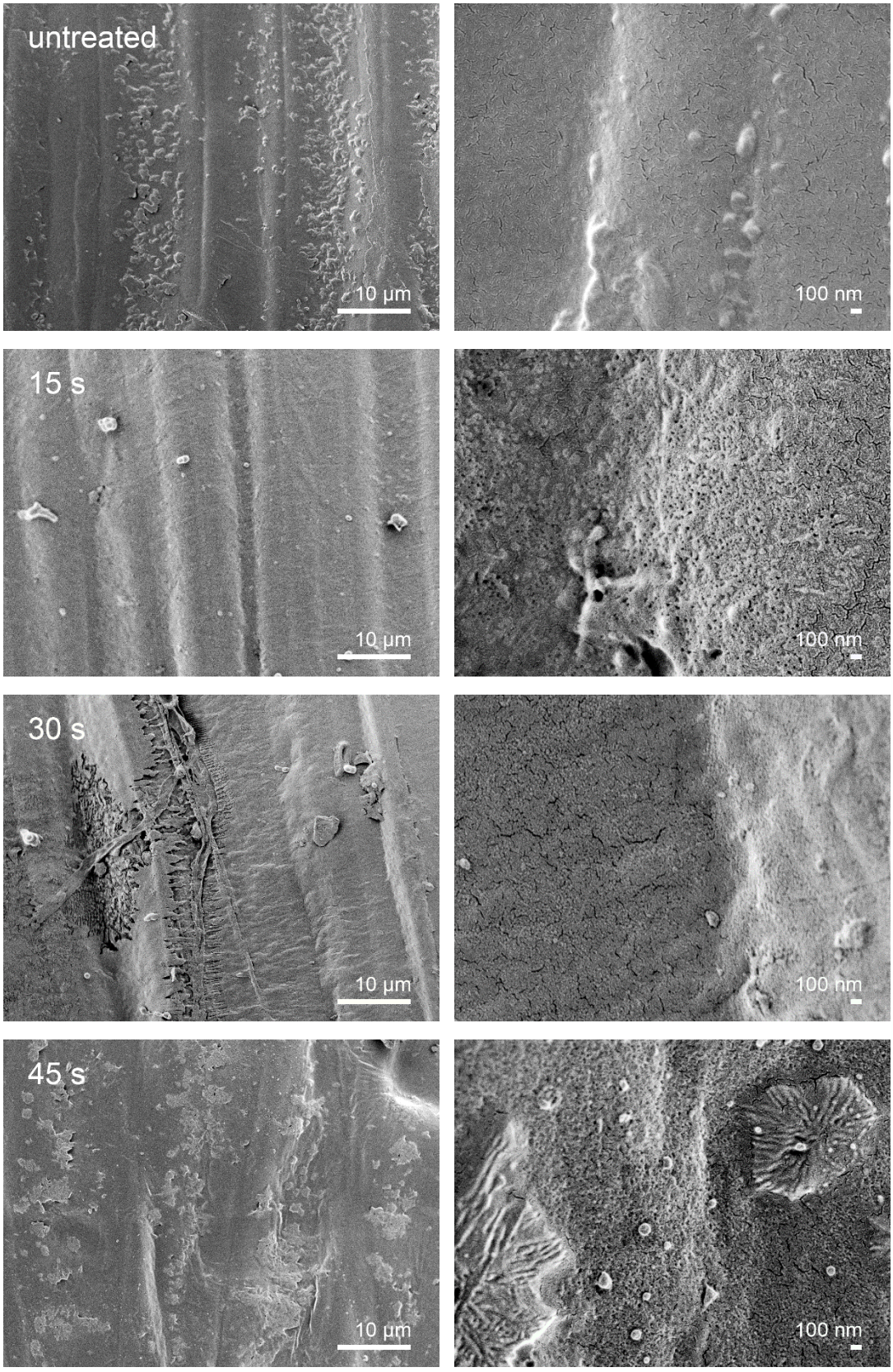

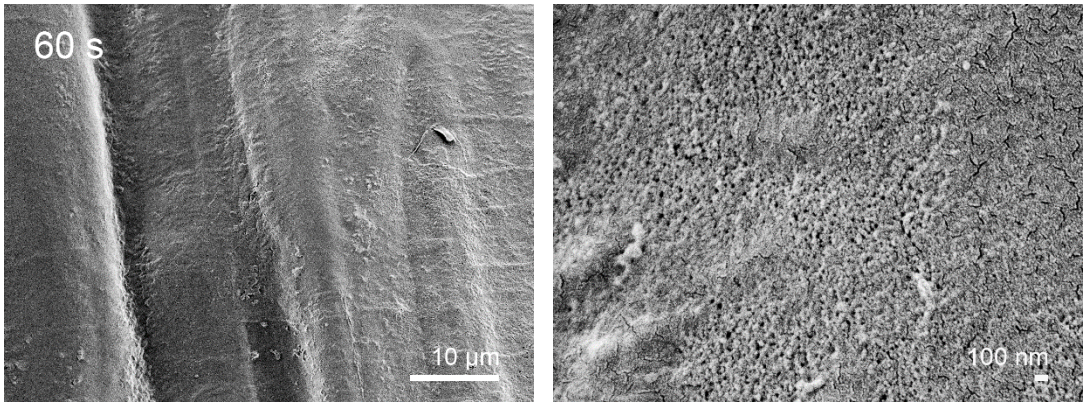

Figure 5.1: SEM images, unpeeled garlic, pilot-scale H-mode afterglow. P_N = 300 W, p = 30 Pa, t = 0 – 60 s. Taken at 2,000 × (left) and 30,000 × (right) magnification.

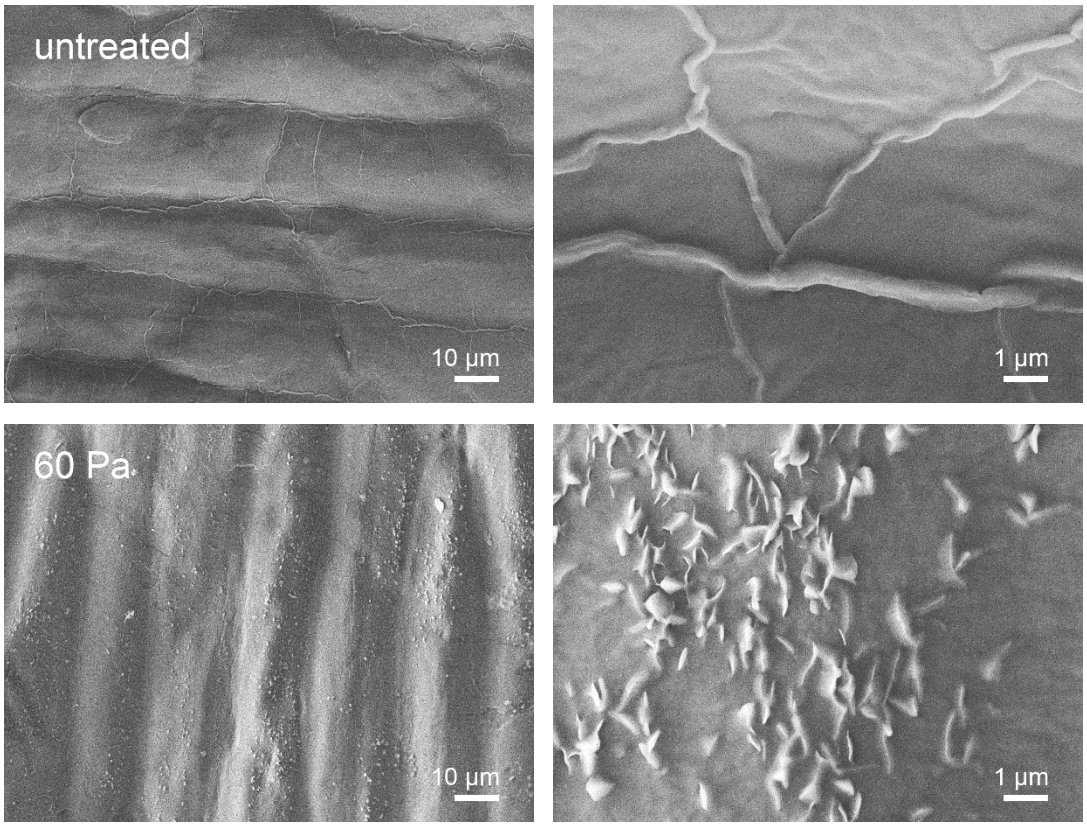

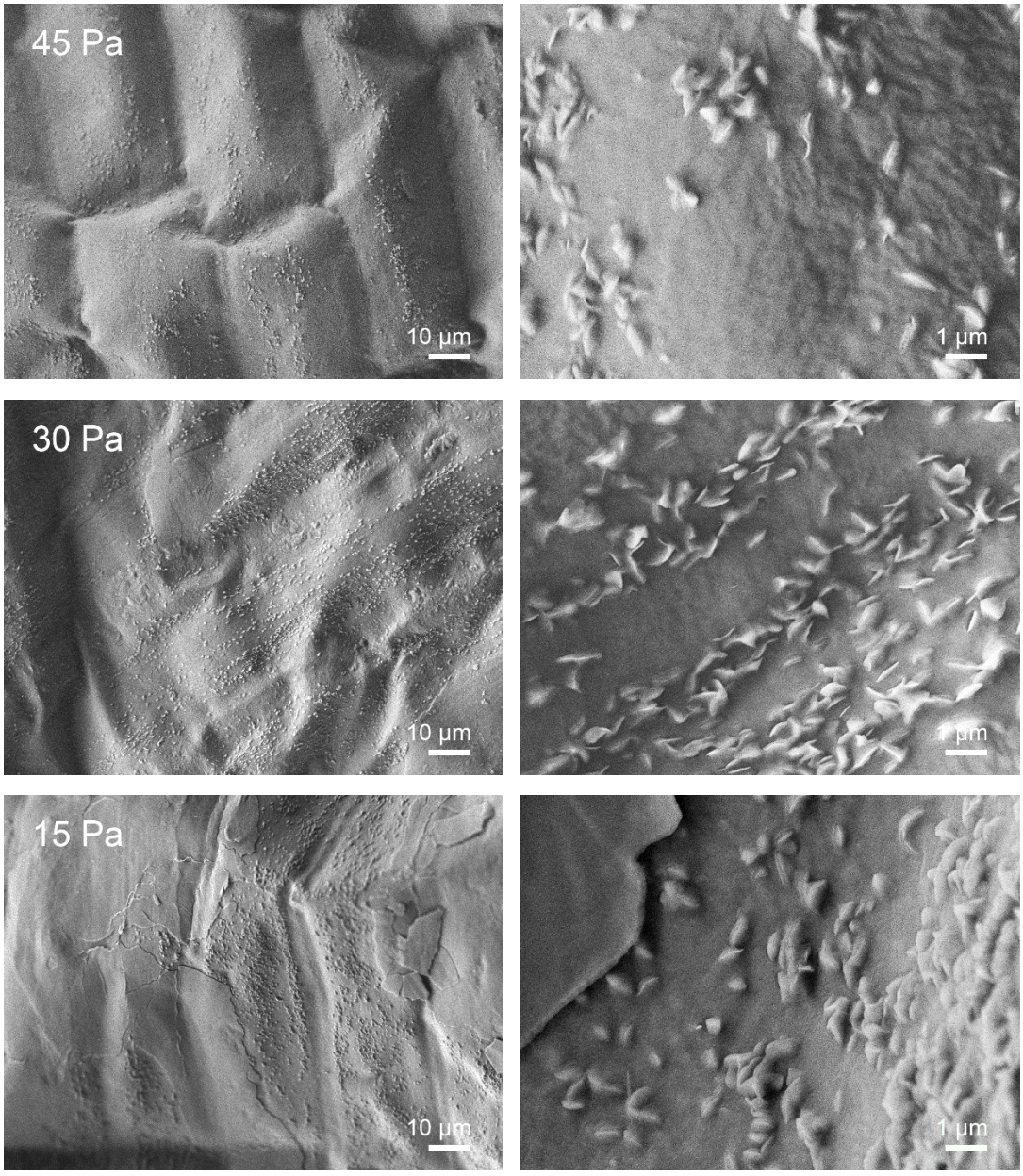

Figure 5.2: SEM images, peeled garlic, industrial-scale E-mode glow. $P_N = \sim 700$ – 900 W, $p = 15$ – 60 Pa, $t = 60$ s. Top to bottom: untreated, 60 Pa, 45 Pa, 30 Pa, 15 Pa. Taken at 1,000 × (left) and 10,000 × (right) magnification.

A.3 Sprout and root growth

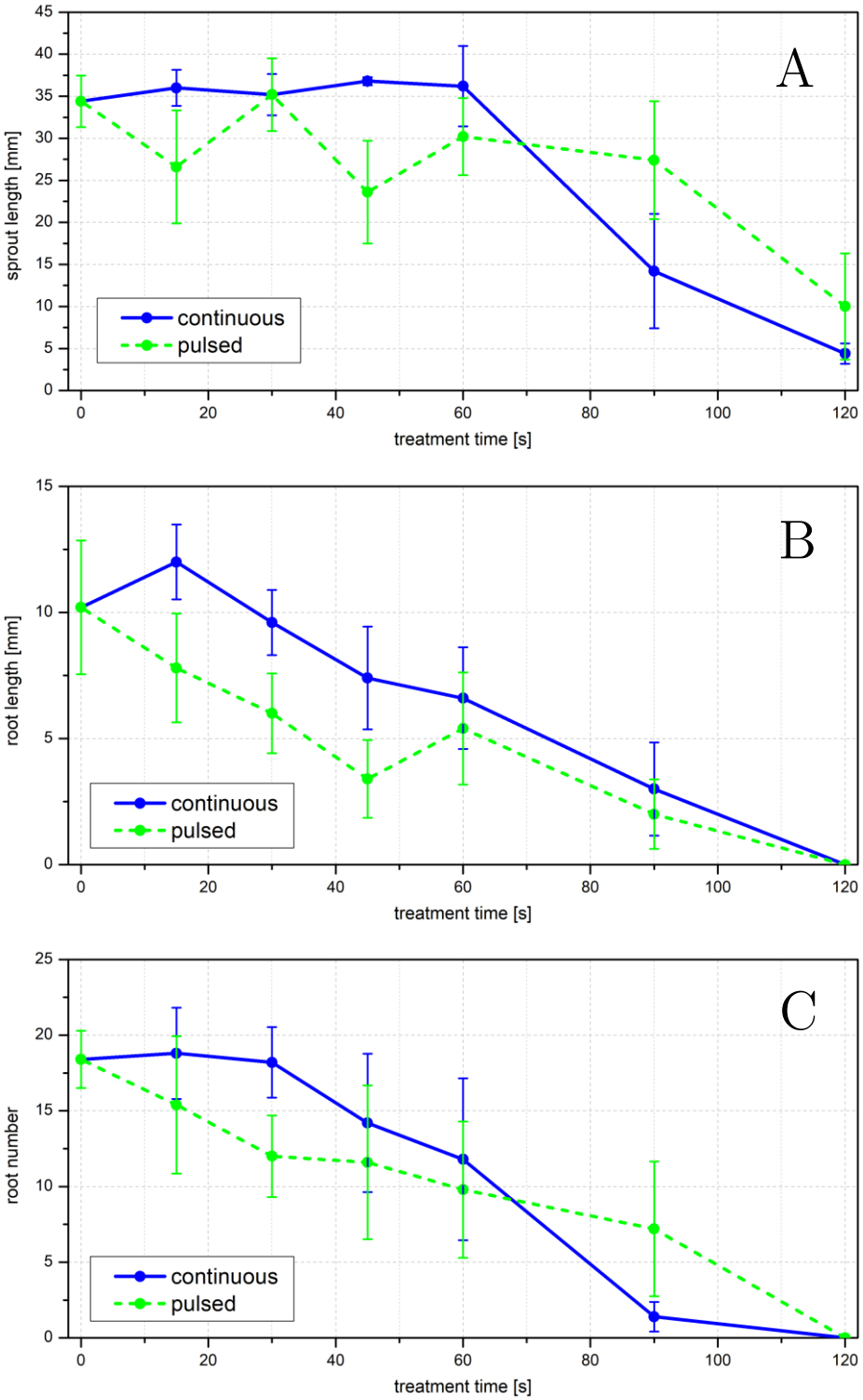

Figure 5.3: Unpeeled clove growth after continuous and pulsed treatment. Pilot-scale E-mode glow, $P_N = 200$ W, $p = 50$ Pa, $t = 0 - 120$ s (pulsed: 5 s on, 5 s off). Recorded at a growth time of 7 days. (A) sprout length; (B) root length; (C) root number.

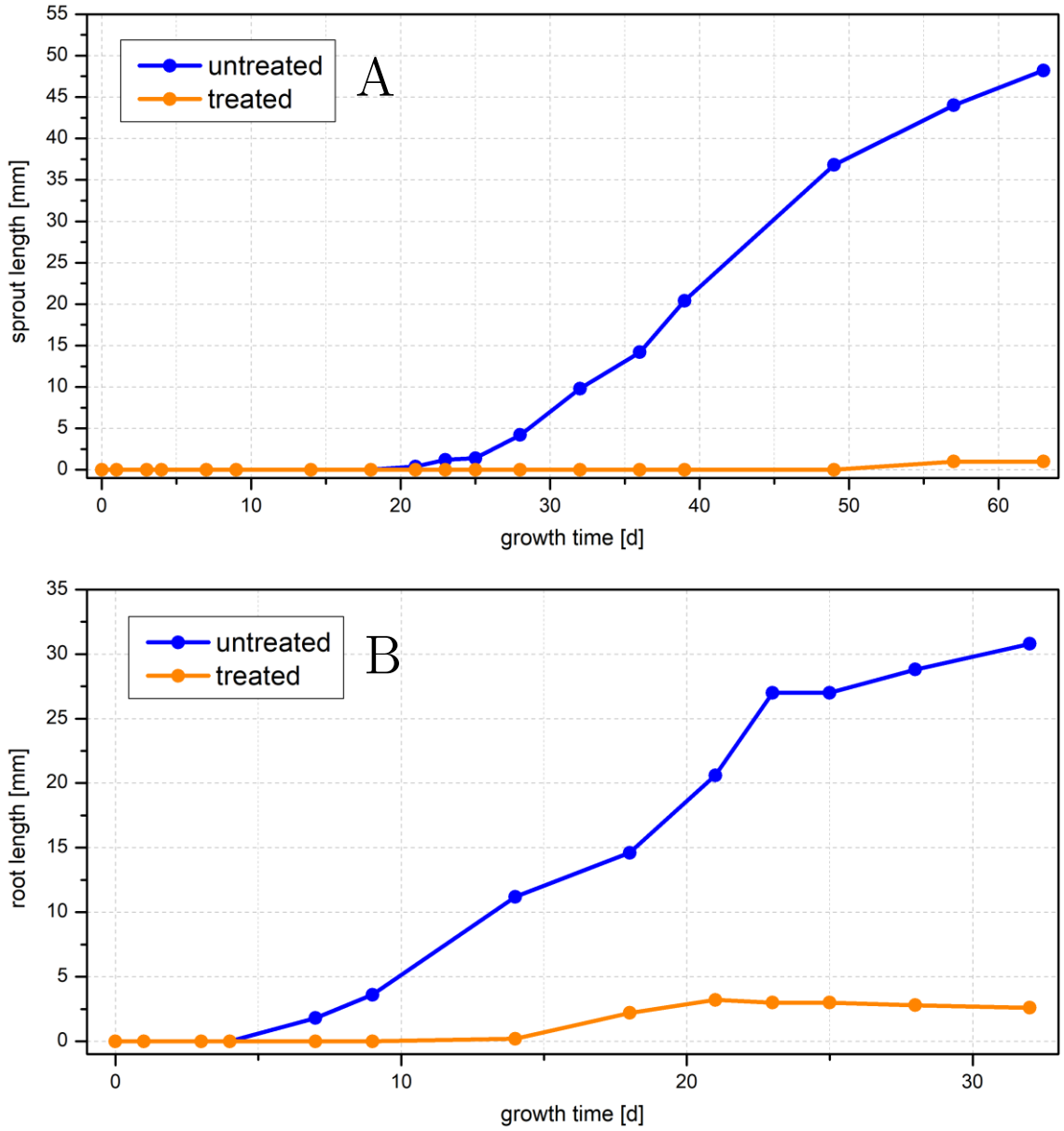

Figure 5.4: Unpeeled clove sprout and root growth after pulsed treatment. Pilot-scale E-mode glow, $P_N = 200$ W, $p = 70$ Pa, $t = 30$ s (6 × 5 s on, 5 s off). (A) sprout length; (B) root length.

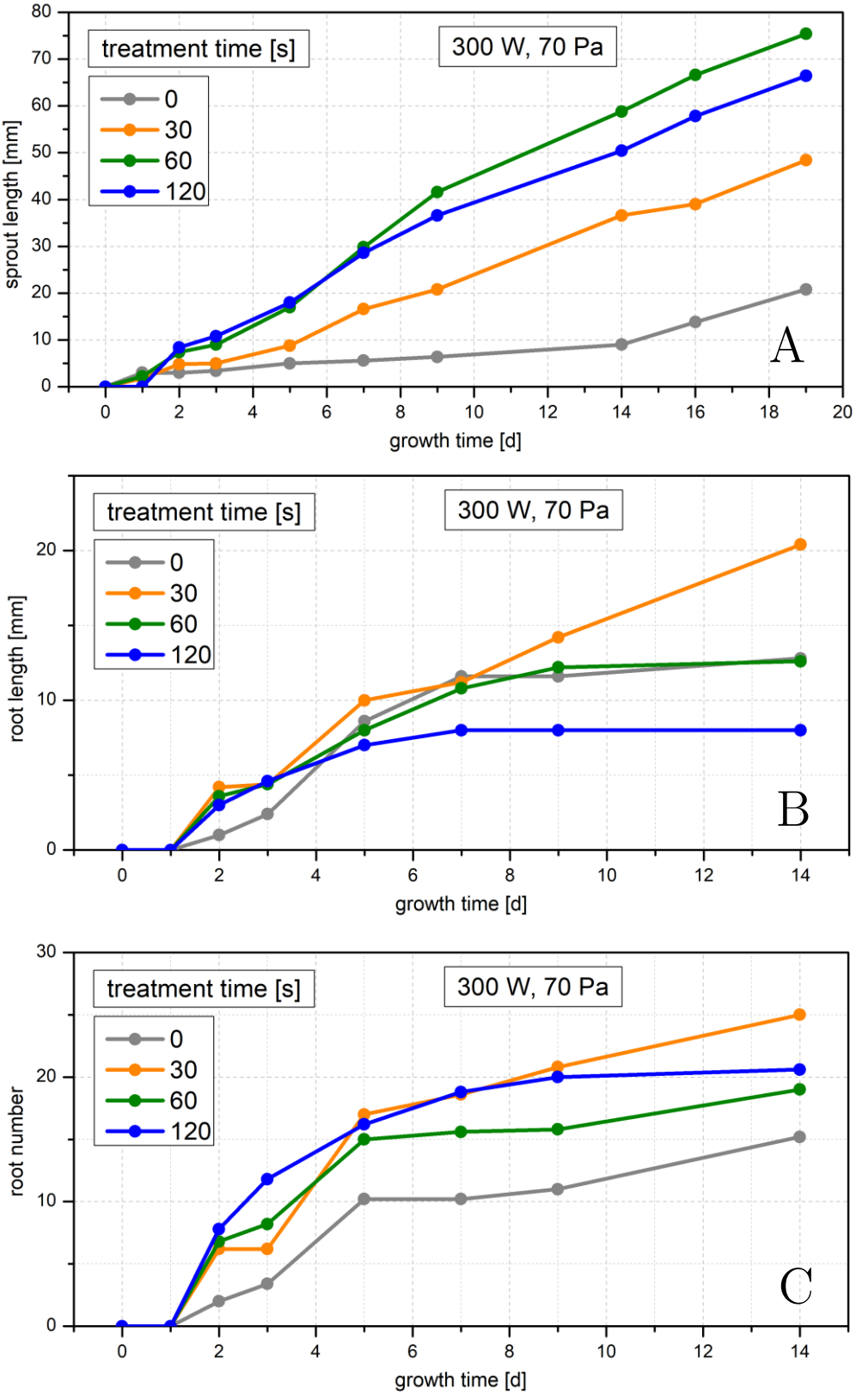

Figure 5.5: Peeled cloves sprout and root growth at 70 Pa. Pilot-scale E-mode glow plasma, $P_N = 300$ W, $p = 70$ Pa, $t = 0 - 120$ s. (A) sprout length; (B) root length; (C) root number.

References

[1] A. Fridman, *Plasma Chemistry*. New York: Cambridge University Press, 2008.

[2] M. A. Lieberman and A. J. Lichtenberg, *Principles of Plasma Discharges and Materials Processing*, 2nd ed.: John Wiley & Sons, 2005.

[3] M. Gorjanc and M. Mozetič, *Modification of Fibrous Polymers by Gaseous Plasma: Principles, Techniques and Applications*. Saarbrücken: Lambert Academic Publishing, 2014.

[4] H. Conrads and M. Schmidt, "Plasma generation and plasma sources," *Plasma Sources Science and Technology,* vol. 9, p. 441, 2000.

[5] U. Cvelbar and M. Mozetič, "Osnove fizike kisikove plazme," *Vakuumist,* vol. 27, pp. 24-33, 2007.

[6] D. Dobrin, M. Magureanu, N. B. Mandache, and M.-D. Ionita, "The effect of non-thermal plasma treatment on wheat germination and early growth," *Innovative Food Science & Emerging Technologies,* vol. 29, pp. 255-260, 2015.

[7] M. Henselová, L. Slováková, M. Martinka, and A. Zahoranová, "Growth, anatomy and enzyme activity changes in maize roots induced by treatment of seeds with low-temperature plasma," *Biologia,* vol. 67, pp. 490-497, 2012.

[8] D. A. Toneli, R. S. Pessoa, M. Roberto, and J. T. Gudmundsson, "On the formation and annihilation of the singlet molecular metastables in an oxygen discharge," *Journal of Physics D: Applied Physics,* vol. 48, p. 325202, 2015.

[9] R. Zaplotnik, A. Vesel, and M. Mozetič, "Atomic oxygen and hydrogen loss coefficient on functionalized polyethylene terephthalate, polystyrene, and polytetrafluoroethylene polymers," *Plasma Processes and Polymers,* p. e1800021, 2018.

[10] Z. Kregar, S. Milošević, and A. Vesel, "Optical Emission From Oxygen Plasma in E and H Modes," *IEEE Transactions on Plasma Science,* vol. 39, pp. 2502-2503, 2011.

[11] I. El-Fayoumi, I. Jones, and M. Turner, "Hysteresis in the E-to H-mode transition in a planar coil, inductively coupled rf argon discharge," *Journal of Physics D: Applied Physics,* vol. 31, pp. 3082-3094, 1998.

[12] A. A. Bol'shakov, B. A. Cruden, R. Mogul, M. Rao, S. P. Sharma, B. N. Khare*, et al.*, "Radio-frequency oxygen plasma as a sterilization source," *Aiaa Journal,* vol. 42, pp. 823-832, Apr 2004.

[13] K. Kutasi, R. Zaplotnik, G. Primc, and M. Mozetic, "Controlling the oxygen species density distributions in the flowing afterglow of O-2/Ar-O-2 surface-wave microwave discharges," *Journal of Physics D-Applied Physics,* vol. 47, Jan 15 2014.

[14] M. Mozetič, G. Primc, A. Vesel, R. Zaplotnik, M. Modic, I. Junkar*, et al.*, "Application of extremely non-equilibrium plasmas in the processing of nano and biomedical materials," *Plasma Sources Science and Technology,* vol. 24, p. 015026, 2015.

[15] R. Molina, C. Lopez-Santos, A. Gomez-Ramirez, A. Vilchez, J. P. Espinos, and A. R. Gonzalez-Elipe, "Influence of irrigation conditions in the germination of plasma treated Nasturtium seeds," *Scientific Reports,* vol. 8, Nov 2018.

[16] S. H. Wheale, C. P. Barker, and J. P. S. Badyal, "Chemical Reaction Pathways at the Plasma−Polymer Interface," *Langmuir,* vol. 14, pp. 6699-6704, 1998/11/01 1998.

[17] R. Zaplotnik, A. Vesel, G. Primc, X. Liu, K. Chen, C. Wei*, et al.*, "Rapid Hydrophilization of Model Polyurethane/Urea (PURPEG) Polymer Scaffolds Using Oxygen Plasma Treatment," *Polymers,* vol. 8, p. 144, 2016.

[18] M. Mozetic, "Surface modification of materials using an extremely non-equilibrium oxygen plasma," *Materiali in Tehnologije,* vol. 44, pp. 165-171, Jul-Aug 2010.

[19] T. Belmonte, C. D. Pintassilgo, T. Czerwiec, G. Henrion, V. Hody, J. M. Thiebaut*, et al.*, "Oxygen plasma surface interaction in treatments of polyolefines," *Surface and Coatings Technology,* vol. 200, pp. 26-30, 10/1/ 2005.

[20] M. Dhayal, S.-Y. Lee, and S.-U. Park, "Using low-pressure plasma for Carthamus tinctorium L. seed surface modification," *Vacuum,* vol. 80, pp. 499-506, 1/26/ 2006.

[21] F. D. Egitto, V. Vukanovic, and G. N. Taylor, "Plasma Etching of Organic Polymers," in *Plasma Deposition, Treatment, and Etching of Polymers*, R. d'Agostino, Ed., ed San Diego: Academic Press, 1990, pp. 321-422.

[22] L. Phan, S. Yoon, and M.-W. Moon, "Plasma-Based Nanostructuring of Polymers: A Review," *Polymers,* vol. 9, p. 417, 2017.

[23] S. d. S. Araujo, S. Paparella, D. Dondi, A. Bentivoglio, D. Carbonera, and A. Balestrazzi, "Physical Methods for Seed Invigoration: Advantages and Challenges in Seed Technology," *Frontiers in plant science,* vol. 7, p. 646, 2016 2016.

[24] S. Mondal, J. E. Rutkoski, G. Velu, P. K. Singh, L. A. Crespo-Herrera, C. Guzman*, et al.*, "Harnessing Diversity in Wheat to Enhance Grain Yield, Climate Resilience, Disease and Insect Pest Resistance and Nutrition Through Conventional and Modern Breeding Approaches," *Frontiers in Plant Science,* vol. 7, p. 991, Jul 2016.

[25] N. Puač, M. Gherardi, and M. Shiratani, "Plasma agriculture: A rapidly emerging field," *Plasma Processes and Polymers,* vol. 15, p. 1700174, 2018.

[26] L. K. Randeniya and G. J. J. B. de Groot, "Non-Thermal Plasma Treatment of Agricultural Seeds for Stimulation of Germination, Removal of Surface Contamination and Other Benefits: A Review," *Plasma Processes and Polymers,* vol. 12, pp. 608-623, Jul 2015.

[27] R. Thirumdas, A. Kothakota, U. Annapure, K. Siliveru, R. Blundell, R. Gatt*, et al.*, "Plasma activated water (PAW): Chemistry, physico-chemical properties, applications in food and agriculture," *Trends in Food Science & Technology,* vol. 77, pp. 21-31, Jul 2018.

[28] R. Thirumdas, C. Sarangapani, and U. S. Annapure, "Cold Plasma: A novel Non-Thermal Technology for Food Processing," *Food Biophysics,* vol. 10, pp. 1-11, Mar 2015.

[29] A. Gomez-Ramirez, C. Lopez-Santos, M. Cantos, J. L. Garcia, R. Molina, J. Cotrino*, et al.*, "Surface chemistry and germination improvement of Quinoa seeds subjected to plasma activation," *Sci Rep,* vol. 7, p. 5924, Jul 19 2017.

[30] L. Li, J. G. Li, H. L. Shao, and Y. H. Dong, "Effects of low-vacuum helium cold plasma treatment on seed germination, plant growth and yield of oilseed rape," *Plasma Science & Technology,* vol. 20, Sep 2018.

[31] L. Li, J. Li, M. Shen, J. Hou, H. Shao, Y. Dong*, et al.*, "Improving Seed Germination and Peanut Yields by Cold Plasma Treatment," *Plasma Science and Technology,* vol. 18, pp. 1027-1033, 2016.

[32] T. Stolárik, M. Henselová, M. Martinka, O. Novák, A. Zahoranová, and M. Černák, "Effect of Low-Temperature Plasma on the Structure of Seeds, Growth and Metabolism of Endogenous Phytohormones in Pea (Pisum sativum L.)," *Plasma Chemistry and Plasma Processing,* vol. 35, pp. 659-676, Jul 2015.

[33] L. Li, J. Jiang, J. Li, M. Shen, X. He, H. Shao*, et al.*, "Effects of cold plasma treatment on seed germination and seedling growth of soybean," *Scientific Reports,* vol. 4, p. 5859, 07/31/online 2014.

[34] J. Jiang, J. Li, and Y. Dong, "Effect of cold plasma treatment on seedling growth and nutrient absorption of tomato," *Plasma Science and Technology,* vol. 20, p. 044007, 2018.

[35] J. Jiang, X. He, L. Li, J. Li, H. Shao, Q. Xu*, et al.*, "Effect of Cold Plasma Treatment on Seed Germination and Growth of Wheat," *Plasma Science and Technology,* vol. 16, pp. 54-58, 2014.

[36] M. Saberi, S. A. M. Modarres-Sanavy, R. Zare, and H. Ghomi, "Amelioration of Photosynthesis and Quality of Wheat under Non-thermal Radio Frequency Plasma Treatment," *Sci Rep,* vol. 8, p. 11655, Aug 3 2018.

[37] B. Zhang, R. H. Li, and J. C. Yan, "Study on activation and improvement of crop seeds by the application of plasma treating seeds equipment," *Archives of Biochemistry and Biophysics,* vol. 655, pp. 37-42, Oct 2018.

[38] N. C. Roy, M. M. Hasan, M. R. Talukder, M. D. Hossain, and A. N. Chowdhury, "Prospective Applications of Low Frequency Glow Discharge Plasmas on Enhanced Germination, Growth and Yield of Wheat," *Plasma Chemistry and Plasma Processing,* vol. 38, pp. 13-28, 2017.

[39] N. C. Roy, M. M. Hasan, A. H. Kabir, M. A. Reza, M. R. Talukder, and A. N. Chowdhury, "Atmospheric pressure gliding arc discharge plasma treatments for improving germination, growth and yield of wheat," *Plasma Science & Technology,* vol. 20, Nov 2018.

[40] M. Yin, M. Huang, B. Ma, and T. Ma, "Stimulating Effects of Seed Treatment by Magnetized Plasma on Tomato Growth and Yield," *Plasma Science and Technology,* vol. 7, pp. 3143-3147, 2005.

[41] Z. Zhou, Y. Huang, S. Yang, and W. Chen, "Introduction of a new atmospheric pressure plasma device and application on tomato seeds," *Agricultural Sciences,* vol. 02, pp. 23-27, 2011.

[42] K. Koga, S. Thapanut, T. Amano, H. Seo, N. Itagaki, N. Hayashi*, et al.*, "Simple method of improving harvest by nonthermal air plasma irradiation of seeds of Arabidopsis thaliana (L.)," *Applied Physics Express,* vol. 9, p. 3, Jan 2016.

[43] E. Bormashenko, R. Grynyov, Y. Bormashenko, and E. Drori, "Cold Radiofrequency Plasma Treatment Modifies Wettability and Germination Speed of Plant Seeds," *Scientific Reports,* vol. 2, p. 741, 10/17/online 2012.

[44] Y. Meng, G. Qu, T. Wang, Q. Sun, D. Liang, and S. Hu, "Enhancement of Germination and Seedling Growth of Wheat Seed Using Dielectric Barrier Discharge Plasma with Various Gas Sources," *Plasma Chemistry and Plasma Processing,* vol. 37, pp. 1105-1119, 2017.

[45] X. Q. Wang, R. W. Zhou, G. Groot, K. Bazaka, A. B. Murphy, and K. K. Ostrikov, "Spectral characteristics of cotton seeds treated by a dielectric barrier discharge plasma," *Sci Rep,* vol. 7, p. 5601, Jul 17 2017.

[46] A. Zahoranova, L. Hoppanova, J. Simoncicova, Z. Tuekova, V. Medvecka, D. Hudecova*, et al.*, "Effect of Cold Atmospheric Pressure Plasma on Maize Seeds: Enhancement of Seedlings Growth and Surface Microorganisms Inactivation," *Plasma Chemistry and Plasma Processing,* vol. 38, pp. 969-988, Sep 2018.

[47] A. R. M. da Silva, M. L. Farias, D. L. S. da Silva, J. O. Vitoriano, R. C. de Sousa, and C. Alves-Junior, "Using atmospheric plasma to increase wettability, imbibition and germination of physically dormant seeds of Mimosa Caesalpiniafolia," *Colloids Surf B Biointerfaces,* vol. 157, pp. 280-285, Sep 1 2017.

[48] P. F. Ambrico, M. Šimek, M. Morano, R. M. De Miccolis Angelini, A. Minafra, P. Trotti*, et al.*, "Reduction of microbial contamination and improvement of germination of sweet basil (Ocimum basilicum L.) seeds via surface dielectric barrier discharge," *Journal of Physics D: Applied Physics,* vol. 50, p. 305401, 2017.

[49] L. Taiz, E. Zeiger, I. M. Møller, and A. Murphy, *Plant Physiology and Development.* New York: Oxford University Press, 2014.

[50] H. H. Chen, Y. K. Chen, and H. C. Chang, "Evaluation of physicochemical properties of plasma treated brown rice," *Food Chemistry,* vol. 135, pp. 74-79, 11/1/ 2012.

[51] K. Graeber, K. Nakabayashi, E. Miatton, G. Leubner-Metzger, and W. J. Soppe, "Molecular mechanisms of seed dormancy," *Plant Cell Environ,* vol. 35, pp. 1769-86, Oct 2012.

[52] N. Hayashi, R. Ono, M. Shiratani, and A. Yonesu, "Antioxidative activity and growth regulation of Brassicaceae induced by oxygen radical irradiation," *Japanese Journal of Applied Physics,* vol. 54, p. 06GD01, 2015.

[53] S. H. Ji, K. H. Choi, A. Pengkit, J. S. Im, J. S. Kim, Y. H. Kim*, et al.*, "Effects of high voltage nanosecond pulsed plasma and micro DBD plasma on seed germination, growth development and physiological activities in spinach," *Archives of biochemistry and biophysics,* vol. 605, pp. 117-28, 2016-Sep-1 2016.

[54] M. C. Pérez Piza, L. Prevosto, C. Zilli, E. Cejas, H. Kelly, and K. Balestrasse, "Effects of non-thermal plasmas on seed-borne Diaporthe/Phomopsis complex and germination parameters of soybean seeds," *Innovative Food Science & Emerging Technologies,* vol. 49, pp. 82-91, Oct 2018.

[55] C. Bailly, H. El-Maarouf-Bouteau, and F. Corbineau, "From intracellular signaling networks to cell death: the dual role of reactive oxygen species in seed physiology," *Comptes Rendus Biologies,* vol. 331, pp. 806-814, 10// 2008.

[56] Food and Agriculture Organization of the United Nations. (2015, Dec 15th). *FAOSTAT, Browse Data / By Domain.* Available: http://faostat3.fao.org/browse/Q/QC/E

[57] J. L. Brewster, *Onions and Other Vegetable Alliums*, 2nd ed. Wallingford: CABI, 2008.

[58] C. Wu, M. Wang, Y. Dong, Z. Cheng, and H. Meng, "Growth, bolting and yield of garlic (Allium sativum L.) in response to clove chilling treatment," *Scientia Horticulturae,* vol. 194, pp. 43-52, 10/14/ 2015.

[59] T. Etoh, "Fertility of the Garlic Clones Collected in Soviet Central Asia," *Journal of the Japanese Society for Horticultural Science,* vol. 55, pp. 312-319, 1986.

[60] H. D. Rabinowitch and J. L. Brewster, *Onions and Allied Crops, Volume III: Biochemistry, Food Science, and Minor Crops*. Boca Raton: CRC Press, 1989.

[61] R. Kamenetsky, "Garlic: Botany and Horticulture," *Horticultural Reviews,* vol. 33, pp. 123-172, 2007.

[62] L. K. Mann, "Anatomy of the garlic bulb and factors affecting bulb development," *Hilgardia,* vol. 21, pp. 195-251, 1952.

[63] R. F. Evert and S. E. Eichorn, *Raven Biology of Plants*, 8th edition ed.: W. H. Freeman, 2012.

[64] M. Riederer and C. Muller, *Biology of the Plant Cuticle*. Oxford, United Kingdom: Blackwell Publishing Ltd, 2006.

[65] C. Buschhaus and R. Jetter, "Composition differences between epicuticular and intracuticular wax substructures: How do plants seal their epidermal surfaces?," *Journal of Experimental Botany,* vol. 62, pp. 841-853, Jan 2011.

[66] J. Graça, L. Schreiber, J. Rodrigues, and H. Pereira, "Glycerol and glyceryl esters of ω-hydroxyacids in cutins," *Phytochemistry,* vol. 61, pp. 205-215, 9// 2002.

[67] K. Koch and W. Barthlott, "Superhydrophobic and superhydrophilic plant surfaces: an inspiration for biomimetic materials," *Philos Trans A Math Phys Eng Sci,* vol. 367, pp. 1487-509, Apr 28 2009.

[68] J. A. Argüello, R. Bottini, R. Luna, G. A. de Bottini, and R. W. Racca, "Dormancy in Garlic (Allium sativum L.) cv. Rosado Paraguayo I. Levels of Growth Substances in “Seed Cloves” under Storage," *Plant and Cell Physiology,* vol. 24, pp. 1559-1563, 1983.

[69] Rahman, "Effects of Gibberellic Acid (GA3) on Breaking Dormancy in Garlic (Allium sativum L.)," *International Journal of Agriculture and Biology,* vol. 8, pp. 63-65, 2006.

[70] L. K. Mann and D. A. Lewis, *Rest and Dormancy in Garlic*, 1956.

[71] A. R. Kramida, Yu., J. Reader, and a. N. A. Team. (2018, June 10). *NIST Atomic Spectra Database (ver. 5.6.1)*. Available: https://physics.nist.gov/asd

[72] J. Musil, J. Matouš, and A. Rajský, "Optical emission spectra from microwave oxygen plasma produced by surfatron discharge," *Czechoslovak Journal of Physics,* vol. 43, pp. 533-540, 1993.

[73] Z. Kregar, M. Biscan, S. Milosevic, K. Elersic, R. Zaplotnik, G. Primc*, et al.*, "Optical Emission Characterization of Extremely Reactive Oxygen Plasma During Treatment of Graphite Samples," *Materiali in Tehnologije,* vol. 46, pp. 25-30, Jan-Feb 2012.

[74] A. Vesel and M. Mozetič, "New developments in surface functionalization of polymers using controlled plasma treatments," *Journal of Physics D: Applied Physics,* 2017.

[75] M. Mozetic, G. Primc, A. Vesel, R. Zaplotnik, M. Modic, I. Junkar*, et al.*, "Application of extremely non-equilibrium plasmas in the processing of nano and biomedical materials," *Plasma Sources Science & Technology,* vol. 24, Feb 2015.

[76] U. Cvelbar, N. Krstulović, S. Milošević, and M. Mozetič, "Inductively coupled RF oxygen plasma characterization by optical emission spectroscopy," *Vacuum,* vol. 82, pp. 224-227, 2007.

[77] S. Wickramanayaka, N. Hosokawa, and Y. Hatanaka, "Variation of the Recombination Coefficient of Atomic Oxygen on Pyrex Glass with Applied RF Power," *Japanese Journal of Applied Physics,* vol. 30, pp. 2897-2900, 1991.

[78] F. Clouet and M. K. Shi, "Interactions of polymer model surfaces with cold plasmas: Hexatriacontane as a model molecule of high-density polyethylene and octadecyl octadecanoate as a model of polyester. I. Degradation rate versus time and power," *Journal of Applied Polymer Science,* vol. 46, pp. 1955-1966, 1992.

[79] M. Gorjanc, V. Bukošek, M. Gorenšek, and A. Vesel, "The Influence of Water Vapor Plasma Treatment on Specific Properties of Bleached and Mercerized Cotton Fabric," *Textile Research Journal,* vol. 80, pp. 557-567, 2009.

[80] R. Zaplotnik, A. Vesel, and M. Mozetič, "Transition from E to H Mode in Inductively Coupled Oxygen Plasma: Hysteresis and the Behaviour of Oxygen Atom Density," *EPL (Europhysics Letters),* vol. 95, p. 55001, 2011.

[81] A. Vesel and M. Mozetič, "Behaviour of catalytic probe during surface activation of polyether sulphone," *Vacuum,* vol. 61, pp. 373-377, 2001.

[82] A. Vesel, M. Mozetič, A. Hladnik, J. Dolenc, J. Zule, S. Milošević*, et al.*, "Modification of Ink-Jet Paper by Oxygen-Plasma Treatment," *Journal of Physics D: Applied Physics,* vol. 40, p. 3689, 2007.

[83] R. Zaplotnik, A. Vesel, and M. Mozetic, "A fiber optic catalytic sensor for neutral atom measurements in oxygen plasma," *Sensors (Basel),* vol. 12, pp. 3857-67, 2012.

[84] H. Sourkova, G. Primc, and P. Spatenka, "Surface Functionalization of Polyethylene Granules by Treatment with Low-Pressure Air Plasma," *Materials (Basel),* vol. 11, May 25 2018.

[85] A. Doliška, A. Vesel, M. Kolar, K. Stana-Kleinschek, and M. Mozetič, "Interaction between model poly(ethylene terephthalate) thin films and weakly ionised oxygen plasma," *Surface and Interface Analysis,* vol. 44, pp. 56-61, 2012.

[86] Engineering ToolBox. (2019, Jun 19th). *Specific Heat of Food and Foodstuff.* Available: https://www.engineeringtoolbox.com/specific-heat-capacity-food-d_295.html

[87] M. Mozetic, A. Vesel, S. D. Stoica, S. Vizireanu, G. Dinescu, and R. Zaplotnik, "Oxygen atom loss coefficient of carbon nanowalls," *Applied Surface Science,* vol. 333, pp. 207-213, 2015.

[88] W. Liu, Y. F. Liu, Y. Q. Tao, Y. J. Yu, H. M. Jiang, and H. Z. Lian, "Comparative study of adsorption of Pb(II) on native garlic peel and mercerized garlic peel," *Environmental Science and Pollution Research,* vol. 21, pp. 2054-2063, Feb 2014.

[89] Y. Zhao, W. Li, Z. Liu, J. Liu, L. Zhu, X. Liu*, et al.*, "Renewable Tb/Eu-Loaded Garlic Peels for Enhanced Adsorption of Enrofloxacin: Kinetics, Isotherms, Thermodynamics, and Mechanism," *ACS Sustainable Chemistry & Engineering,* vol. 6, pp. 15264-15272, 2018.

[90] J. A. Heredia-Guerrero, R. de Lara, E. Dominguez, A. Heredia, J. Benavente, and J. J. Benitez, "Chemical-physical characterization of isolated plant cuticles subjected to low-dose gamma-irradiation," *Chemistry and Physics of Lipids,* vol. 165, pp. 803-808, Dec 2012.

[91] T. Hietala, N. Mozes, M. J. Genet, H. Rosenqvist, and S. Laakso, "Surface lipids and their distribution on willow (Salix) leaves: A combined chemical, morphological and physicochemical study," *Colloids and Surfaces B-Biointerfaces,* vol. 8, pp. 205-215, Apr 10 1997.

[92] M. C. Perkins, C. J. Roberts, D. Briggs, M. C. Davies, A. Friedmann, C. A. Hart*, et al.*, "Surface morphology and chemistry of Prunus laurocerasus L. leaves: a study using X-ray photoelectron spectroscopy, time-of-flight secondary-ion mass spectrometry, atomic-force microscopy and scanning-electron microscopy," *Planta,* vol. 221, pp. 123-134, Apr 2005.

[93] L. J. Gerenser, "X-Ray photoemission study of plasma modified polyethylene surfaces," *Journal of Adhesion Science and Technology,* vol. 1, pp. 303-318, 1987/01/01 1987.

[94] S. K. Øiseth, A. Krozer, B. Kasemo, and J. Lausmaa, "Surface modification of spin-coated high-density polyethylene films by argon and oxygen glow discharge plasma treatments," *Applied Surface Science,* vol. 202, pp. 92-103, 2002.

[95] J. De Giorgi, U. Piskurewicz, S. Loubery, A. Utz-Pugin, C. Bailly, L. Mene-Saffrane*, et al.*, "An Endosperm-Associated Cuticle Is Required for Arabidopsis Seed Viability, Dormancy and Early Control of Germination," *PLoS Genet,* vol. 11, p. e1005708, Dec 2015.

[96] T. Dufour, J. Minnebo, S. A. Rich, E. C. Neyts, A. Bogaerts, and F. Reniers, "Understanding polyethylene surface functionalization by an atmospheric He/O2 plasma through combined experiments and simulations," *Journal of Physics D: Applied Physics,* vol. 47, p. 224007, 2014.

[97] V. Štěpánová, P. Slavíček, J. Kelar, J. Prášil, M. Smékal, M. Stupavská*, et al.*, "Atmospheric pressure plasma treatment of agricultural seeds of cucumber (Cucumis sativus L.) and pepper (Capsicum annuum L.) with effect on reduction

of diseases and germination improvement," *Plasma Processes and Polymers,* vol. 15, p. 1700076, 2018.

[98] S. Kitazaki, K. Koga, M. Shiratani, and N. Hayashi, "Growth Enhancement of Radish Sprouts Induced by Low Pressure O 2 Radio Frequency Discharge Plasma Irradiation," *Japanese Journal of Applied Physics,* vol. 51, p. 01AE01, 2012.

[99] H. Suhr, "Application of nonequilibrium plasmas in organic chemistry," *Plasma Chemistry and Plasma Processing,* vol. 3, pp. 1-61, 1983.

[100] P. Patiño, F. E. Hernández, and S. Rondón, "Reactions of O(3P) with secondary C-H bonds of saturated hydrocarbons in nonequilibrium plasmas," *Plasma Chemistry and Plasma Processing,* vol. 15, pp. 159-171, 1995.

[101] M. Zhang, J. K. Oh, L. Cisneros-Zevallos, and M. Akbulut, "Bactericidal effects of nonthermal low-pressure oxygen plasma on S. typhimurium LT2 attached to fresh produce surfaces," *Journal of Food Engineering,* vol. 119, pp. 425-432, Dec 2013.

[102] S. A. Nasim, B. Dhir, R. Kapoor, S. Fatima, Mahmooduzzafar, and A. Mujib, "Alliin production in various tissues and organs of Allium sativum grown under normal and sulphur-supplemented in vitro conditions," *Plant Cell Tissue and Organ Culture,* vol. 101, pp. 59-63, Apr 2010.

[103] P. Bocchini, C. Andalò, R. Pozzi, G. C. Galletti, and A. Antonelli, "Determination of diallyl thiosulfinate (allicin) in garlic (Allium sativum L.) by high-performance liquid chromatography with a post-column photochemical reactor," *Analytica Chimica Acta,* vol. 441, pp. 37-43, 2001.

[104] R. Leontiev, N. Hohaus, C. Jacob, M. C. H. Gruhlke, and A. J. Slusarenko, "A Comparison of the Antibacterial and Antifungal Activities of Thiosulfinate Analogues of Allicin," *Scientific Reports,* vol. 8, p. 6763, 2018/04/30 2018.

[105] G. G. Freeman, "Distribution of flavour components in onion (Allium cepa L.), leek (Allium porrum) and garlic (Allium sativum)," *Journal of the Science of Food and Agriculture,* vol. 26, pp. 471-481, 1975.

[106] L. Schreiber, "Polar paths of diffusion across plant cuticles: new evidence for an old hypothesis," *Ann Bot,* vol. 95, pp. 1069-73, Jun 2005.

[107] P. K. Hepler, "Calcium: a central regulator of plant growth and development," *Plant Cell,* vol. 17, pp. 2142-55, Aug 2005.

[108] T. Vukušić, A. Vesel, M. Holc, M. Ščetar, A. Režek Jambrak, and M. Mozetič, "Modification of Physico-Chemical Properties of Acryl-Coated Polypropylene Foils for Food Packaging by Reactive Particles from Oxygen Plasma," *Materials (Basel),* vol. 11, Mar 3 2018.

[109] J. F. Ma, Y. Miyake, and E. Takahashi, "Chapter 2: Silicon as a beneficial element for crop plants," in *Studies in Plant Science*. vol. 8, L. E. Datnoff, G. H. Snyder, and G. H. Korndörfer, Eds., ed: Elsevier, 2001, pp. 17-39.

[110] A. F. Abdel-Fattah and M. Edrees, "A study on the composition of garlic skins and the structural features of the isolated pectic acid," *Journal of the Science of Food and Agriculture,* vol. 23, pp. 871-877, 1972.

[111] (June 30th). *Infrared Spectroscopy Absorption Table.* Available: https://chem.libretexts.org/Ancillary_Materials/Reference/Reference_Tables/Spectroscopic_Parameters/Infrared_Spectroscopy_Absorption_Table

[112] J. A. Hardin, C. L. Jones, P. R. Weckler, N. O. Maness, J. W. Dillwith, and R. D. Madden, "Rapid Quantification of Spinach Leaf Cuticular Wax Using Fourier Transform Infrared Attenuated Total Reflectance Spectroscopy," *Transactions of the Asabe,* vol. 56, pp. 331-339, Jan-Feb 2013.

[113] S. H. Ji, S. H. Ki, M. H. Kang, J. S. Choi, Y. Park, J. Oh*, et al.*, "Characterization of physical and biochemical changes in plasma treated spinach seed during germination," *Journal of Physics D: Applied Physics,* vol. 51, p. 145205, 2018.

[114] F. M. Mirabella, *Internal reflection spectroscopy: theory and applications.* New York: Marcel Dekker, 1993.

[115] M. Lehocký, H. Drnovská, B. Lapčíková, A. M. Barros-Timmons, T. Trindade, M. Zembala*, et al.*, "Plasma surface modification of polyethylene," *Colloids and Surfaces A: Physicochemical and Engineering Aspects,* vol. 222, pp. 125-131, 2003.

[116] F. Grzegorzewski, S. Rohn, L. W. Kroh, M. Geyer, and O. Schlueter, "Surface morphology and chemical composition of lamb's lettuce (Valerianella locusta) after exposure to a low-pressure oxygen plasma," *Food Chemistry,* vol. 122, pp. 1145-1152, Oct 15 2010.

[117] S. H. Ji, T. Kim, K. Panngom, Y. J. Hong, A. Pengkit, D. H. Park*, et al.*, "Assessment of the Effects of Nitrogen Plasma and Plasma-Generated Nitric Oxide on Early Development of Coriandum sativum," *Plasma Processes and Polymers,* vol. 12, pp. 1164-1173, Oct 2015.

[118] J. Tong, R. He, X. Zhang, R. Zhan, W. Chen, and S. Yang, "Effects of Atmospheric Pressure Air Plasma Pretreatment on the Seed Germination and Early Growth of Andrographis paniculata," *Plasma Science and Technology,* vol. 16, p. 260, 2014.

[119] B. Šerá, P. Spatenka, M. Sery, N. Vrchotova, and I. Hruskova, "Influence of Plasma Treatment on Wheat and Oat Germination and Early Growth," *IEEE Transactions on Plasma Science,* vol. 38, pp. 2963-2968, 2010.

[120] D. Korzec, J. Rapp, D. Theirich, and J. Engemann, "Cleaning of metal parts in oxygen radio frequency plasma: Process study*," *Journal of Vacuum Science & Technology A,* vol. 12, pp. 369-378, 1994.

[121] N. Sprang, D. Theirich, and J. Engemann, "Plasma and ion beam surface treatment of polyethylene," *Surface and Coatings Technology,* vol. 74-75, pp. 689-695, 1995.

[122] H. Puliyalil and U. Cvelbar, "Selective Plasma Etching of Polymeric Substrates for Advanced Applications," *Nanomaterials (Basel),* vol. 6, Jun 07 2016.

[123] G. N. Taylor and T. M. Wolf, "Oxygen plasma removal of thin polymer films," *Polymer Engineering and Science,* vol. 20, pp. 1087-1092, 1980.

[124] J. Barros, H. Serk, I. Granlund, and E. Pesquet, "The cell biology of lignification in higher plants," *Ann Bot,* vol. 115, pp. 1053-74, Jun 2015.

[125] A. Niemietz, K. Wandelt, W. Barthlott, and K. Koch, "Thermal evaporation of multi-component waxes and thermally activated formation of nanotubules for superhydrophobic surfaces," *Progress in Organic Coatings,* vol. 66, pp. 221-227, 2009.

[126] Y. Rhee, A. Hlousek-Radojcic, J. Ponsamuel, D. H. Liu, and D. Post-Beittenmiller, "Epicuticular wax accumulation and fatty acid elongation activities are induced

during leaf development of leeks," *Plant Physiology,* vol. 116, pp. 901-911, Mar 1998.

[127] H. J. Ensikat, M. Boese, W. Mader, W. Barthlott, and K. Koch, "Crystallinity of plant epicuticular waxes: electron and X-ray diffraction studies," *Chem Phys Lipids,* vol. 144, pp. 45-59, Oct 2006.

[128] J. Pawłat, A. Starek, A. Sujak, M. Kwiatkowski, P. Terebun, and M. Budzeń, "Effects of atmospheric pressure plasma generated in GlidArc reactor on Lavatera thuringiaca L. seeds' germination," *Plasma Processes and Polymers,* vol. 15, p. 1700064, 2018.

[129] J. Pawłat, A. Starek, A. Sujak, P. Terebun, M. Kwiatkowski, M. Budzen*, et al.*, "Effects of atmospheric pressure plasma jet operating with DBD on Lavatera thuringiaca L. seeds' germination," *PLoS One,* vol. 13, p. e0194349, 2018.

[130] S. Srisonphan, "Tuning Surface Wettability through Hot Carrier Initiated Impact Ionization in Cold Plasma," *ACS Appl Mater Interfaces,* vol. 10, pp. 11297-11304, Apr 4 2018.

[131] E. Bormashenko, Y. Shapira, R. Grynyov, G. Whyman, Y. Bormashenko, and E. Drori, "Interaction of cold radiofrequency plasma with seeds of beans (Phaseolus vulgaris)," *Journal of Experimental Botany,* vol. 66, pp. 4013-4021, Jul 2015.

[132] V. Azharonok, I. Filatova, N. Poklonski, N. Lapčuk, and A. Gajdarov, "Electron Paramagnetic Resonance Study of the Efficiency of RF Electromagnetic Field and RF Plasma Seed Pretreatments for Germination Stimulation of Carrot Seeds," in *VII International conference Plasma Physics and Plasma Technology*, Minsk, Belarus, 2012.

[133] N. Hayashi, A. Nakahigashi, M. Goto, S. Kitazaki, K. Koga, and M. Shiratani, "Redox Characteristics of Thiol Compounds Using Radicals Produced by Water Vapor Radio Frequency Discharge," *Japanese Journal of Applied Physics,* vol. 50, p. 5, Aug 2011.

[134] B. Šerá, P. Špatenka, M. Šerý, N. Vrchotová, and I. Hrušková, "Influence of Plasma Treatment on Wheat and Oat Germination and Early Growth," *IEEE Transactions on Plasma Science,* vol. 38, pp. 2963-2968, 2010.

[135] V. Mildaziene, G. Pauzaite, Z. Naucienė, A. Malakauskiene, R. Zukiene, I. Januskaitiene*, et al.*, "Pre-sowing seed treatment with cold plasma and electromagnetic field increases secondary metabolite content in purple coneflower (Echinacea purpurea) leaves," *Plasma Processes and Polymers,* vol. 15, p. 1700059, 2018.

[136] V. Mildaziene, G. Pauzaite, A. Malakauskiene, R. Zukiene, Z. Nauciene, I. Filatova*, et al.*, "Response of perennial woody plants to seed treatment by electromagnetic field and low-temperature plasma," *Bioelectromagnetics,* Aug 30 2016.

[137] A. De Souza, D. García, L. Sueiro, and F. Gilart, "Improvement of the seed germination, growth and yield of onion plants by extremely low frequency non-uniform magnetic fields," *Scientia Horticulturae,* vol. 176, pp. 63-69, 2014.

[138] M. Orlowski, E. Rekowska, and R. Dobromilska, "Effect on the yield of garlic (Allium sativum L.) of autumn and spring planting using different methods of seedstalk trimming," *Folia Horticulturae (Poland),* 1994.

[139] A. Zahoranová, M. Henselová, D. Hudecová, B. Kaliňaková, D. Kováčik, V. Medvecká*, et al.*, "Effect of Cold Atmospheric Pressure Plasma on the Wheat Seedlings Vigor and on the Inactivation of Microorganisms on the Seeds Surface," *Plasma Chemistry and Plasma Processing,* vol. 36, pp. 397-414, Mar 2016.

[140] M. Holc, I. Junkar, G. Primc, J. Iskra, P. Titan, S. G. Mlakar*, et al.*, "Improved Sprout Emergence of Garlic Cloves by Plasma Treatment," *Plasma Medicine,* vol. 6, pp. 325-338, 2016.

[141] M. Modic, I. Junkar, A. Vesel, and M. Mozetic, "Aging of plasma treated surfaces and their effects on platelet adhesion and activation," *Surface and Coatings Technology,* vol. 213, pp. 98-104, 2012.

Bibliography

Publications Related to the Thesis

Journal Articles

M. Holc, I. Junkar, G. Primc, J. Iskra, P. Titan, S. G. Mlakar, J. Kovač, and M. Mozetič, "Improved Sprout Emergence of Garlic Cloves by Plasma Treatment," *Plasma Medicine*, vol. 6, pp. 325-338, 2016.

Conference Papers

M. Holc, I. Junkar, G. Primc, J. Iskra, P. Titan, S. G. Mlakar, J. Kovač, and M. Mozetič, "Garlic sprout emergence improvement by low-pressure oxygen plasma treatment," in *81st Workshop on Response of Biological Materials to Plasma Treated Medium*, Rogla, Slovenia: Plasmadis, 2017.

M. Holc, I. Junkar, G. Primc, and M. Mozetič, "Disinfection and germination of cloves and bulbs by weakly ionized low-pressure plasma," in *ICMAP 2018, 7th International Conference on Microelectronics and Plasma Technology*, Incheon, Korea: Korean Vacuum Society, 2018

M. Holc, I. Junkar, G. Primc, and M. Mozetič, "Stimulation of garlic sprouting by brief treatment in oxygen plasma," in *IWOPA2, 2nd International Workshop on Plasma Agriculture*, Gifu, Japan: 2018.

Patents

M. Holc, I. Junkar, G. Primc, M. Mozetič, J. Iskra, and P. Titan, "Metoda za obdelavo strokov česna," patent SI 25440 A, Ljubljana, Slovenia: Urad RS za intelektualno lastnino, 2018.

Other Publications

Journal Articles

T. Vukušić, A. Vesel, M. Holc, M. Ščetar, A. Režek Jambrak, and M. Mozetič, "Modification of Physico-Chemical Properties of Acryl-Coated Polypropylene Foils for Food Packaging by Reactive Particles from Oxygen Plasma," *Materials (Basel)*, vol. 11, 2018.

M. Holc, R. Zaplotnik, M. Mozetič, and A. Vesel, "Surface Modification and Aging of Polyacrylonitrile Butadiene Styrene Polymer Induced by Treatment in RF Oxygen Plasma," *IEEE Transactions on Plasma Science*, pp. 1-8, 2018.

Conference Papers

A. Vesel, T. Vukušić, M. Holc, and M. Mozetič, "Modification of polypropylene foil for packaging applications," in *Book of abstracts, 24th International Scientific Meeting on Vacuum Science and Technology*, Zadar, Croatia: Croatian Vacuum Society, 2017.

Biography

The author of this dissertation was born in Murska Sobota, Slovenia, on October 11th, 1986. After completing Gimnazija Franca Miklošiča high school in Ljutomer, he enrolled into the University of Ljubljana, Faculty of Pharmacy, study program Pharmacy. During his studies, he completed a 6-month research internship in the field of pharmaceutical technology at AstraZeneca R&D Mölndal, Sweden. He prepared his Master's thesis in the field of biotechnology at the Vrije Universiteit Brussel, Belgium. On April 10th, 2013, he completed his studies, receiving the title Master of Pharmacy. Between May 2014 and October 2015, he was employed as a Quality Assurance Manager at Lek d. d., Ljubljana. In November 2015, he started his position as a Young Researcher at the Jožef Stefan Institute, Department of Surface Engineering and Optoelectronics (F4). There, the author performed low-pressure plasma treatments of various materials, primarily biological samples, paper, and polymers. He analyzed the germination and growth of garlic in laboratory and agricultural settings. He performed surface analyses using scanning electron microscopy and atomic force microscopy, as well as wettability assessments of materials using water uptake and water contact angle measurements.